RECOGNITION AND SENSING OF BIOLOGICALLY AND ENVIRONMENTALLY SIGNIFICANT ANALYTES

THESIS SUBMITTED TO ACSIR FOR THE AWARD OF

THE DEGREE OF

DOCTOR OF PHILOSOPHY

IN CHEMICAL SCIENCES

By

GANDRA UPENDAR REDDY

(10CC11J26134)

UNDER THE GUIDANCE OF

Dr. AMITAVA DAS

CSIR-NATIONAL CHEMICAL LABORATORY

PUNE: 411008, MAHARASHTRA, INDIA.

JULY 2015

CANDIDATE'S STATEMENT

I hereby declare that the work incorporated in the present thesis is original and has not been submitted to any University/Institution for the award of a Diploma or a Degree. I further declare that the results presented in the thesis and the considerations made therein, contribute in general to the advancement of knowledge in Chemistry and in particular to “**Recognition and sensing of Biologically and Environmentally Significant Analytes**".

Gandra Upendar Reddy

Fax: +91-020-25902629
☎: (O) +91-020-25902385

E-Mail: a.das@ncl.res.in

National Chemical Laboratory

Dr. Homi Bhabha Road, Pune: 411008, Maharashtra INDIA

Dr. Amitava Das*, F.A.Sc., F.N.Sc*
Chief Scientist and Prof AcSIR
Organic Chemistry Division

Date: July 30, 2015

CERTIFICATE BY THE GUIDE

This is to certify that the contents of this thesis entitled “Recognition and sensing of Biologically and Environmentally Significant Analytes” is the original research work of Gandra Upendar Reddy carried out under my supervision at CSIR-National Chemical Laboratory, Pune.

I further certify that the work has not been submitted either partly or fully to any other University or Institution for the award of any degree.

[Amitava Das]
Signature of Guide

ACKNOWLEDGEMENTS

I express my deep sense of gratefulness to **Dr. Amitava Das**, my research supervisor. His passion for chemistry has been the source of inspiration to me. I am extremely grateful to him for the freedom that I have enjoyed during my research career as a Ph.D. student. I dedicate all my success, whatever I have achieved as a Ph.D. student, to this wonderful person and his family.

I wish to convey my gratefulness to ***Dr. Biswajit Ganguly*** of CSIR-Central Salt & Marine Chemicals Research Institute at Bhavnagar for his guidance and support with all computational studies. These studies constitute an important part of this thesis. I also express my sincere gratitude to **Dr. *Samit Chattopadhyay*** of National Center for Cell Science in Pune for all the help and guidance that he has extended for biological studies.

I sincerely thank ***Dr. Sourav Paul*** (ex-Director), **Dr. Vijayamohanan K. Pillai,** (Director), CSIR-National Chemical Laboratory, **Dr. Pushpito K. Ghosh** of (ex-Director of CSIR-Central Salt and Marine Chemicals Research Institute at Bhavnagar for providing me the necessary infrastructure for carrying out my research work. I wish to convey my gratefulness to ***Dr. Padip Kumar Tripathi*****,** Chair person of Organic Chemistry Division and ***Dr. Parimal Paul***, Discipline Coordinator of Analytical Chemistry Discipline, for their support and providing me all analytical/departmental facilities.

My special thanks to ***Dr. R. Khureshy*** and ***Dr. C.G. Suresh*** for their unconditional support and advices during my AcSIR course work period and completion of thesis.

I would like to extend my gratitude towards ***Dr. C. S. Gopinath, Dr. Santhosh B Mhaske, Dr. Sakya Sen, Dr. Kumar Vanka, Dr. N.H. Khan, Dr. Divesh N. Srivastava, Dr. Surendhar Singh*** (University of Delhi), ***Prof. Vasudeva Reddy*** (Kakatiya University) and ***Prof. Manoj Kumar*** (Guru Nanak Dev University) for their timely help and support.

I wish to express thanks to ***Dr. R. Meena, Dr. Kamalesh Prasad*** and ***Dr. Vibhav Manthri*** for their guidance and valuable advices during my AcSIR 800 level course work.

I wish to express my sincere thanks to ***Dr. Vinod Boricha*** for recording NMR spectra, ***Mr. Vinod Agarwal*** for recording FTIR spectra, ***Mr. Arun Das*** for Mass Spectroscopic results and **Dr. *Harsad Brambhatt*** for elemental analysis at CSIR-CSMCRI.

I would like to express my special thanks to all my laboratory seniors, ***Dr. Atindra D. Sukla***, ***Dr. D.Krishna Kumar***, ***Dr. D. Amilan Jose***, ***Dr. Prasenjit Kar, Dr. Amrita***

Ghosh**, **Dr. Moorthy Suresh**, **Dr. Prasenjit Mahato**, **Dr. Amal Kumar Mandal**, **Dr. Priyadip Das**, **Dr.Sukdeb Saha**, **Dr. Tanmay Banerjee. They all taught me intricacies in initial days of my research and took me along with them until their final days at CSIR-CSMCRI.

I feel fortunate enough to have, ***Dr. Praveen L.**, **Dr. Sovan Roy**, **Dr. Suman Pal**, **Dr. Ajay Pal**, **Dr. Shilpi**, **Hridesh Agarwalla**, **Arunava Maity**, **Monalisa Gangopadhyay**, **Firoj Ali**, **Sunil Aute**, **Anila H.A**, **Anantha Dey and Koushik Maji*** *as* my research colleagues, with whom I worked all these years in my laboratory either at 101 (at CSIR-CSMCRI) and/or at 172 (at CSIR-NCL). Each one of them has helped and contributed in my research. They all stood by me and caring me from being fallen. I thank all of them individually from the bottom of my heart.

I am sincerely thankful to ***Dr. Shafee*** and ***Vadde Ramu*** for their effort, which brought me to CSIR-CSMCRI and for enormous helps during in my whole PhD journey.

I am extremely thankful to my friends ***Ch. Pradeep Reddy**, **R.C. Reddy**, **K.Tarun, N.Vishwanath*** *and* ***B. Kiran Reddy*** for their friendly and moral support in day to day life of CSIR-CSMCRI & CSIR-NCL.

I owe a lot to Mr. ***Nandaraj Taye***, my friend and a research scholar from NCCS (Pune). Without his help and discussions in biological studies, it would not have been possible for me to put things together for this thesis.

My sincere thanks are due to all my friends and well-wishers ***N. Prasad Reddy**, **Dr.K.Chaitanya**, **Bhuma Naresh**, **Sathish**, **R Suresh**, **KCB Naidu**, **Ram Reddy**, **Ganesh**, **ThriNath**, **Senthil**, **Krishna Prasad**, **Anoop**, **Goudappa**, **Y. Shanthi**, **S. Gopal Mandal**, **Dr.Kethan**, **Swamy**, **J Sagar**, **Prathap**, **V. Kashayap**, **Korra Praveen**, **Veer**, **Santhosh, Indrapal**, **Roby**, **Rahul**, **Ullas**, **Yashpal**, **Anand**, **D. Pratap**, **Sandip Sharma***, ***Raju Thombal**, **Pranab**, **Abhijit**, **Shiva, Navanath, Afthab**, **Moshina**, **Apoorva**, **Mayuri**, **Dr.Sovankar**, **DevraJ*** and all my CSIR-NCL friends for their help and friendly atmosphere in NCL.

I wish to express thanks to ***Bhanu**, **Veera Babu**, **SN Rao**, **Stalin, G. Sreedhar**, **GVS Rao**, **CM**, **Sampath**,**V.Narayana**, **Dr. Ravi Gunupuru**, **Dr. Mastan**, **Dr. Krishna Mohan Shiva**, **Debdeep Da**, **Rabin Da**, **Apurba**, **Muni Swamy**, **V.Ramakrishna**, **Cnu**, **Pankaj**, **Sham**, **Bharat Bhai***, and all my CSIR-CSMCRI friends for their help during my stay at CSIR-CSMCRI.

I sincerely thank all other scientists, technician and other staff Members of CSIR-***CSMCRI*** and CSIR-***NCL*** for their keen help and co-operation.

Acknowledgement

I would like to acknowledge ***UGC and DST*** (New Delhi)**,** Government of India for financial assistance in the form of a research fellowship.

Finally, I thank the most important people in my life, my ***Parents*** and ***Brother*** for their love, prayers, patience and unconditional support, which has helped me to fulfill my dream.

ABBREVIATIONS

CD_2Cl_2	Deuterated dichloromethane
$CDCl_3$	Deuterated chloroform
CD_3OD	Deuterared Methanol
DMF-d_7	Deuterated N, N'-dimethylformamide
DMSO-d_6	Deuterated Dimethyl sulfoxide
CD_3CN	Deuterated acetonitrile
DMF	N,N'-dimethylformamide
DMSO	Dimethyl sulfoxide
ESI	Electrospray Ionization
ET	Energy Transfer
FRET	Forster Resonance Energy Transfer
TBET	Through Bond Resonance Energy Transfer
HOMO	Highest Occupied Molecular Orbital
LUMO	Lowest Unoccupied Molecular Orbital
LED	Light Emitting Diode
(λmon)	Monitoring Wavelength
(λexc)	Excitation Wavelength
(λemi)	Emission Wavelength
MLCT	Metal to Ligand Charge Transfer
ns	nanosecond
ps	picosecond
ICT	Intramolecular Charge Transfer
TICT	Twisted Intramolecular Charge Transfer
PET	Photo induced electron transfer
RET	Resonance Energy Transfer
TCSPC	Time Correlated Single Photon Counting

THF	Tetrahydrofuran
TBAH	Tetrabutylammonium hydroxide
TBAF	Tetrabutylammonium fluoride
(λ_{Abs}^{max})	Absorption Wavelength at maximum fluorescence intensity
(λ_{Ems}^{max})	Emission Wavelength at maximum fluorescence intensity
Hz	Hertz
MHz	Megahertz
h	Hour
NIR	Near Infrared
μM	Micro molar
mM	Millimolar
μl	Micro litre
ITC	Isothermal Titration Calorimeter
SEM	Scanning electron microscopy
HEPES	4-(2-hydroxyethyl)-1-piperazineethanesulfonic acid
DNA	Deoxyribonucleic acid
EDTA	Ethylene diamine tetraacetic acid
PBS	Phosphate buffered saline
SD	Standard deviation
NMR	Nuclear Magnetic Resonance
FTIR	Fourier transform infrared
ppm	Parts per million
ppb	Parts per billion

CHAPTER 1

INTRODUCTION

1. Photoinduced processes and recognition of biologically important analytes

1.1 Introduction

Certain ions and molecules are essential for human and other living organisms. However, presence of such analytes beyond a threshold value may have some adverse consequences.[1-3] Specific recognition and quantitative estimation of such specific analytes is essential for a variety of applications ranging from diagnostic, clinical biology, environmental sample analysis and developing imaging reagent for important biomarkers.[4] For this, appropriate design and synthesis of purpose built molecules are crucial. In general, various traditional analytical techniques like titrimetric, voltammetric, potentiometric, electrochemical methods and ion chromatography, are being conventionally used for the detection and quantitative estimation of such analytes. However, many of the above mentioned techniques are expensive and need multistep sample preparation and/or use of sophisticated instrumentation. These procedures often require samples of large size/volume and do not allow real time monitoring. Such methodologies often suffer from interference problem from competing analytes. Further, these sophisticated instrumental techniques are neither well-suited for quick in-field detection of these ions nor for in-vivo studies.

In contrast, method based on the molecular sensors for the detection of such analytes offer distinct advantages in terms of selectivity and sensitivity, response time, local observation (e.g. by fluorescence imaging spectroscopy).[5] Such a procedure also offers the option of real time monitoring. Chromogenic sensors that allow visual detection are of special significance as it offers the choice for semi quantitative naked eye detection of targeted analytes without resorting to any spectroscopic instrumentation. Whereas fluorescent sensors have edge for higher sensitivity and for the possibility of using such reagents for imaging application for living cells with temporal and spatial resolution.[6]

A review of the literature reports reveals that the designing of popular molecular sensors for recognition and quantitative estimation of analytes that have biological and environmental significance involve (i) covalently coupled receptor-signalling subunit, (ii) dye displacement methodology and (iii) chemodosimetric approach (Figure 1.1). In the first approach, receptors and the optical signalling subunit are covalently bonded in such a way that the interaction of the analyte with the binding site influences the energies of the frontier orbitals of the signalling unit, which eventually resulted a modified optical responses either in the form of changes in electronic or/and fluorescence spectral properties (Figure 1.1a). Choice of the receptor fragment depends on the nature and the charge of the analyte for achieving the desired specificity in receptor-analyte binding or interaction. Receptor-analyte binding could also be achieved either by covalent or coordinate covalent interactions or by utilizing various non-bonded interactions, namely, ion-ion,[7] ion-dipole,[8] dipole-dipole,[9] hydrogen bonding,[10] π-π interactions.[11]

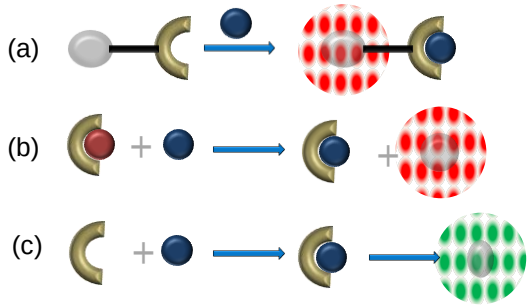

Figure 1.1. Three main approaches for molecular recognition: (a) probe molecule bearing a signalling subunit as well as a binding site; (b) displacement approach; (c) chemodosimetric approach.

In dye displacement approach, receptors and signalling subunits are not covalently bound; rather these fragments form a molecular assembly. Higher thermodynamic stability of the analyte specific receptor binding causes the release of dye that was earlier held in an assembly with the receptor and such process is usually associated with changes in optical responses (Figure 1.1b).

Chemodosimetric approach (Figure 1.1c) is generally adopted for recognition and sensing of ionic analytes having high enthalpy of hydration, as the even higher reaction enthalpy exceed the hydration enthalpy of the ionic analyte and allow the chemical reaction to prevail over the deleterious solvation enthalpy of the ionic analyte. For neutral analyte, receptor analyte interactions are generally governed by the weak dipole-dipole or dipole-induced dipole interactions and such weak interactions affects the receptor-analyte binding efficiency and the detection process. To get around this problem, researchers have adopted the chemodosimetric approach for detection of certain neutral analyte either in aqueous medium or in biofluids. The chemodosimetric process generally leads to an irreversible reaction with an associated change in electronic or luminescence spectral properties that allow monitoring of these analytes.

1.2 Various photoinduced phenomena utilized for recognition processes

Signaling fragment constitutes one of the major components of any efficient sensors. Change in output signal, either in the form of fluorescence or electronic spectral change(s), of the reporter functionality in response to the receptor-analyte interaction is basically the expression of the relative change in the difference in the energy level of the orbitals as well as the differences in the ground and excited state properties of the photoactive unit in the free and the bound form. Such spectral responses generally involve mechanistic pathways like, photo-induced electron transfer (PET), intramolecular charge transfer (ICT), fluorescence resonance energy transfer (FRET), through bond energy transfer (TBET) and excited state intrarmolecular proton transfer (ESIPT) etc.[12]

Among various fluorophores, xanthene moiety having rhodamines are being used extensively for molecular recognition because of high emission quantum yield, cell membrane permeability, non-toxic nature towards live cells and finally the switch on

fluorescence response upon conversion of a cyclic lactam form to the acyclic one. However, such reagents generally have a Stokes shift of about 50 nm with single emission intensity changes. It provides the single emission intensity change, which tend to be affected by variety of factors such as instrumental efficiency and environmental conditions, as well as the concentration of probe molecule. However, quantification of a target analyte using single fluorescence based probe is great difficult. These interferences can be eliminated by employing ratiometric fluorescent probes, which allow the measurement of changes of the intensity ratio at two emission bands induced by analytes. Such ratiometric probes can be designed by attaching suitable fluorophore to rhodamines, which exhibits different photo physical mechanisms with large pseudo Stokes shift, which further helps in various biological applications. Photophysical properties of a fluorophore can be easily tuned using various strategies such as PET, electron transfer, ICT, ESIPT, FRET and TBET, which are to be discussed in the following section.

1.2.1. Photoinduced Electron Transfer (PET)

Photoinduced electron transfer (PET) is one of the most attractive photophysical signalling mechanisms that has been extensively used for cation recognition studies. PET involves donation of the lone pair of the electrons of hetero atoms like N, O, S or P of the receptor fragment to the HOMO of the excited fluorophore (Figure 1.2), which accounts for the luminescence quenching the covalently bound fluorophore preferably through a $–CH_2–$ linkage. On formation of a coordinate covalent bond to a metal ion or on protonation, energy of the HOMO of the receptor having that lone pair of electron is significantly lowered in energy and this interrupt the PET process and attributes to a luminescence ON response.[13]

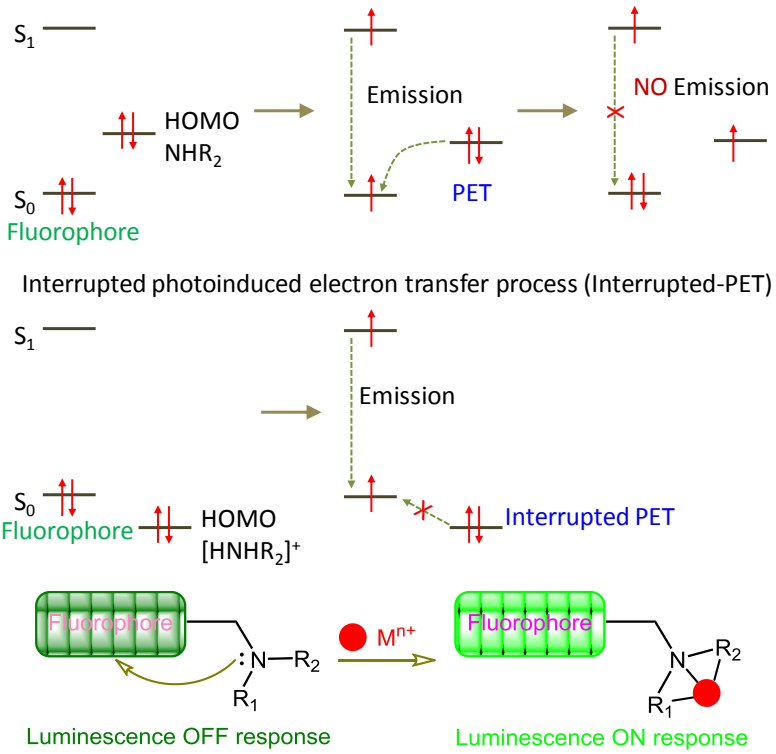

Figure 1.2. Photo physical mechanism of photo induced electron transfer (PET).

A. P. de Silva and his co-workers were the first to demonstrate the PET-based process for developing a luminescence ON probe having N-(9-Anthrylmethyl) monoaza-18-crown-6 moiety **1** (Figure 1.3).[14] The probe was initially non fluorescent (Φ=0.003), as an effective PET process was operational.

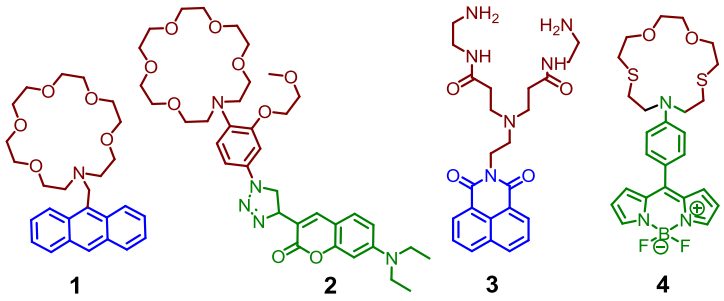

Figure 1.3. Molecular structures of the PET based chemosensors **1** - **4**.

However, a *switch ON* luminescence response was observed on binding to K^+ in methanol (Φ = 0.14) upon. Despite interference from Na^+ and H^+, this report opened up the new area on utilizing interrupted PET process for metal ion recognition. Holdt *et al.* reported probe **2** for recognition of K^+/Na^+ based on PET mechanism.[15] Probe **2**

contains phenylaza-[18]-crown-6 lariat ether with a coumarin fluorophore (Figure 1.3). Free probe **2** displayed a weak emission peak at 493 nm and with low quantum yield (Φ=0.062). Upon addition of K^+ (100 mM) to the solution of probe **2** results in strong emission with high quantum yield (Φ = 0.184). However, any possibility of the intramolecular charge transfer (ICT) process was not discussed. Furthermore, probe **2** was also embedded with in a polymer matrix to demonstrate its application as a continuous sensor. Fluorescence microscopy experiments revealed that probe **2** has possessed excellent cell membrane permeability. Bojinov *et.al* reported a probe **3** (Figure 1.3) having 1,8-naphthalimide moiety as a fluorophore and tertiary amine as a receptor for high specificity towards H^+ over Co^{2+}, Cu^{2+}, Fe^{3+}, Ni^{2+}, Cd^{2+}, Pb^{2+}, Zn^{2+}, Hg^{2+} and Ag^+ and a luminescence ON response was observed on binding to H^+ due to an interrupted PET process.[16] A violet-blue fluorescence was observed at lower solution pH. By utilising the PET mechanism, Kaur *et.al* described a molecular probe **4** having a N-aryl derivative dithia-dioxa-aza crown ether as a specific Pd^{2+} ion receptor and BODIPY moiety as the signalling fragment (Figure 1.3).[17] The probe was found to be highly stable over broad pH range (1 -11). The free ligand (10 μM in ACN solution) showed an absorption shoulder at 484 nm and weak emission band at 520 nm (Φ= 0.0018 for λ_{Ext} = 480 nm). It was argued that upon addition to Pd^{2+} ion, significant emission enhancement was observed due to an interrupted PET process. However, the role of any ICT process was not discussed in this report. Despite sparing solubility of the reagent **4**, authors could successfully demonstrate the cell imaging studies for breast cancer cell line.

Yang *et al.* reported a NIR active fluorescent probe **5** (Figure 1.4) for the selective detection of Cys over Hcy/GSH by utilizing a PET based response.[18] Probe **5** made up with an IR-780 fluorophore, functionalized with nitro group. It was proposed that the probe fluorescence was mostly quenched as a PET process was operational and a weak emission band maximum at 830 nm was observed.

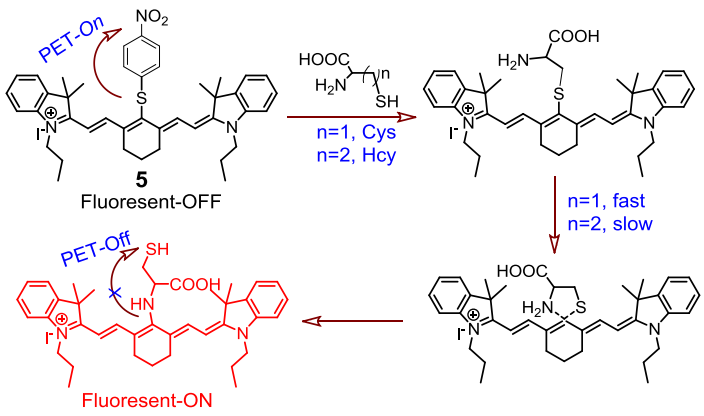

Figure 1.4. Proposed mechanism of **5** for detection of Cys.

Reaction with Cys caused elimination of the nitro phenyl moiety, which consequently interrupted the PET process and a strong emission band with maximum at 750 nm appeared. Once again the shift of emission maximum tends to support ICT process over the PET process, while no such possibility was discussed in that report. For GSH, an increase in luminescence at 830 nm was observed, while for Hcy, a dual emission at both 745 nm and 820 nm was observed. Reactivity of **5** for Hcy and GSH was reported to be slow compared to Cys. The lower detection limit for Cys was found to be 1.26 μM. Moreover, probe **5** was successfully applied for maping intracellular Cys in live cells.

Kim *et al.* reported a water-soluble BODIPY derivative (Figure1.5) for selective recognition of HOCl/OCl$^-$ over the other anions.[19] This probe was initially non fluorescent owing to the quenching of the singlet excited state by an efficient PET process involving electron-rich catechol group as the donor functionality with higher HOMO energy than does the BODIPY moiety. The free ligand exhibited a sharp absorption band at 497 nm and a weak emission maximum at 519 nm (Φ = 0.001). On reaction with HOCl/OCl$^-$, a 80 fold fluorescence enhancement was observed in phosphate buffer solution. It was proposed that hypochlorite oxidized the catechol moiety to o-quinone form, which inhibit the PET process. The LOD of probe **6** for

HOCl is found to be 0.3 μM. Once again the possibility of ICT process was ignored while explaining the results of the photoinduced processes.

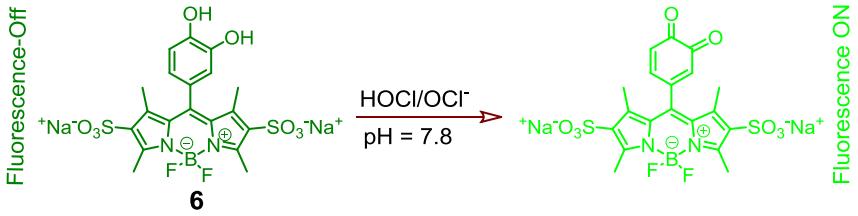

6

Figure 1.5. Proposed mechanism of **6** for detection of HOCl.

Hong *et al.* reported a Co(II)-salen based fluorescent sensor **7** (Figure 1.6) for recognition of CN^- over other anions.[20] In CH_3CN, the solution of probe **7** was found to be non fluorescent due to an efficient PET process involving electron transfer from the photo-excited coumarin moiety to the central Co(II)-centre in **7**. In presence of CN^-, Co(II)-CN^- coordination raised the LUMO level of the cobalt-salen complex and this inhibited the PET process, which eventually resulted for the luminescence enhancement at ~750 nm. Large Stroke's shift and shift in emission maxima tends to suggest involvement of ICT process. Other anions either failed to coordinate to Co(II) were bond weakly to Co(II) centre, which failed to alter the energies of the frontier orbital's and consequently the luminescence response remained unchanged for **7**. Therefore, the selectivity of **7** plausibly comes from the higher affinity of the CN^- for coordination to Co(II) ion. Experimental results confirmed binding stoichiometry of 1: 2 and based on this the following coordination mode was proposed.

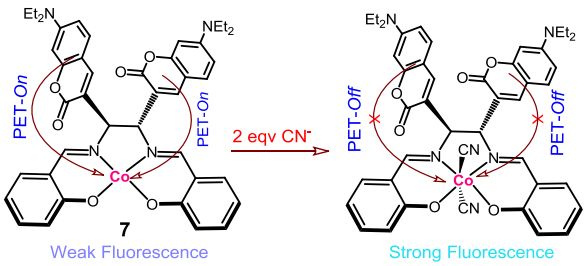

7

Weak Fluorescence

Strong Fluorescence

Figure 1.6. Reaction mechanism of the fluorescence change of **7** with CN^-.

1.2.2. Energy Transfer Quenching (ET)

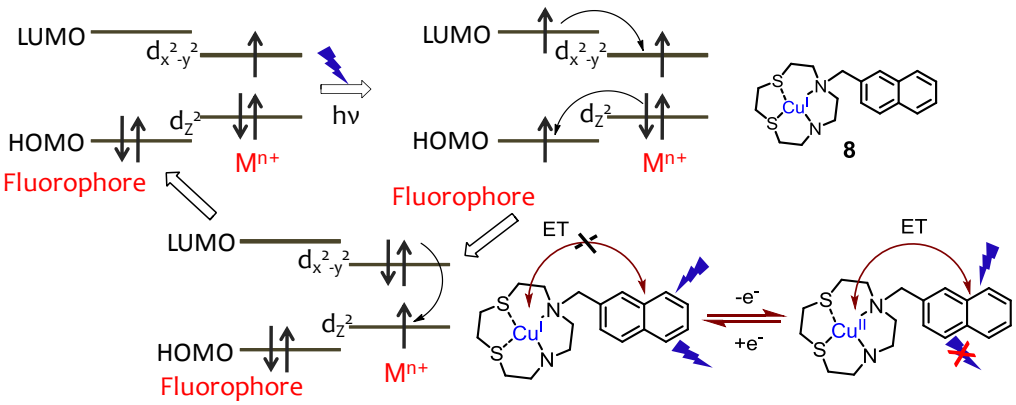

Figure 1.7. Energy transfer mechanism (double-electron exchange) between excited fluorophore and d^9–metal ion (elongated-octahedral arrangement).

In some cases, complexation of Cu^{2+} does not induce the chelation enhanced fluorescence effect (CHEF) but causes the quenching the luminescence of the excited state of a fluorophore via energy transfer (ET) to the metal ion, that lead to rapid non radiative decay.[21] Cu^{2+}-ion, with elongated-octahedron d^9 configuration is known to participate in such energy transfer (ET) process. The d^9 metal ion quenches the fluorescence through double electron exchange as shown in the Figure.1.7 and there is no net change in distribution of electron(s) (Dexter type electron transfer).

Probe **8** was reported by Bergonzi *et al.* and this was comprised of a NS_3 macrocycle, which was linked to a naphthalene fluorophore by a $-CH_2-$ group. Cu(II) ion, with elongated−octahedron d^9 configuration, is capable of quenching the fluorescence of the naphthalene moiety in **8** by energy transfer (ET) mechanism.[21]

1.2.3. Intramolecular Charge Transfer (ICT)

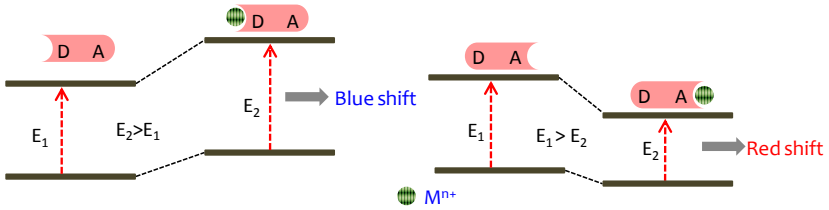

Figure 1.8. Representation of an ICT process on interaction with a bound cation with a receptor.

The ICT strategy for cation sensing was introduced by Valeur.[2] This mechanism involves the transfer of an electron between electron donor (D) and acceptor (A) functionalities within the molecule, which eventually results an altered ‘‘push–pull’’ interaction in the excited state in a π-electron system. Modification of D or A as a metal ionophore results in metal coordination-induced blue or red shift of emission via an altered photo-induced internal charge transfer excited state with modified fluorescence quantum yields and lifetimes. This could be probed for monitoring the metal ion recognition process. Binding of the metal ion to the donor part of an ICT-based fluorophore would cause a decrease in the HOMO energy and induce the hypsochromic (blue) shift of emission maxima. Metal ion coordination to its acceptor part would favour the ICT process further and would cause an opposing influence in the luminescence response (Figure 1.8). Therefore, ICT mechanism is an efficient strategy for the construction of ratiometric metal ion probes, which allow quantitative determination of target metal ions in living cells, tissues and animals. Various representative examples of ICT based cation sensors are given in Figure 1.9. Molecular probes **9**[22] and **10**[23] were reported to be specific for Pd(II) ions, while **11**[24] was found to be specific towards Cu(II) ion. Bathochromic shifts were observed for these three receptors in their absorption and emission spectra upon binding of these cations. On the other hand, molecular probes **12**,[25] **13**[26] and **14**[27] belonged to the other class of ICT based chemosensors where the receptor-metal ion binding

favored the ICT process and thereby induced hypsochromic shift in absorbance and emission spectra.

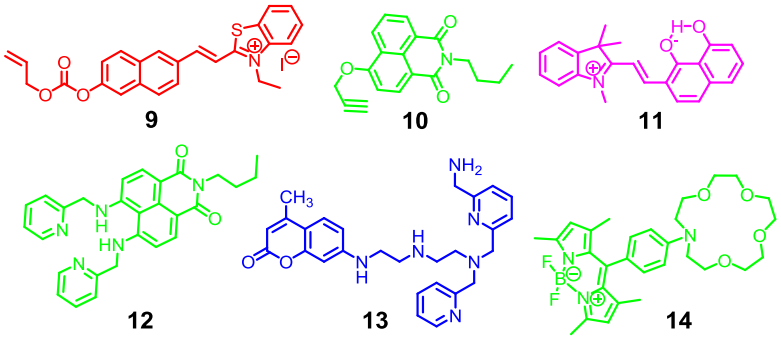

Figure 1.9. Molecular structures of ICT based probes **9** - **14**.

The 1,1-dicyanovinyl group has been used as a specific chemodosimetric probe for CN^-. CN^- being a strong nucleophile underwent a conjugate addition to the 1,1-dicyano-vinyl group to produce a stabilized anionic adduct. Using this strategy, Li and his co-workers designed a chemodosimetric reagent **15** (Figure 1.10) for detection of CN^- in CH_3CN solution by utilizing the ratiometric changes in electronic spectrum.[28] On reaction of CN^- with **15**, an adduct (15A) formation with consequential decrease in the extent of conjugation and the ICT process.

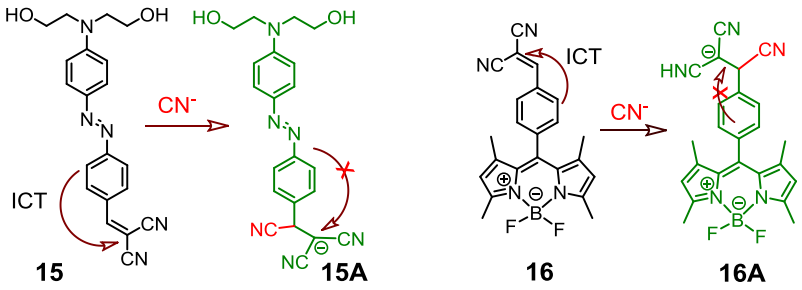

Figure 1.10. Addition of CN^- to Diazo-malononitrile **15** and BODIPY-malononitrile **16** conjugate leads to change in colour as well as fluorescence.

This was accounted for the observed shift in the absorption band maximum from 515 to 435 nm with a distinct isobestic point at 475 nm. Lowest detection limit reported for the reagent was 1.1 μM and this reagent could be used for developing a ‘‘dip-stick’’ colorimetric sensor for [CN^-] of ~ 3 ×10^{-5} mol/L.

Jang *et al.* designed a turn-*on* molecular probe **16** (Figure 1.10) for detection of CN^- in THF:H_2O medium (1:99, v/v).[29] Free receptor exhibited strong absorption bands at around 320 and 500 nm. Luminescence for this molecule was found to be completely quenched due to an efficient ICT process and a narrow energy gap among the frontier orbitals. On reaction with CN^-, disruption of π-conjugation between the phenyl and dicyano-vinyl groups was well anticipated and accounted for a less efficient ICT process, which in turn would enhanced HOMO-LUMO energy gap. This presumably interrupted the non-radiative deactivation of the excited state and a luminescence *ON* response at 510 nm (for λ_{Ext} of 480 nm) was observed. In ^{1}H NMR spectrum, aromatic proton signals exhibited an up-field shift after addition of CN^-. Moreover, the signal for the olefinic proton at 7.8 ppm was found to disappear upon addition of CN^- (1 equiv.), while a new peak appeared at 4.4 ppm. These observations further corroborated the proposed addition reaction of CN^-. This reagent could also be used as an imaging reagent for the detection of cyanide (2 μM) in HeLa cells.

Analogous mode of detection based on dicyano-vinyl receptor for cyanide based on ICT mechanism was achieved by using probes **17**,[30] **18**,[31] **19**[32] and **20** (Figure 1.11).[33]

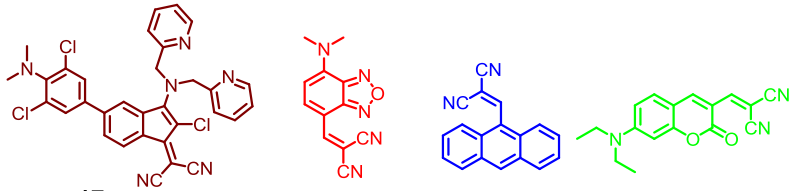

Figure 1.11. Molecular structures of **17** - **20**.

Kim *et al.* reported an indole conjugated coumarin skeleton **21** (Figure 1.12) for recognition of KCN in H_2O-CH_3CN solution (5: 95, v/v).[34] Compound **21** displayed two characteristic UV-Vis absorbance bands cantered at 398 and 609 nm. Among the tested anions, only CN^- induced a significant change in the absorption spectra: band at 398 nm was red-shifted to 409 nm and the band at 610 nm completely

disappeared with associated colour change in solution colour from blue to yellow. For the product formed on reaction with CN^-, a less efficient ICT process resulted with coumarin as the donor moiety and the positive charged indole group as an acceptor fragment. Such a proposition was also supported by detailed ^1H NMR studies. As anticipated, on reaction with CN^-, vinyl protons at $\delta = 8.1$ ppm (H_b) and $\delta = 7.9$ ppm (H_a) were found to be upfield shifted to $\delta = 6.9$ (H'_b) and $\delta = 6.7$ ppm (H'_a), respectively.

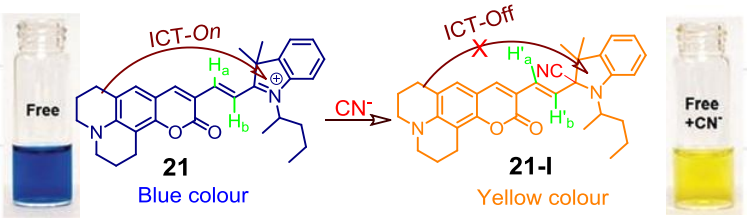

Figure 1.12. Reaction mechanism of cyanide with **21**.

Wu *et al.* reported a fluorescent probe **22** for fast and selective detection of cysteine (Cys) based on a response-assisted electrostatic attraction (Figure 1.13).[35] The probe reagent underwent a Michael addition reaction with the thiol group of Cys and this resulted modified colorimetric and fluorescent responses. Free ligand **22** was found to be non-fluorescent in PBS buffer solution ($\Phi = 0.001$, $\lambda_{Ext} = 450$ nm) due to an efficient ICT process involving diethylamino group as donor and electron-deficient pyridinium moiety as acceptor. Among the tested amino acids, only those with free thiol functionality (Cys, Hcy and GSH) showed *turn-on* fluorescence response and a blue shifted absorbance spectrum. This molecule showed preference for Cys among these three biothiols and the reactivity followed the order Cys > Hcy > GSH. Upon treatment of Cys, **21**-Cys adduct was formed and accounted for the new emission band at 500 nm with significant increase (140 fold) in its intensity. Adduct formation disfavoured the ICT process, which results in the observed optical spectral changes. The LOD for Cys was evaluated as low as 25 nM. To demonstrate the hypothesis, the cationic pyridinum derivative **22** and the neutral precursor **23** were investigated

under same experimental conditions. Reactivity of the cationic derivative **22** was much higher than the neutral precursor **23**.

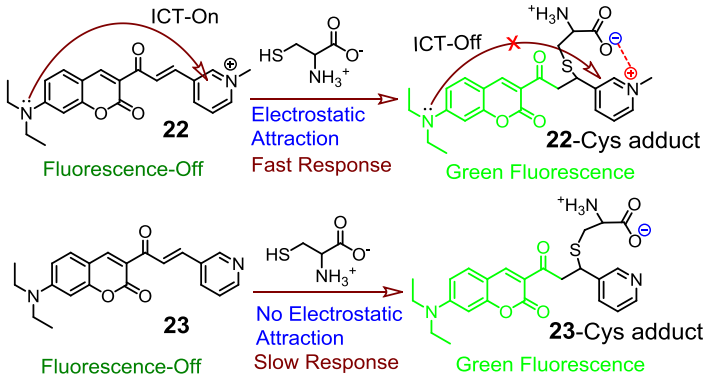

Figure 1.13. The design concept for molecular probe **22** and **23** for Cys detection.

The probe **22** was used as an imaging reagent for detection of free Cys residue within proteins as well as in live HeLa cells. Lin *et al.* designed a ratiometric fluorescent probe **24** for Cys and Hcy (Figure 1.14).[36] Probe **24** consists of a electron rich phenanthroimidazole moiety, which acted both as a fluorescent dye as well as electron donor, while the aldehyde group acted as a electron acceptor as well as a receptor for thiols. In presence of Cys or Hcy, absorption spectra for **24** (20 μM in HEPES buffer-DMF (1:3, v/v; pH 7.4); λ_{Max} ~ 375 nm) were found to be blue shifted by 46 nm and a decrease in the intensity of the ICT emission band at 519 nm was observed with concomitant growth of a new emission band at 394 nm.

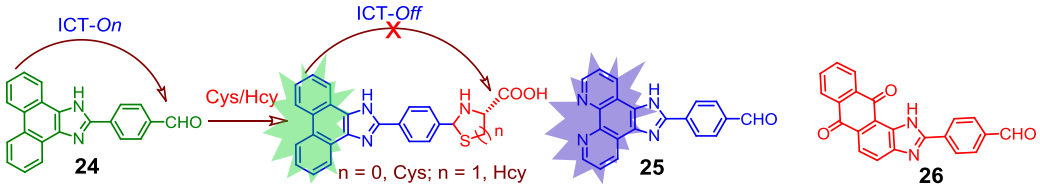

Figure 1.14. Reaction of Cys/Hcy with **24** with and molecular structures of **25** and **26**.

This was attributed to an effective interruption of ICT process. Further the binding mechanism was established by ^{1}HNMR and ESI-Ms studies. Analogous mode of detection for Cys/Hcy was achieved by Das *et.al* while using reagents **25** and **26** (Figure 1.14).[37]

1.2.4. C=N isomerization

The photo-isomerisation of a C=N double bond was originally inferred by Kuhn and Weitz to explain a reversible colour change resulting from irradiation of triphenylformazan.[38a] The first spectroscopic observation of the trans-cis photo-isomerisation of imines was reported by Fischer and Frei in 1957, through a significant change of the absorption spectrum.[38b] Energy barrier for this Cis→trans isomerisation is generally low (20-75 kJ/mol) for unhindered imine derivatives and is generally lower than the isomerisation process for azine derivatives.[38c] This is being used successfully as a signalling mechanism on specific binding to a targeted cationic analyte. Compounds with a facile C=N isomerization generally have short lived excited state due to a fast non-radiative deactivation of the photo excited states and accounts for a poor luminescence quantum yield value.[39] In contrast, fluorescence of probes having covalently bridged C=N structure increases dramatically due to the suppression of C=N isomerization in the excited states. Based on this hypothesis, Wang *et.al* designed a novel fluorescent chemosensor **27** (Figure 1.15) for recognition of Zn^{2+} ions over other cations.[40] The free ligand **27** showed a low Φ value due to a rapid isomerization of the C=N double bond in the excited state.

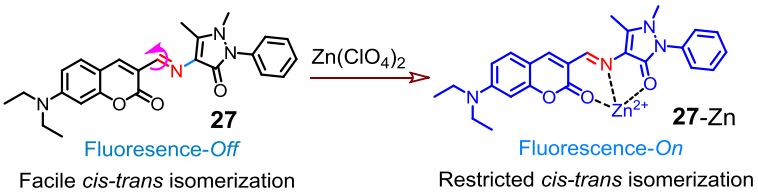

Figure 1.15. Proposed interaction mode between **27** and Zn^{2+}.

However, upon coordination to Zn(II) ion restricted the isomerization process and resulted a significant enhancement in fluorescence intensity (220 fold) with a red shift in the emission maxima from 500 to 522 nm. Similar strategy was also exploited by Das and his co-workers using azine and imine based receptor (**28**[41] and **29**[42]) for

efficient recognition of Hg^{2+} over other cations in mixed aqueous-organic medium (Figure 1.16). Both probes were non-emissive in solution form due to a rapid N=N or C=N isomerization. Coordination to Hg^{2+} ion had interrupted the isomerisation process in **28-**Hg and **29-Hg**, which resulted a significant enhancement in fluorescence intensity. Similar mechanism was also operation for probe **30** and was utilized for preferential binding to Hg^{2+} and Au^{+} (Figure 1.16).[43]

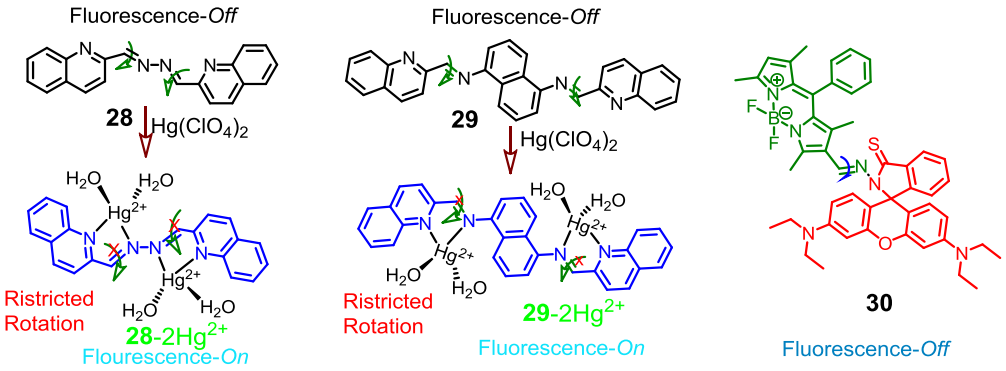

Figure 1.16. Mode of binding of Hg^{2+} with **28** and **29** and molecular structure of **30**.

1.2.5. Excited-state Intramolecular Proton Transfer (ESIPT)

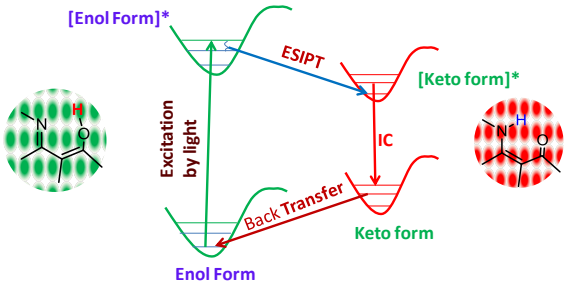

Figure 1.17. Excited-state intramolecular proton transfer (ESIPT) mechanism.

Organic fluorescent molecules having excited-state intramolecular proton transfer (ESIPT) properties have received significant attention due to their unique photophysical properties. A photoinduced proton transfer process through an intramolecular hydrogen bond (H-bond) is generally referred as an ESIPT process and this is generally a fast process happened within nano second time domain.[44] For following the ESIPT mechanism, a molecule should possesses intramolecular H-bond between proton donor (-OH, $-NH_2$) and proton acceptor (-C=O, -N=) groups in

close proximity to each other in a molecule. ESIPT active molecules typically exist exclusively in the enol form, which is better stabilized by strong intramolecular H-bond formation. Upon photo excitation, the redistribution of electronic charge causes an increase in the acidity of the proton donor and the basicity of the proton acceptor. This favors a fast proton transfer reaction along the excited-state potential energy surface via the intramolecular H-bond and eventually leads to a tautomeric transformation from the excited enol form to the excited keto form in sub-picoseconds time scale. ESIPT and the subsequent reverse proton transfer in the ground state helps in achieving a fully reversible reaction cycle (Figure 1.17). As anticipated, ESIPT process is influenced by solvent polarity.

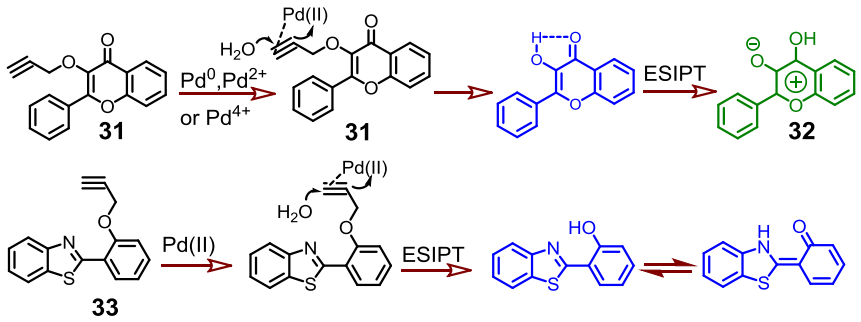

Figure 1.18. ESIPT mechanism of **31** and **33** with Pd species.

Bai *et al.* reported a new ratiometric probe **31** (Figure 1.18) for Pd-species based on ESIPT process in CH_3CN-HEPES buffer (1: 4, v/v) medium.[45] 3-(prop-2-ynyloxy) hydroxyl flavone was used as a fluorophore for this molecular probe. On binding to $PdCl_2$, emission intensity at 412 nm was found to decrease and it was attributed to the formation of adduct as an intermediate product (Figure 1.18). Presumably, the heavy atom effect of Pd-centre caused an effective luminescence quenching. After a delay of ~ 30 min, emission band intensity was found to increase, as the PET-induced fluorescence quenching influence was over along with the subsequent completion of depropargylation as well as deprotection of the hydroxyl group of **31**, which resulted in the formation of **32**. Final product **32** was ESIPT active and contributed to the luminescence enhancement after the initial delay of ~ 30 min.

However probe could not discriminate the Pd^{2+} from Pd^{0} and Pd^{4+} species. This reagent was not suitable for bio-imaging application owing to the slow response time and limited solubility in aqueous medium. Using similar strategy (Palladium promoted depropargylation) Manoj Kumar *et.al* derived a probe **33** (Figure 1.18) for detection of Pd(II) ions in mixed organic aqueous medium.[46] Despite its limited solubility and slow response time, authors had explored the possibility of using this reagent for intracellular imaging of palladium ions.

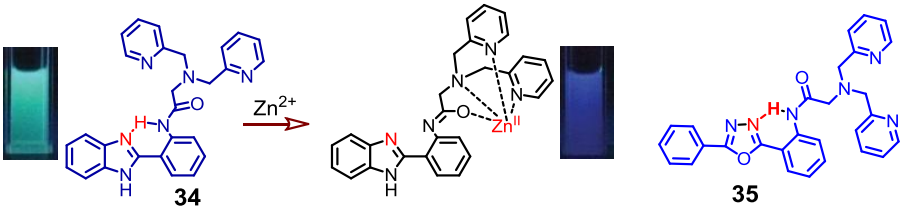

Figure 1.19. Proposed binding mode for Zn^{2+} to **34** and molecular structure of **35**.

Tang *et al.* designed a ratiometric probe **34** (Figure 1.19) for recognition of Zn^{2+} and Cd^{2+} ions over other cations based on ESIPT mechanism in CH_3CN-HEPES (2:8, v/v; pH 7.4) solution.[47] Upon gradual addition of Zn^{2+}, the emission intensities at 367 nm and 502 nm were found to bleach and a new emission band cantered at 424 nm appeared simultaneously.

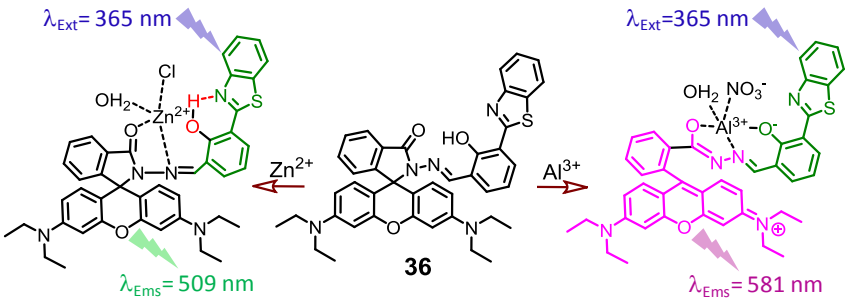

Figure1.20. Proposed binding mode of Zn^{2+} and Al^{3+} with **36**.

For Cd(II), new emission band appeared at 479 nm. The mode of binding for Zn^{2+} ions was explained by ^{1}H NMR studies. Same group reported another ratiometric probe **35** for efficient recognition of Zn^{2+} ions by utilizing an ESIPT process.[48] Probe molecule was also used for intracellular detection of Zn(II) ion.

Goswami *et al.* designed rhodamine-HBT-dyad (RHD) **36**, which selectively could detect two biologically important ions (Al^{3+} and Zn^{2+}) at two different wavelengths through different mechanisms (FRET and ESIPT).[49] Free ligand showed two emission bands centred at 398 nm and 556 nm following excitation at 365 nm. Shorter wavelength band at 398 nm was associated with 'enol' and the longer wavelength band at 556 nm peak was associated with the corresponding 'keto' form. On addition of Al^{3+} ions (3 mole equiv.), a gradual red shift ($\Delta\lambda = 25$ nm) for band maxima at 559 nm was observed. Simultaneously, the emission intensity at 398 nm was enhanced as the ESIPT process was interrupted due to an interaction of Al^{3+} with the probe molecule. Thus, the excitation energy was transferred from HBT to the xanthene form of rhodamine moiety, which was an essential condition for successful FRET. Interestingly upon addition of Zn^{2+} ions, ESIPT was suppressed and that resulted characteristic green fluorescence from the HBT fragment.

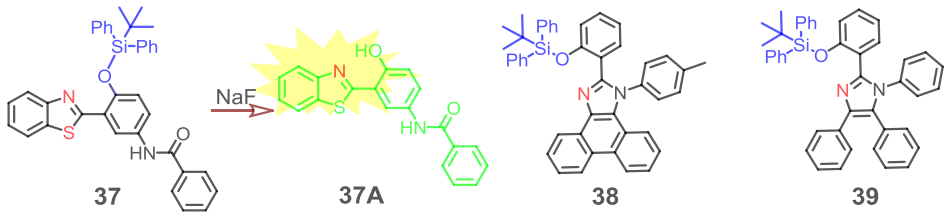

Figure 1.21. ESIPT mechanism of **37** with NaF and molecular structures of **38** and **39**.

Yang *et al.* reported a probe **37** (Figure 1.21) for recognition of F^- over other anions in aqueous medium.[50] Due to limited solubility of the probe, authors had used CTAB solution for their spectroscopic studies. Free ligand showed strong emission band at 418 nm (blue violet emission) under excitation at 350 nm.

F^- ion induced a selective cleavage of Si-O bonds in presence and this led to the formation of a desilylated product **37A**, which was appropriate for the ESIPT based emission response. A blue-violet emission band was found to decrease and simultaneously, a new emission band appeared with maximum at 560 nm. The LOD for F^- ion was 0.38 ppm, which was much lower than the limit set by W.H.O for safe

drinking water. The authors could develop a paper strip that was suitable for convenient and reliable detection of F^-. Similar methodology was adopted for designing receptors like **38** and **39** (Figure 1.21) for F^- ion detection.[51, 52]

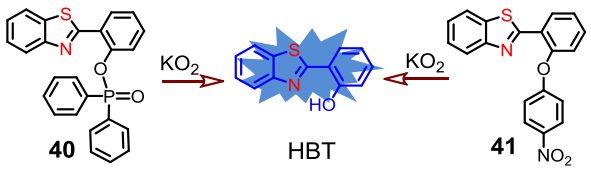

Figure 1.22. Reaction of KO_2 with **40** and **41** in aqueous medium.

Probes **40** and **41** showed enol-based emission at 375 nm due to the inhibition of the ESIPT process, which was induced by the presence of the HBT fragment as the protecting group (Figure 1.22).[53]

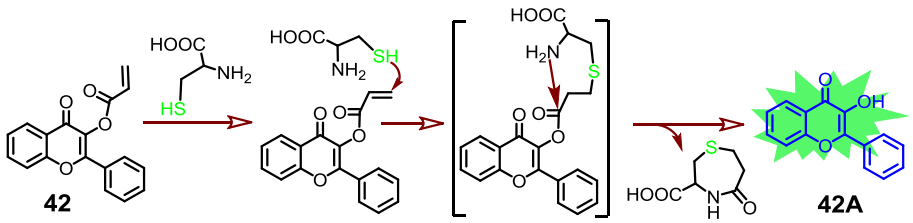

Figure 1.23. Reaction of Cys with the reagent **42**.

Reaction with reactive oxygen species (superoxide) caused a hydrolytic cleavage of the O-P (for **40**) or O-$C_{4\text{-nitro Phenyl}}$ (for **41**) bond in aqueous media and this led to the generation of free 2-(benzothiazol-2-yl)-phenol (HBT) with a strong emission band at 475 nm. Pang *et al.* reported flavone-based ratiometric probe **42** (Figure 1.23) for detection of Cys in living cells primarily based on the ESIPT-based response.[54] This receptor initially showed a weak blue fluorescence on excitation at 350 nm. Cys as a nuleophile induced an acrylate hydrolysis in **42**, which resulted in the elimination of 3-carboxy-5-oxoperhydro-1,4-thiazepine and generation of the coumarin derivative **42A**. This showed strong green luminescence, instead of a weak blue emission due to an ESIPT-based response. The LOD of probe **42** for Cys was estimated as 1 μM.

1.2.6. Forster Resonance Energy Transfer (FRET)

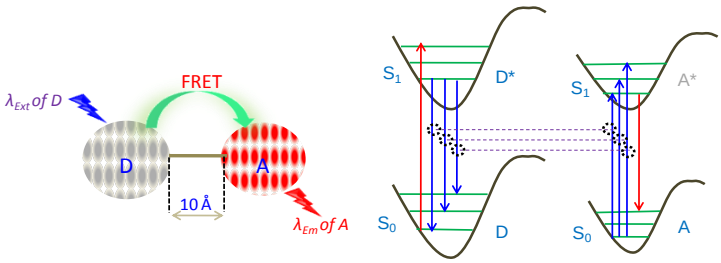

Figure 1.24. Schematic representation of FRET mechanism: Spectral overlap between donor emission and acceptor absorbance.

Förster (Fluorescence) resonance energy transfer (FRET) or resonance energy transfer (RET), is a photophysical mechanism in which energy transfer occurs from an excited state of a donor fluorophore (D) to the ground state of an acceptor fluorophore (A) via a non-radiative long range dipole–dipole coupling (Figure 1.24). It is a distance dependent phenomenon and is generally operation for D to A distance of 10 to 100 Å. The critical or Förster distance (R_0, distance for which energy transfer efficiency of 50% is achieved) is calculated using the following equitation 1.

$$R_0 = 0.211\ [(J(\lambda))\ Q\ (\eta^{-4})\ (\kappa^2)]^{1/6} \qquad 1$$

where η is the refractive index of the medium, κ^2 is the dipole orientation factor, Q is the fluorescence quantum yield of the donor in the absence of acceptor and J(λ) is the spectral overlap integral between the emission spectrum of the D and the absorption spectrum of the A. The energy transfer efficiency (E) from D-moiety to A-moiety can be measured by the following equitation 2.

$$\Phi_{ET} = 1-(F'_D/F_D) \qquad 2$$

where F_D and F'_D denote the donor fluorescence intensities of the donor moiety in absence and presence of an acceptor, respectively. The rate of energy transfer depends upon the extent of spectral overlap of the absorption spectrum of the A and emission spectrum of the D, the quantum yield of D and the distance between the D and A moieties.[55]

In the FRET based process, one can quantify the ratio of fluorescence intensities at two different wavelengths as this process is independent of the concentration of interacting donor and acceptor fluorophores. Luminescence studies, in principal, allow quantitative measurements as the linear relationship exists between luminescence intensity and the [fluorophore]; however, this may not be known with sufficient accuracy in the case of aggregation or photo bleaching. For FRET based processes, the ratio of the emission intensities at two different wavelengths varies as a function of the analyte concentration; while it remains independent of the concentration of interacting donor and acceptor fluorophores, path length, or spectral sensitivity of the instrument. Thus, FRET based process helped in eliminating experimental artefacts. For biological applications FRET-based probe molecules are more advantages than other ratiometric probes based on ICT and ESIPT mechanism.[56] Also, FRET based response generally helped in achieving larger Stokes's shift value.

a. FRET based probes for Hg^{2+} ion recognition

A number of colorimetric as well as fluorescent chemosensors have been reported for Hg^{2+} ions in the literature.[57] However, reports of FRET-based probes are relatively less in the contemporary literature. Das *et.al* reported a FRET-based reagent **43** for specific recognition of Hg(II) ion in CH_3CN/water medium (Figure 1.25).[58] Free probe showed a strong emission of the dansyl moiety at 490 nm on excitation at 340 nm. Specific binding of **43** to Hg^{2+} resulted a conversion from the cyclic lactam form to the corresponding xanthenes form, which showed a strong luminescence 555 nm with simultaneous quenching of the dansyl emission at 490 nm. The singlet-singlet energy transfer efficiency (Φ_{ET}) and the rate constant for the energy transfer process between dansyl to xanthenes form of the rhodamine moiety as acceptor was 83% and 2.84 x 10^8 s^{-1}, respectively. Association constant for the

formation of **43** was evaluated as $(5.0 \pm 0.2).10^4$ M^{-1}. The LOD for Hg^{2+} detection was found to be 0.1 ppm. This reagent was also utilised as a staining agent for detection of uptake of Hg^{2+} in *Pseudomonas putida*.

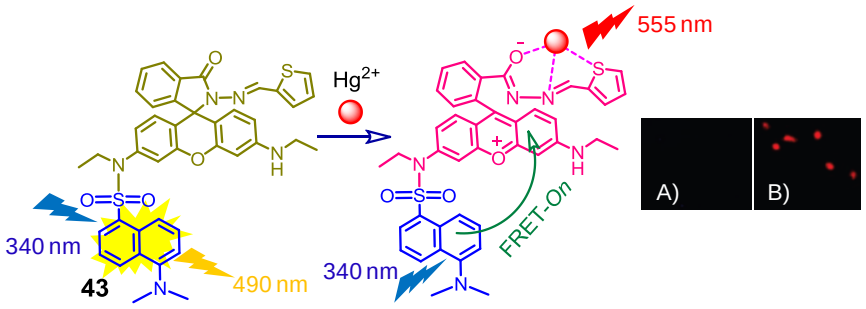

Figure 1.25. Hg^{2+}-induced FRET-on in **43**; Inset Use of receptor **43** for the recognition of Hg^{2+} within the *Pseudomonas putida* bacteria viewed under confocal laser microscopy; a) only **43** in the cells, b) **43** in presence of Hg^{2+} within the cells.

FRET process was also effectively used by Zeng and his co-workers.[59] They reported a water soluble ratiometric probe **44** (Figure 1.26) for detection of Hg^{2+} ion by using a self-assembly process. The rhodamine acceptor was covalently linked to outer hydrophilic rim of β-CD, while the donor fluorescein moiety functionalized with adamantyl moiety formed an inclusion complex with β-CD through non-bonding interactions between the hydrophobic interior of β-CD and the ademantyl fragment.

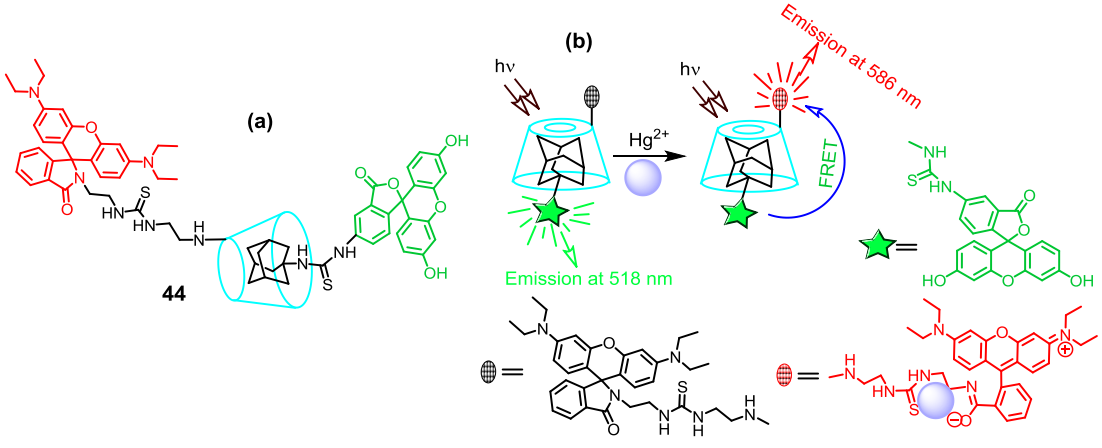

Figure 1.26. (a) Hg^{2+}-induced FRET in β-CD-based compound **44**; (b) Cartoon representation for the FRET-based ratiometric sensing system for Hg^{2+} with β-CD as vehicle.

The probe underwent a ring-opening process of rhodamine moiety upon addition of Hg^{2+} ions, which consequently resulted in the generation of acyclic xanthenes

moiety. A strong emission at 586 nm was observed on excitation of the donor fluorophore at 495 nm (with λ_{Ems} = 518 nm) due to an efficient FRET process. A lower detection limit of the 10 nM was reported.

A calix[4]arene derivative **45** functionalized with pyrene as donor and rhodamine as acceptor moiety was reported by Kim *et al.* FRET (Figure 1.27).[60] Upon excitation at 343 nm, free ligand showed strong excimer emission of the pyrene moiety at 460 nm and weak monomer emissions at 375 and 395 nm.

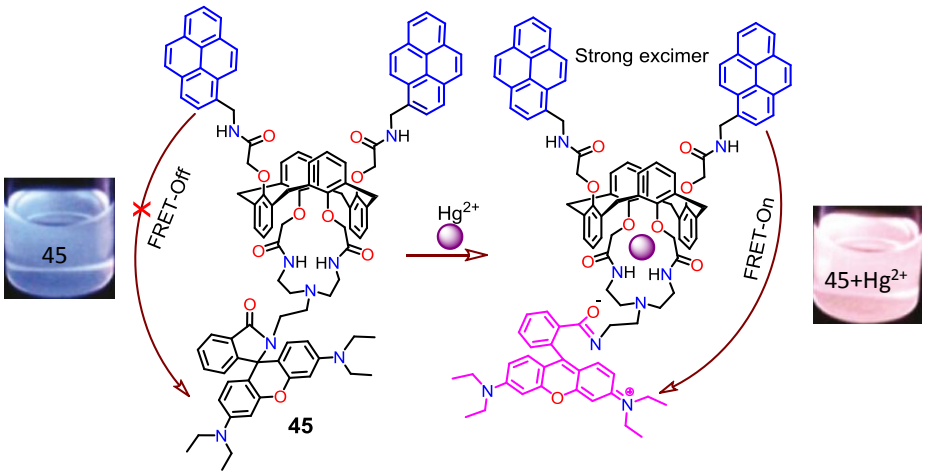

Figure 1.27. Structure of the molecular probe **45** and Hg^{2+} induced FRET response.

This reagent showed a FRET-based response on selective binding to Hg^{2+} ion with an enhancement in emission at 576 nm (for λ_{Ext} of 343 nm) for the conversion to the xanthene form of rhodamine fragment with simultaneous quenching of the pyrene-based excimer emission at 460 nm. The LOD reported for the Hg^{2+} ion detection was 5 μM.Wu *et al.* designed a FRET- based probe **46** (Figure 1.28) for recognition of Hg^{2+} ion in aqueous medium. A rhodamine derivative, in its spirolactam form, was covalently linked to the silica surface modified with the Cd-Te QDs/silica core. In absence of Hg^{2+}, the nanosurface did not show any optical (electronic and fluorescence) responses in the visible region of the spectrum. Upon specific binding to Hg^{2+}, FRET process was operational and a strong luminescence, having maxima at 590 nm (λ_{Ext}^{Donor}: 410 nm) and a strong pinkish red colouration was observed as

an output signal. These optical responses could be utilized for probing the Hg^{2+} concentration. Lower detection limit reported for this organic-inorganic hybrid reagent was 260 nM.[61] The close proximity of the QDs as a donor and rhodamine as a acceptor favoured the FRET process to be operational (Figure 1.28).

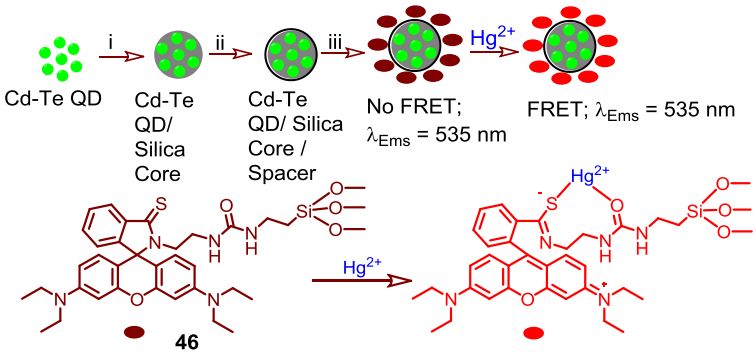

Figure 1.28. QDs/silica composite nano particles based approach for the detection of Hg^{2+} ions.

Das *et al.* reported a naphthalimide–rhodamine conjugate **47** (Figure 1.29), which was found to bind preferentially to Hg^{2+} or Cr^{3+} in the presence of other competing metal ions.[62] On binding to Hg^{2+} or Cr^{3+}, FRET process was operational and a strong luminescence, having maximum at 583 was observed with concomitant decrease in luminescence for the donor naphthalimide moiety at 533 nm (for λ_{Ext}^{Donor} of 455 nm) was observed.

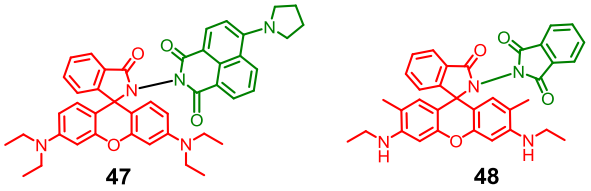

Figure 1.29. Molecular structures of **47** and **48**.

The binding stoichiometry of 1:1 was ascertained for Hg^{2+} or Cr^{3+} by Jobs plot, BH plot and results of the ESI-Ms studies. In order to explain the binding mechanism and photophysical properties of **47** upon binding to specific metal ions model compound **48** (Figure 1.29) was synthesized. The binding constant values for two metal ions were evaluated (K_{Hg}^{2+} = (1.09 ± 0.02)10^5 M^{-1} and K_{Cr}^{3+} = (1.12 ± 0.01)10^5 at 25°C) from the systematic emission titration experiments. Further, confocal laser

microscopic experiments confirmed that probe **47** was cell membrane permeable and could be used as an imaging reagent for the cellular uptake of these ions.

Analogous mode of detection for Hg^{2+} was achieved by using several probes (**49** to **53**), in which rhodamin+e moiety was used as an acceptor fragment in a FRET-based luminescence response (Figure 1.30).[63,64,65,66,67]

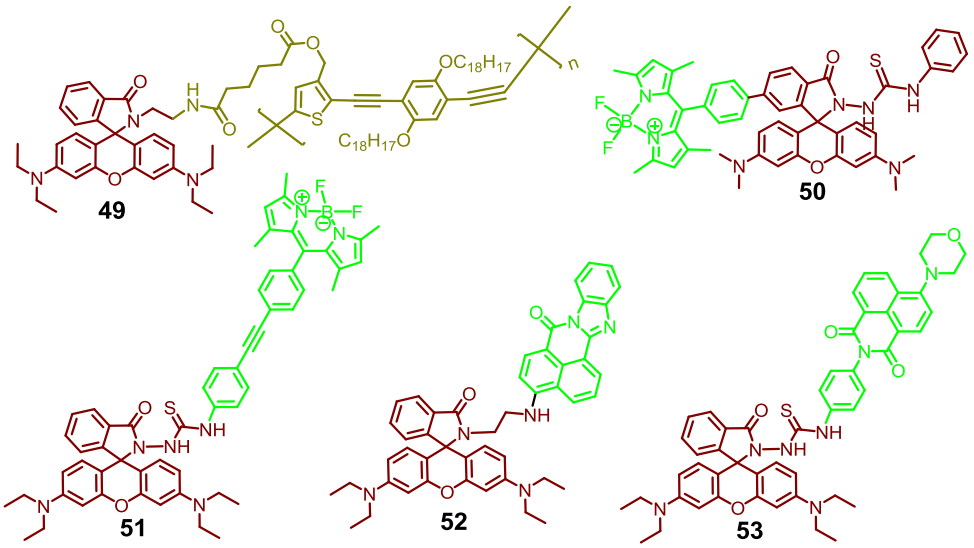

Figure 1.30. Molecular structures of **49** to **53**.

Akkaya *et al.* designed a probe **54** (Figure 1.31), functionalized with two different BODIPY units having a thio-crown ether moiety as the receptor fragment for Hg^{2+} or Fe^{2+} ions in THF solution. In this conjugate, one of the two BODIPY moieties acted as a donor and the other one acted as an acceptor.[68]

Jiang *et al.* reported a probe **55** (Figure 1.31) for recognition of Hg^{2+} ion using a covalently bound 8-hydroxyquinoline benzoate moiety to a bodipy as well as to a porphyrin moiety.[69] Probe **55** exhibited FRET response, in which BODIPY unit acted as a donor fragment and porphyrin unit acted as a acceptor fragment. It was proposed that the flexible 8-hrdoxy quinoline moiety not only facilitated the energy transfer process but also acted as a receptor for preferential binding to Hg^{2+} or Fe^{2+} cations. Chang *et al.* designed fluorescent probes **56**[70] and **57**,[71] having covalently coupled coumarin and fluorescein moieties for the ratiometric detection of Hg^{2+} ions

in aqueous media. Upon excitation at 340 nm (λ_{Max}^{Abs} for donor coumarin moiety), both probes **56** and **57** showed strong emission at ~ 525 nm (λ_{Max}^{Ems} for fluorescein moiety) and weak emission at ~ 440 nm (λ_{Max}^{Ems} for coumarin moiety), as an efficient FRET process was operational. Upon binding to Hg^{2+} ion, significant quenching in emission intensity at 525 nm was observed due to the Hg^{2+}-induced suppression of FRET between coumarin and the fluorescein moiety.

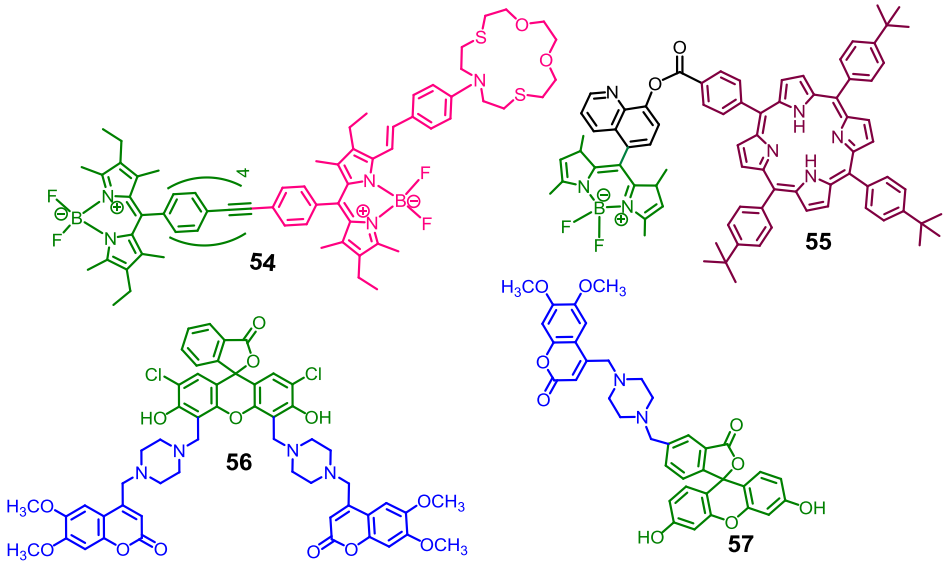

Figure 1.31. Molecular structures of **54** to **57**.

b. FRET based probes for Cu^{2+} ions

Cu(II) is an essential metal ion for human physiology, as it plays important roles in many essential biological processes and chemical systems. However, abnormal level of intracellular Cu^{2+} is also responsible for several physiological disorders.[72] Thus, it is pertinent to develop efficient fluorescence ON reagent for Cu(II) detection in aqueous medium with physiological relevance. However, Cu(II) being a paramagnetic d^9 system, is known to quench the fluorophore emission effectively and it is always challenging to develop a reagent that is specific for Cu(II) and capable of exhibiting fluorescence ON response on binding to Cu(II). Duan *et al.* developed FRET-based probes **58**[73] and **59**[73] consisting of a coumarin moiety as

donor and a rhodamine moiety as an acceptor for the selective detection of metal ions (Figure 1.32).

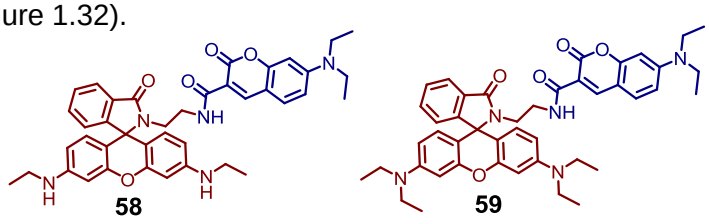

Figure 1.32. Molecular structures of **58** to **59**.

Among the tested cations, these probes were highly selective towards Cu^{2+} ion. On binding to Cu^{2+}, probe molecule **58** (20 μM) showed a strong emission at 550 nm on excitation of the donor coumarin moiety at 415 nm in acetonitrile solution. For **59**, the emission intensity for coumarin fragment at 460 nm was found to decrease with simultaneous increase in emission intensity at 585 nm on excitation at 415 nm. As the spectral overlap between the acceptor and donor of **58** was more significant than that for **59**, higher FRET efficiency of (90%) was achieved for 58 than that for **59** (33%) at identical condition.

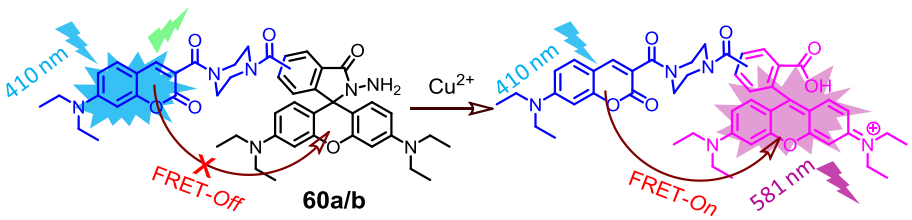

Figure 1.33. Cu^{2+} -induced FRET in **60**.

Lin *et al.* reported molecular probes **60a** and **60b** (Figure 1.33) for ratiometric detection of Cu^{2+} ions in living cells and they could successfully exploited the FRET process.[74] Using coumarin as a donor rhodamine as the acceptor moieties, which were linked through a rigid piperazine linker. The rigid linker restricted the static fluorescence quenching and provided an appropriate distance between the donor coumarin and acceptor rhodamine for achieveing high energy transfer efficiency. On binding to Cu^{2+}, similar quenching of coumarin based emission was evident with simultaneous enhancement in the acceptor moiety (xanthenes form of the

rhodamine) at around 581 nm. The LOD of probe **60a** for Cu^{2+} ion was found to be 0.008 μM.

More recently, Guo *et al.* reported FRET based probe **61** (Figure 1.34) for ratiometric detection of Cu^{2+} ions in CH_3CN: aq. tris buffer (9: 1, v/v) medium (pH =7.4).[75]

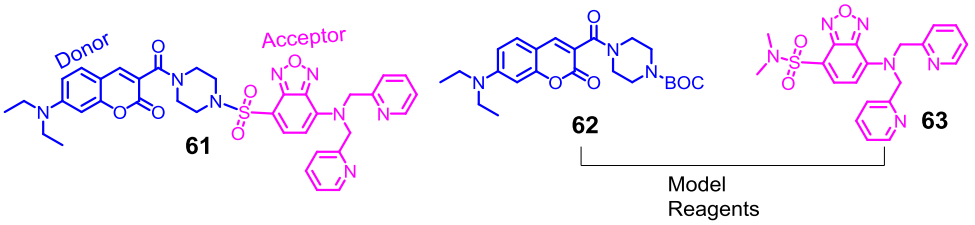

Figure 1.34. (a) Molecular structures of **61**, **62** and **63**.

The probe molecule **61** consisted of coumarin & 4-amino-7-sulfamoyl benzoxadiazole (ASBD) as donor & acceptor pair, respectively, for a FRET process. Free probe **61** showed two absorptions bands at 405 (coumarin based) and 455 nm (ASBD based). Upon excitation at 405 nm probe **61** showed a weak emission band centred at 460 nm (coumarin emission) and a strong emission band centred at 555 nm (ASBD emission).This was confirmed by spectral results of model reagents **62** and **63**. On binding of Cu^{2+} (0 to 25 mole equiv.) to **61**, a distinct decrease in the emission intensity for ASBD and a subsequent enhancement in emission intensity at 460 nm was evident along with an isoemissive point of 480 nm.

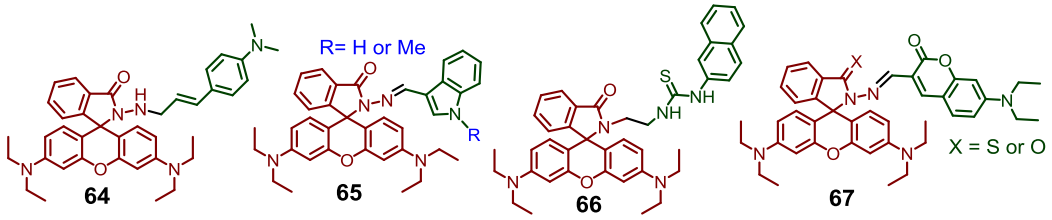

Figure 1.35. Molecular structures for **64** to **67**.

The LOD of (3σ/slope) of this probe was determined as 3 μM, which, a value lower than the lowest value (20 μM) set by the W.H.O for safe drinking water. The probe was successfully applied for the intracellular detection of Cu(II) ions in MCF-7 cells. Analogous mode of detection and FRET based responses for Cu^{2+} ion detection

were utilized while designing probe molecules like **64**[76],**65**[77],**66**[78] and **67**[79] (Figure 1.35).

1.2.7. Through bond energy transfer (TBET)

Unlike FRET, energy transfer can occurs through bonds via a Dexter mechanism, in which energy transfer from donor (D) fluorophore to an acceptor (A) fluorophore happens predominantly via twisted π-electron systems or bonds For such a process, spectral overlap between the D and A is not required.[80a] In case of TBET-cassettes, the donor fluorophore (D) is to be linked directly with the acceptor fluorophore (A) by an electronically conjugated bond. This prevents the donor and acceptor fragments from becoming planar, which helps to delineate the possibility of π-orbital overlap between them.[80b] TBET provides a large wavelength difference between the two emission peaks with improved imaging resolution by choosing suitable dye pairs and higher energy transfer efficiency than that of the classical FRET system.

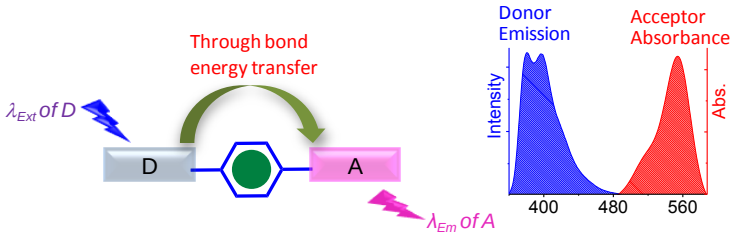

Figure 1.36. Schematic representation of through bond energy transfer: Spectral overlap between donor emission and acceptor absorbance.

a. TBET based probes For Hg^{2+} ions

Manoj Kumar and his co-workers reported a TBET based probe **68** (Figure 1.37) for specific recognition and detection of Hg^{2+} ions in mixed solvent medium.[81] Design of the probe **68**, involved covalent linking of naphthalimide as a donor and rhodamine as an acceptor through a phenyl group as the spacer. Free probe showed two prominent absorption bands at 320 and 363 nm for the naphthalimide moiety, whereas emission spectra showed weak emission at 472 nm for the naphthalimide moiety ($\lambda_{Ext}^{Naphthalimide}$ of 360nm).

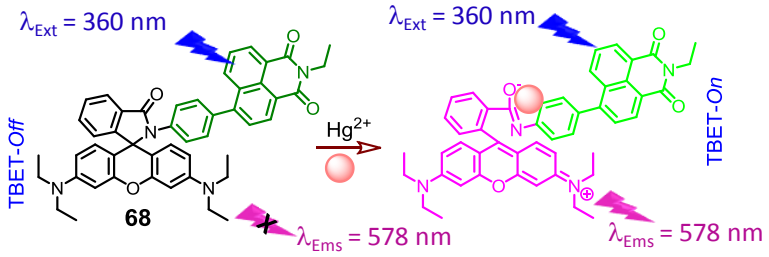

Figure 1.37. Hg^{2+} -induced TBET based response of the receptor **68**.

Upon addition of Hg^{2+}, to the THF-H_2O (9.5: 0.5, v/v) solution of **68**, a new absorption band appeared at 565 nm along with a visually detectable change in solution colour from colourless to pink. Simultaneously, a strong emission band for acyclic xanthenes form of rhodamine appeared at 578 nm for $\lambda_{Ext}^{Naphthalimide}$ of 360nm. The LOD of probe **68** for Hg^{2+} ion was found to be 2 μM. Stoichiometries for the binding mode (1:1) and binding constant (7.1 x10^4 M^{-1}) were reported based on various spectral studies. The authors utilised **68** as a potential fluorescence imaging agent for the detection of Hg^{2+} in live prostate cancer (PC3) cells.

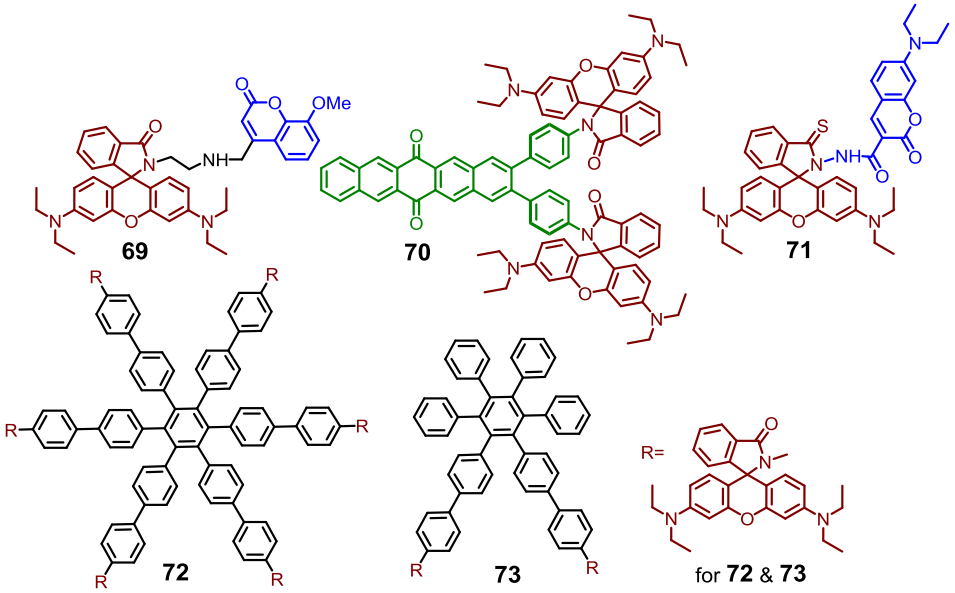

Figure 1.38. Molecular structures of **69** to **73**.

Das and his co-workers reported an unique example of interrupted PET coupled TBET phenomenon using a coumarin-rhodamine conjugate **69** (Figure 1.38) for selective recognition of Hg^{2+} in MeOH-aq. HEPES buffer (1: 1, v/v; pH 7.2).[82]

Free probe showed an absorption spectral band at 320 nm and weak luminescence at 405 nm in absence of Hg^{2+} ion. Binding of Hg^{2+} to the probe **69** results initiated a TBET based luminescence from the acceptor rhodamine moiety at 585 nm following excitation at the donor coumarin moiety at 402 nm. Ligand design allowed an interrupted PET based luminescence response from the coumarin moiety on binding to Hg(II) ion and this initiated the TBET process further. Two appropriate model reagents were synthesized for unambiguous assignment of the spectral responses of **69** upon binding to Hg^{2+} ions under identical experimental conditions. The LOD of probe **69** for Hg^{2+} ion was found to be 2 ppb. Binding stoichiometry (1:1) and binding constant (7.3 ($\pm$ 0.06) x10^4 M^{-1}) were also reported. Analogous design strategy was utilized for developing other sensors for Hg^{2+} like **70**,[83] **71**,[84] **72**[85] and **73**[85] (Figure 1.38).

b. TBET based probes For Cu^{2+} ions

Recently, Fan and Peng *et al.* developed a TBET-based fluorescent probe **74** for the detection of Cu^{2+} ion over other cations in mixed solvent medium.[86] The reported probe molecule was a conjugate of two fluorophores, naphthalimide & rhodamine, having acylhydrazide functionality as the metal ion receptor (Figure 1.39). On excitation at 420 nm ($\lambda_{Ext}^{Naphthalimide}$), free probe **74** showed a naphthalimide-based emission at 535 nm. On binding to Cu^{2+} ion, TBET process was initiated and a rhodamine based emission at 577 nm was achieved with TBET efficiency of ~ 81% and a detection limit of 38 μM.

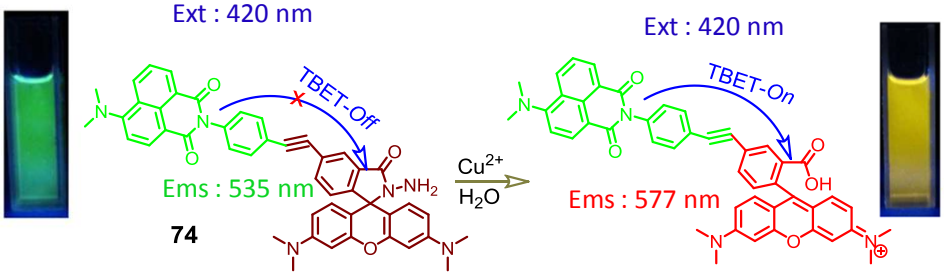

Figure 1.39. Cu^{2+}-induced TBET process for receptor **74**.

Very recently Tan *et al.* reported TBET-based two-photon fluorescent probe **75** (Figure 1.40) for ratiometric detection of Cu^{2+} ions in living cells and tissues.[87] Free ligand **75** showed only one naphthalene-based absorption band at 395 nm. However, on binding of Cu^{2+} (0−50 mole equiv.) a new absorption band appeared at 525 nm, which belonged to the xanthenes form of rhodamine B. On excitation at 395 nm, a strong emission at 525 was observed for an efficient TBET process. Simultaneously, a distinct bleaching of the emission band at 475 nm for the naphthalene core was also observed (Figure 1.40). The energy transfer efficiency was calculated as 93.7% with a detection limit of 0.3 μM. Authors have investigated two-photon active absorption cross-section of the probe, using the following formula: $\delta = \delta_r(S_s\Phi_r\phi_r c_r)/(S_r\Phi_s\phi_s c_s)$ (δ =115 GM), where the subscripts s and r denote the sample and reference molecule, respectively.

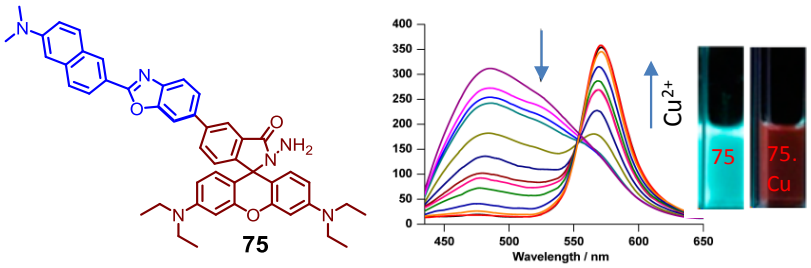

Figure 1.40. Molecular structure of **75** and one-photon-excited fluorescent changes of **75** (5 μM) varying concentrations of Cu^{2+} from 0 to 50 equiv) in Tris- HCl/EtOH (9:1, v/v, 10 mM), pH = 7.4. λ_{Ext} = 420 nm. The inset picture shows fluorescence before and after the addition of Cu^{2+} [Figure partially adopted from ref. 75].

Free ligand **75** showed two-photon emission at 475 nm upon excitation at 780 nm. On binding to Cu^{2+}, on laser excitation at 780 nm, the donor's fluorescence peak at 475 nm was found to be complete bleached and a new strong fluorescent peak appeared at 575 nm.

c. TBET based probe for Pd^{2+} ions

Zhang *et al.* reported TBET-based two-photon fluorescent probe **76** for ratiometric detection of Pd^{2+} ions (Figure 1.41).[88] Probe **76** comprised of two-photon fluorophore as an energy donor, which was linked to an anthracene appended rhodamine B in its

spirolactam form. In the absence of Pd^{2+} ions, free ligand **76** showed one absorption peak at 395 nm for the anthracene moiety. However, in presence of Pd^{2+} ion (40 μM), a new absorption band appeared at 550 nm, which belonged to the acceptor (rhodamine B moiety) with associated colour change from light yellow to red. In presence of Pd^{2+} ion, excitation at 415 nm revealed a dramatic increase in fluorescence intensity at 595 nm and an obvious decrease in fluorescence intensity at 495 nm.

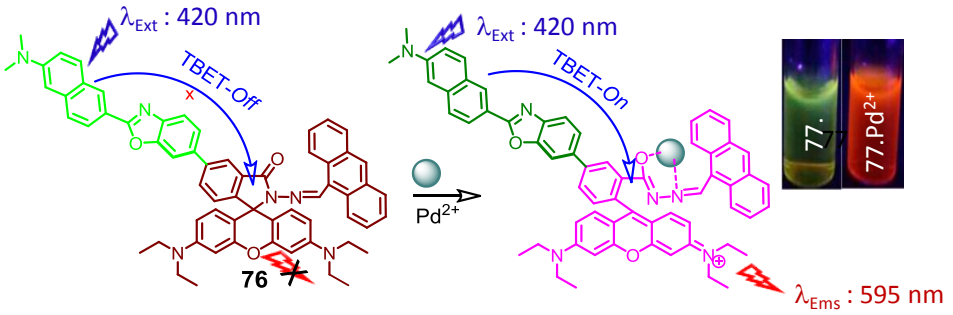

Figure 1.41. Pd^{2+} -induced TBET in **77**and the inset picture shows fluorescence before and after the addition of Pd^{2+} under excitation by UV light.

Such a fluorescence response was utilized for detection of Pd^{2+} with LOD of 23 μM. The energy transfer efficiency was evaluated as 90%. The authors could successfully use this probe for fluorescence imaging of Pd^{2+} ions in live cells and tissue. Tissue slices, under two-photon excitation (λ_{Ext} = 780 nm), showed significant tissue-imaging depths (90−270 μm) with superior resolution for imaging.

1.3. References

1. J. S. Kim and D. T. Quang, *Chem. Rev*., 2007, **107**, 3780.
2. M. H. Lee, J. S. Kim and J. L. Sessler, *Chem.Soc.Rev*., DOI: 10.1039/C4CS00280F.
3. G. T, Spence and P. D. Beer, *Acc. Chem. Res*. 2013, **46**, 571.
4. X. Lou, D. Ou, Q. Li and Z. Li, *Chem. Commun*., 2012, **48**, 8462.
5. (a) X. Wang, C. Drew, S. H. Lee, K. J. Senecal, J. Kumar and L. A. Samuelson, *Nano Lett.,* 2002, **2**, 1273; (b) R. Metivier, I. Leray and B. Valeur, *Chem. Eur. J.,* 2004, **10**, 4480; (c) A. P. de Silva, H. Q. N. Gunaratne, T. Gunnlaugsson, A. J. M. Huxley, C. P. McCoy, J. T. E. Rademacher, and Rice, *Chem. ReV.* 1997, **97***,* 1515.
6. (a) E. Palomares, R. Vilar and J. R. Durrant, *Chem. Commun.,* 2004, 362; (b) J. Liu and Y. Lu, *J. Am. Chem. Soc.* 2004, **126**, 12298; (c) J. M. Nam, C. S. Thaxton and C. A. Mirkin, *Science.,* 2003, **301**, 1884.
7. T. M. Rygowski and W. R. Fawcett, *J. Am. Chem. Soc*., 1975, **97**, 2143.
8. S. Mangani and M. Ferraroni, Supramolecular Chemistry of Anions (Eds.: A. Bianchi, K. Bowman-James, E. Garcia-EspanÄ a), WILEYVCH, New York, 1997, 63.
9. R. Meyer, J. K. Ha and H. S. Gunthard, *Chem. Phys*. 1975, **9**, 393.
10. L. Pu, *Chem. Rev*., 2004, 104, 1687.
11. J. B. Lambert and K. M. Taba, *J. Org. Chem.*, 1980, **45**, 452.
12. J. Wu, W. Liu, J. Ge, H. Zhang and P. Wang, *Chem. Soc. Rev*., 2011, **40**, 3483.
13. (a) A. J. Bryan, A. P. de Silva, S. A. de Silva, R. A. D. D. Rupasinghe and K. R. A. S. Sandanayake, *Biosensors.,* 1989, **4**, 169; (b) A. P. de Silva, T. S. Moody and G. D. Wright, *Analyst*., 2009, **134**, 2385-2393.
14. A. P. de Silva and S. A. de Silva, *J. Chem. Soc. Chem. Commun.,* 1986, 1709.
15. S. Ast, T. Schwarze, H. Muller, A. Sukhanov, S. Michaelis, J. Wegener, O. S. Wolfbeis, T. Kçrzdçrfer, A. Durkop and H.-J. Holdt, *Chem. Eur. J*., 2013, **19**, 14911.
16. N. I. Georgiev, S. M.Dimov, A. M. Asiri, K. A. Alamry, A. Y.Obaid and V. B. Bojinov, *J. Luminescence*., 2014, **149**, 325-332.
17. P. Kaur, N. Kaur, M. Kaur, V. Dhuna, J. Singh and K. Singh, *RSC Adv.*, 2014, **4**, 16104.
18. Y.-S. Guan, L.-Y. Niu, Y.-Z. Chen, Li-Z. Wu, C.-H. Tung and Q.-Z. Yang, *RSC Adv.*, 2014, **4**, 8360-8364.
19. J. Kim and Y. Kim, *Analyst*., 2014, **139**, 2986.
20. J. H. Lee, A. R. Jeong, I.-S. Shin, H.-J. Kim and J.-I. Hong, *Org. Lett.,* 2010, **12**, 764.
21. R. Bergonzi, L. Fabbrizzi, M. Licchelli and C. Mangano, *Coord. Chem. Rev*., 1998, **170**, 31-46.
22. X. Chen, H. Li, L. Jin and B. Yin, *Tetrahedron Letters.,* 2014, **55**, 2537-2540.

23. B.Zhu, C. Gao, Y.Zhao, C. Liu, Y. Li, Q. Wei, Z. Ma, B.Du and X. Zhang, *Chem. Commun*., 2011, **47**, 8656-8658.

24. Z.-Q. Guo, W.-Q. Chen and X.-M. Duan, *Org. Lett.,* 2010, **12**, 2203-2205.

25. Z. Xu, Y. Xiao, X. Qian, J. Cui and D.Cui, *Org. Lett.,* 2005, **7** , 889-892.

26. M. Taki, M. Desaki, A. Ojida, S. Iyoshi, T. Hirayama, I. Hamachi and Y. Yamamoto, *J. Am. Chem. Soc.,* 2008, **130**, 12564-12565.

27. M. Kollmannsberger, K. Rurack, U. R. –Genger and J. Daub, *J. Phys. Chem. A.,* 1998, **102***,* 10211-10220.

28. X. Cheng, Y. Zhou, J. Qin and Z. Li, *ACS Appl. Mater. Interfaces.,* 2012*,* **4***,* 2133.

29. C.-H. Lee, H.-J. Yoon, J.-S. Shim and W.-D. Jang, *Chem. Eur. J.,* 2012, **18**, 4513.

30. T. Gomez, D. Moreno, B. D. GreÇu, A. C. Fernandez, T. Rodriguez, J. Rojo, J. V. Cuevas and T. Torroba, *Chem. Asian J*., 2013, **8**, 1271-1278.

31. Z. Liu, X. Wang, Z. Yang and W. He, *J. Org. Chem.*, 2011, **76**, 10286−10290.

32. M. Shahid and A. Misra, *Anal. Methods.*, 2013, **5**, 434.

33. X. Cheng, R. Tang, H. Jia, J. Feng, J. Qin and Z. Li, *ACS Appl. Mater. interfaces*, 2012, **4**, 4387.

34. H. J. Kim, K. C. Ko, J. H. Lee, J. Y. Lee and J. S. Kim, *Chem. Commun*., 2011, 47, 2886-2888.

35. X. Zhou, X. Jin, G. Sun, D. Li and X. Wu, *Chem. Commun*., 2012, **48**, 8793-8795.

36. W. Lin, L. Long, L. Yuan, Z. Cao, B.Chen, and W.Tan, *Org. Lett.,* 2008, **10**, 5577.

37. P. Das, A. K. Mandal, N. B. Chandar, M. Baidya, H. B. Bhatt, B. Ganguly, S. K. Ghosh and A. Das, *Chem. Eur. J*., 2012, **18**, 15382 -15393.

38. (a) R. Kuhn and H. M. Weitz, Chem. Ber., 1953, **86**, 1199; (b) E. Fischer and Y. Frei, *J. Chem. Phys*., 1957, **27**, 808; (c) Y. Luo, M. Utecht, J. Dokic, S. Korchak, H.-M. Vieth, R. Haag and P. Saalfrank, *Chem.Phys.Chem*, 2011, **12**, 2311.

39. J. Wu, W. Liu, J. Ge, H. Zhang and P. Wang*, Chem. Soc. Rev*., 2011, 40, 3483.

40. J.-S. Wu, W.-M. Liu, X.-Q. Zhuang, F. Wang, P.-F. Wang, S.-L. Tao, X.-H. Zhang, S.-K.Wu and S.-T.Lee, *Org. Lett*., 2007, **10**, 33-36.

41. M.Suresh, A. K. Mandal,.S. Saha, E. Suresh, A. Mandoli, R.D. Liddo, P. P. Parnigotto and A. Das, *Org. Lett*., 2010, **12**, 5406-5409.

42. A. K.Mandal, M. Suresh, P. Das, E. Suresh, M. Baidya, S. K. Ghosh and A. Das, *Org. Lett*., 2012, **14**, 2980-2983.

43. E. Karakus, M.U¨çu¨ncu¨ and M. Emrullahog˘lu, *Chem. Commun.,* 2014, **50**, 1119.

44. J. E. Kwon and S.Y. Park, *Adv. Mater*., 2011, **23**, 3615-3642.

45. B. L., H. Wang, T. Wang, Y. Bao, F. Du, J. Tian, Q. Li and Ruke Bai, *Chem. Commun*., 2012, **48**, 2867-2869.

46. M. Kumar, N, Kumar and V. Bhalla, *RSC Adv.*, 2013, **3**, 1097-1102.

47. L. Tang, M. Cai, P. Zhou, J. Zhao, K. Zhong, S. Hou and Y. Bian, *RSC Adv*., 2013, **3**, 16802–16809.

48. L. Tang, X.Dai, K. Zhong, D. Wu and X. Wen, *Sensors and Actuators B*., 2014, **203**, 557-564.

49. S. Goswami, A. Manna, S. Paul, A. K. Maity, P. Saha, C. K. Quahc and H.-K. Fun, *RSC Adv*., 2014, **4**, 34572.

50. R. Hu, J. Feng, D. Hu, S. Wang, S. Li, Y. Li and G. Yang, *Angew. Chem. Int. Ed*., 2010, **49**, 4915 -4918.

51. K. Dhanunjayarao, V. Mukundam and K. V. Subbaiah, *J. Mater. Chem. C*, 2014, **2**, 8599-8606.

52. X. Li, B. Hu, J. Li, P. Lu and Y. Wang, *Sensors and Actuators B*., 2014, **203**, 635.

53. D. P. Murale, H. Kim, W. S. Choi and D. G. Churchill, *Org. Lett*., 2013,**15**, 3947.

54. B. Liu, J. Wang, G. Zhang R. Bai and Y. Pang, *ACS Appl. Mater. Interfaces,* 2014, **6**, 4402−4407.

55. Z. Liu, W. He and Z. Guo, *Chem. Soc. Rev.,* 2013, **42**, 1568.

56. N. Kumar, V. Bhalla and M. Kumar, *Analyst*., 2014, **139**, 543.

57. P. Mahato, S. Saha, P. Das, H. Agarwalla and A. Das, *RSC Adv*., 2014, **4**, 36140.

58. M. Suresh, S. Mishra, S. K. Mishra, E. Suresh, A. K. Mandal, A. Shrivastav and A. Das, *Org. Lett.,* 2009, **11**, 2740.

59. G. Fang, M. Xu, F. Zeng and S. Wu, *Langmuir.,* 2010, **26**, 17764-7771.

60. Y. H. Lee, M. H. Lee, J. F. Zhang and J. S. Kim, *J. Org. Chem.,* 2010, **75**, 715960.

61. B. Liu, F. Zeng, G. Wu and S. Wu, *Analyst*., 2012, **137**, 3717.

62. P. Mahato, S. Saha, E. Suresh, R. D. Liddo, P. P. Parnigotto, M. T. Conconi, M. K. Kesharwani, B. Ganguly and A. Das, *Inorg. Chem*., 2012, 51, 1769-1777.

63. M. Zhu, C. Zhou, Y. Zhao, Y. Li, H. Liu and Y. Li, *Macromol. Rapid Commun*., 2009, **30**, 1339.

64. H. Yu, Y. Xiao, H. Guo and X. Qian, *Chem. Eur. J*., 2011, **17**, 3179.

65. X. Zhang, Y. Xiao and X. Qian, *Angew. Chem. Int. Ed*., 2008, **47**, 8025.

66. V. Luxami, M. Verma, R. Rani, K. Paul and S. Kumar, *Org. Biomol. Chem*., 2012, **10**, 8076.

67. Y. Liu, X. Lv, Y. Zhao, M. Chen, J. Liu, P. Wang and W. Guo, *Dyes Pigm*., 2012, **92**, 909.

68. A. Coskun and E. U. Akkaya, *J. Am Chem Soc*., 2006, **128**, 14474.

69. Y. Chen, L. Wan, X. Yu, W. Li, Y. Bian and J. Jiang, *Org. Lett*., 2011, **13**, 5774.

70. H. J. Kim, J. E. Park, M. G. Choi, S. Ahn and S.-K. Chang, *Dyes Pigm*., 2010, **84**, 54.

71. D. H. Ryu, J. H. Noh and S.-K. Chang, *Bull. Korean Chem. Soc*., 2010, **31**, 246.

72. D. G. Barceloux, *J. Toxicol. Clin. Toxicol.*, 1999, 37, 217; (b) D. Strausak, J. F. Mercer, H. H. Dieter, W. Stremmel and G. Multhaup, *Brain Res. Bull.*, 2001, **55**, 175.

73. G. He, X. Zhang, C. He, X. Zhao and C. Duan, *Tetrahedron*, 2010, **66**, 9762.

74. L. Yuan, W. Lin, B. Chen and Y. Xie, *Org. Lett*., 2012, **14**, 432.

75. Y. Chen, C. Zhu, J. Cen, J. Li, W. He, Y. Jiao and Z. Guo, *Chem. Commun*., 2013, **49**, 7632.

76. M. Kumar, N. Kumar, V. Bhalla, P. R. Sharma and T. Kaur, *Org. Lett*., 2012, **14**, 406.

77. C. Kar, M. D. Adhikari,A. Ramesh and G. Das, *Inorg. Chem*., 2013, **52**, 743.

78. C. Kaewtong, J. Noiseephum, Y. Uppa, N. Morakot, N. Morakot, B. Wanno, T. Tuntulanic and B. Pulpoka, *New J. Chem*., 2010, **34**, 1104.

79. D. Maitya, D. Karthigeyan, T. K. Kundu and T. Govindaraju, *Sens. Actuators, B.*, 2013, **176**, 831.

80. (a)Through-bond Energy Transfer Cassettes, *Reviews*., A. Loudet, C. Thivierge, and K. Burgess, Texas A & M University, Box 30012, College Station, TX 77841, USA; (b) R. Bandichhor, A. D. Petrescu, A. Vespa, A. B. Kier, F. Schroeder and K. Burgess, *J. Am. Chem. Soc.,* 2006, **128**, 10688-10689.

81. M. Kumar, N. Kumar, V. Bhalla, P. R. Sharma and T. Kaur, *Org. Lett*., 2011, **13**, 1422.

82. S. Saha, P. Mahato, M. Baidya, S. K. Ghosh and A. Das, *Chem.Commun*., 2012, **48**, 9293.

83. V. Bhalla, Roopa, M. Kumar, P. R. Sharma and T. Kaur, *Inorg. Chem*., 2012, **51**, 2150.

84. Y.-J. Gong, X.-B. Zhang, C.-C. Zhang, A.-L. Luo, T. Fu, W. Tan, G.-L. Shen and R.-Q. Yu, *Anal. Chem*., 2012, **84**, 10777.

85. V. Bhalla, V. Vij, R. Tejpal, G. Singh and M. Kumar, *DaltonTrans*., 2013, **42**, 4456.

86. J. Fan, P. Zhan, M. Hu, W. Sun, J. Tang, J. Wang, S. Sun, F. Song and X. Peng, *Org. Lett*., 2013, **15**, 492.

87. L. Zhou, X. Zhang, Q. Wang, Y. Lv, G. Mao, A. Luo, Y. Wu, Y. Wu, J. Zhang and W. Tan, *J. Am. Chem. Soc*., 2014, **136**, 9838−9841.

88. L. Zhou, Q. Wang, X.-B. Zhang and W. Tan, *Anal. Chem*., 2015, **87**, 4503−4507.

CHAPTER 2

TURN-ON PHOSPHORESCENT PROBE FOR CYANIDE, A BIOLOGICALLY ACTIVE ANION AND ITS APPLICATION AS AN IMAGING REAGENT AS WELL AS FOR DEVELOPING AN ENZYMATIC ASSAY

Publication:
Chem. Commun., 2013, ***49***, 255-257

2.1. Introduction

Among the biologically active anions, cyanide (CN^-) ion is the most significant one. Although substances containing cyanide have been used as poisons for centuries, it was not until 1782 that this anion was first isolated by the Swedish chemist Scheel.[1] Acute toxicity of the cyanide ion towards mammalians results from its ability to interfere with the electron transport process and thus, inhibits the cellular respiration. Despite such a detrimental effect on human health, cyanide as a reagent has been used widely in various industries.[2] Accumulation of a higher level of cyanide could also happen through consumption of certain foods and plants.[3] Over 2000 plants species, including fruits and vegetables, contain cyanogenic glycosides that release cyanide on acid hydrolysis (e.g., as occurs when ingested). Among them, cassava (tapioca, manioc) and sorghum are staple foods for hundreds of millions in tropical countries.[3]

The LD_{50} (estimated dose that is lethal to 50% of the exposed population) of hydrogen cyanide has been reported to be 2500–5000 mg.min/m^3 and according to the World Health Organization, the maximum acceptable concentration level of cyanide in drinking water is 1.9 mM. The LD_{50} of hydrogen cyanide in humans is 1.0 mg/kg, and the estimated LD_{50} for cyanide solutions applied to the skin is approximately 100 mg/kg.[1] Cyanide poisoning is a form of histotoxic hypoxia because the cells of an organism are unable to use oxygen, primarily through the inhibition of cytochrome c oxidase of the mitochondrial respiratory chain.[4]

Cyanide affects practically all metalloenzymes, but its principal toxicity derives from the binding to the iron-centre in the heme groups in cytochrome oxidase (cytochrome a_3), inhibiting the functioning of the Electron Transport Chain.[4] Cyanide is a potent inhibitor of cellular respiration and works to inhibit ATP production by blocking the electron transport chain in mitochondria. Cyanide can act as an inhibitor

towards many metallo-enzymes and nonmetallo-enzymes and also act on visual, cardiac, endocrine and on the metabolic systems.[5]

Its acute toxicity accounts for a very low tolerance limit and according to the regulatory bodies (U.S. EPA) the maximum acceptable level of cyanide in drinking water and environmental primary standards is 0.2 and 0.5 ppm, respectively.[6] Prevalent industrial use as well as the increasing threat of its use with malicious intention has actually led to a recent surge of interest for the development of suitable reagents for selective detection of CN^- in water or in an aqueous environment. Further, the possibility of using such a reagent to develop an enzymatic assay for probing the in situ CN^- generation initiated by an important enzyme like hydroxynitrile lyase (HNL) is an added motivation and challenge.[7] Several methodologies have been adopted for designing an efficient CN^- sensor, which include recognition through hydrogen bonded adduct formation,[8] chemodosimetric detection,[9] utilizing the metal–cyanide ion coordination in a metal ion based receptor,[10] or by adopting the displacement reaction pathway.[11] However, many such systems suffer from the problem of achieving the specificity either due to the interference of other anions like fluoride, acetate, phosphate etc., and/or the desired sensitivity owing to the high solvation energy of CN^- in water (-339 kJ mol^{-1}).[12] The affinity of CN^- towards Cu^{2+}-ions and the consequential displacement methodology is utilized for its recognition in an aqueous environment.[13] Hydrated CN^-, which is present predominantly in aq. medium, also attributes to its poor reactivity as a neucleophile towards a chemodosimetric reagent. Thus, the issue of specific, efficient and instantaneous recognition of CN^- in aqueous medium is a challenging one and any new reagent that works under physiological conditions as well as address these issues has significance in the area of cyanide detection.

2.2. Experimental Section

2.2.1. Materials

2-phenylpyridine(ppy), $IrCl_3.3H_2O$, di-(2-picolyl) amine(dpa), Sodiumcyanoborohydrate, 4,4'-dimethyl-2,2' bipyridyl were obtained from Sigma Aldrich. Selenium dioxide was purchased from Acros India. Glacial acetic acid, $Cu(ClO_4)_2.H_2O$, NaCl, NaBr, KI, KNO_3, NaCN, $CH_3COONa.3H_2O$, $NaIO_4$, Na_2SO_3, NaF, $Na_2HPO_4.2H_2O$, $NaH_2PO_4.2H_2O$ were purchased from SD Fine Chemicals in India.

2.2.2. Analytical Methods

FTIR spectra were recorded as KBr pellets in a cell fitted with a KBr window, using a Perkin-Elmer Spectra GX 2000 spectrometer. ^1H NMR spectra were recorded on a Bruker 200 MHz FT NMR (Model: Avance-DPX 200) or on a Bruker 500 MHz FT NMR (Model: Avance-DPX 500) using CD_3CN and CD_3OD as the solvent and tetra methyl silane (TMS) as an internal standard. ESI-MS measurements were carried out on a Waters QTof-Micro instrument. Electronic spectra were recorded with a Shimadzu UV-3101 PC spectrophotometer; while fluorescence spectra were carried out using the Edinburg instruments Xe 900 spectro fluorometer.

2.2.3. Details of the Biological Study

HeLa cells were grown in Dulbecco's Modified Eagle Medium supplemented with 10% fetal bovine serum at 37°C were trypsinized, and $1x10^4$ cells were added in each well in a 24-well culture plate. After 48 h of growth, HeLa cells were then stained with a 5 μM solution of **1.Cu** dissolved in acetonitrile/aqueous HEPES buffer (99.6:0.4, v/v; pH 7.6) medium for 20 min at 37°C. The pre-treated live HeLa cells were further treated with different concentrations (0.2 ppm, 0.5 ppm, 1ppm) of NaCN in aqueous media for 5 min. Cells were viewed under a laser scanning confocal microscope (FV100, Olympus) in the red channel (590 $\pm$ 10 nm). Cytotoxicity of

1.Cu on HeLa cells was determined by conventional MTT assay. HeLa cells in their exponential growth phase were trypsinised and seeded in 96-well flat-bottom culture plates at a density of 3 x 10^3 cells per well in 100 µl DMEM complete medium. The cells were allowed to adhere and grow for 24 h at 37ºC in CO_2 incubator (New Brunswick Scientific, U.S.A.), and then the medium was replaced with 100 µl fresh in complete medium containing various concentrations of **1.Cu** (0 to 25 µM). The assay was performed in quadruplet for each concentration. Cells were then incubated for 12h, after which the culture medium was removed, and 100 µl of 1 mg/ml MTT reagent in PBS was added to each well. Thereafter, it was incubated for 4 h; during this period active mitochondria of viable cells reduce MTT to purple formazan. Unreduced MTT were then discarded and DMSO (100 µl) was added into each well to dissolve the formazan precipitate, which was then measured spectrophotometrically using a microplate reader at 570 nm. The cytotoxic effect of each treatment was expressed as percentage of cell viability relative to the untreated control cells. [MTT= (3-(4, 5-Dimethylthiazol-2-yl)-2, 5-diphenyltetrazolium bromide, a yellow tetrazole].

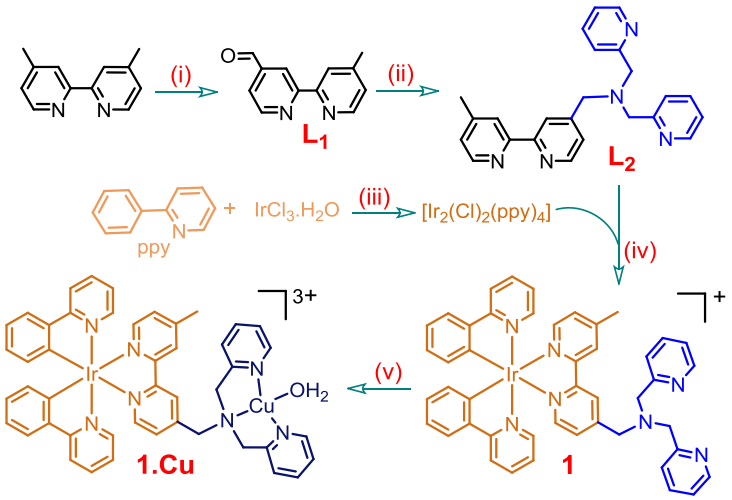

Conditions: (i) SeO_2, Dioxane; (ii) Di-(2-picolyl) amine, Glacial acetic acid (Catalytic amount); MeOH, Sodium cyano borohydrate (excess); (iii) 2-Methoxy ethanol, water; (iv) CH_2Cl_2/MeOH, NH_4PF_6; (v) $Cu(ClO_4)_2.H_2O$, MeOH/Water.

Scheme 1. Methodology that was adopted for synthesis of the L_1, L_2, $Ir_2(ppy)_4(Cl)_2$, **1** and **1.Cu**. **I.Cu** was used for CN^- ion detection by utilizing higher the affinity of CN^- towards Cu(II)-species.

2.3. Synthesis and Characterization

2.3.1. Synthesis of $[(ppy)_2Ir(\mu\text{-}Cl)]_2$[14]

A mixture of 2-methoxy ethanol and water (3:1, v/v) was added to round bottom flask containing $IrCl_3.H_2O$ (0.5 g, 1.58 mmol) and 2-phenylpyridine (0.612 g, 3.95 mmol). The mixture was refluxed for 36 h. After cooling to room temperature, yellow solid was precipitated and was filtered to give crude cyclo metalated Iridium(III) chloro-bridged dimer ($[(ppy)_2Ir(\mu\text{-}Cl)]_2$ and ppyH is 2-phenyl pyridine), which was further washed with cold methanol and water to isolate the desired compound (Yield: 0.6 g; 33%).

2.3.2. Synthesis of 4'-Methyl-2,2'-bipyridyline-4-Carbaldehyde (L_1)[15]

The compound 4,4'-dimethyl-2,2'-bipyridyl (1.8 g, 9.78 mmol) and SeO_2 (1.1 g, 9.9 mmol) were added to 1,4-dioxane (50 mL) and the mixture was heated at reflux under an inert atmosphere for 24 h. The solution was filtered while hot to remove precipitate Se, cooled to room temperature, and allowed to stand for 1 h. Filtrate removed a pale yellow precipitate of 4,4'-dimethyl-2,2'-bipyridine, redissolved in Ethyl acetate (300 mL). The Ethyl acetate solution was treated with aqueous Na_2CO_3 (0.1M, 20 mL) to remove residue carboxylic acids and extracted with 0.2 M aqueous solution of sodium bisulphite (3.0 x 30 mL). The combined aqueous extracts were adjusted to pH 9 by the addition of Na_2CO_3 and re extracted with dichloromethane (3 x 30 mL). The dichloromethane extracts were combined and evaporated to give 4'-Methyl-2,2'-bi pyridyline 4-Carbaldehyde (Yield: 0.6 g; 40%). ESI-MS (*m/z*): Calculated for $C_{12}H_{10}N_2O$: 198.08, Observed: 199.10 $[M + H]^+$; ^1H NMR [200 MHz, $CDCl_3$: δ (ppm)] 10.19 (1H, s, -CHO); 8.90 (1H, d, *J* = 4.8 Hz, H^5 (bpy)); 8.83 (1H, s, H^3 (bpy)); 8.58 (1H, d, *J* = 4.6 Hz, H^6 (bpy)); 8.28 (1H, s, $H^{3'}$ (bpy)); 7.72(1H, d, *J* = 4.2

Hz, $H^{6'}$ (bpy)); 7.20 (1H, d, *J* = 4.4 Hz, $H^{5'}$ (bpy)); 2.47 (3H, s, (bpy-CH_3)). IR (KBr), γ/cm^{-1}: 1702 (s, -CHO).

2.3.3. Synthesis of (L_2)[16]

L_1 (0.4 g, 2.08 mmol) and di-(2-picolyl) amine (0.413 g, 2.08 mmol) were dissolved in fresh methanol (35 mL). A catalytic amount of (two drops) glacial acetic acid was added to the solution, which was refluxed for half an hour. The reaction mixture was cooled by using an ice bath, and then $NaBH_3CN$ (0.262 g, 416 mmol) was slowly added to the solution. The ice bath was removed and the reaction mixture was stirred overnight at room temperature. Basic work-up using saturated aqueous sodium carbonate solution and subsequent extraction using dichloromethane was performed. The organic layer was recovered dried over anhydrous Na_2SO_4 and concentrated by vacuum. The crude product was subjected to neutral alumina gel chromatography. (Ethyl acetate: Hexane, 40:60) affording a sticky oil solid. (Yield (50%), 0.396 g). ESI-MS (*m/z*): Calculated for $C_{24}H_{23}N_5$ – 381, Observed – 382 $[M + H]^+$; ^1H NMR [200 MHz, MeOD: δ (ppm)]. 8.43 (1H, d, *J* = 5.2 Hz, H^6 (bpy)); 8.39 (1H, d, J = 5.2 Hz, $H^{6'}$ (bpy)); 8.32 (2H, d, *J* = 4.8 Hz, H^6 and $H^{6'}$ pyridyl rings of (dpa)); 8.19 (1H, s, H^3 (bpy)); 7.98 (1H, s, $H^{3'}$ (bpy)); 7.90 (1H, *J* = 5.0 Hz, H^5 (bpy)); 7.73-7.58 (4H, m, H^3 and $H^{3'}$, H^4 and $H^{4'}$ pyridyl rings of (dpa)); 7.40 (1H, d, *J* = 5.0Hz, H^5 (bpy)); 7.16 (2H, d, *J* = 5.4 Hz, H^2 and $H^{2'}$ pyridyl rings of (dpa)); 7.14 (1H, *J* = 5.6 Hz, $H^{5'}$ (bpy)); 3.74 (4H, s, -CH_2 (dpa)); 3.70 (2H, s,-CH_2 (bpy)); 2.34 (3H, s, -CH_3 (bpy)).

2.3.4. Synthesis of the $[Ir(ppy)_2L_2]PF_6$(1) complex[16]

A mixture of $[(ppy)_2Ir(\mu\text{-}Cl)]_2$ (0.3 g, 0.28 mmol) and L_2 (0.245 g, 0.644 mmol) in methanol-dichloromethane (60 mL; 1:3 (v/v)) were refluxed with exclusion of light for 4 h. After cooling to ambient temperature, removed the solvent (45 mL) by vacuum, to the solution was added a methanol solution (5 mL) of ammonium hexafluorophosphate (0.2 gm) with stirring for 30 minutes. The solution was filtered.

Solid was dissolved in dichloromethane and purified by column chromatography on alumina gel. The desired product was eluted with dichloromethane- methanol (9:1, v/v) (Yield: 0.24 g; 94%). ESI-MS (m/z): Calculated for $C_{46}H_{39}F_6IrN_7P$: 1027, Observed: 882 $[M- PF_6]^+$. ^1H NMR [500 MHz, CD_3CN: δ (ppm)]. 8.66(1H, s, H^3 (bpy)); 8.48 (2H, d, J = 4.0 Hz, H^6 and $H^{6'}$ pyridyl rings of (dpa)); 8.40 (1H, s, $H^{3'}$ (bpy)); 8.06 (2H, t, J = 7.5 Hz, H^4 and $H^{4'}$ pyridyl rings of (dpa)); 7.86-7.77 (6H, m, H^5 and $H^{5'}$ pyridyl rings of (dpa), H^6 and $H^{6'}$ pyridine of (ppy), H^3 and $H^{3'}$ phenyl of (ppy)); 7.65 (2H, t, J = 7.5 Hz, H^3 and $H^{3'}$ pyridine of (ppy)); 7.6 (1H, d, J = 5.5 Hz, H^6 (bpy)); 7.55-7.51 (3H, m, H^6 and $H^{6'}$ phenyl of (ppy), 1H, H^5 (bpy)); 7.47 (1H,d, J = 5.0 Hz, $H^{6'}$ (bpy)); 7.33 (1H, d, J = 5.0 Hz, $H^{5'}$ (bpy)); 7.17-7.15 (2H, m, H^5 and $H^{5'}$ pyridine of (ppy)); 7.05-6.8 (4H, m, H^4 and $H^{4'}$ pyridine of (ppy), H^4 and $H^{4'}$ phenyl of (ppy)); 6.9 (2H, t, J = 7.5 Hz, H^5 and $H^{5'}$ phenyl of (ppy)); 6.3 (2H, d, J = 7.5 Hz, H^3 and $H^{3'}$ pyridyl rings of (dpa)); 3.95(2H, s, $-CH_2$ (bpy)); 3.88(4H, s, $-CH_2$ (dpa)); 2.59(3H, s, $-CH_3$ (bpy)). IR(KBr): γ/cm^{-1}: 846(s, PF_6).

2.3.5. General Methodology Adopted for Spectroscopic Studies

1.0×10^{-4} M solution of the **1** and **1**.Cu in aq.-HEPES buffer-CH_3CN (98: 2; 99.6: 0.4(v/v); pH 7.6) medium was prepared and stored in dark. This solution was used for all spectroscopic studies after appropriate dilution. The effective ratio for the aq.-HEPES buffer-CH_3CN in the final solution was 99.6: 0.4. 1.0×10^{-3} M solutions of inorganic salt of respective anions were prepared in HEPES buffer (pH = 7.6). Solution of the compound **1** and **1.Cu** was further diluted for spectroscopic titrations, and the effective final concentration of the solution of compound **1** and **1.Cu** used for the fluorescence study was 2.0×10^{-5} M, while the final analyte concentration during emission spectral scanning was 8.0×10^{-4} M. For emission spectral titration effective $[CN^-]$ was varied between (0 to 6.0×10^{-4} M), while maintaining [**1.Cu**] as 2.0×10^{-5} M. For the evaluation of the formation constant of **1.Cu**, emission spectral titration

was carried out using effective [Cu^{2+}] between (0 to 1.4 x 10^{-4} M), while maintaining [1] unchanged as 2.0 x 10^{-5} M. All emission studies were performed in aq.- HEPES buffer-CH_3CN (99.6: 0.4(v/v); pH 7.6) medium using λ_{Ext} = 380 nm, λ_{Mon} = 583 nm and a slit width of 2.5 nm. The relative fluorescence quantum yields (ϕ_f) were estimated using equation 1 in aq.-HEPES buffer-CH_3CN (99.6:0.4 (v/v); pH 7.6) medium by using the integrated emission intensity of $Ru(bpy)_3^{2+}$ (ϕ_f = 0.042 in aqueous at RT) as a reference:[17]

$$\phi_f = \phi_f' \, (I_{sample}/I_{std})(A_{std}/A_{sample})(\eta^2_{sample}/\eta^2_{std}) \qquad \text{Eq. 1}$$

where, $\phi f'$ is the absolute quantum yield for the $Ru(bpy)_3^{2+}$, used as reference; I_{sample} and I_{std} are the integrated emission intensities; A_{sample} and A_{std} are the absorbance at the excitation wavelength, and η_{sample} and η_{std} are the respective refractive indices.

2.3.6. Evaluation of the Association Constant for the Formation of 1.Cu. from spectrophotometric titration

Receptor **1** was dissolved in CH_3CN: HEPES buffer (98: 2, v/v; pH 7.2) medium and was stored in dark conditions. This solution composition was maintained for all spectrophotometric titration studies. A stock solution of $Cu(ClO_4)_2$, having a concentration of 1.0 x 10^{-3} M, was prepared using the same solvent composition. A solution of receptor **1** having an effective concentration of 20 μM was used for spectroscopic titrations, while final concentrations for the CN^- ion were varied between 0.0 M and 8.0 x 10^{-4} M. The solution pH was adjusted to 7.2 using an aqueous HEPES buffer solution having an effective concentration of 10 mM. On the other hand, all solutions were stored at 25°C and all photophysical experiments were carried out at the same temperature unless mentioned otherwise.

2.4. Results and Discussions

Ligand **L_2** was synthesized following a two-step procedure. Initially **L_1** was synthesized by oxidation of 4,4'-dimethyl-2,2'-bipyridyl with selenium dioxide

following a reported procedure. **L_1** was then allowed to react with dpa in methanol to yield an intermediate that was further reduced in-situ by sodium cyanoborohydrate to yield crude **L_2**. After necessary purification using gravity chromatography, **L_2** was used for reaction with $[(ppy)_2Ir(\mu\text{-}Cl)]_2$ in appropriate mixed-solvent system for the synthesis of the complex **1**, which was isolated as hexa fluorophosphate salt and further purified by column chromatography. Complex **1** on further treatment with $Cu(ClO_4)_2$ in methanol resulted the desired product **1.Cu**. Synthetic methodologies that were adopted are shown in Scheme 1. The intermediate ligands (**L_1** and **L_2**), and corresponding complexes **1** and **1.Cu** were properly characterized using various analytical and spectroscopic techniques. Analytical data for these confirmed the desired purity for **L_2**, **1** and **1.Cu**. EPR spectrum for **1.Cu** was also recorded in CH_3CN at 77 K. The observed spectrum is typical of mononuclear Cu(II) complexes with tetrahedral distortion. The value of $g_{||} > g_{\perp} > 2.0$ is consistent with the fact that the contribution to the ground state arises from $dx^2\text{-}y^2$ orbital (Figure 2.1).

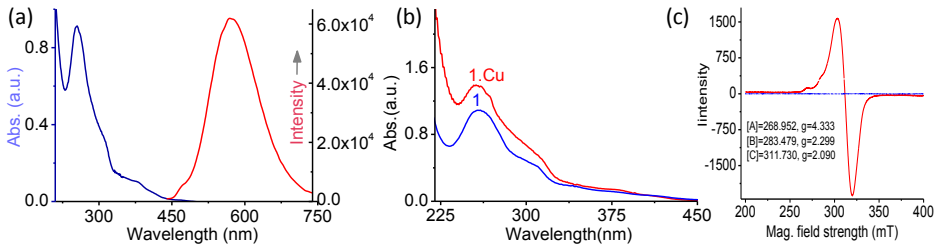

Figure 2.1. (a) Electronic and luminescence (λ_{Ext} = 380 nm) spectra of **1** (20 μM); (b) Absorbance spectra of **1** (20 μM) and **1.Cu** (20 μM) was performed in ACN: HEPES buffer (98:2, v/v; pH 7.6) medium; (b) Electronic spectra of **1** in absence and presence of $Cu(ClO_4)_2$; (c) EPR spectra of **1** in absence and presence of externally added tetra butyl amminium cyanide (TBACN) in acetonitrile at 77K.

The absorption and photoluminescence spectra of **1** were recorded in aqueous HEPES buffer (pH 7.6) medium at room temperature (Figure 2.1). As shown in the figure 2.1a, the intense absorption band maximum for **1** at 260 nm (ε = 5.2 x 10^4 $mol^{-1}L\ cm^{-1}$) was assigned to typical ppy and L_2 based ligand centered (LC) $\pi-\pi^*$ transitions. Whereas, a moderately less intense absorption shoulder appeared at 311

nm (ε = 1.5 x 10^4 $mol^{-1}L\ cm^{-1}$), which was accounted for the n–π*-based transitions of ppy and L_2. The relatively weak broad band at 380 nm (ε = 4.7 x 10^4 $mol^{-1}L\ cm^{-1}$) is attributed to a spin allowed $d\pi_{Ir(III)} \rightarrow \pi^*_{L2/ppy}$-based metal-to-ligand charge transfer (^{1}MLCT) transition; while even weaker longer wavelength tail could be accounted for a $d\pi_{Ir(III)} \rightarrow \pi^*_{L2/ppy}$-based ^{3}MLCT transition.[18] These assignments (as ^{1}LC, ^{1}MLCT and ^{3}MLCT states) should only be considered as a guideline, as mixing between different states could be significant due to the efficient spin-orbit coupling process. The electronic spectra for **1.Cu** was recorded in aq.HEPES buffer (pH =7.6) medium and no detectable change in the absorption spectral pattern for **1** was observed on formation of **1.Cu** (Figure 2.1b). Upon excitation at 380 nm, complex **1** exhibited a strong ^{3}MLCT emission band with λ_{max} 583 nm (Figure 2.1a). The relative emission quantum yield (Φ_1) for **1** in aq.HEPES buffer (pH 7.6) medium was found to be 0.0379 using $Ru(bpy)_3^{2+}$ as a standard. Photo luminescence spectra recorded for **1.Cu** (λ_{Ext} = 380 nm and λ_{Ems}^{Mon} = 583 nm) in aqueous HEPES buffer (pH =7.6) revealed that the phosphorescence for **1** was virtually quenched ($\Phi_{1.Cu}$ =0.00477) on formation of the binuclear complex **1.Cu** (Figure 2.2a). This is understandable as the paramagnetic Cu^{2+} ion with d^9 electronic configuration is known to quench the receptor luminescence rather efficiently.[19]

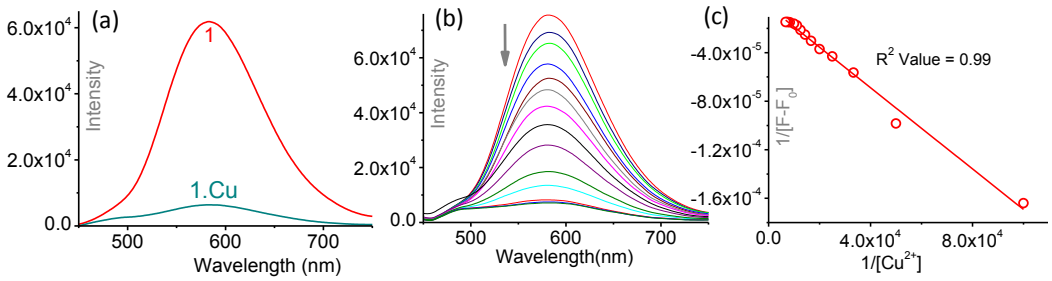

Figure 2.2. (a) Luminescence spectra of **1** (20 μM) and **1** in Presence of Cu^{2+} (2 equiv); (b) Emission spectral responses of **1** (20 μM) towards varying [$Cu(ClO_4)_2$] (0 to 1.4 x 10^{-4} M); (c) Benesi-Hildebrand plot of **1** (20 μM) for varying [Cu(II)] (0 to 1.4 x 10^{-4} M) Good linear fit confirms the 1: 1 binding stoichiometry. All studies were performed in aq.-HEPES buffer-CH_3CN (99.6: 0.4(v/v); pH 7.6) medium using λ_{Ext} =380 nm and λ_{Mon} = 583 nm. Slit width 2.5 nm. 10 mM HEPES buffer solution was use for maintaining solution pH.

As luminescence of **1** was found to be quenched on formation of **1.Cu**, systematic luminescence titration was carried out for **1** with varying [$Cu(ClO_4)_2$] in aq. HEPES buffer medium following excitation at 380 with λ_{Ems}^{Mon} of 583 nm. Formation of **1.Cu** was also associated with a change in solution luminescence colour from orange red to colourless. A binding stoichiometry of 1:1 was ascertained for the formation of **1.Cu** from the Job's plot and a binding constant of 8.8 x 10^3 M^{-1} was evaluated from the B-H plot (Figure 2.2b). In order to examine the luminescence response of the receptor **1.Cu** towards different anionic analytes, we had recorded the luminescence spectra of the receptor **1.Cu** (20 μM) in the absence and presence of 20 mole equiv. excess of various anionic analytes like F^-, Cl^-, Br^-, I^-, CN^-, $CH_3CO_2^-$, $H_2PO_4^-$, $P_4O_7^{4-}$, HSO_4^-, NO_3^-, NO_2^-, N_3^-, ClO_4^-, $PhCO_2^-$ and IO_4^- in aqueous HEPES buffer (pH 7.6) medium. Among all these anions, only CN^- showed a "*turn-on*" emission response λ_{Ems}^{Max} of 583 nm (for λ_{Ext} = 380 nm), which incidentally was identical with the emission spectra recorded for complex **1** under the identical experimental condition (Figure 2.3a).

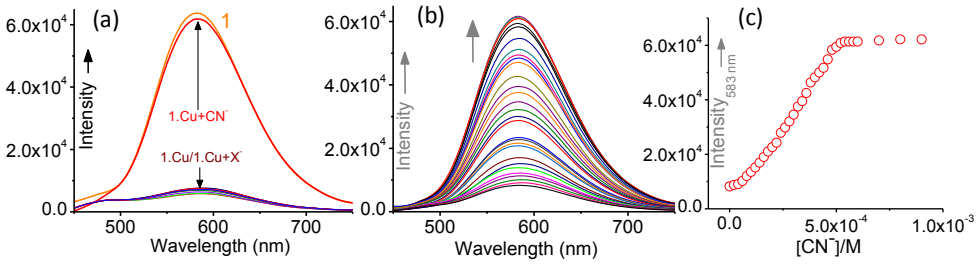

Figure 2.3. (a) Luminescence spectra (λ_{Ext} = 380 nm) of **1.Cu** in the absence and presence of various anions (X= F^-, Cl^-, Br^-, I^-, CN^-, $CH_3CO_2^-$, $H_2PO_4^-$, $P_2O_7^{4-}$, HSO_4^-, NO_3^-, NO_2^-, N_3^-, ClO_4^-, $PhCO_2^-$ and IO_4^-); (b) Luminescence response of **1.Cu** (20 μM) towards varying [CN^-]; (c) Luminescence titration profile of **1.Cu** (20 μM) towards varying [CN^-] (0 to 6.0 x 10^{-4} M); (c) with λ_{Ext} = 380 nm and λ_{Mon} = 583 nm. All studies were performed in aq. HEPES buffer–CH_3CN (99.6: 0.4, v/v; pH 7.6).

It is worth mentioning here that similar studies with **1.Cu** and CN^- did not show any detectable change in electronic spectra on or before addition of CN^-. It may be mentioned that luminescence changes on addition of CN^- were instantaneous.

Systematic luminescence titration with **1.Cu** (2.0 x 10^{-5} M) in aq. HEPES buffer (pH 7.6) medium with increasing [CN^-] (0 to 6 x 10^{-4} M) resulted in the regeneration of the original emission maxima at 583 nm (Figure 2.3.b). Thus an "*Off-On*" type luminescence response in absence and presence of excess of CN^- could be achieved.

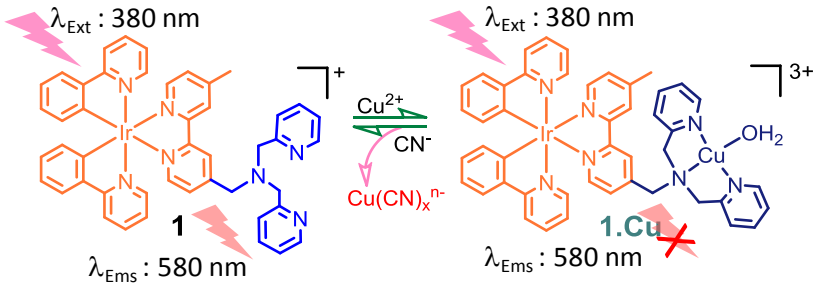

Scheme 2. Schematic representation of the luminescence response of **1.Cu** in presence of Cyanide ion in aq. buffer medium (pH = 7.6).

Restoration of the luminescence spectra of **1** on addition of CN^- to the solution of **1.Cu** (20 μM) in aq. HEPES buffer medium (pH 7.6) as well as strong affinity of CN^- towards Cu(II)-centre suggest the possible de-complexation and formation of $Cu(CN)_2$ with simultaneous regeneration of the complex **1** (Scheme 2). EPR spectral pattern for **1.Cu** was found to change in presence of TBACN, which also confirmed the generation of a distinctly different Cu(II)-species (Figures 2.1c & 2.4a). EPR spectra for instances revealed that the corresponding spectrum for Cu(II)-center in each solution was typical of an isolated Cu(II)-complex with tetrahedral distortion. The value of $g_{\|} > g_{\perp} > 2.0$ is consistent with the fact that the contribution to the ground state arises from $d_{x^2-y^2}$ orbital. The weaker in-plane covalent bonding after addition of CN^- indicates a more distortion. This was further confirmed from the ESI-Ms studies.

The *turn-on* luminescence response due to the regeneration of **1** from the reaction **1.Cu** with CN^- was also confirmed from the time resolved phosphorescence studies using Xenon flash Lamp (100 Watt) as an excitation source (Figure 2.5). The

emission decay traces was monitored at 583 nm following excitation at 380 nm for solution having **1**, **1.Cu** and **1.Cu** + CN^-.

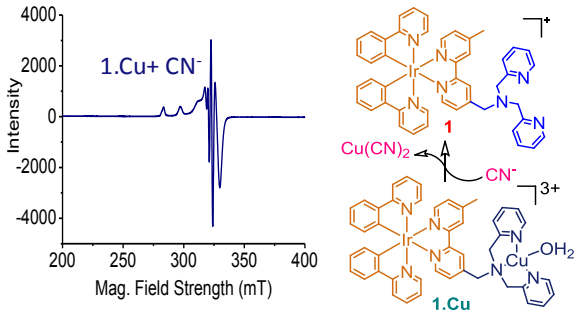

Figure 2.4. (a) EPR spectra for **1.Cu** in presence of externally added tetra butyl amminium cyanide (TBACN) in acetonitrile at 77K.

The phosphorescence decay trace at 583 nm for **1** could be best fitted to a bi-exponential function with (τ_1 = 3.71 μs (8.65 %), τ_2 = 60.23 μs (91.35%) with χ^2 = 1.20. In contrast, similar studies with **1.Cu** revealed much lower values for the multi-exponential time constants (τ_1 = 0.7 μs (44.58%), τ_2 = 6 μs (55.42%); χ^2 = 1.24)), which agreed well with its reduced phosphorescence quantum value due to the presence of the paramagnetic Cu^{2+} ion. The phosphorescence decay traces for **1.Cu**+CN^- (added as TBACN in 20 mole equivalent) showed a bi exponential decay trace with time constants (τ_1 = 3.59 μs (10.20%), τ_2 = 60.10 μs (89.80%); χ^2 = 1.44) that were almost similar to those observed for **1**. This further corroborates the proposed demetalation of the **1.Cu** by CN^- (Scheme 2).

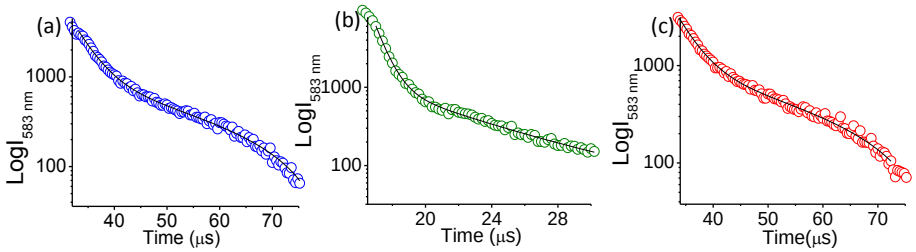

Figure 2.5. Time resolved phosphorescence decay profile for (a) **1**, (b) **1.Cu** and (c) **1.Cu** + CN^- at 583 nm. Time resolved study were performed in presence of TBACN in CH_3CN medium.

We also explored the possibility of using the **1.Cu** reagent for probing the *in-situ* cyanide (CN^- and/or HCN) generation following an enzymatic process initiated by

hydroxynitrile lyase (HNL), an enzyme that was known to catalyze the decomposition of mandelonitrile (mdnl) and liberate cyanide at pH 6.5. mdnl is the cyanide releasing source in presence of hydroxynitrilase and it occurs in the pits of some fruit. As shown in figure 2.6, HNL has an inherent emission band with maxima at 437 and 453 nm in aq. HEPES buffer medium of pH 6.5.

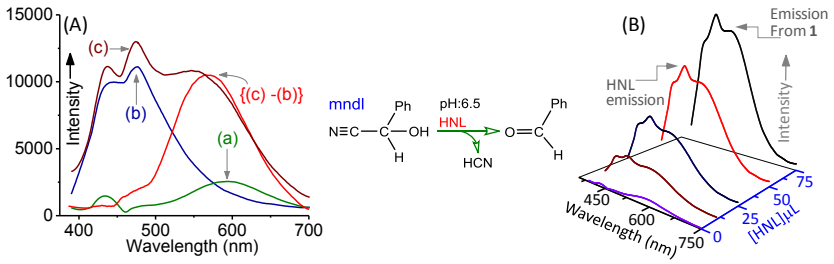

Figure 2.6. (A) Emission spectra of (a) **1.Cu**, (b) HNL, (c) **1.Cu** + mdnl + HNL; {(c)-(b)} was generated after subtracting the spectra of HNL (b) from the spectra of the solution having **1.Cu** + mdnl + HNL (c) to nullify the emission due to the HNL.[**1.Cu**] = 0.02 mM, [mdnl] = 0.8 mM, [HNL] = 10 μL; (B) Emission spectra of {**1.Cu** (0.02 mM) + mdnl (0.8 mM)} in the absence and presence of varying [HNL] (0-75 μL) in 10 mM HEPES buffer medium pH = 6.5 at λ_{Ext} = 380 nm.

Evaluation of Michaelis Constant of the enzymatic reaction for the generation of cyanide from the mandelonitrile using hydroxynitrile lyase (HNL)

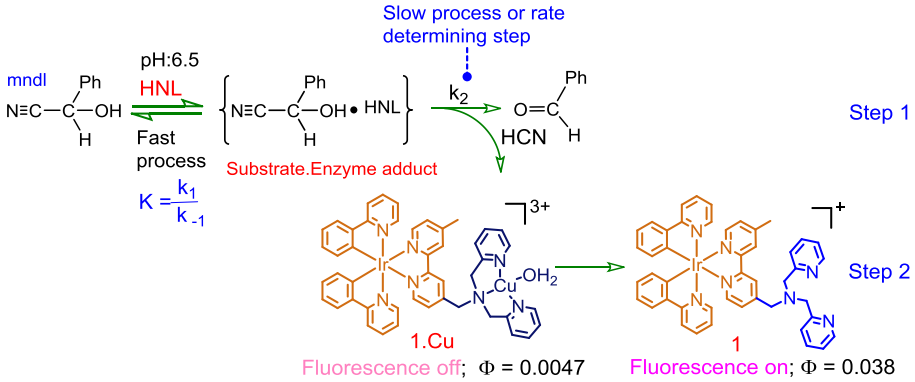

Scheme 3. Schematic presentation of the methodology that was adopted for developing an enzymatic assay.

A distinct increase in emission intensity at ~ 583 nm with an increase in [HNL] in the solution mixture containing mdnl and **1.Cu** suggests an increase in the formation of **1** and thus, the enhanced in situ generation of cyanide species with higher [HNL]. We could evaluate the Michaelis constant (K_m = 9.99 x 10^{-4} M) from the plot of v (v being

the overall rate constant) vs. 1/[mdnl] ([mdnl] = 0.5 mM to 50 mM), while [HNL](30 μL) and [**1.Cu**] (20 μM) were kept unchanged. A moderately low value of K_m implies that the enzyme has a moderately high affinity for the substrate mdnl.

Liberated cyanide could de-metalate **1.Cu** to generate **1** with subsequent enhancement in emission at ~ 583 nm, i.e., the switch on emission response. Please note that relative quantum yield for **1.Cu** was much lower than that for **1** (Scheme 3). Studies reveal that the displacement of Cu(II) from **1.Cu** for the generation of **1** and $Cu(CN)_x^{2-X}$ is an instantaneous process and thus the reaction rate is fast. In step 1, generation of HCN at pH 6.5 is the slow step or rate determining step. As mentioned in the above scheme decomposition of the {**mndl.HNL**} adducts into corresponding acetaldehyde and HCN in Step-1 is the rate determining step with overall rate constant of k.

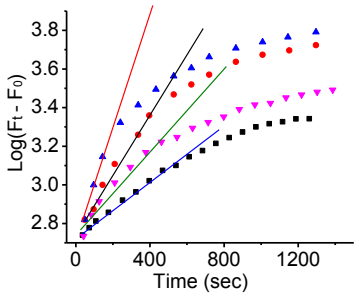

Figure 2.7. HNL assay using **1.Cu** (20 μM), [mdnl] = 1.5 x 10^{-4} M to 5 x 10^{-4} M with λ_{mon} = 586 in 10 mM HEPES buffer medium pH = 6.5 at λ_{Ext} = 380 nm.

For the above reaction shown in step 1, the rate of the reaction (v) is as follows:

$$v = k_2[\text{mndl.HNL}] = \frac{k_2[\text{HNL}]_0[\text{mndl}]}{K_m + [\text{mndl}]}$$

where $K_m = (k_{-1} + k_2) / k_1$

$$\frac{1}{v} = \frac{K_m}{k_2[\text{HNL}]_0[\text{mndl}]} + \frac{1}{1/k_2[\text{HNL}]_0}$$

Overall rate constant (v) for a certain [mndl] with [HNL] = 30 μL, [**1.Cu**] = 20 μM and pH = 6.5 (10 mM HEPES buffer-CH_3CN (99.6: 0.4) solution) was evaluated from the plot of Log [F_t-F_0] v_s time (in sec), where F_t is the luminescence intensity for **1** at 583

nm (λ_{Ext} = 380 nm) at time t and F_0 is the initial luminescence intensity of **1.Cu** at 570 nm.

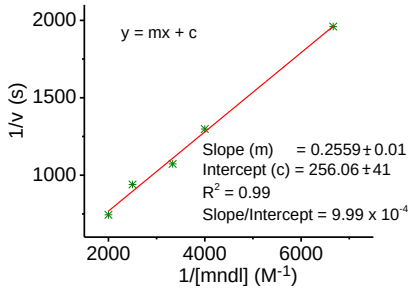

Figure 2.8. 1/v v_s. 1/[mndl] plot, while [HNL] = 30 μL, [**1.Cu**] = 20 μM; pH was maintained at 6.5 with 10 mM HEPES buffer-CH_3CN (99.6: 0.4) solution having temperature of 22°C.

Kinetics of the individual reaction was studied for initial 60% of the total reaction (based on the change in luminescence intensity at 570 nm). A reasonably linear plot was obtained for v vs. [mndl] for [mndl] varying from 1.5 x 10^{-4} M to 5 x 10^{-4} M. Beyond the concentration of 5.0 x 10^{-4} M, a deviation from linearity was observed due to the saturation effect and thus, were not considered for the 1/v vs. 1/[mndl] for the evaluation of K_m. Thus, a plot of 1/v v_s. 1/[mndl] would give intercept of $1/k_2[HNL]_0$ and slope of $K_m/k_2[HNL]_0$. Thus, {slope/intercept} would result K_m (9.99 x 10^{-4}).

2.5. Cell Imaging Study

The switch *ON* luminescence response on regeneration of the reagent **1** from **1.Cu** on interaction with CN^- offered us the possibility for checking the feasibility of using the reagent (**1.Cu**) as an imaging reagent for the detection of the cellular uptake of CN^- in pre-exposed live HeLa cells (Cervical cancer cell). Suitable amphipathicity and insignificant cytotoxicity of **1.Cu** further reinforced such an opportunity. To examine this, live HeLa cells (pre-exposed to an aq. HEPES buffer solution of 5.0 μM **1.Cu**) were treated with various concentrations of NaCN (0.2 to 1.0 ppm) in aq. HEPES buffer solution (pH 7.6) and were visualized under the laser scanning confocal microscope (FV1000, Olympus). Images (Figure 2.9) clearly revealed a

distinct increase in intracellular emission intensity with an increase in the [CN^-] in the aq. Buffer solution to which live cells were exposed.

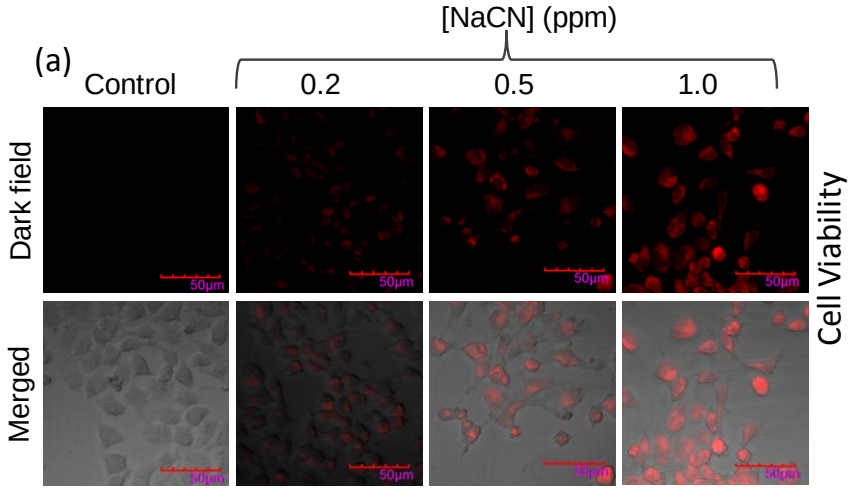

Figure 2.9. (a) Confocal micrographs HeLa cells in the presence **1.Cu** (5 μM). The phophorescence images were acquired after 2 mins of traetment of NaCN (0.2, 0.5, 1 ppm) on HeLa cells. Bottom pannels show an overlay of the image with a confocal phase contrast image. Time Correlated single photon counting Experiment.

Higher [CN^-] accounted for the more effective regeneration of the luminescent Ir(III)-complex (**1**) from non-luminescent binuclear complex **1.Cu**, which accounted for the enhanced intercellular emission. No significant change of the cell morphology or floating appearance of the cells was observed.

Thus, studies presented in this chapter, reveal that the reagent **1.Cu** is capable of detecting CN^- either in a pure aqueous environment at a concentration lower than the safe limit of environmental primary standards or in live HeLa cells pre-exposed to aqueous solution with [CN^-] of 0.2 ppm, the permissible limit set by the world regulatory body for safe drinking water. Initial studies clearly reveal that **1.Cu** could be used to develop a phosphorescence turn-on assay for studying the enzymatic activity of HNL on a cyanohydrin compound. No such example was reported earlier using a receptor for cyanide. Recognition process occurs through the demetalation of Cu from **1.Cu** and formation of formation of $Cu(CN)_n^{-(n-2)}$ (n = 2 or 4).

2.6. References

1. S. I. Baskin and T. G. Brewer, Medical Aspects of Chemical and Biological Warfare, ed. F. Sidell, E. T. Takafuji and D. R. Franz, TMM Publication, Washington, DC, 1997, ch. 10, 271.

2. R. M. Glead, W. J. Foley and I. E. Woodrow, *Plant, Cell Environ*.,1998, **21**, 12.

3. C. Young, L. Tidwell and C. Anderson, Cyanide: Social, Industrial, and Economic Aspects, Minerals, Metals, and Materials Society, Warrendale, 2001.

4. Z. Xu, S. K. Kim and J. Yoon, *Chem. Soc. Rev*., 2010, **39**, 1457.

5. K. W. Kulig; *Cyanide Toxicity*, U.S. Department of Health and Human Services, Atlanta, GA, 1991.

6. Guidelines for Water Reuse, U.S. Environmental Protection Agency, EPA/625/R-04/108-2004, Washington, DC.

7. (a) Y. Asano1, M. Dadashipour, M. Yamazaki, N. Doi and H. Komeda, *Protein Eng., Des. Sel*., 2011, **24**, 607; (b) R. J. H. Gregory, *Chem. Rev*.,1999, **99**, 3649.

8. (a) S.-S. Sun and A. J. Lees, *Chem. Commun*., 2000, 1687; (b) H. Miyaji and J. L. Sessler, *Angew. Chem., Int. Ed*., 2001, 40, 154; (c) S. Saha, A. Ghosh, P. Mahato, S. Mishra, S. K. Mishra, E. Suresh, S. Das and A. Das, *Org. Lett*., 2010, 12, 3406.

9. (a) K.-S. Lee,H.-J. Kim, G.-H. Kim, I. Shin and J.-I. Hong, *Org. Lett*., 2008, **10**, 49; (b) H.-J.Mo, Y. Shen and B.-H. Ye, *Inorg. Chem*., 2012, **51**, 7174; (c) M. Schmittel and S. Qinghai, *Chem. Commun*., 2012, **48**, 2707.

10. (a) Y. H. Kim and J.-I. Hong, *Chem. Commun*., 2002, 512; (b) P. Anzenbacher, D. S. Tyson, K. Jursikova and F. N. Castellano, *J. Am. Chem. Soc*., 2002, **124**, 6232.

11. (a) S. Y. Chung, S. W. Nam, J. Lim, S. Park and J. Yoon, *Chem. Commun*., 2009, 2866; (b) X. Chen, S. Nam, G. Kim, N. Song, Y. Jeong, I. Shin, S. K. Kim, J. Kim, S. Park and J. Yoon, *Chem. Commun*., 2010, **46**, 8953; (c) K. P. Divya, S. Sreejith, B. Balakrishna, P. Jayamurthy, P. Anees and A. Ajayaghosh, *Chem. Commun*., 2010, 6069; (d) H. S. Jung, J. H. Han, Z. H. Kim, C. Kang and J. S. Kim, *Org. Lett*., 2011, **13**, 5056; (e) V. Bhalla, H. Singh and M. Kumar, DaltonTrans., 2012, 41, 11413.

12. (a) G. Eaton, A. S. Pena-Nun˜ez, M. C. R. Symons, M. Ferrario and I. R. McDonald, *Faraday Discuss. Chem. Soc*., 1988, **85**, 237; (b) G. J. Kim and H. J. Kim, *Tetrahedron Lett*., 2010, **51**, 185; (c) J. H. Lee, A. R. Jeong, I. S. Shin, H. J. Kimand J. I. Hong, *Org. Lett*., 2010, **12**, 764; (d) S. Park and H. J. Kim, *Chem. Commun*., 2010, **46**, 9197.

13. (a) Y. Liu, X. Lv, Y. Zhao, J. Liu, Y.-Q. Sun, P. Wang and W. Guo, *J. Mater. Chem*., 2012, **22**, 1747; (b) J. Rosenthal and S. J. Lippard, *J. Am. Chem. Soc*., 2010, **132**, 5536.

14. Q. Zhao, F. Li, S. Liu, M. Yu, Z. Liu, T. Yi and C. Huang. *Inorganic Chemistry.,* 2008, **47**, 9257.

15. F. S. Geoffrey, J. R. Schoonover, R. Duesing, S. Boyde, Wayne E. Jr. Jones and J. M. Thomas, *Inorg. Chem.,* 1995, ***34***, 473.

16. Y. You, S. Lee, T. Kim, K. Ohkubo, W.-S. Chae, S. Fukuzumi, G.-J. Jhon, W. Nam and S. J. J. Lippard, J. Am. Chem. Soc., 2011,**133**, 18328.

17. D. Bruce and M. M. Richter, *Anal. Chem*., 2002, **74**, 1340.

18. (a) P.-K. Lee, W. H. T. Law, H. W. Liu and K. K.-W. Lo, *Inorg. Chem*., 2011, **50**, 8570; (b) K. K.-W. Lo, P.-K. Lee and J. S. Y. Lau, *Organometallics*., 2008, **27**, 2998; (c) J. Liu, Y. Liu, Q. Liu, C. Li, L. Sun and F. Li, *J. Am. Chem. Soc*., 2011, **133**, 15276.

19. M. Suresh, A. Ghosh and A. Das, *Chem. Commun*., 2008, 3906.

CHAPTER 3

FRET-BASED RECOGNITION OF FUMARIC AND MALEIC ACIDS IN PHYSIOLOGICAL CONDITION AND IN COMMERCIAL FRUIT JUICE

Publication:
Chem. Commun., 2013, ***49***, 9818-9820

3.1. Introduction

Molecular recognition studies of dicarboxylic acids are of great importance because of their presence as key structural moiety in many bioactive molecules.[1] Certain carboxylates have significant biological importance due to their role in innumerable metabolic processes. These are also known to take part in the biosynthesis of some important intermediates.[2] Certain organic acids are known to exhibit antimicrobial activity and are commonly being utilized either as food additives or preservatives for preventing food deterioration and extending the shelf life of perishable food ingredients.[3] Among such acids, fumaric and maleic acids find a broad range of usages in medicine and food industries. Fumaric acid is also important in the manufacture of unsaturated polyester resins. Fumaric acid derivatives are being tested for treatment of multiple sclerosis, the most common cause of neurological disability in young adults.[4] Fumaric acid, a by-product of the Krebs cycle, is known to be present in living cells.[5] Deficiency in fumaric acid is responsible for the skin lesion in-patients with Psoriasis.[6] Maleic acid, the cis isomer of the fumaric acid, is the inhibitor of Krebs cycle, and its presence in different kidney diseases has been widely described.[5c] However, this apparently benign reagent is toxic to lungs and mucous membranes on prolonged exposure, which could eventually led to a target organs damage. Maleic acid is irritant to eye and skin, while severe over-exposure can produce lung damage, choking, unconsciousness and eventually death. Considering the widespread use of these two acids as ingredients in food as well as beverages and their possible adverse influences on human physiology on prolonged exposure, it is almost imperative to develop an efficient reagent for their recognition and quantitative estimation in neutral aqueous medium. During the past few years, considerable progress has been made in the recognition of various dicarboxylic acids through hydrogen bonded adduct formation using hydrogen bond donors like urea/thiourea/amide subunits,[7,8] guanidium groups,[9] and allosteric phosphate-based

receptors.[10] But use of such detection processes are mostly limited to studies in non-aqueous medium due to an adverse solvation energy of these two dicarboxylate ion at pH ~ 7.0 in aqueous medium. There are two literature reports that describe either the recognition of several diacids and amino acids in mixed CH_3OH-aq.HEPES buffer (1:1, v/v; pH 7.4) medium or recognition of tartaric acid in CH_3OH-H_2O (3:1, v/v) medium utilizing hydrogen bond interactions of a thiourea based receptors.[7d,19] The only report that reveals the recognition of certain dicarboxylate ions in pure aqueous tris buffer medium of pH 7.5 also lacks the desired specificity towards maleate or fumarate.[9a] More recently, Bencini et. al. have reported a BINOL-based chiral polyammonium receptor that could act as a selective sensor for (S,S)-tartaric acid over its (R,R)/meso forms.[9c] Thus, reports on recognition of a certain diacid in aqueous environment or at neutral pH are scanty.[9]

The most commonly used techniques for the determination of fumaric and maleic acids are gas chromatography (GC) and high-performance liquid chromatography (HPLC) in a wide variety of samples. However, these methods often require complicated, multi-step sample pre-treatment or need expensive equipment. However, one drawback with these techniques is the lack of any selectivity among various dicarboxylic acids. To get around this problem of high solvation enthalpy of these dicarboxylate ions in aqueous medium, researchers have adopted the alternate approach of coordinative interactions of these dicarboxylate ions to certain metal ion or Lewis acid based receptors with even higher free energy changes. However, such reports are truly limited.[11] Among these, two independent reports have stated the specific recognition of oxalate ion utilizing the dye-displacement technique. Fabbrizzi *et. al.* have reported a homo binuclear Cu(II)-complex for recognition studies with imidazole and certain amino acids at pH 9.6, while this did not show any affinity towards acetate ion.[11c] While Delgado and co-workers have reported non-specific binding of several dicarboxylate ions as well as imidazole in H_2O-DMSO/CH_3OH

medium.[11d] Ghosh *et. al*. have reported an amide based receptor that could discriminate maleic and fumaric acids based on the opposite influences on the fluorescence response as output signal in chloroform medium; however, tartaric acid showed comparable fluorescence enhancement as that was observed for fumaric acid.[12a] Delgado *et.al*. reported protonated macro bicyclic amine derivatives for recognition of several dicarboxylate ions by potentiometric titration method with very little preference for fumarate over maleate. The only report on chemo dosimetric detection of certain diacids (oxalate, malonate, phthalate, maleate) in dioxane-aq. HEPES buffer (7:3, v/v) medium reveals that the reagent could clearly delineate fumarate and maleate based on the visually detectable colour and electronic spectral changes.[12b] Thus the issue of specificity in binding of these two biologically significant dicarboxylate ions like maleate and fumarate ions in an ensemble of all other mono- as well as di-carboxylate ions in aqueous medium at physiological pH has eluded researchers till date.

Fumaric acid provides more sourness per unit weight than other acidulants used in fruit juice drinks and this has triggered an indiscriminate use of this compound in commercially available fruit juices. According to the regulatory body like Association of the Industry of Juices and Nectars (AIJN) the maximum acceptance of fumaric acid in apple juice is considered as 3.0 - 5.0 $mgkg^{-1}$.[13] Thus, development of an efficient methodology for fast, specific and quantitative detection of this acid in fruit juices in presence many other probable mono and dibasic acids is crucial. Anslyn and his co-workers have successfully applied two different synthetic tripodal receptors having imidazolium ion as the H-bond donor fragment for estimating citrate or tartrate/malate in beverages in CH_3OH-aq. HEPES buffer (4:1, v/v) medium.[9b] To the best of our knowledge there is no report in the contemporary literature that describes the specific recognition of fumaric or maleic acid in aq. medium or at physiological pH, which further could help in estimation of fumaric acid in

commercially available nectar. In this present study, we have tried to address this issue using a novel receptor that could act as a reversible sensor for fumaric and maleic acid in aq. medium under physiological conditions with FRET-based fluorescence responses. This reagent could even be used for quantitative estimation of fumaric acid in commercially available apple juice. To the best of our knowledge, this is the first report that describes the specific detection and estimation of on the fumaric acid in any commercial juice.

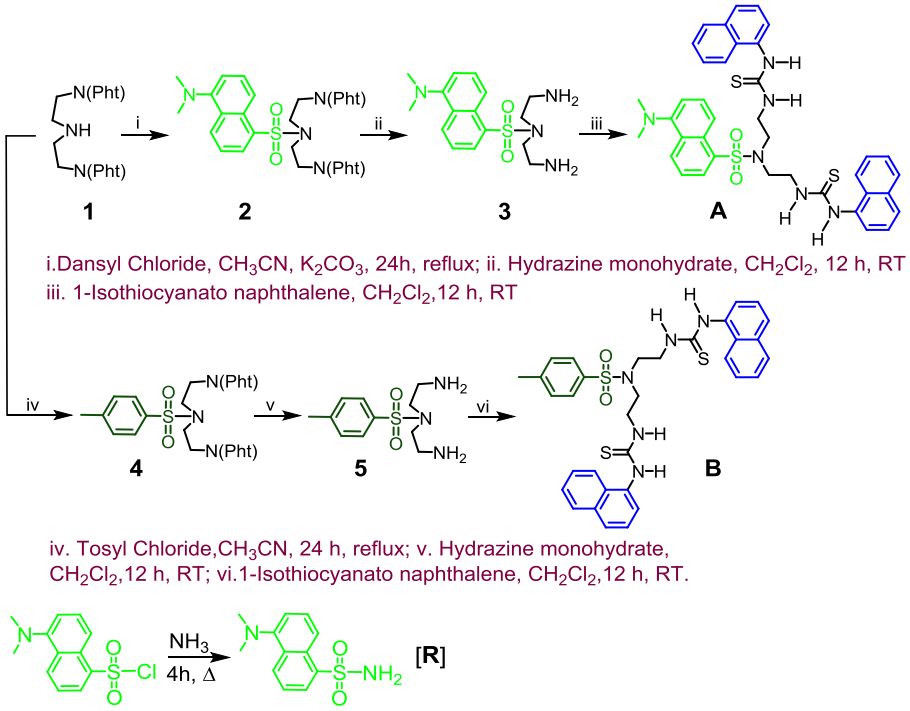

Scheme 1. Methodologies that were adopted for synthesis of **A**, **B** and **R.**

3.2. Experimental Section

3.2.1. Materials

Dansyl chloride, hydrazine monohydrate (98%), 1-isothiocyanato-naphthalene, tosyl chloride, phthalic anhydride were obtained from Sigma Aldrich and were used as received. 2,2'-Diaminodiethylamine was obtained from Koch-Light laboratory in India. AR grade mono- and di-carboxylic acids, such as oxalic acid, maleic acid, fumaric acid, suberic acid, sebasic acid, malonic acid, acetic acid, glutaric acid, adipicacid, citric acid, malic acid were purchased from SD Fine Chemicals in India. Tetra butyl

ammonium (TBA) salts of fumaric and maleic acids were prepared following standard procedure and used for further studies.[7b] Compound **1** was synthesized by following the method reported in the literature.[14a] Reference compound (R) was synthesized following a previously reported methodology.[15a] Solvents used for synthesis of various intermediates and final compounds were of AR grade (S.D. Fine Chemicals) and were used as received without further purification. Solvents used for various spectroscopic and HPLC studies were of HPLC grade (S.D. Fine Chemicals). Solvents were dried, as and when necessary, following standard procedures.

3.2.2. Analytical Methods

^{1}H NMR spectra were recorded on a Bruker 200 MHz FT NMR (Model: Avance-DPX 200) or on a Bruker 500 MHz FT NMR (Model: Avance-DPX 500) using CD_3CN, CD_2Cl_2 and CD_3OD as the solvent and tetra methyl silane (TMS) as an internal standard. ESI-Ms measurements were carried out on a Waters QTof-Micro instrument. Electronic spectra were recorded with a Shimadzu UV-3101 PC spectrophotometer; while fluorescence spectra were recorded using an Edinburgh instrument Xe 900 spectrofluorimeter.

3.2.3. General experimental procedure for UV-Vis and Fluorescence studies

1.0×10^{-4} M (spectral titration), 1.0×10^{-3} M (for HPLC studies) solution of the **A** and 1.0×10^{-4} M solution of **B** in aq. HEPES buffer-acetonitrile (1:1, v/v; pH 7.4) was prepared and stored in dark. This solution was used for all spectroscopic studies after appropriate dilution. 10 mM solution of aq. HEPES buffer was used for all spectroscopic studies unless mentioned otherwise. 1.0×10^{-2} M of diacid solutions was prepared in aq. HEPES buffer: acetonitrile (1: 1, v/v; pH 7.4). Solution of the compound **A** was further diluted for spectroscopic titrations, and the effective final concentration of the solution of compound **A** used for the fluorescence study was 2.0×10^{-5} M, while the final analyte concentration during emission spectral scanning was

4.0 x 10^{-3} M. For all luminescence measurements, λ_{Ext} = 290 nm with an emission slit width of 2 nm were used. The relative fluorescence quantum yields (ϕ_f) were estimated using equation 1 in acetonitrile medium by using the integrated emission intensity of dansyl amide (ϕ_f = 0.37) as reference for **A** and naphthalene (ϕ_f = 0.23) as reference for **7**.

$$\Phi_f = \Phi_f'.(I_{sample}/I_{std})(A_{std}/A_{sample})(\eta^2_{sample}/\eta^2_{std}) \quad \text{Eq. 1}$$

where, Φ_f' is the absolute quantum yield for the dansyl amide and naphthalene used as references; I_{sample} and I_{std} are the integrated emission intensities; A_{sample} and A_{std} are the absorbances at the excitation wavelength, and η_{sample} and η_{std} are the refractive indices.

3.2.4. General experimental procedure for ^{1}H NMR

3.0 x 10^{-3} M solution of **A** in CD_3CN (500 μL) was taken in an NMR tube. Complexation studies with maleate and fumarate as their tetra butyl ammonium (TBA) salts,[7b] were studied by ^{1}H NMR technique. Concentration for the stock solutions for both fumarate (in CD_3CN:DMSO-d_6; 99:1, v/v) and maleate (in CD_3CN) ions were maintained at 150 x 10^{-3} M. ^{1}H NMR spectra of the guest molecule (**A**) were recorded with increasing concentration of the host ions (fumarate and maleate ions). Such addition was continued until no further change in the chemical shifts was observed.

3.2.5. HPLC Instrument & Methodology

Apple juice was analysed by HPLC (Waters Alliance model with Waters 2996 Photo diode array Detector) using the Supelco Gel 610-H Column (Length: 30 cm, ID: 7.8 mm), in conjugation with a column heating device at 30ºC. Solutions with known [Fumaric acid] was analysed by HPLC method under the identical conditions. Elution was carried out with water (100%), containing 0.1% of phosphoric acid at a flow rate of 0.5 ml/min for 30 min. The mobile phase was filtered through 0.2 μM PVDF

membrane filter and degassed before use. Detection was performed with photo diode array detector (PDA). For generating the calibration plot, standard solution of fumaric acid was freshly prepared with concentrations of 0.78, 1.56, 3.125, 6.25, 12.5, 25 and 50 ppm in distilled water. The elution was monitored using an UV-detector at 210 nm and for each standard fumaric acid solution injection volume was 20 µL to get the standard plot for obtaining the calibration plot, while that for commercial apple juice was 40 µL. The standard curve for fumaric acid passed virtually through the origin and a good linear fit (R^2 = 0.999) was obtained.

3.2.6. Computational methods

Conformational searches for probe **A** was performed using the Monte Carlo algorithm for the random variation of all of the rotatable bonds combined with Semi empirical PM3 in Spartan 06.[16] For each calculation, 5000 Monte Carlo steps were carried out. Lowest energy conformers were taken for the energetic comparisons with semi empirical calculations. All the geometries of probe **A** were fully optimized at the PM3 level[17] of theory using the Gaussian 03 program.[18] The lowest energy conformer is taken for the complexation study. We have also optimized fumaric and maleic acids (in neutral, mono and bis deprotonated form) at PM3 level of theory in gas phase. The optimized geometries were checked with imaginary frequencies to identify the ground-state minimum. Next we have taken probe **A** for complexation with diastereomeric diacids (fumaric and maleic acid) in neutral, mono and bis deprotonated form optimised at PM3 level of theory in gas phase. Single-point calculations were performed for these complexes at the B3LYP/6-31G* level using the PM3 level[19] optimized complex geometries for more accurate estimation of the energies. The binding energies were computed using the equation, $\Delta E = \Delta E_{complex} - (\Delta E_{probe4} + \Delta E^{diacid/mono/bisdeprotonated})$.

3.3. Synthesis and Characterization

3.3.1 Synthesis of 2

Compound **1** (700 mg, 1.92 mmol) and dansyl chloride (647 mg, 2.40 mmol) were dissolved in 50 ml dry acetonitrile. To this solution, Na_2CO_3 (407 mg, 3.84 mmol) was added and allowed to reflux for 24 h. Then the reaction mixture was filtered to separate out Na_2CO_3. Filtrate was completely evaporated and redissolved in minimum volume of dichloromethane. To this solution, 20 mL of ethanol was added to precipitate the desired compound. This was collected through filtration and was washed further with ethanol. This isolated light yellow compound was further dried over P_2O_5 in a dissector. Yield: 550 mg, 48%. ESI-Ms (m/z) calculated for $C_{32}H_{28}N_4O_6S$: 596, observed: 597 [M + H^+]. ^{1}H NMR [500 MHz, $CDCl_3$: δ (ppm)]: 8.16 (1H, d, *J* = 8.5 Hz, ArH); 8.12 (1H, d, *J* = 7.5 Hz, ArH); 7.76 (1H, d, *J* = 8.5 Hz, ArH); 7.65 - 7.60 (8H, m, ArH); 7.38 (1H, t, *J* = 8.0 Hz, ArH); 7.22 (1H, t, *J* = 8.0 Hz, ArH); 6.18 (1H, d, *J* = 7.5 Hz, ArH); 3.94 (4H, t, *J* = 5.0 Hz, -CH_2); 3.88 (4H, t, *J* = 5.0 Hz, -CH_2); 2.70 (6H, s, -CH_3).

3.3.2. Synthesis of 3[14a]

To a dichloromethane solution of compound **2** (500mg, 0.84 mmol), hydrazine monohydrate (16.8 mmol) was added. Reaction mixture was stirred for 12 h at room temperature, while a white precipitate was formed. Precipitate was removed through filtration using a G_4 sintered crucible. Filtrate was collected and evaporated under reduced pressure. Solid residue was redissolved in dichloromethane and undesired impurities were subsequently extracted is aqueous layer. The organic layer was collected and dried over anhydrous Na_2SO_4 and evaporated in vacuum. A sticky pale green compound was obtained. Yield: 250 mg; 89 %. ESI-Ms (m/z) calculated for $C_{16}H_{24}N_4$ O_2S: 336, observed: 337 [M + H^+]. ^{1}H NMR [500 MHz, $CDCl_3$: δ (ppm)]. 8.53 (1H, d, *J* = 8.5 Hz, ArH); 8.30(1H, d, *J* = 8.5 Hz, ArH); 8.15 (1H, d, *J* = 7.5 Hz,

ArH); 7.56-7.49 (2H, m, ArH); 7.17 (1H, d, *J* = 8 Hz, ArH); 3.38 (4H, t, *J* = 6 Hz, -CH_2); 2.91 (4H, t, *J* = 6Hz, -CH_2); 2.87 (6H, s, -CH_3).

3.3.3. Synthesis of A

Compound **3** (130 mg, 0.39 mmol) and 1-isothiocyanato naphthalene (144 mg, 0.78 mmol) were dissolved in 10 ml dichloromethane and stirred at room temperature for 24 h. Progress of the reaction was monitored by checking the TLC and the reaction was stopped when no further change could be observed. Volume of the reaction mixture was reduced to 5 ml under reduced pressure. To this, diethyl ether was added to precipitate the desired compound. A white solid compound was isolated through filtration and was further washed with cold dichloromethane. Yield: 180mg, 66%. ESI-Ms(m/z) calculated for $C_{38}H_{38}N_6\ O_2S_3$: 706, observed: 707 [M + H^+]. ^{1}H NMR [500 MHz, $CDCl_3$: δ (ppm)]: 8.47 (1H, d, *J* = 8.0 Hz, ArH); 7.98 (1H, d, *J* = 8.5 Hz, ArH); 7.98 (2H, d, *J* = 5.0 Hz, ArH); 7.88-7.86 (4H, m, ArH); 7.82 (1H, d, *J* = 7.0 Hz, ArH);7.76 (2H, s, NH); 7.54-7.53 (4H, m, ArH); 7.48 (2H, t, *J* = 7.5 Hz, ArH); 7.42-7.35 (4H, m, ArH); 7.08 (1H, d, *J* = 7.0 Hz, ArH); 6.28(2H, s, -NH); 3.65 (4H, t, *J* = 8.0 Hz, -CH_2); 3.39 (4H, t, *J* = 8.0 Hz, -CH_2); 2.84 (6H,s,CH_3).^{13}C NMR (125 MHz, CD_3CN + 1% DMS0-d_6: δ (ppm)]: 183.72, 152.64, 135.71, 135.34, 134.96, 131.18, 130.70, 130.03, 129.14, 128.31, 127.45, 126.62, 124.57, 123.91, 120.17, 116.23, 47.90, 45.74, 43.81.

3.3.4. Synthesis of 4

Synthetic procedure that was adopted for **4** was similar to that of **2**, except 4-toluene sulphonyl chloride (104 mg, 0.55 mmol) was used for the reaction instead of dansylchloride. Similar workup procedure was also followed for isolating the desired white solid compound **4**. Yield: 140 mg, 50%. ESI-Ms (m/z) calculated for $C_{27}H_{23}N_3O_6S$: 517, observed: 556 [M + K^+]. ^{1}H NMR [200 MHz, $CDCl_3$: δ (ppm)]:

9.71 (8H, m, ArH); 9.38 (2H, d, *J* = 7.6Hz, ArH); 8.86 (2H, d, *J* = 7.8 Hz, ArH); 5.83 (4H, t, *J* = 5.6 Hz, -CH_2); 5.63 (4H, t, *J* = 5.6 Hz, -CH_2); 4.06 (3H, s, -CH_3).

3.3.5. Synthesis of 5

Procedure that was adopted for synthesis of **5** was similar to that of **3**, except **4** (150 mg, 0.3 mmol) was used for the reaction instead of the intermediate compound **2**. After following the similar work-up procedure a white sticky compound was isolated. Yield: 40 mg, 58 %. ESI-Ms (m/z) calculated for $C_{11}H_{19}N_3O_2S$: 257, observed: 258[M + H^+]. ^{1}H NMR [200 MHz, $CDCl_3$: δ (ppm)]: 9.67 (2H, d, *J* = 7.8 Hz, ArH); 9.28 (2H, d, *J* = 7.4 Hz, ArH); 5.08 (4H, t, *J* = 12 Hz, -CH_2); 4.82 (4H, t, *J* = 12 Hz, -CH_2); 4.39 (3H, s, -CH_3).

3.3.6. Synthesis of B

Procedure that was adopted for synthesis of **B** was similar to that of **A**, except **5** (40 mg, 0.15 mmol) instead of **3** and accordingly 57 mg (0.31 mmol) of 1-isothiocyanato naphthalene were used for the reaction. After following the similar work-up procedure, as it was adopted for **A**, desired compound **B** was isolated as a white solid. Yield: 17 mg, 18%. ESI-Ms (m/z) calculated for $C_{33}H_{33}N_5O_2S_3$: 627, observed: 628 [M + H^+]. ^{1}H NMR [500 MHz, CD_2Cl_2: δ (ppm)]. 7.95 (2H, d, *J* = 7.5 Hz, ArH); 7.92 - 7.87 (4H, m, ArH); 7.83 (2H, s, NH); 7.58 - 7.53 (4H, m, ArH); 7.51 - 7.47 (4H, m, ArH); 7.42 (2H, d, *J* = 10 Hz); 6.33 (2H, s, -NH); 3.66 (4H, t, *J* = 10 Hz, -CH_2); 3.19 (4H, t, *J* = 10 Hz, -CH_2); 2.37 (3H, s, CH_3). ^{13}C NMR (125 MHz, $CDCl_3$, δ (ppm)]: 182.04, 143.81, 134.97, 134.64, 131.36, 129.88, 129.03, 128.55, 127.38, 127.03, 126.91, 125.89, 122.36, 48.67, 44.43, 29.7, 21.5.

3.4. Results and Discussions

Dansyl chloride and *p*-toulene sulphonyl chloride was allowed to react with the secondary amine derivative **1** to yield intermediate compounds **2** or **4**, respectively (Scheme 1). Purity of these two intermediates was checked and were further reacted

with hydrazine monohydrate for deprotection reaction and conversion of two terminal amide functionalities to corresponding amine moieties (compounds **3** and **5**), which were also characterized using various analytical techniques. Intermediate compounds **3** and **5** were allowed to react with 1-isothiocyanato naphthalene to yield two desired thiourea derivatives **A** and **B** respectively. These two compounds were characterized following standard analytical (ESI-Ms, elemental analysis) and spectroscopic (^{1}H and ^{13}C NMR, Uv-vis and Fluorescence spectroscopic) techniques. Analytical data for these two compounds agreed well with the data that were anticipated for the proposed formulation of the respective compound.

The electronic and emission spectra for compound **A** and **B** were recorded in aq. HEPES buffer: acetonitrile (1:1, v/v; pH 7.4) medium at room temperature. Electronic spectrum of compound **A** showed three shoulders at ~ 353 nm, ~ 290 nm and ~ 244 nm, whereas in case of compound **B** one distinct absorption band at 290 nm was observed. The common shoulder observed at 290 nm could be ascribed to a charge transfer (CT) transition that is typical for naphthalene based Chromophore.[15b] The other shoulder at about 353 nm from **A** was ascribed to a dansyl-based CT transition (Figure 3.1). Electronic spectra for **A** and **B** remained unchanged in the presence excess of all mono and di-carboxylate ions in aq. HEPES buffer-acetonitrile (1:1, v/v; pH = 7.4) medium.

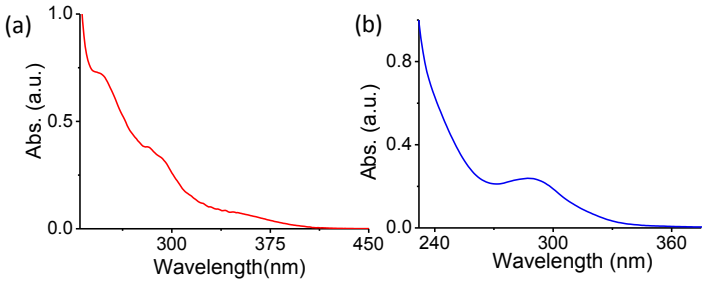

Figure 3.1. Electronic spectra recorded for 20 μM solution of (a) **A** and (b) **B**; Uv-vis spectra of **R**; All spectra were recorded in 10 mM aq. HEPES buffer:acetonitrile (1:1, v/v; pH 7.4) medium.

A solution of the probe molecule **A** in aq.HEPES buffer: acetonitrile (1:1, v/v; pH 7.4) medium showed a strong emission band at 542 nm on excitation at 290 nm. It is worth mentioning here that compound **A** has two fluorophores as an integral part of the molecule. Emission spectra recorded for compound **B**, having only a comparable naphthalene moiety as the fluorescence active unit with λ_{Ext} of 290 nm, under the identical experimental condition. This showed three emissions bands at 313 nm, 390 nm (broad) and 464 nm (Figure 3.2). The bands at 313 and 390 nms were assigned as the vibronic-bands of the naphthyl moiety, whereas relatively less intense emission band at 464 nm was assigned to an emission process from an excited naphthyl dimer.[7g] Multiple emission bands within the 310 - 390 nm are known to be typical for the naphthalene derivatives with λ_{Ext} of 290 nm. Similar experiment with other model compound **R** showed an emission band at 528 nm following excitation at 355 nm, while a very weak emission band was observed when excited at 290 nm. A comparison of the emission spectra of **A**, **B** and **R** clearly revealed a complete absence of the naphthalene-based emission bands and presence of strong dansyl-based emission band in compound **A** on excitation at 290 nm (where naphthalene absorb predominantly). All these tend to suggest that a FRET process was being operational for the probe molecule **A** (λ_{Ext} = 290 nm), with naphthalene moiety as the donor and dansyl moiety as the acceptor fragment.

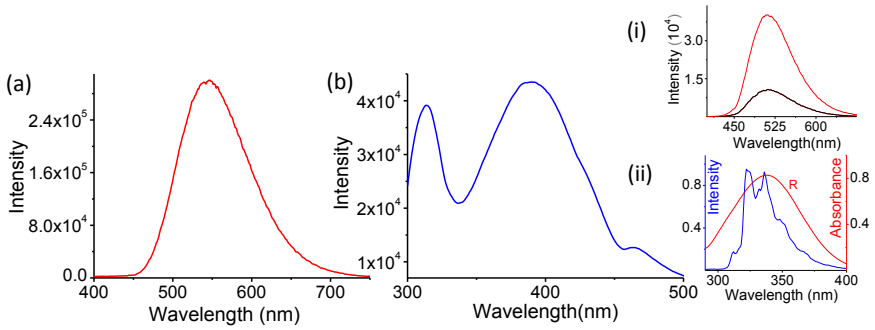

Figure 3.2. Luminescence (λ_{Ext} = 290 nm) spectra recorded for 20 μM solution of (a) A (slit width: 2/2 nm) and (b) B (slit width: 3/3 nm); Inset i: Emission spectra for R following excitation at 355 (Red line) and 290 (Black line) nm; ii: Spectra showing the strong overlap

between the emission spectra of naphthalene and Uv-vis spectra of **R**; Inset All spectra were recorded in 10 mM aq. HEPES buffer: acetonitrile (1: 1, v/v; pH 7.4) medium.

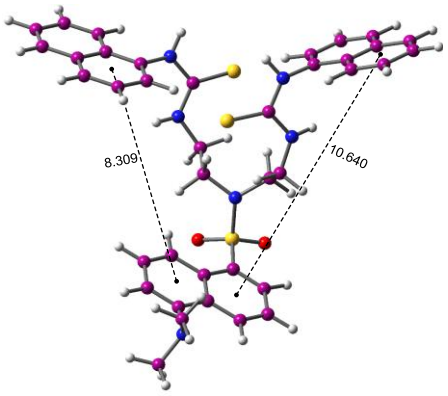

Figure 3.3**.** RHF/PM3 optimized geometry of probe A. Distances are given in Å. (Atom colour code: red = oxygen; blue = nitrogen; white = hydrogen; yellow = sulphur; dark magenta = carbon).

Such a possibility is further supported by the fact that two model compounds **R** (showed predominantly dansyl-based absorption) and **B** (with naphthalene-based emission) showed a significant spectral overlap (Figure 3.2, Inset ii). Feasibility of the FRET process between naphthyl donor and dansyl acceptor was reported earlier and for such a process, R_0 (Förster distance) was found to be ~34 Å between naphthyl and dansyl moieties, separated by poly-L-proline.[20]

Energy optimized structures for the receptor **A** (Figure 3.3) revealed that the distance between the donor dansyl moiety and two naphthalene-based acceptors were of 8 Å and 10 Å, respectively (*vide infra*). This further supported the feasibility of such an energy transfer process. Efficiency of the FRET process for the energy transfer between napthyl and dansyl moieties in **A** was evaluated as 75% in aq. HEPES buffer:acetonitrile (1:1, v/v; pH 7.4) medium using the equation 2.

$$\Phi_{ET} = 1 - (F_{DA} / F_D) \qquad \text{Eq. 2}$$

Energy transfer efficiency (Φ_{ET}) was evaluated using the expression shown in Eq. 2, where F_{DA} and F_D denote the donor fluorescence intensity with and without an acceptor, respectively.

Emission quantum yield (Φ_F) for the model compound **B** was evaluated as 0.0137 in aq. HEPES buffer-acetonitrile (1:1, v/v; pH 7.4) medium using naphthalene as the reference compound. Our earlier reports on urea/thiourea based receptors clearly revealed that urea/thiourea moiety could act as a hydrogen bond donor for polar hydrogen bond (H-bond) acceptor solvent molecules like DMSO.[21] Water molecule being a good H-bond acceptor is also expected to interact with the model compound **B**. Such interactions are expected to favour solvation and thereby the non-radiative deactivation pathway of the naphthalene based excited state. This could be attributed for the apparently lower quantum yield value for FRET based energy transfer (Φ_{ET} = 75 %) despite a strong overlap of the emission spectra for **B** and the absorption spectra of **R** (Figure 3.2, inset ii), one of the few essential criteria for an efficient FRET process.

In order to examine the luminescence response of the probe molecule **A** towards different carboxylic acids, we had recorded the luminescence spectra of **A** in the absence and presence various mono-, di- and tri-carboxylic acids (Figure 3.4). Emission spectra (λ_{Ext} = 350 nm) were recorded for **A** (20 μM) in the presence of 200 mole equivalents of various carboxylic acids (acetic, malonic, citric, succinic, adipic, glutaric, suberic, malic, maleic and fumaric acids) in 10 mM of aq.HEPES buffer: acetonitrile (1:1, v/v, pH 7.4) medium. Emission spectra for **A** remained virtually unchanged when recorded in presence of all other carboxylic acids, except maleic and fumaric acids. For maleic and fumaric acids, a significant quenching (~ 85 %) of the FRET based luminescence at 542 nm for **A** was observed (Figure 3.4), which was presumably due to the formation of H-bonded adduct between the reagent **A** and maleate or fumarate ion. To understand the nature of the species (mono- and/or bis-deprotonated species) of these two acids that could actually prevail at pH 7.4, pKa for these two acids were evaluated. Respective values for pK_1 & pK_2 for maleic and fumaric acids were found to be 1.92 & 6.23 and 3.02 & 4.38.18.

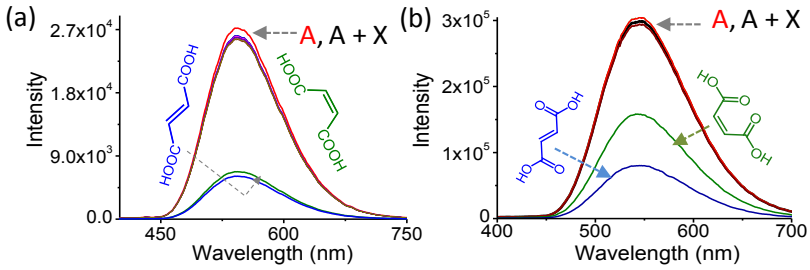

Figure 3.4. Emission spectra of probe A (20 μM) in absence and presence of 200 mole equivalent various carboxylic acids X (X = acetic, oxalic, malonic, citric, succinic, adipic, glutaric, suberic, malic) as well as maleaic and fumaric acids; (a) in 10 mM aq. HEPES buffer: acetonitrile (1: 1 (v/v); pH 7.4) medium; (b) in 10 mM aq. HEPES buffer: acetonitrile (1:1, v/v; pH 6) medium using λ_{Ext} = 290 nm and λ_{Mon} = 542 nm. Slit width 2 nm.

These data tend to suggest that predominantly mono-deprotonated species, along with certain proportion of bis-deprotonated species actually exist in the equilibrated mixture of the respective acids at pH 7.4. To ensure the luminescence responses of the receptor **A** on binding to the mono-deprotonated form of the respective acid, similar experiments were also repeated at pH 6.0. Observed luminescence responses at 542 nm (λ_{Ext}= 290 nm) were similar to that was observed at pH 7.4; except, extent of changes were more pronounced for fumarate ion than maleate.

To understand the photo induced process that could be responsible for this dansyl-moiety based luminescence quenching for **A** at 542 nm, luminescence responses (λ_{Ext} = 290 nm) of the model receptor **B** were recorded in presence of 200 mole equivalent excess of maleic and fumaric acids (Figure 3.4). Analogous quenching of the naphthalene-based luminescence for a urea/thiourea based receptors were also observed on binding to different acetate drivatives.[21b] This clearly suggested that the binding of the maleate/fumarate ion to either of two receptors (**A** and **B**) could cause an efficient quenching of the naphthalene-based luminescence. Such an observation is anticipated for the binding of the anionic analytes to a fluorophore without much change in the molecular rigidity.

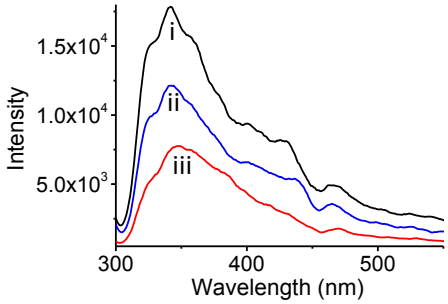

Figure 3.5. Luminescence response of (i) B, (ii) B with Maleic acid (iii) B with Fumaric acid was recorded in 10 mM aq. HEPES buffer:acetonitrile (1:1, v/v; pH 6) medium. λ_{Ext} = 290 nm.

Binding of an anion is expected to enhance the energy of the highest occupied molecular orbital (HOMO) and thereby narrowing down the HOMO-LUMO energy gap.[21c,d] This in turn, is expected to favour the non-radiative deactivation pathway following the energy gap law. Once the naphthalene based emission is effectively blocked/quenched, no FRET based energy transfer and consequently dansyl-based emission at 542 nm is anticipated for **A** following excitation at 290 nm. Thus, the observed fluorescence quenching of the receptor **A** at 542 nm (λ_{Ext} = 290 nm) could be attributed to the quenching of the luminescence of the napthyl fragment and with consequent interruption of the FRET process.

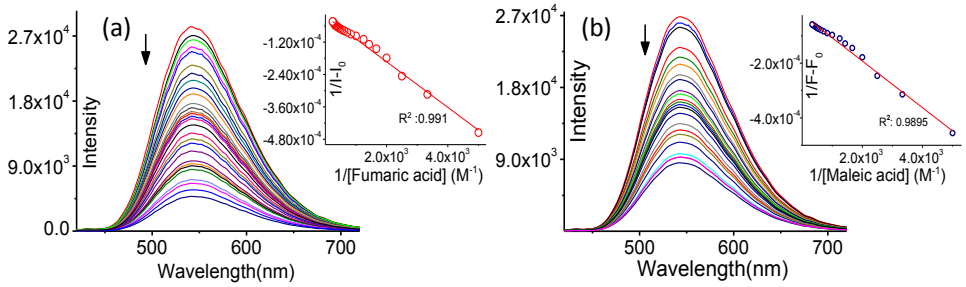

Figure 3.6. (a) Changes in luminescence spectral pattern for **A** (20 μM) upon addition of increasing [fumaric acid] (0 to 4.2 x 10^{-3} M) and (b) [maleic acid] (0 to 3.4 x 10^{-3} M); Insets in Figures a and b show the respective Benesi-Hildebrand plot for fumaric and maleic acids. For both B-H plots, good linear fit confirms the 1:1 binding stoichiometry. For all studies λ_{Ext} = 290 nm, λ_{Mon} = 542 nm with slit width: 2 nm was used. All measurements were performed in 10 mM HEPES buffer: acetonitrile (1:1, v/v; pH 7.4) medium.

The residual luminescence of the receptor **A** in presence of excess of maleate/fumarate ion could be accounted as the weak dansyl-based emission on

excitation at 290 nm. Low emission quantum yield for the other model compound **R** at 528 nm for λ_{Ext} of 290 nm further corroborated this. Systematic luminescence titrations were carried out for **A** (20 μM) with varying [fumaric acid] (0 to 4.2 x 10^{-3} M) and [maleic acid] (0 to 3.4 x 10^{-3} M) in aq. HEPES buffer: acetonitrile (1:1, v/v; pH 7.4) medium using λ_{Ext} of 290 nm and λ_{Mon} of 542 nm. A gradual decrease in emission intensity at 542 nm was observed upon addition of either of these two carboxylic acids (Figure 3.6 (a) and (b)). The binding stoichiometry for the adduct formation between the receptor **A** and the respective carboxylic acids was evaluated as 1:1 based on the Benesi-Hildebrand plot of the data obtained from the systematic fluorescence titration. This 1:1 binding stoichiometry was also confirmed from the data obtained from the ESI-Ms analysis. ESI-Ms signals at m/z of 843.21 and m/z 843.71 were attributed to [**A** + fumarate + Na^+] and [**A** + maleate + Na^+], respectively. Binding affinity of **A** towards fumaric and maleic acids was evaluated as (6.1± 0.05) x 10^2 M^{-1} and (5.16 ± 0.04) x 10^2 M^{-1} from fluorescence titration experiments and the subsequent B-H plot at aq.HEPES buffer: acetonitrile (1:1, v/v; pH 7.4) medium. Respective binding affinity of **A** towards maleate (2.1± 0.04) x 10^2 M^{-1} and fumarate (8.6 ± 0.02) x 10^2 M^{-1} ions were also evaluated at aq.HEPES buffer: acetonitrile (1:1, v/v; pH 6.0) medium, which showed a slightly different trend in binding affinities.

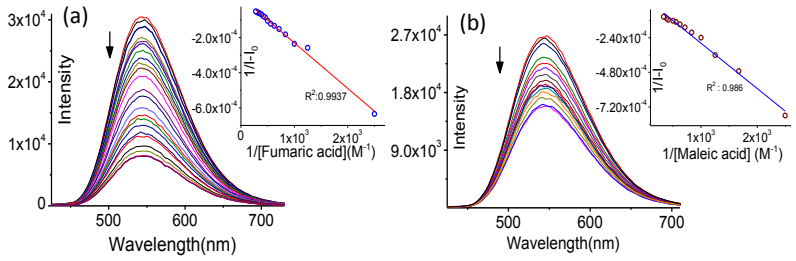

Figure 3.7. Changes in luminescence spectral pattern for **A** (20 μM) upon addition of increasing (a) [fumaric acid] (b) [maleic acid]; Insets in Figures (a) and (b) show the respective Benesi-Hildebrand plot for fumaric and maleic acids. For both B-H plots, good linear fit confirms the 1:1 binding stoichiometry. For all studies λ_{Ext} = 290 nm, λ_{Mon} = 542 nm with slit width: 2 nm was used. All measurements were performed in 10 mM HEPES buffer: acetonitrile (1:1, v/v; pH 6) medium.

This change in preference of **A** towards maleic and fumaric acids at two different media pH (e.g. 6.0 and 7.4) could be attributed to the presence of these two diacids virtually in different de-protonated forms at pH 6.0 and pH 7.4.Such a presumption was further substantiated by molecular modelling and simulation studies (*vide infra*). Please note that all reported binding constants evaluated were average of at least three independent fluorescence titrations.

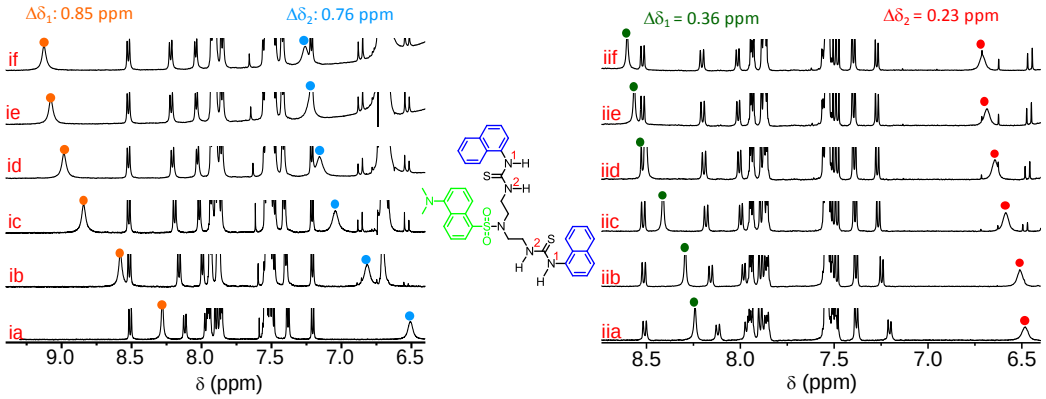

Figure 3.8. Partial ^{1}H NMR spectra of **A** (2.83 mM) in (ia/iia) absence and in presence of varying concentration of (ib - if and iib - iif) X (X is fumarate and maleate); (ib and iib): [X] = 11.32 mM; (ic and iic): [X] = 19.81 mM; (id and iid): [X] = 28.3 mM; (ie): [fumarate] = 36.79 mM and (iie): [maleate] = 33.96 mM. All spectra were recorded for fumarate in CD_3CN-DMSO (d_6) (99:1, v/v) medium and for maleate in CD_3CN.

The hydrogen bonding interaction between TBA salt of fumaric acid (TBAF) and maleic acid (TBAM) with **A** was also investigated by systematic ^{1}H NMR titration with varying [TBAF] or [TBAM]. For fumarate ^{1}H NMR titration studies were performed in CD_3CN-DMSO (d_6) (99:1, v/v) medium; while for maleate, titrations were performed in CD_3CN. The initial chemical shifts for signals for the four protons of two dissymmetric thiourea (two -N_1H and two -N_2H protons) functionalities in **A** appeared as two sharp singlet at δ = 8.28 ppm and δ = 6.52 ppm respectively, with integration for each signal was consistent for two protons (Figure 3.8).This signified that two thiourea functionalities were magnetically anisotropic with thiourea protons (belonged to N_1-atom), adjacent to the naphthyl ring, were most down filed shifted (δ = 8.28 ppm). On subsequent increase in the [TBAF], signals for these four thiourea-protons in **A**, were found to shift downfield, e.g. 8.28 to 9.13 ppm ($\Delta\delta_1$ = 0.85 ppm for two -N_1

protons) and 6.51 to 7.27 ppm ($\Delta\delta_2$ = 0.76 ppm for two $-N_2$ protons). These downfield shifts were attributed to the net desheilding effect induced by the hydrogen-bonding interaction between the thiourea protons and the fumarate anion. Higher shift for the N_1-thiourea protons signified a stronger interaction with fumarate ion than that of N_2-protons. Upon addition of TBAF to **A**, no significant changes in chemical shift value of either aromatic (dansyl and naphthyl) or aliphatic protons were noticed. These revealed that there were no interactions between the protons of the aromatic rings and the fumarate ions. For similar ^{1}H NMR studies with TBAM, relatively smaller downfield shifts for two sets of the thiourea protons ($\Delta\delta_1$ = 0.36 ppm for two -N_1 protons and $\Delta\delta_2$ = 0.23 ppm for two $-N_2$ protons) were observed, which signified a weaker hydrogen-bonded interaction between the thiourea functionality of **A** and the maleate ion than that was observed for fumarate in CD_3CN-DMSO (d_6) (99:1, v/v) medium. No appreciable shifts in the signals for the aromatic as well as aliphatic protons of **A** were observable during titration with TBAM. We addressed the issue of most favourable conformation for **A** for binding to fumarate and maleate ions and thus, the observed preferences at different pH through detailed molecular modelling studies.

Fumaric acid is one of the most common additives for use in fruit juice drinks as it provides more sourness per unit weight than other acidulants used in fruit juice drinks as well as it provides more buffering capacity than other acidulants. The hydrophobic nature of the fumaric acid allows this to interact better with lipid material of the microbial cell wall to disrupt the microbial activity and thus acts as an effective antimicrobial agent.[22] However, this apparently benign food additive also has detrimental influences on human physiology on prolong exposure to a higher concentration than that is allowed for fruit juice drinks. Higher content of fumaric acid in apple juice indicates adulteration and over processing of the apple juice.[23] Moreover, fumaric acid content in fruit products may indicate the certain degree of

microbial degradation of raw material. According to the recent guidelines of the Association of the Industry of Juices and Nectars from Fruits and Vegetables of the European Union (AIJN) the limiting concentration for fumaric acid in apple juices is 5.0 mgkg^{-1}. Thus, we explored the possibility of using this reagent (**A**) for quantitative estimation of the fumaric acid in commercially available apple juice.

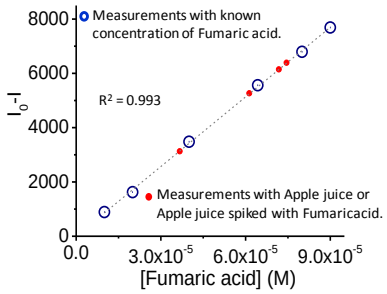

Figure 3.9. Calibration plot obtained from I_0-I *vs* [Fumaric acid]. (a) Block dots on linear plot shows known fumaric acid concentration. (b) Red dots on linear plot show apple juice and apple juice spiked with fumaric acid (20 μM, 40 μM and 60 μM).

To evaluate the ability of probe **A** in the detection of fumaric acid concentration, the probe reagent was treated with different concentrations of fumaric acid (0 to 1.0 x 10^{-4} M). The final concentration of **A** was maintained at (1.0x 10^{-4} M) for all measurements. The linearity of the method was tested by preparing a calibration curve by plotting $\Delta[I_0\text{-}I]$ vs. [Fumaric acid] (Figure 3.9). An average value of the three measurements of fluorescence intensity for each concentration level was used for preparing the linear calibration curve (R^2 = 0.999). Consequently, for the lowest concentration (9.95 x 10^{-6} M for fumarate ion) that was used for preparing the calibration curve, the ΔI ($\Delta I = I_0\text{-}I$) to noise ratio was measured with three replicates and was found to be appreciably higher than 10 ppm. These data support the suitability of the proposed method for its application to real samples.

For analysis of the commercial sample of apple juice, 0.2 ml of this was used, which was eventually adjusted to the final volume to 5 ml after adding appropriate amount of the reagent **A** (1.0 x 10^{-4} M) and aq. HEPES buffer: acetonitrile (1:1, v/v; pH 7.4)

as solvent. This solution, along with the solutions spiked with known concentration of fumaric acids (20 μM, 40 μM and 60 μM) as an internal standard were used for emission measurements without further treatment. The Fumaric acid concentration in the commercial apple juice was determined to be 3.8 x 10^{-5} M, which is within the allowed limit for fumaric acid concentration in good apple juice.[13] Absence of any Maleate ion or maleic acid in this sample of commercial apple juice was confirmed from the HPLC analysis (vide infra). To validate our results for the evaluation of the [Fumaric acid] in commercial apple juice, same apple juice was also analysed by HPLC technique (Figure 3.10). First, solutions with known [Fumaric acid] were analysed by HPLC method under the identical conditions. Calibration curve was generated by using freshly prepared standard solution of fumaric acid having concentrations of 0.78, 1.56, 3.125, 6.25, 12.5, 25 and 50 ppm in double distilled water. The elution was monitored at 210 nm using UV detector and injection volume used was 20 μL each for different standard fumaric acid solution and 40 μL for neat apple juice for generating the standard plot. A good linear fit was obtained for the standard curve (R^2 = 0.999).

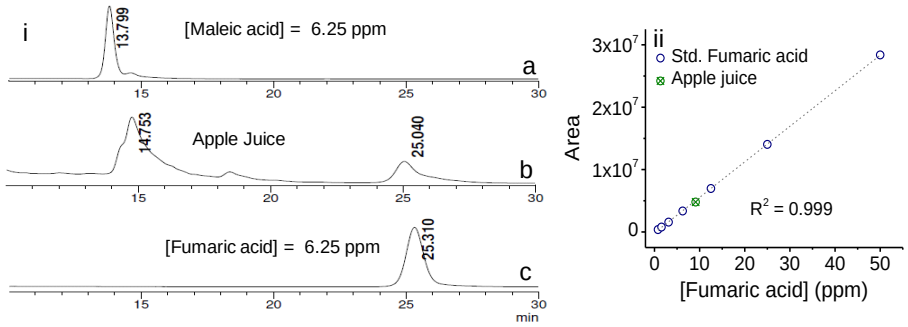

Figure 3.10. (i) HPLC chromatogram of (a) standard Maleic acid (6.25 ppm) solution with retention time 13.799 min. (b) commercial apple juice and (c) standard fumaric acid (6.25 ppm) with retention time 25.221 min; (ii) Standard calibration curve obtained from the HPLC data for different standard fumaric acid (0.78, 1.56, 3.125, 6.25, 12.5, 25 and 50 ppm) solutions and the use of that calibration plot for evaluation of [Fumaric acid] in the commercial sample of apple juice.

The concentration of fumaric acid in this apple juice was estimated as 3.84 x10^{-5} M by this HPLC method after considering the ratio of the volume injected for standard

fumaric acid solution and commercial apple juice. Experiment was also repeated for detection of maleic acid in apple juice, which revealed either its complete absence or its presence below the detection limit in the sample of the commercial apple juice. Thus, the concentration of fumaric acid obtained from HPLC technique was in very good agreement with that obtained from fluorescence measurements using the new probe reagent **A**.

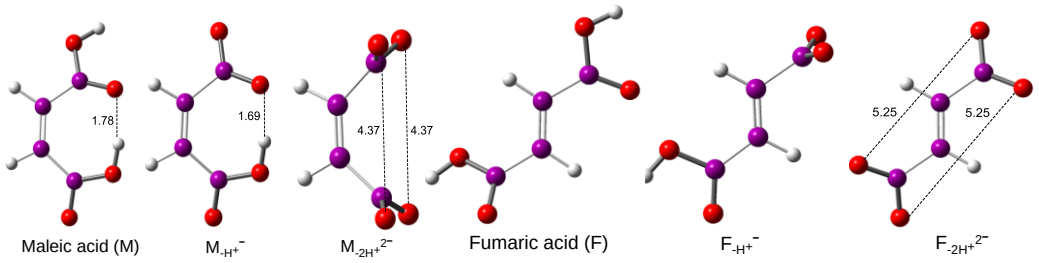

Figure 3.11. Energy optimized structures for the neutral, mono and bis-deprotonated form of maleic and fumaric acid. Structures were optimized in PM3 level.

The binding of maleic and fumaric acids with the receptor **A** could occur with the mono- or bis-deprotonated state of these diacids. Proton affinities (PAs) for the mono- and bis-deprotonated forms were calculated for maleic and fumaric acids (Figure 3.11). The PA values for mono and bis ionic forms of respective acids were computed with B3LYP/6-31G*//RHF/PM3 level of theory. The first proton affinity of maleic acid (333.7 kcal/mol) was found to ~15.0 kcal/mol lower than the corresponding first PA of fumaric acid (349.9 kcal/mol). The lowering in the PA of maleic acid is attributed to the stabilization achieved by the conjugate base via strong intra molecular hydrogen bonding (Figure 3.11). However, the second PA was found to be higher for the maleic acid (468.7 kcal/mol) compared to the fumaric acid (437.2 kcal/mol). The electrostatic repulsion between the carboxylate ions in bis-deprotonated maleic acid is expected to be higher due to their proximity (4.36 Å) than the corresponding fumaric acid (5.25 Å). The calculated results show that the occurrence of the different forms of these acids is greatly influenced by the pH of the reaction medium. To examine the calculated results better, we evaluated the

fractional distribution curves using reported experimental pK_a values for fumaric and maleic acids[24] (Figure 3.12). These curves revealed that the formation of α_1 (mono-deprotonated form) and α_2 (bis-deprotonated form) of fumaric and maleic acid at different pH range.

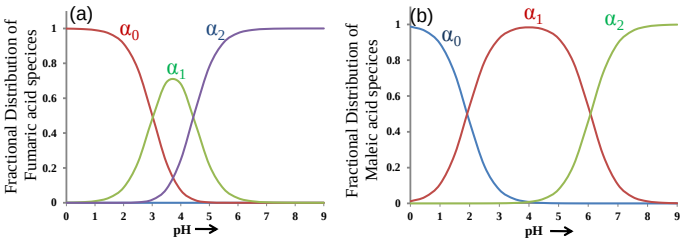

Figure 3.12. Fractional distributions of the various forms of (a) fumaric acid and (b) maleic acid that was calculated using the p*K*a values are plotted as a function of pH value.

It is evident from Figure 3.12 that the deprotonated forms of these two acids vary with respect to the pH of the medium. This clearly reveals that at pH 6 maleic acid exist as an equilibrium mixture of mono and bis-deprotonated forms, whereas fumaric acid exists almost exclusively in bis-deprotonated form. Further, both of the diacids exist as bis-deprotonated forms at pH 7.4. These results suggest that at pH 6, the existence of bis-deprotonated form of fumaric acid is appreciable compared to maleic acid.

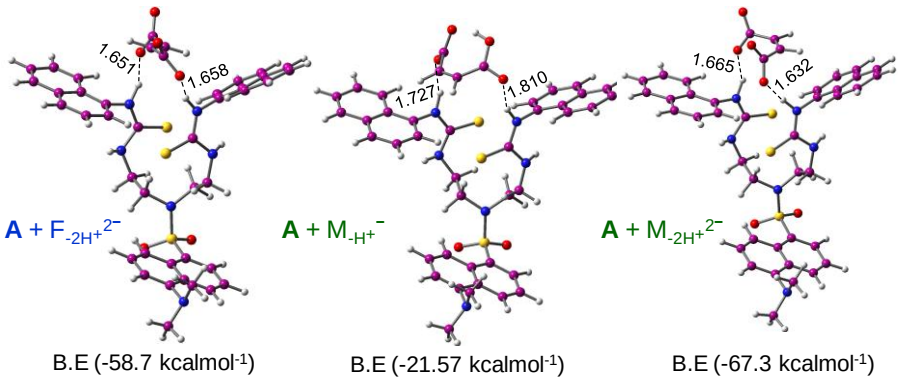

Figure 3.13. RHF/PM3 optimized complex geometries for probe **A** with Fum^{2-} and **A** with $Male^{1-}$ and $Male^{2-}$ in gas phase. Binding energies are calculated at B3LYP/6-31G* level using the RHF/PM3 level optimized complex geometries. Distances are given in Å. (Atom colour code: red = oxygen, blue = nitrogen, white = hydrogen, yellow = sulphur, dark magenta = carbon).

In earlier studies, it has been reported that all the four hydrogen atoms of thiourea in anthraquinone based anion receptors are involved for binding with the acid anion.[7i] However, the optimized geometry of probe **A** illustrates a different picture and it shows that only one set of thiourea–N_1H protons (adjacent to naphthyl rings) are oriented in such a way that they can participate in hydrogen bonding interactions with the diacids (Figure 3.13). The other thiourea–N_2H protons are not appropriately oriented or positioned for such interactions with analytes.

Experimental studies clearly revealed that these analytes showed a marked difference in binding with **A** at pH 6. Hence, we have examined the binding energies of fumaric and maleic acid with B3LYP/6-31G*//RHF/PM3 level of theory. The fraction distribution curves reveal that maleic acid exists in mono- and bis-deprotonated forms at pH 6 though reasonably in lower concentrations than the case of fumaric acid, which is predominantly present in bis-deprotonated form. The binding energy calculated of bis-deprotonated fumaric acid with **A** shows that the analyte interacts quite efficiently (-58.7 kcal/mol).

The higher binding energy of the bis-deprotonated fumaric acid with probe **A** arise due to the interaction of two -N_1H groups adjacent to the naphthyl ring via strong hydrogen bonding with the two carboxylate oxygens of the analyte (Figure 3.13). In the case of mono-deprotonated maleic acid, weaker interaction has been predicted with the probe **A** (-21.6 kcal/mol), however, the bis-protonated form showed a much stronger interaction (-67.3 kcal/mol) with the receptor molecule **A**. The binding mode of the deprotonated maleic acid is similar to that of fumaric acid (Figure 3.13). Therefore, it appears that the fluorescence titration would have given the higher binding energy of maleic acid with **A** as observed in the case of fumaric acid at pH 6. The binding affinity of maleic acid is compromised due to the presence of both mono- and bis-deprotonated forms under this pH condition, where, both the forms can have the affinity to bind with probe **A**. The binding mode of these analytes with **A** was

found to be in agreement with the observed experimental ^{1}H NMR titration results. The downfield shifts of -N_1H protons are relatively more than the -N_2H protons upon addition of fumaric acid and maleic acid to probe **A**, which confirms that the all thiourea protons have not participated in binding with analytes.

Thus, this chapter reveals that a thiourea based receptor **A** designed for recognition of fumaric and maleic acids based on FRET based fluorescence off response. Experimentally observed preferences of the receptor **A** towards mono- and bis-deprotonated species of maleic and fumaric acids at different media pH could be rationalized based on the quantum chemical calculations. More importantly, this reagent could even be used for quantitative estimation of fumaric acid in commercially available nectar and such result was further validated by results of the HPLC studies. Design of the receptor **A** enabled us to probe the binding processes through changes in solution fluorescence, which was initiated by a PET coupled FRET response. This was ascertained by comparing optical responses of the receptor **A** with analogous model compounds **B** and R. To the best of our knowledge, this is the first report that describes the specific detection and estimation of on the fumaric acid in any commercial juice.

3.5. References

1. D. Voet and J. G. Voet, Biochemistry, 2nd ed.; Wiley: New York., 1995.

2. (a) H. Nohta, J. Sonoda, H. Yoshida, H. Satozono, J. Ishida and Yamaguchi, *M. J. Chromatogr A*., 2003, **1010**, 37; (b) V. Kra´l, A. Andrievsky and J. L. Sessler, *J. Am. Chem. Soc*., 1995, **117**, 2953.

3. C. Ricke, *Poultry Science*., 2003, **82**, 632.

4. D. M. Khiabani, A. Blank, T. Skripuletz, E. Miller, A. Kotsiari, V. Gudi and M. Stangel, *PLoS ONE*., 2010, **5**, e11769.

5. (a) J. Stepinski, D. Pawlowska and S. Angielski, *Acta Biochim. Pol*., 1984, **31**, 229; (b) A. Gougoux, G. Lemieux and N. Lavoie, *Am. J. Physiol*., 1976, **231**, 1010; (c) S. Eiamong, M. Spohn, N. A. Kurtzman and S. Sabatini, *Kidney Int*., 1995, **48**, 1542.

6. P. J Altmeyer, U. Matthes, F. Pawlak, K. Hoffmann, P. J Frosch, P. Ruppert and S. W. Wassilew, *J Am Acad Dermatol*.,1994, **30**, 977.

7. (a) E. Fan, S. A.V. Arman, S. Kincaid and A. D. Hamilton, *J. Am. Chem. Soc*., 1993, **115**, 369; (b) T. R. Kelly and M. H. Kim, *J. Am. Chem. Soc*., 1994, **116**, 7072; (c) J. M. Benito, M. G´omez-Garc´ıa, J. L. J. Blanco, C. O. Mellet and J. M. G. Fern´andez, *J. Org. Chem*., 2001, **66**, 1366; (d) S.-Y. Liu, L. Fang, Y.-B. He, W.-H. Chan, K.-T.Yeung, Y.-K.Cheng and R.-H. Yang, *Org. Lett*., 2005, **7**, 5825; (e) M. H. Mei and S. K. Wu, *New J. Chem*., 2001, **25**, 471; (f) Y.-P. Yen and K.-W. Ho, *Tetrahedron Lett*., 2006, **47**, 7357; (g) Z. H. Lin, L. X. Xie, Y. G. Zhao, C. Y. Duan and J. P. Qu, *Org. Biomol. Chem*., 2007, **5**, 3535; (h) A. M. Costero, M. Colera, P. Gavin˜a and S. Gil, *Chem. Commun*., 2006, 761; (i) Y. P. Tseng, G. M. Tu, C. H. Lin, C. T. Chang, C. Y. Lin and Y. P. Yen, *Org. Biomol. Chem.*, 2007, **5**, 3592; (j) Y.-S. Lin, G.-M. Tu, C.-Y. Lin, Y.-T. Chang and Y.-P. Yen, *New J. Chem*., 2009, **33**, 860; (k) M. B. Jim´enez, V. Alca´zar, R. Pela´ez, F. Sanz, A. L. F. Arriba and M. C. Caballero, *Org. Biomol. Chem.*, 2012, **10**, 1181; (l) T. Gunnlaugsson, A. P. Davis, J. E. O'Brien and M. Glynn, *Org*. *Biomol. Chem.*, 2005, **3**, 48.

8. S. Goswami, K. Ghosh and S. Dasgupta, *J. Org. Chem*., 2000, **65**, 1907.

9. (a) J. Raker and T. E. Glass, *J. Org. Chem.*, 2002, **67**, 6113; (b) A. Metzger and E. V. Anslyn, *Angew. Chem. Int. Ed*., 1998, **37**, 649; (c) J. J. Lavigne and E. V. Anslyn, *Angew. Chem. Int. Ed*., 1999, **38**, 3666.

10. (a) D. A. Jose, I. Mon, H. F. Perez, E. C. E. Adan, J. B. Buchholz and A. V. Ferran, *Org. Lett*., 2011, **13**, 3632; (b) M. Takeuchi, T. Imada and S. Shinkai, *Angew. Chem. Int. Ed*., 1998, **37**, 2096; (c) T. Ikeda, O. Hirata, M. Takeuchi and S. Shinkai, *J. Am. Chem. Soc*., 2006, **128**, 16008.

11. (a) M. Hu and G. Feng, *Chem. Commun*., 2012, **48**, 6951; (b) L. Tang, J. Park, H- J. Kim, Y. Kim, S. J. Kim, J. Chin and K. M. Kim, *J. Am. Chem. Soc*., 2008, **130**, 12606; (c) L. Fabbrizzi, M. Licchelli and A. Taglietti, *Dalton Trans*., 2003, 3471; (d) F. Li, S. Carvalho, R. Delgado, M. G. B. Drew and V. Félix, *Dalton Trans*., 2010, **39**, 9579.

12. (a) K. Ghosh and T. Sen, *J. Phys. Chem. B*., 2011, **115**, 8597; (b) F. Sanceno´n, R. Martı´nez-Ma´n˜ez, M. A. Miranda, M.-J. Segu and J. Soto, *Angew. Chem*., 2003, **115**, 671; (c) P. Mateus, R. Delgado, P. Brandão and V. Félix, *J. Org. Chem.*, 2012,**77**, 4611.

13. V. Gokmen and J. Acar*, Food Additives and Contaminants*., 2004, **21**, 626.

14. (a) S. O. Kang, D. Powell, V. W. Day and K. Bowman-James, *Angew. Chem. Int. Ed*., 2006, **45**, 1921; (b) P. Das, A. Ghosh and A. Das, *Inorg. Chem*., 2010, **49**, 6909.

15. (a) J. Guy, K. Caron, S. Dufresne, S. W. Michnick, W. G. Skene and J. W. Keillor, *J. Am. Chem. Soc*., 2007, **129**, 11969; (b) P. Das, M. K. Kesharwani, A. K. Mandal, E. Suresh, B. Ganguly and A. Das, *Org. Biomol. Chem*., 2012, **10**, 2263.

16. Spartan'06, Wave function Inc.: Irvine, California.

17. J. J. P. Stewart, *J. Comp. Chem*., 1989, **10**, 209.

18. M. J. Frisch, G. W. Trucks, H. B. Schlegel, G. E. Scuseria, M. A. Robb, J. R. Cheeseman, J. A. Montgomery, Jr., T. Vreven, K. N. Kudin, J. C. Burant, J. M. Millam, S. S. Iyengar, J.Tomasi, V. Barone, B. Mennucci, M. Cossi, G. Scalmani, N. Rega, G. A. Petersson, H. Nakatsuji, M. Hada, M. Ehara, K. Toyota, R. Fukuda, J. Hasegawa, M. Ishida, T. Nakajima, Y. Honda, O. Kitao, H. Nakai, M. Klene, X. Li, J. E. Knox, H. P. Hratchian, J. B. Cross, V. Bakken, C. Adamo, J. Jaramillo, R. Gomperts, R. E. Stratmann, O. Yazyev, A. J. Austin, R. Cammi, C. Pomelli, J. W. Ochterski, P. Y. Ayala, K. Morokuma, G. A. Voth, P. Salvador, J. J. Dannenberg, V. G. Zakrzewski, S. Dapprich, A. D. Daniels, M. C. Strain, O. Farkas, D. K. Malick, A. D. Rabuck, K. Raghavachari, J. B. Foresman, J. V. Ortiz, Q. Cui, A. G. Baboul, S. Clifford, J. Cioslowski, B. B. Stefanov, G. Liu, A. Liashenko, P. Piskorz, I. Komaromi, R. L. Martin, D. J. Fox, T. Keith, M. A. Al-Laham, C. Y. Peng, A. Nanayakkara, M. Challacombe, P. M. W. Gill, B. Johnson, W. Chen, M. W. Wong, C. Gonzalez and J. A. Pople, Gaussian 03, Revision E.01, Gaussian, Inc., Wallingford CT, **2004**.

19. (*a*) A. D. Becke, *J. Chem. Phys*., 1993, ***98***, 5648; (*b*) C. Lee, W. Yang and R. G. Parr, *Phys.Rev. B*, 1988, **37**, 785; (*c*) W. J. Hehre, L. Radom, P. v. R Schleyer and J. A. Pople, *Abinitio Molecular Orbital Theory*, Wiley, New York, **1988**.

20. L. Stryer and R. P. Haugl, *Proc. Natl. Acad. Sci. USA*., 1967, **58**, 719.

21. (a) D. A. Jose, D. K. Kumar, P. Kar, S. Verma, A. Ghosh, B. Ganguly, H. N. Ghosh and A. Das, Tetrahedron., 2007, **63**, 12007; (b) D. A. Jose, A. Singh, A. Das and B. Ganguly, *Tetrahedron Letters*, 2007, **48**, 3695; (c) A. Ghosh, B. Ganguly, and A. Das, *Inorg. Chem*., 2007, **46**, 9912; (d) A. Ghosh, S. Verma, B. Ganguly, H. N. Ghosh and A. Das, Eur. *J. Inorg. Chem*., 2009, 2496.

22. C. E. Justin and R. B Beelman, *Journal of Food Protection*., 2002, **65**, 476.

23. J. Acar, V. Gökmen and E. E. Taydas*, Eur Food Res Technol*., 1999, **209**, 308.

24. (a) D. A. Skoog, D. M. West, F. J. Holler and S. R. Crouch, *Analytical Chemistry An Introduction*, Pub:-Holt, Rinehart and Winston, 7th ed., 1965, 317; (b) A. Sen and B. Ganguly, *Angew. Chem*. Int. Ed., 2012, **51**, 11279.

CHAPTER 4

METAL BASED RECEPTOR FOR CYSTEINE AND HISTIDINE: RECOGNITION STUDIES UNDER PHYSIOLOGICAL CONDITION, IN HUMAN BLOOD PLASMA AND IMAGING OF ENDOGENOUS CYSTEINE IN LIVE HCT116 CELLS

Publication:
Chem.Commun., 2014, ***50***, 9899-9902

4.1. Introduction

Thiol-containing small molecules such as cysteine (Cys), homocysteine (Hcy), and glutathione (GSH) play key roles in living organism. These key amino acids are also useful biomarkers for early stage detection of some crucial diseases or physiological processes.[1] Abnormal level of cellular thiols have been linked to a number of diseases, such as leucocyte loss, psoriasis, liver damage, cancer, and AIDS.[2-4] Among the twenty amino acids commonly found in proteins, two thiol based amino acids (cysteine (Cys) and histidine (His)) are of immense significance, as these play vital roles in many critical bioactivities.[5] Cys acts as an intracellular redox buffer that influences detoxification and critical metabolic functions.[6] Deficiency in Cys causes oxidative damage, haematopoiesis, psoriasis, leukocyte loss and metabolic disorders.[7] A higher level of Cys in the human blood plasma (HBP) is known to cause cardiovascular and Alzheimer's diseases. Moreover, the total cellular Cys concentration is significantly related with a high risk of a wide variety of tumor progressions.[8] His can act as a neurotransmitter in the central nervous system of mammals. Its deficiency could affect the human growth factor and may cause the impaired nutritional state of patients with chronic kidney disease.[9] A higher level of His could cause metabolic disorders like histidinemia.[10] The respective concentration level of Cys and His in human plasma is typically 240-360 μM and 15-75 μM.[11] Accordingly, detection of these biomolecules in biological fluids is very important to understand the role of these in the pathogenesis of vascular diseases. HPLC,[12] capillary electrophoresis,[13] and gas chromatography[14] are most common determination techniques for estimation of Cys in human plasma and urine. However, all these methodologies involve intricate sample preparation and use of expensive instrumentation techniques. Cys possesses a very low molar extinction coefficient and lacks a suitable chromophore for spectrometric detection in the detector used for HPLC methods and this led to the use of post derivatizaton of the Cys with suitable

Uv-active chromophore prior to the detection process. More recently, fluorescence based chemodosimetric reagents and electrochemical methods are being used.[15] Fluorescent-labeling reagents contain a functional group, e.g., N-substituted maleimide, reactive halide or aziridine, which reacts with the thiol group in general with an associated modified luminescence response.[16] These methods are widely used in both research and clinical analysis. However, one drawback of these agents is the lack of any selectivity among various thiols, and thus not specific to Cys. Recent studies have focused on the development of direct fluorescent methods for the detection of Cys and other biological thiols, aiming at high sensitivity, higher sensitivity as well as developing an imaging reagent for detection of the cellular uptake of the analyte with spatial resolution and suitability as a fluorescent tag for labeling or as an imaging tool for diagnostics.[17]

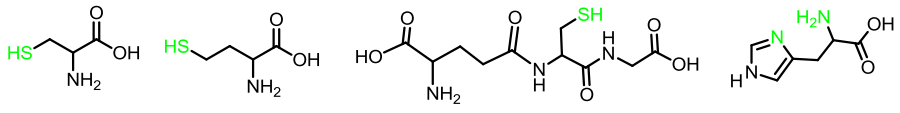

Figure 4.1. Molecular structures of Cysteine (Cys), Homocysteine (Hcy), Glutathione (GSH) and Histidine (His) with their respective pK$_a$ value.

Numbers of thiol-specific chemodosimetric probes have been developed on the basis of various strategies. Examples of molecular probes that could specifically detect Cys, even in the presence of Hcy and GSH, under pure physiological conditions are scanty due to the similarities in their structural and reactivity properties. However, Cys has a lower pK$_a$ value (8.30) than those of Hcy (8.87) and GSH (9.20).[18] Under physiological conditions at pH 7.4, His is expected to exist predominantly in its thiolate from, while a certain fraction of Cys is also expected to be present in this thiolate form, which becomes a better nucleophile than the corresponding thiol form. Apart from this, the thiol group in Cys is sterically less hindered than those of Hcy and GSH.[18] By utilising these two advantages, we designed a new Cu(II)-based

receptor, that showed luminescence ON response on specific recognition of Cys and His in an ensemble of several other amino acids.

4.2. Experimental Section

4.2.1. Materials

Dansyl chloride, Hydrazine monohydrate (98%), Phthalic anhydride, 2-Pyridinecarboxaldehyde, Sodium triacetoxyborohydride, Copper(II) perchlorate hexahydrate were obtained from Sigma Aldrich and were used as received. Cysteine, Histidine, Glutathione, Arginine, iso-Leucine, Proline, Methionine, Glycine, Alanine, Serine, Threonine, Tryptophan, Tyrosine, Valine, Leucine were purchased from SD Fine Chemicals in India. Solvents used for synthesis of various intermediates and final compounds were of AR grade (S.D. Fine Chemicals) and were used as received without further purification. HPLC grade (S.D. Fine Chemicals) solvents were used for various spectroscopic studies.

4.2.2. Analytical Methods

^{1}H NMR spectra were recorded on a Bruker 500 MHz FT NMR (Model: Avance-DPX 500) using $CDCl_3$ as the solvent and tetra methyl silane (TMS) as an internal standard. ESI-Ms measurements were carried out on a Waters QTof-Micro instrument. Uv spectra's was recorded with a Shimadzu UV-3101 PC spectrophotometer; while fluorescence spectra were recorded using an Edinburgh instrument Xe 900 spectrofluorometer.

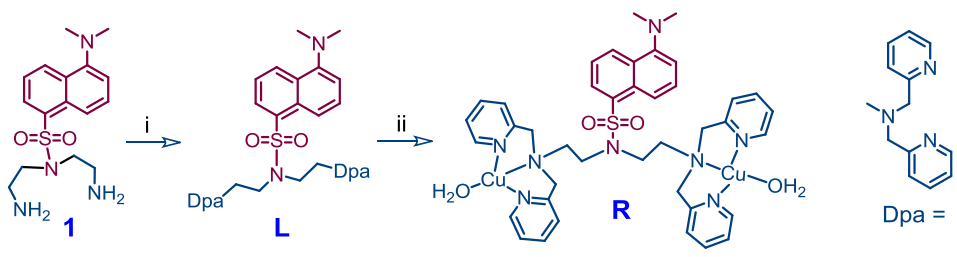

i. 2-Pyridine carboxyldehyde, $NaBH(OAC)_3$, 1,2-Dichloroethane, RT, 48 h.; ii.$Cu(ClO_4)_2.H_2O$, MeOH, RT, 8h.

Scheme 1. Methodologies that were adopted for synthesis of **1**, **L** and **R**.

4.2.3. General experimental procedure for UV-Vis and Fluorescence studies

1.0×10^{-4} M, solution of the **L** in aq. HEPES buffer: CH_3CN (96:4, v/v) and **R** in pure aq.HEPES buffer medium was prepared and stored in dark. This solution was used for all spectroscopic studies after appropriate dilution. Aq. HEPES buffer (10 mM for maintaining pH 7.4) was used for all spectroscopic studies unless mentioned otherwise. Amino acid solutions (1.0×10^{-2} M) were prepared in 10 mM HEPES buffer (pH 7.4) medium. Solution of the compound **R** was further diluted for spectroscopic titrations, and the effective final concentration of compound **R**, used for the fluorescence studies, was 2.0×10^{-5} M; while, the final [Cys] during emission spectral scanning was 4.0×10^{-3} M. For all luminescence measurements, λ_{Ext} = 350 nm with an emission slit width of 3 nm. The relative fluorescence quantum yields (Φ_f) were estimated (using an equation that is discussed in the previous chapter) in acetonitrile medium by using the integrated emission intensity of dansyl amide (Φ_f = 0.37) for **L** and **R** as a reference.[19]

4.2.4. Cell culture and fluorescence imaging

Hct116 cells (3×10^5) were seeded on cover slips placed in 6 well plates. After 24 hours cells were treated with **R** (10 µM) for 30 minutes or pre-treated with N-ethyl maleimide (NEM, a thiol specific blocking reagent (1 mM) for 30 minutes before adding **R** (10 µM) for 30 minutes. Cells were then washed thrice with Phosphate Buffer Saline (1X PBS) and fixed with 4% PFA for 20 minutes and washed again with 1X PBS. Permeabilization of the cells was done using 0.2% Triton X 100 for 5 minutes. Again three washes were given and then cover slips mounted using Fluor shield with DAPI (Sigma) mounting medium. Nail paints was used to seal the cover slips mounted on the glass slides. Images were acquired in Olympus Fluoview Microscope.

The *in-vitro* cytotoxicity of **R** on Hct116 cells (Colon cancer cells) were determined by conventional MTT (3-(4,5-Dimethylthiazol-2-yl)-2,5-diphenyltetrazolium bromide, a yellow tetrazole) assay. Hct116 colon cancer cells (7×10^3) were seeded in each well of a 96 well plate and cultured in a 37°C incubator supplied with 5% CO_2. Cells were maintained in DMEM medium, supplemented with 10% Fetal Bovine Serum and 100 Units of Penicillin Streptomycin antibiotics. After 24 hours the cells were treated with different concentrations of the **R** in triplicates for 12 hours. After treatment cells were added with 0.5 µg/ml of MTT reagent. The plate was then incubated for 4 hours at 37°C and then later added to each well with 100 µl of Isopropyl Alcohol. The optical density was measured at 570 nm using Multiskan Go (Thermo Scientific) to find the concentration of the cell inhibition. IC_{50} value has been calculated to be 200 µM. Formula used for the calculation of the MTT assay for evaluation of the cell viability is as follows:

Cell viability (%) = (means of Absorbance value of treated group/ means of Absorbance value of untreated control) X 100.

4.2.5. Determination of detection limit[22]

The detection limit was calculated based on the fluorescence titration. To determine the S/N ratio, the emission intensity of **R** without Cys was measured by 10 times and the standard deviation of blank measurements was determined. The detection limit (DL) of **R** for Cys was determined from the following equation:

$DL = K * Sb_1/S$

where, K = 2 or 3 (we take 2 in this case); Sb_1 is the standard deviation of the blank solution; S is the slope of the calibration curve. From the graph we get slope = 4.85×10^4, and Sb_1 value is 0.0004. Thus using the formula we get the Detection Limit = 1.64×10^{-8} M.

4.2.6. Pre-treatment of human blood plasma sample for estimation of C_{Cys} & C_{His}

Fresh and human blood samples (5 mL) with added lithium anticoagulant were centrifuged in a vacutainer tube at 3000 rpm for 15 min. The supernatant solution (plasma), which contains proteins and amino acids, was collected. 2 ml of collected plasma was vigorously mixed with appropriate amount of $NaBH_4$ and incubated for 5 minutes at room temperature in order to hydrolyse the disulphide bond. Various protein residues present in the sample after reduction were precipitated by the addition of methanol, followed by centrifugation (18,500g) of the sample for 15 minutes. The supernatant liquid, which contained Cys and His in blood plasma, was used for the spectroscopic studies.

4.3. Synthesis and Characterisation

4.3.1. Synthesis of 1

Synthetic procedure that was adopted for synthesis of **1** from our previous report.[19]

4.3.2. Synthesis of L

Synthetic procedure was adopted from a previous report and was further modified for synthesis of the reagent **L**.[20] Compound **1** (210 mg, 0.625 mmol) and 2-pyridinecarboxaldehyde (401 mg, 3.75 mmol) were dissolved in 7 ml of 1,2-dichloroethane and refluxed it for 1 hr. To this reaction mixture, Sodium triacetoxyborohydride (791 mg, 3.75 mmol) in 1,2-dichloroethane (10 mL) was added. The reaction mixture was allowed to stirr at room temperature for 48 h. Progress of the reaction was monitored by checking the TLC. The reaction mixture was treated with saturated aq. $NaHCO_3$ solution and subsequent extraction was performed with chloroform. The organic layer was recovered, dried over anhydrous Na_2SO_4 and concentrated under reduced pressure. The crude product was subjected to neutral alumina gel chromatography using $CHCl_3$:CH_3OH (99.5: 0.5, v/v) as eluent.

Major fraction was collected and dried under vacuum, which afforded pure product as a sticky oil. Yield: 270 mg, 61.78 %. ESI- Ms (m/z) calculated for $C_{40}H_{44}N_8O_2S$: 700, observed: 701 [M + H^+]. ^{1}H NMR [500 MHz, $CDCl_3$: δ (ppm)]: 8.46 (5H, d, *J* = 4.0 Hz, ArH); 8.18 (1H, d, *J* = 8.5 Hz, ArH); 8.10 (1H, d, *J* = 6.5 Hz, ArH); 7.59 (4H, t, *J* = 8.0 Hz, ArH); 7.47-7.44 (1H, m , ArH);7.39 (5H, t, *J* = 12 Hz, ArH); 7.15-7.10 (5H, ArH); 3.67 (8H, s, CH_2); 3.39 (4H, t, *J* = 7.0 Hz, CH_2); 2.77 (6H, s, CH_3); 2.54 (4H, t, *J* = 7.0 Hz, CH_2). ^{13}C NMR (125 MHz, $CDCl_3$, δ (ppm)): 173.60, 164.71, 161.18, 145.80, 138.00, 137, 135.17, 129.00, 127.74, 124.24, 119, 50.24, 40.17, 32 and 31.60.

4.3.3. Synthesis of R[21]

The compound **L** (120 mg, 0.17 mmol) was dissolved in 7.5 mL methanol; to this $Cu(ClO_4)_2.6H_2O$ (126 mg, 0.342 mml) was added. Solution colour was changed immediately. The reaction mixture was stirred for 8 h and then transferred into a beaker and allowed to evaporation at room temperature to precipitate the desired compound. A previous reported procedure was adopted for synthesis of this reagent **R**.[21] Light bluish white solid compound was isolated through filtration and was further carefully washed with cold Dichloromethane. Yield 120 mg, 42.25%. ESI-Ms (m/z) calculated for $C_{40}H_{44}Cu_2N_8.2H_2O$: 862, observed: 863 [M+$H^+$].

4.4. Results and Discussions

The UV-vis spectrum of **L** (Figure 1a) is showed Figure 4.2. This clearly revealed two distinct bands at 256 and 329 nm. The band at 256 nm was attributed to a charge transfer (CT) transition involving N-amine as a donor and a dansyl moiety as an acceptor. The other band at 329 nm was ascribed to a dansyl-based CT transition.[19] These two bands for **R** appeared at 252 and 324 nm, respectively. Observed blue shifts in **R** were ascribed to a less favoured CT process, as compared to those in **L** (Figure 4.2). All studies with **L** were performed in the aqueous HEPES buffer-

acetonitrile (96: 4, v/v; pH 7.4) medium, while studies with **R** were performed in pure aq.HEPES buffer (pH 7.4) medium.

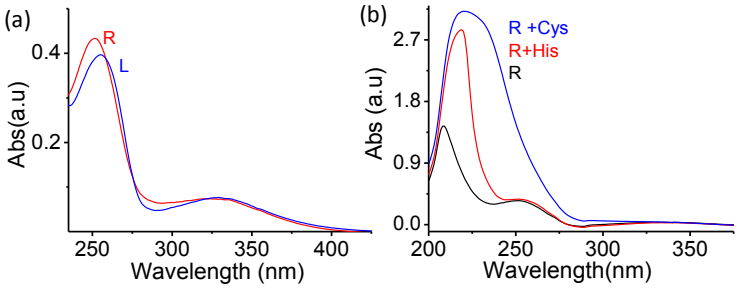

Figure 4.2. (a) Absorbance spectra of **L** (20 μM) and **R** (20 μM); (b) Absorbance spectra of **R** (20 μM) in presence of His & Cys. All studies were performed in aq. HEPES buffer medium (10 mM, pH 7.4).

Electronic spectra recorded for **R** in the presence of Cys and His were little different, which signified a distinct difference in the nature of interaction between the Cu (II)-centre in **R** and Cys or His (Figure 4.2(b)). Fluorescence responses of **L** (20 μM) towards Cu^{2+} in aq.HEPES buffer-CH_3CN (96:4 v/v; pH 7.4, RT) medium are shown in Figure 4.3. Upon excitation at 350 nm, compound **L** showed strong emission band at λ_{max} of 552 nm. The relative emission quantum yield (Φ_L) for **L** in buffer (pH 7.6) medium was found to be 0.068, using dansyl amide as a standard.[19] Upon addition of Cu^{2+} to the solution of **L**, hypsochromic shift ($\Delta\lambda_F$) of 52 nm in emission maxima was observed with anticipated quenching of the dansyl-based fluorescence. This luminescence quenching was attributed to the binding to the Cu^{2+}-centre (d^9).[21] A very weak emission band with λ_{Max} of ~ 500 nm was assigned to a new CT-based process on formation of a bis-Cu(II) complex (Figure 4.3.a). Systematic luminescence titrations were carried out for **L** (20 μM) with varying [Cu^{2+}] (0 to 46 μM) in aq. HEPES buffer:acetonitrile (96:4, v/v; pH 7.4) medium using λ_{Ext} of 350 nm and λ_{Mon} of 552 nm. A gradual decrease in emission intensity at 552 nm was observed upon addition Cu^{2+} solution (Figure 4.3.b). This was also confirmed from

the data obtained from the ESI-MS analysis, signal appeared at m/z of 863.2952 was attributed to [**L**.2Cu.2H_2O+H^+].

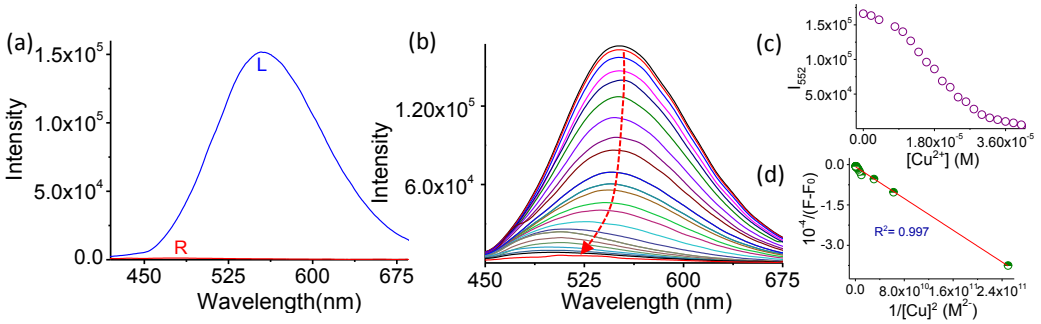

Figure 4.3. (a) Emission spectra of **L** (20 μM) and R; (b) Emission spectra of **L** in the presence of varying [$Cu(ClO_4)_2$] (0 to 4.6 x 10^{-5} M); (c) B-H plot for **L** (20 μM) with varying [Cu^{2+}] (0 to 46 μM) λ_{Ext} = 350 and λ_{Mon} = 552 nm. Good linear fit confirms the 1:2 binding stoichiometry; (d) Luminescence titration profile. All studies were performed in aq.-HEPES buffer-CH_3CN (96: 4, v/v; 10 mM, pH 7.4) medium. (λ_{Ext} = 350 nm; slit width 3/3 nm).

Luminescence spectra of the receptor **R** (20 μM) in the absence and presence of 200 mole equivalent of various aminoacids such as tryptophan (Trp), leucine (Leu), isoleucine (Ile), methionine (Met), threonine (Thr), tyrosine (Tyr), valine (Val), alanine (Ala), serine (Ser), glycine (Gly), cysteine (Cys), Glutathione (GSH), homocysteine (Hcy), proline (Pro) and arginine (Arg) in buffer media (pH 7.6) were recorded to examine the luminescence response of this receptor towards different and physiologically significant aminoacids (Figure 4.4). The high selectivity of Cys over other thiols could be attributed to the low pK_a of value of the thiol group in Cys is 8.00, which is lower than those for Hcy (8.87) and GSH (9.20). At this pH, Cys exists predominantly in its thiolate form and thus acts as a better coordinating ligand for Cu(II) than other biothiols. These studies clearly revealed that an increase in emission intensity was observed at 552 nm when Cys or His was added to the aq.-buffer solution of **R**. Other thio-amino acids, especially Hcy and GSH could not induce any change in emission spectral pattern. This result is significant, as Hcy or/and GSH generally interfere with the Cys detection. Further the discrimination in

between Cys and His was achieved by the thiol specific reagent n-ethyl malemide (NEM).

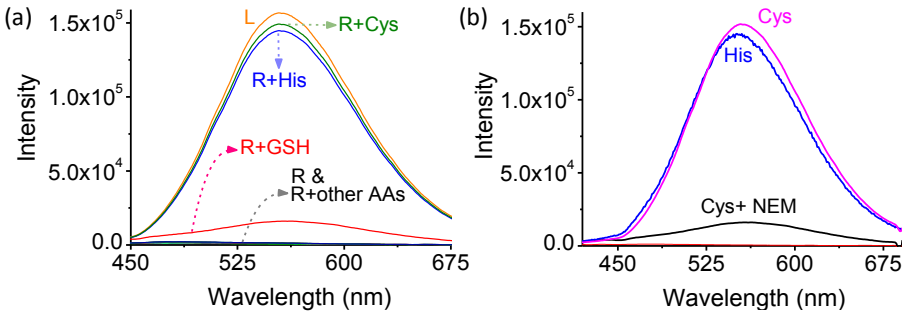

Figure 4.4. (a) Luminescence spectra of **R** (20 μM) in the absence and presence of various amino acids (AAs); e.g. tryptophan (Trp), leucine (Leu), isoleucine (Ile), methionine (Met), threonine (Thr), tyrosine (Tyr), valine (Val), alanine (Ala), serine (Ser), glycine (Gly), cysteine (Cys), glutathione (GSH), homocysteine (Hcy), proline (Pro) and arginine (Arg); (b) Luminescence spectra of **R** in absence and presence of Cys, His and Cys+NEM.

Systematic luminescence titrations were carried out for **R** (20 μM) with varying [Cys] (0 to 2.8 x 10^{-3} M) and [His] (0 to 3.2 x 10^{-3} M) in pure aq.HEPES buffer medium (10 mM, pH 7.4). Increase in [Cys] or [His] caused a concomitant increase in emission intensity at ~ 552 nm (Figure 4.5). Titration profiles revealed linear range of 90 - 2800 μM and 200 - 3200 μM, for Cys and His, respectively

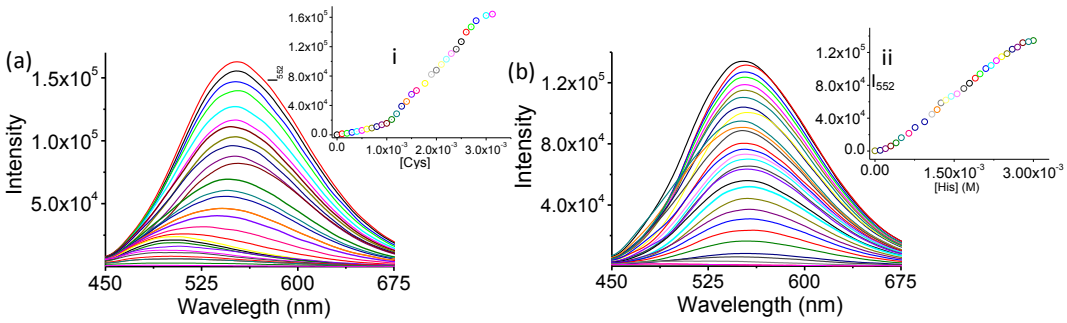

Figure 4.5.Changes in luminescence spectra of **R** (20 μM) in the presence of varying (a) [Cys] (0 - 2.8 x 10^{-3} M) and (b) [His] (0 - 3.2 x 10^{-3} M); Insets titration profiles of (i) Cysteine (Cys) and (ii) Histidine (His). All studies were performed in pure aq.HEPES buffer (10 mM, pH 7.4) medium using λ_{Ext} = 350 nm; slit width 3/3 nm.

. The fluorescence changes shown in Figure 4.5 for Cys involved several competing equilibriums and it was not possible to evaluate equilibrium constant for each individual process. However, a B-H plot for emission titration with varying [His]

(Figure 4.5) helped us to evaluate the binding constant ($K_{R.2His}$ = (1.4 ± 0.03) x 10^4 M^{-2}) for the formation of **L** $(Cu^{II}\text{-His})_2$ (Scheme 2).

The emission enhancement observed upon binding of Cu(II) centres in **R** to His could be explained based on the much weaker and elongated Cu^{II}–N_{Amine} bond in **L** $(Cu^{II}\text{–His})_2$ as compared to that in (Scheme 2). Such an elongation of the metal–N_{Amine} bond with a consequential fluorescence enhancement has been reported earlier for other Cu(II) complexes upon binding to an anionic analyte.[22] This effectively nullifies the quenching influence induced by the d^9 Cu(II)-centre induced by the d^9 Cu(II)-centre. The emission spectral pattern of **R** was found to be invariant for the pH range of 3 - 12.

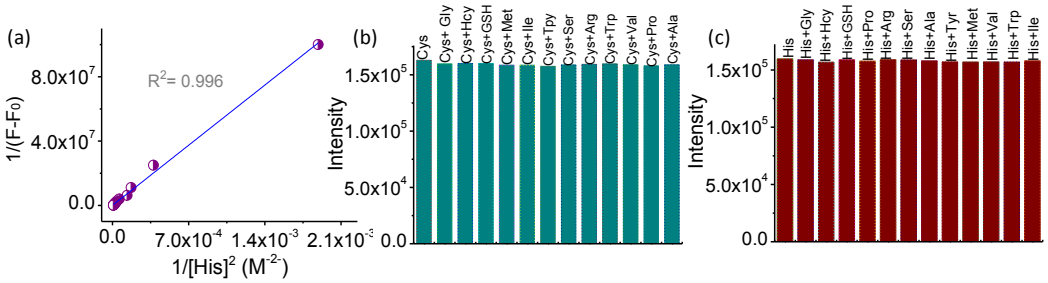

Figure 4.6. (a) Benesi-Hildebrand plot of **R** (20 μM) for varying [His] (0 to 3.2x 10^{-3} M) λ_{Ext} = 350 and λ_{Mon} = 552 nm. Good linear fit confirms the 1: 2 binding stoichiometry in aq.-HEPES (10 mM, pH 7.4) medium. (b) Spectrophotometric interference study of **R** (20 μM) with (a) Cys (2.8 x 10^{-3}M) (b) Histidine (2.8x 10^{-3}) M in presence of various amino acids (2.8 x 10^{-4}M) in HEPES buffer by using λ_{Ext} = 350 and λ_{Mon} = 552 nm.

To examine the spectrophotometric interference study of **R** (20 μM) with Cys/His in presence of various amino acids were performed in HEPES buffer by using λ_{Ext} = 350 and λ_{Mon} = 552 nm. In order to understand the mechanism, we have been recorded X-band EPR spectra of **R** in the absence and presence of Cys and His in aq. Buffer medium (Figure 4.7). For **R**, solution spectra were isotropic with g_{av} = 2.099. **R** in presence of His, the X-band EPR spectrum of the copper complex showed well-resolved four-line hyperfine splitting in the frozen state at 77 K. The g values with $g_{||} > g_{\perp} > 2.0023$ indicate that an unpaired electron resides predominantly in the $dx^2\text{-}y^2$ orbital with the copper centre is in axial symmetry ($g_{||}$, $g_{\perp}$ and $A_{||}$ values are 2.230,

2.035 and 166.2 x 10^{-4} cm-1, respectively).[23] The absence of any band corresponding to ms = ± 2 transition and the value of G ($g_{||}$-2/ $g_{\perp}$-2) rule out any Cu--Cu interaction in the complex. The $g_{||}$/ $A_{||}$ value is considered as an empirical index of tetrahedral distortion for copper complexes of N, O, and S donor ligands. This ratio for the present complex is 134 cm, typical of square-planar geometry without any tetrahedral distortion. The spectral parameters further indicate the presence of significant covalent bonding in the complex. Affinity of Cu(II) to form mixed ligand coordination complexes with His is well documented and this presumably supports the formation of **L** (Cu^{II}–His)$_2$ (Scheme 2).[24] Interestingly, the EPR spectrum recorded for **R** in the presence of Cys was significantly different. Cu^{2+} is known to be reduced to Cu^{+} by Cys with stoichiometric production of cystine.[24]

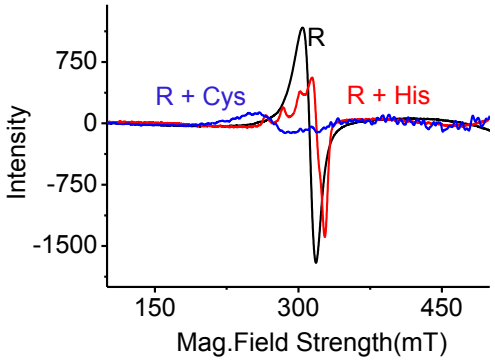

Figure 4.7. X-band EPR spectrum of probe **R** (1.0 mM) in the absence and presence of Cys (3.0 mM) and His (3.0 mM). All studies were performed in aq.-HEPES buffer (10 mM, pH 7.4) medium at 298 K.

Previous reports revealed that this Cu(I) forms a coordination complex with the excess of Cys present in the reaction medium under the conditions that are very similar to those of the present study.[24] It is reported that O_2 (present in the reaction medium) could oxidize the Cys–Cu(I) complex to cystine with simultaneous generation of Cu(0), which could undergo partial disproportionation to generate Cu(II) and Cu(I). This presumably accounts for the insignificantly small EPR signal (Figure 4.7) for **R** treated with Cys.[24] The m/z signals in the ESI-MS spectra were observed

at 701.68 [(**R**-2Cu) + H^+] and 1235.66 [**R** + 2His + ClO_4^-], respectively, when spectra of **R** were recorded in the presence of excess Cys and His, respectively.

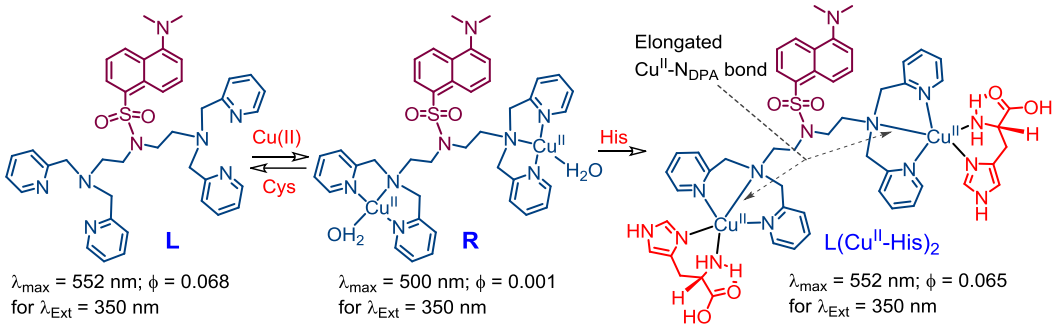

Scheme 2. Sensing mechanism of **R** with Cys and His with associated steady state fluorescence properties.

These data supported the eventual demetalation reaction of **R** with Cys and complex formation reaction with His (Scheme 2). All these confirmed that different reaction pathway for interaction of **R** with Cys and His led to the fluorescence on response.

The respective concentration level of Cys and His in human plasma is typically 240 - 360 μM and 15 - 75 μM. In order to estimate the unknown concentration of Cys and His in human blood plasma we have generated fluorescence calibration plots. The final concentration of the probe molecule **R** in each solution used for estimation of Cys and His in HBP samples was maintained at 20 μM. Please note that emission intensities at 552 nm for HBP samples treated with a standard solution of **R** gave the total amount (C_T = [Cys] + [His]) of these two AAs present in the HBP sample. Emission intensity measurements for HBP samples treated with the reagent **R** directly gave the summation of concentration of C_{Cys} and C_{His} ($C_T = C_{Cys} + C_{His}$). Thus, $C_T - C_{His} = C_{Cys}$.

Detection of His (C_{His}) in human blood plasma (Methodology 1)

Calculation of the C_{His} in Human Blood Plasma (HBP) sample that contains Cys and His. To the 20 μl HBP sample 10 mM NEM was added. NEM is known to react irreversibly with Cys and yield a non fluorescent compound (Scheme 3). This resultant solution was used for quantitative analysis of His.

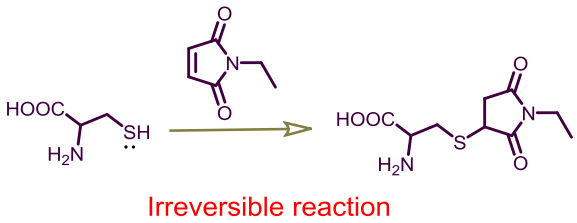

Scheme 3. Irreversible reaction of cysteine with malemide.

Concentration of His in HBP is low and thus to avoid any error in its detection, HBP samples (pre-treated with excess NEM) were spiked with two known concentration of His (100 μM and 200 μM, respectively). Thus fluorescence intensity of such HBP samples spiked with 200 and 300 μM of His was $I_{HBP+200}$ and $I_{HBP+300}$, respectively. Fluorescence intensities for pure aqueous HEPES buffer solution having pH of 7.4 was evaluated for [His] of 200 and 300 μM and these values were I_{200} and I_{300}, respectively. Thus, the difference between $I_{HBP+200}$ and I_{200} should lead to the actual concentration of His ($[His]_1$) in HBP sample. Similarly, the difference between $I_{HBP+300}$ and I_{300} should lead to the actual concentration of His ($[His]_2$) in HBP sample. Arithmetic mean of $[His]_1$ and $[His]_2$ led us to the value ((23 ± 2.1) μM) for C_{His} in HBP sample. Please note that the data reported for C_{His} is an average of three independent evaluations for $[His]_1$ and $[His]_2$.

Detection of Cys (C_{cys}) in human blood plasma (Methodology 2)

C_{Cys} was also evaluated from the experiments with NEM, which reacted specifically with Cys. Emission intensity for HPB samples treated with **R** was evaluated (I_T), which reflected the total concentration of Cys and His present in HBP sample. Then this solution was treated with NEM. NEM reacted with Cys present in HBP sample and the product was non emissive. The emission intensity (I_{NEM}) for the resulting solution was recorded and the difference in intensities ($\Delta I = I_T - I_{NEM}$) was used for evaluation of [Cys] in HBP sample. Value evaluated for [Cys] in HBP sample, following this methodology, agreed well with the value that was evaluated by adopting the methodology1. The difference (CT - C_{His}) yielded the actual [Cys] (239 ±

7.5 μM) in the HBP sample. Thus the evaluated [Cys] and [His] in HBP were within the allowed limit for a healthy human being.

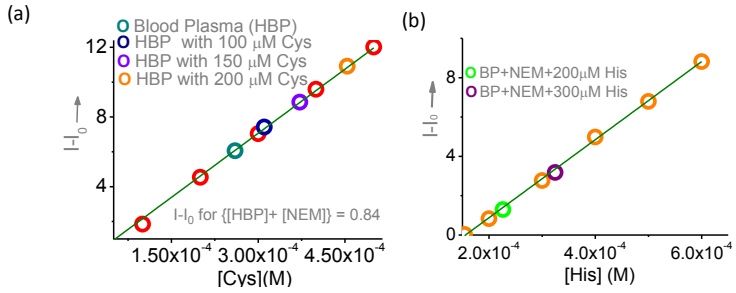

Figure 4.7. (a) Plot of $\Delta I = (I - I_0)$ vs. [Cys], where I_0 and I are emission intensities of aq. HEPES buffer solution (pH = 7.4) of **R** at 552 nm (λ_{Ext} = 350 nm) in the absence and presence of known [Cys] (o) as well as in blood plasma/blood plasma samples spiked with three different known [Cys];(b) Plot of $\Delta I = (I - I_0)$ vs. [His], where I_0 and I are emission intensities of receptor **R** at 552 nm (λ_{Ext} = 350 nm) in presence of known [His] and blood plasma samples spiked with a known [His] + 10 mM NEM.

The switch *ON* luminescence response on regeneration of the reagent **L** from **R** on interaction with Cys offered us the possibility for checking the feasibility of using the reagent (**R**) as an imaging reagent for the detection of endogenous Cys in live Hct116 cells (Colon cancer cells). Furthermore, to assess the possibility of using this reagent **R** as an imaging reagent for detection of intracellular Cys that could be present in live Hct116 cells, confocal laser microscopic studies were performed. Live Hct116 cells were incubated with **R** (10 μM) in aq.-HEPES buffer solution (pH 7.4) at 37°C and then washed thrice with phosphate buffer solution (PBS) to remove the surface adhered probe molecules. Control experiments were performed without exposing live Hct116 cells to the probe reagent solution; otherwise maintaining the identical experimental conditions. The bright-red fluorescence images were observed for Hct116 cells treated with **R**, while no such fluorescence images were observed for Hct116 cells used in control experiments (Figure 4.8.vi). These results confirmed the cell membrane permeability of this reagent and its ability to react with the intracellular Cys to initiate the demetallation reaction (Scheme 2) and regenerate **L** with fluorescence on response.

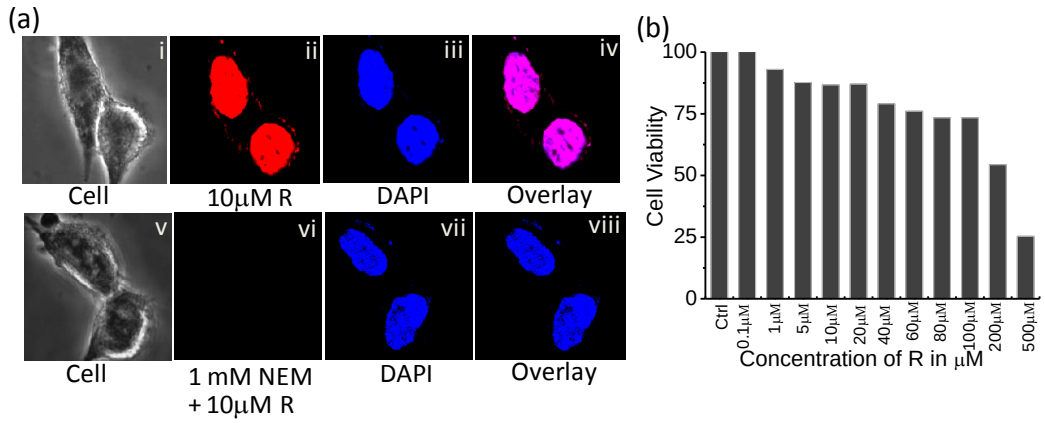

Figure 4.8. (a) Confocal laser microscopic images of Hct116 cells treated with 10 μM of **R** in HEPES buffer and various reagents mentioned in (a). Fig. iv & viii are overlay of the merged images and confirmed the intracellular fluorescence; (b) MTT assay to determine the cell viability percentage in Hct116 colon cancer cells. The concentration of the **R** ranges from 0.1-500 μM and treated for 12 hours. IC_{50} has been calculated to be 200 μM.

In order to confirm that this fluorescence on response was due to the reaction of **R** with intracellular Cys, live Hct116 cells were pre-incubated with 1 mM of NEM for 30 min prior to the incubation with reagent **R** (10 μM) for a further period of 30 min. NEM is known to react specifically with Cys and would not interfere with the further detection of His. Insignificant fluorescence from cells of this control experiment (Figure 4.8.a(vi)) due to the interaction of reagent **R** with endogenous His was lower than the lowest detection limit for His and thus could evade such detection. Thus, confocal images confirmed the ability of this reagent to detect endogenous Cys. MTT assay revealed insignificant cytotoxicity of this probe towards Hct116 cells with an IC_{50} of 200 μM.

Thus, this chapter reveals a new binuclear Cu(II)-based receptor (**R**) designed for recognition of cysteine and histidine based on fluorescence on response. More importantly, this reagent could even be used for quantitative estimation of Cys and His in human blood plasma. Furthermore, probe **R** utilized for the detection of endogenous cysteine present in the Hct116 cell lines. All studies were performed in aq.HEPES buffer (10 mM, pH 7.4) medium at 298 K.

4.5. References

1. (a) D. M. Townsend, K. D Tew and H. Tapiero, *Biomed. Pharmac-other.,* 2003, **57**, 145; (b) L. A. Herzenberg, S. C. De Rosa, J. G. Dubs, M. Roederer M. T. Anderson, S. W. Ela, S. C. Deresinski and L. A. Herzenberg, *Proc. Natl. Acad. Sci. U. S. A.* 1997, **94**, 1967.

2. M. T. Heafield, S. Fearn, G. B. Stevenson, R. H. Waring, A. C. Williams and S. G. Sturman, *Neurosci. Lett*., 1990, **110**, 216−220.

3. H. Refsum, P. M. Ueland, O. Nygard and S. E. Vollset, *Annu. Rev. Med*., 1998, **49**, 31−62.

4. T. P. Akerboom, M. Bilzer and H. J. Sies, *Biol. Chem*., 1982, **257**, 4248−4252.

5. Y. Xun, T. Yuanqi, D. Xinyue, L. Zhentao, T. L. David, X. Jianping, *Anal. Chem.,* 2013, **85**, 1913−1919.

6. X. Yuan, Y. Tay, X. Dou, Z. Luo, D. T. Leong and J. Xi, *Anal. Chem*., 2013, 85, 1913; (b) M. Zhang,M. Yu, F. Li, M. Zhu, M. Li, Y. Gao, L. Li, Z. Liu, J. Zhang, D. Zhang, T. Yi and C. Huang, *J. Am. Chem. Soc*., 2007,**129**, 10322;

7. (a) S. Shahrokhian, Anal. Chem., 2001, 73, 5972–5978; (b) E. Weerapana, C. Wang, G. M. Simon, F. Richter, S. Khare, M. B. D Dillon, D. A. Bachovchin, K. Mowen, D. Baker and B. F. Cravatt, Nature, 2010, 468, 790–795.

8. J. Lin, I. M. Lee, Y. Song, N. R. Cook, J. Selhub, J. E. Manson, J. E. Buring, S. M. Zhang, *Cancer Res*., 2010, **70**, 2397- 2405.

9. (a) J. D. Kopple and M. E. Swendseid, *J. Clin. Invest*., 1975, **55**, 881; (b) Y. Kusakari, S. Nishikawa, S.-i. Ishiguro and M. Tamai, *Curr. Eye Res*., 1997, **16**, 600–604.

10. P. M. Kovach and M. E. Meyerhoff, *Anal. Chem*., 1982, **54**, 217; (b) A. L. Jones, M. D. Hulett and C. R. Parish, Immunol. *Cell Biol*., 2005, **83**, 106–118.

11. (a) P. Das, A. K. Mondal, N. B. Chandar, M. Baidya, H. B. Bhatt, B. Ganguly, K. S. Ghosh, A. Das, *Chem.-Eur. J*., 2012, **18**, 15382; (b) S.-M. Liao, Q.-S. Du, J.-Z. Meng, Z.-W. Pang and R.-B. Huang, *Chem. Cent. J*., 2013, **7**, 44.

12. K. Kusmierek, R. Glowacki and E. Bald, *Anal. Bioanal. Chem*., 2006, **385**, 855–860; (b) T. M. Huang, B. Yang, Y.J. Yu, X. W. Zheng and G. L Duan, *Anal. Chim. Acta.,* 2006, **565**, 178–182.

13 (a) P. Kubalczyk, E. Bald, *Anal. Bioanal. Chem*., 2006, **384**, 1181–1185; (b) A. Musenga, R. Mandrioli, P. Bonifazi, E. Kenndler, A. Pompei and M. A. Raggi, *Anal. Bioanal. Chem*., 2007, **387**, 917–924.

14 (a) J. Radfordknoery and G. A. Cutter, *Anal. Chem*., 1993, 65, 976–982; (b) P. G. Hill and R. M. Smith, *J. Chromatogr. A*, 2000, **872**, 203-213.

15 (a) H. Kamencic, A. Lyon, P. G. Paterson, B. H. J. Juurlink, *Anal. Biochem*., 2000, **286**, 35-37; (b) E. Kaniowska, G. Chwatko, R. Glowacki, P. Kubalczyk and E. Bald, *J. Chromatogr. A.,* 1998, **798**, 27–35.

16. T. M. Huang, B. Yang, Y. J. Yu, X. W. Zheng and G. L. Duan, *Anal. Chim. Acta.,* 2006, **565**, 178–182.

17. P. Hanjing, C. Weixuan, C. Yunfeng, H. Lovemore and S. R. W. Binghe, *Sensors* 2012, **12**, 15907-15946.

18. Z. Xin, J. Xuejun, S. Guangyan, W. Xue, *Chem. Eur. J.*, 2013, **19**, 7817-7824.

19. U. Reddy G, R. Lo, S. Roy, T. Banerjee, B. Ganguly and A. Das, *Chem. Commun*., 2013, **49**, 9818–9820.

20. U. Reddy G, P. Das, S. Saha, M. Baidya, S. K. Ghosh and A. Das, *Chem. Commun*., 2013, **49**, 255-257.

21. (a) M. Suresh, A. Ghosh and A. Das, Chem. Commun., 2008, 3906; (b) W. Hao, A. McBride, S. McBride, J. P. Gao and Z. Y.Wang, J. Mater. Chem., 2011, **21**, 1040.

22. (a) P. Das, N. B. Chandar, S. Chourey, H. Agarwalla, B. Ganguly and A. Das, *Inorg. Chem*., 2013, **52**, 11034–11041; (b) P. Das, S. Bhattacharya, S.Mishra and A. Das, *Chem. Commun*., 2011, **47**, 8118–8120.

23. O. Das and T. K. Paine, *Dalton Trans*., 2012, **41**, 11476–11481.

24. (a) A. Rigo, A. Corazza, M. Luisa di Paolo, M. Rossetto, R. Ugolini and M. Scarpa, *J. Biol. Chem*., 2004, **98**, 1495; (b) M. Remko, D. Fitz and B. M. Rode, *Amino Acids*, 2010, **39**, 1309.

CHAPTER 5

RHODAMINE BASED PROBES: LIGAND DESIGN, USE OF DIFFERENT PHOTOINDUCED PROCESSES FOR RECOGNITION OF BIOLOGICALLY SIGNIFICANT ANALYTES AND IMAGING APPLICATIONS

Publication:

Chem. Commun., 2014, ***50***, 14421-14424
Chem. Commun., 2015, **51**, 3649-3652
Manuscript communicated

5A. A specific probe for Hg^{2+} to delineate even H^+ in pure aqueous buffer/Hct116 colon cancer cells: Hg(II)–η^2-arene π-interaction and a TBET-based fluorescence response

5A.1. Introduction

Intramolecular triplet–triplet energy transfer is being pursued more recently for developing efficient fluorescence-based receptors, as the average lifetime of the triplet state is much longer than the singlet state.[1] However, such a triplet–triplet energy transfer is spin forbidden by the dipole-dipole mechanism (Förster-type mechanism) and is only allowed by the electron exchange mechanism (Dexter-type mechanism).[1] Such a triplet–triplet energy transfer requires either an effective orbital overlap or coupling mediated by an appropriate conduit. More importantly, such a through bond energy transfer (TBET) process is not limited by the fact that donor and acceptor fragments ought to have a spectral overlap. This offers the opportunity to achieve a large pseudo-Stokes shift to avoid self-quenching of the donor fluorophore and fluorescence detection errors because of excitation backscattering effects.[2] Additionally such an energy transfer dyad also helps in avoiding the problem of photo-bleaching of the probe fluorophore.[2,3] For fluorophore dyad systems that have an insignificant spectral overlap between the donor emission and acceptor absorption, the FRET process could be operational along with the TBET process. The challenge of demonstrating the TBET process in a small molecule based fluorophore dyad without the complete absence of the spectral overlap has not been met to date, barring one recent example.[4] Among various fluorophores, acyclic xanthene forms of different rhodamine derivatives have been widely used as imaging reagents because of their high emission quantum yield, cell membrane permeability, non-toxic nature towards live cells and finally the switch on fluorescence response upon conversion of a cyclic lactam form to the acyclic one.[5] However, such reagents generally have a Stokes shift of about 50 nm and respond to H^+ as well as certain metal ion(s) with a fluorescence on response.[5] More recently, a much larger Stokes

shift was reported for a receptor with TBET-based response on specific binding to Hg^{2+}.[6] However, there existed a small spectral overlap between the donor and the acceptor fragments and this did not completely exclude the possibility of the FRET-based response along with the predominant TBET process. Thus, examples of TBET-based cassettes for intracellular imaging applications are actually rare.[3,6] Among various metal ions, Hg^{2+} is one of the most potent neurotoxins known and its deleterious influences on human as well as plant physiology are well documented in literature and the lowest Hg(II) concentration that is allowed in safe drinking water is 0.2 ppb.[7-9] Keeping this in mind, it is imperative to develop a reagent that could specifically recognize, detect and quantitatively estimate mercury ion concentration as low as the above referred limit in pure aqueous/buffer medium having physiological pH. Hg^{2+} is known to be an efficient quencher of molecular fluorescence due to a facile spin-orbit coupling process.[10] The solvation enthalpy for Hg^{2+} is also significant (1824 kJ mol^{-1}). Thus, designing an ultrasensitive probe that is specific for Hg(II) and responds with fluorescence ON response and a high Stokes shift is a challenging issue.

5A.2. Experimental Section

5A.2.1. Materials

Rhodamine B, Ethylenediamine, 9,10-Phenanthrenequinone, Terephthalaldehyde, 4-Methylbenzaldehyde, Trifluoroacetic acid, all metal perchlorate salts such as $NaClO_4$, $KClO_4$, $Mg(ClO_4)_2$, $Ca(ClO_4)_2$, $Cu(ClO_4)_2$, $Zn(ClO_4)_2$, $Co(ClO_4)_2$, $Ni(ClO_4)_2$, $Cr(ClO_4)_2$, $Fe(ClO_4)_2$, $Cd(ClO_4)_2$, $Hg(ClO_4)_2$, $Pb(ClO_4)_2$ salts and $PdCl_2$ were obtained from Sigma-Aldrich and were used as received. Solvents used for synthesis of intermediates and final compounds were of AR grade and HPLC grade solvents for spectroscopic studies from S.D. Fine Chemicals in India.

5A.2.2. Analytical Methods

^{1}H NMR spectra were recorded AV 400 MHz or AV-500 MHz Bruker NMR spectrometers using DMSO-d_6 and CD_3CN as the solvent and tetra methyl silane (TMS) as an internal standard. ESI-Ms measurements were carried out on a Waters QTof-Micro instrument. Electronic spectra were recorded with a Shimadzu UV-3101 PC spectrophotometer; while fluorescence spectra were recorded using Qunata Master 400, PTI spectrofluorometer.

5A.2.3. General experimental procedure for UV-Vis and Fluorescence studies

5.0 x 10^{-2} M solution of the perchlorate salts of the respective ion (Na^+, K^+, Fe^{3+}, Na^+, Mg^{2+}, Ni^{2+}, Co^{2+}, Cu^{2+}, Cd^{2+}, Pb^{2+}, Zn^{2+}, Cr^{3+} and Hg^{2+}) were prepared in pure aqueous medium, while $PdCl_2$ in brine solution for all studies. The effective final concentrations of all metal salts were maintained at 5.0 x 10^{-5} M. A stock solution of the receptor **L** and $\mathbf{R_1}$ and $\mathbf{R_2}$ (5.0 x 10^{-3} M) was prepared in dimethylsulphoxide (DMSO) medium and 20 μL of this stock solution was added to 4.98 ml of 0.4 mM TX100 in 10 mM HEPES aqueous buffer medium having solution pH 7.2 to make the effective ligand concentration of 20 μM. For all luminescence measurements, λ_{Ext} = 400 nm with an emission slit width of 1 nm was used. The relative fluorescence quantum yields (Φ_f) were estimated using Rhodamine B (Φ_f = 0.3 in aq. medium at RT) as a reference.

5A.2.4. General experimental procedure for ^{1}H NMR spectroscopy

3 mM stock solution of **L** and $\mathbf{R_1}$ were prepared in DMSO-d_6 and CD_3CN, respectively. 500 μl of each stock solution of **L** and $\mathbf{R_1}$ were taken in an NMR tube. Complexation studies of **L** and $\mathbf{R_1}$ with $Hg(ClO_4)_2$ (in CD_3CN), was studied by ^{1}H NMR technique. Concentration for the stock solutions for $Hg(ClO_4)_2$ (in CD_3CN) was maintained at 1.0 x 10^{-1} M. ^{1}H NMR spectra of the guest molecule **L** and $\mathbf{R_1}$ were

recorded with increasing concentration of the host ions (Hg^{2+} ions). Such addition was continued until no further change in the chemical shifts was observed.

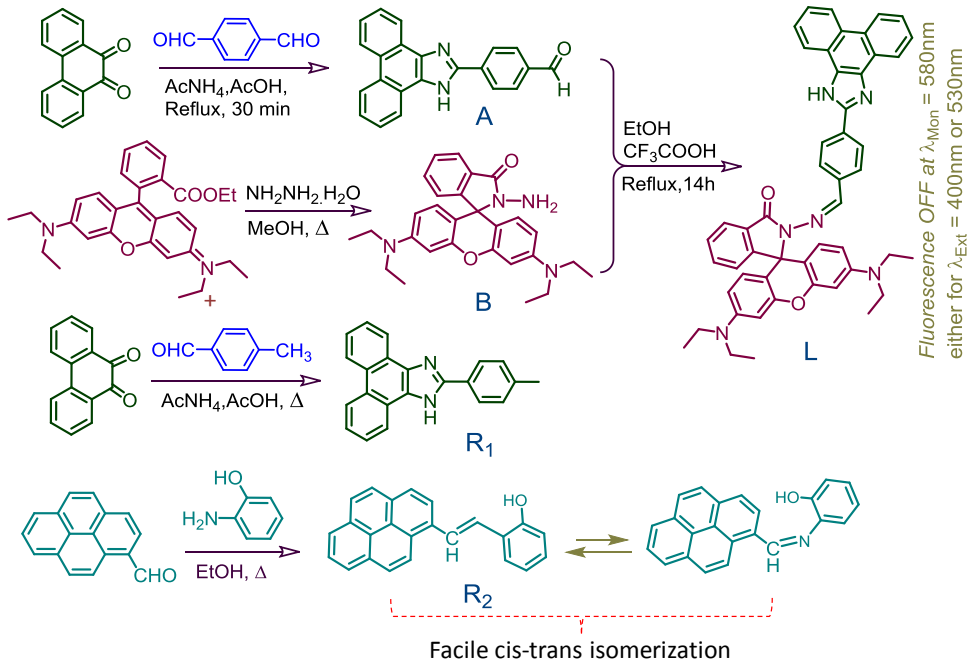

Scheme 1. Methodologies that were adopted for synthesis of **A, B, R_1, R_2** and **L.**

5A.3.1. Synthesis of A[12a]

A mixture of 9,10-phenanthroquinone (700 mg, 3.365 mmol), terephthalaldehyde (1352 mg, 10.08 mmol), and ammonium acetate (5182 mg, 67.29 mmol) were stirred in glacial acetic acid (15 mL) under reflux condition. After 30 min reaction was stopped, the hot solution was cooled to room temperature and the resulting yellow solid was collected by filtration and washed with excess amount of water and methanol to remove starting materials. Yield: 850 mg, 78.50 %. ESI-Ms (m/z) calculated for $C_{22}H_{14}N_2O$: 322.11, observed: 323 [M + H^+]. ^{1}H NMR [400 MHz, DMSO-d_6: δ (ppm)]: 13.71 (1H, s, -NH); 10.10 (1H, s, -CHO); 8.67(2H, d, *J* = 8 Hz, ArH); 8.60 (2H, d, *J* = 7.6 Hz, ArH); 8.53 (2H, d, *J* = 8.4 Hz, ArH); 8.13 (2H, d, *J* = 8 Hz, ArH); 7.77 (2H, t, *J* = 7.6 Hz, ArH); 7.67 (2H, t, *J* = 7.6 Hz, ArH). ^{13}C NMR (100 MHz, DMSO-d6, δ (ppm)): 193.00, 172.58, 149.08, 148.74, 13.91, 136.51, 135.90, 130.56, 128.58, 127.76, 127.32, 127.05, 127.00, 126.13, 124.44 and 122.56.

5A.3.2. Synthesis of R_1[12a]

A mixture of 4-methylbenzaldehyde (288 mg, 2.4 mmol), 9,10-phenanthroquinone (500 mg, 2.4 mmol), and ammonium acetate (3696 mg, 48 mmol) were stirred in glacial acetic acid (10 mL) under reflux condition for 30 min. After 30 min the hot solution was cooled to room temperature, and the resulting white solid was collected by filtration and washed with excess amount of water and methanol to remove starting materials. Yield: 600 mg, 81 %. ESI- Ms (m/z) calculated for $C_{22}H_{16}N_2$: 308, observed: 308 [M]. ^{1}H NMR [500 MHz, DMSO-d_6: δ (ppm)]: 13.36 (1H, s, -NH); 8.84 (2H, d, *J* = 8 Hz, ArH); 8.56 (2H, d, *J* = 7.4 Hz, ArH); 8.21 (2H, d, *J* = 8 Hz, ArH); 7.77-7.60 (4H, m, ArH); 7.41 (2H, d, *J* = 8 Hz, ArH); 2.41 (3H, s, -CH_3). ^{13}C NMR (100 MHz, DMSO-d_6, δ (ppm)): 149.77, 139.33, 137.41, 130.00, 128.18, 128.03, 127.54, 126.56, 125.62, 124.50, 124.23, 122.29 and 21.15.

5A.3.3. Synthesis of R_2

Synthetic procedure that was adopted for synthesis **R_2** from previous literature.[11c]

5A.3.4. Synthesis of L

Rhodamine 6G hydrazine (B) (150 mg, 0.33 mmol) and compound **A** (106 mg, 0.33 mmol) were dissolved in 40 mL of ethanol. To this was added approximately 2 drops of acetic acid, and the resulting solution was refluxed for 16 h. The solution was filtered while hot to remove starting materials and yellow precipitate was collected. The residue was washed thoroughly with methanol and acetone to isolate pure form of **L**. Yield: 160 mg, 64 %. ESI-Ms (m/z) calculated for $C_{50}H_{46}N_6O_2$: 762, observed: 763 [M + H^+]. ^{1}H NMR [400 MHz, DMSO-d_6: δ (ppm)]: 8.89 (1H, s, -CH=N-); 8.87 (2H, d, *J* = 10 Hz, ArH); 8.57 (2H, d, *J* = 10 Hz, ArH); 8.26 (2H, d, *J* = 10 Hz, ArH); 7.96 (1H, t, *J* = 9.0 Hz, ArH); 7.76 (3H, t, *J* = 9Hz, ArH); 7.70-7.61 (6H, m, ArH); 7.15 (1H, d, *J* = 9.5 Hz, ArH); 6.55 (1H, s, ArH); 6.50 (2H, d, *J* = 11, Hz, ArH); 6.40 (2H, d, *J* = 9.5, ArH); 3.33 (8H, q, *J* = 8.5 Hz, CH_2); 1.08 (12H, t, *J* = 8.5 Hz, CH3). ^{13}C NMR

(100 MHz, DMSO-d_6, δ (ppm)): 189.77, 182.95, 175.76, 173.74, 169.54, 154.73, 152.55, 145.71, 144.87, 144.20, 144.02, 143.45, 142.47, 139.98, 138.87, 137.57, 66.83, 54.98, 39.98 and 31.60.

5A.4. Results and Discussions

The absorption and emission properties of **L** and **R** (20 μM) were investigated in aq. solution of 0.4 mM TX100 and HEPES buffer (10 mM; pH 7.2) by using λ_{Ext} of 400 nm and slit width of 1/1 nm. A biologically benign neutral surfactant (TX100) allowed reagent **L** to get trapped inside its miceller structure and to solubilise in pure aqueous buffer medium, and this solution was used for all studies unless mentioned otherwise. Solution of **L** showed one absorption band at 385 nm due to the phenanthroimidazole moiety, while no detectable absorbance at $\lambda > 400$ nm was observed. The electronic spectral band for the model compound **R** also appeared at 375 nm. These spectral observations established two crucial facts: firstly, there was no electronic interaction between the donor and acceptor in the ground state and compound behaves as a single molecule instead of cassette. **L** was present almost exclusively in the spirolactam form of rhodamines derivative under the experimental conditions. A characteristic signal at ~ 66.83 ppm for the tertiary C-atom in the ^{13}C NMR spectrum for **L** also confirmed its spirolactam structure.[6] Absorbance spectra of **L** (20 μM) in absence and presence of 40 mole equivalent of various metals analytes (M^{n+}) in buffer media (pH 7.2) were recorded (Figure 5A.1). Among all these analytes, only Hg^{2+} showed a new absorption band at 564 nm for the acyclic xanthenes form of rhodamine moiety, along with another band at 385 nm. Such a large red shift (179 nm) in absorption behavior changed the color of the solution from color less to pink, allowing colorimetric detection of Hg^{2+} by the naked eye. Thus, in the presence Hg^{2+} ions, compound **L** showed an absorption spectrum that was characteristic of both the donor and acceptor components. Further interference

studies in presence of 50 mole excess of all other metal ions ensured that the reagent, **L** was specific towards Hg^{2+} even in an ensemble of all other common competing cationic analytes. For all of the other ions used for this study, no change in the absorption spectra of **L** was observed. It may be mentioned that the extent of absorbance changes as a function of [Hg^{2+}] was linear [Hg^{2+}] of (0 - 30 mole equiv.) in solution of 0.4 mM TX100 and HEPES buffer (10 mM; pH 7.2). The binding stoichiometry for the adduct formation between the receptor **L** and the Hg^{2+} was evaluated as 1:1 based on the Benesi-Hildebrand plot of the data obtained from the systematic UV-vis titration (Figure 5A.1). B-H plots, obtained by using data available from systematic absorption spectral titrations at 25 °C, revealed an association constant of (2.9 ± 0.5) x 10^3 M^{-1}.

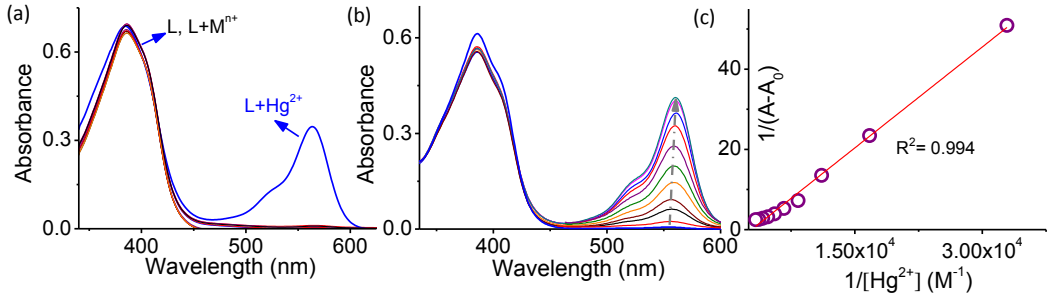

Figure 5A.1. Changes in (a) absorption of the receptor **L** (20 μM) in presence and absence of different metal ions (M^{n+}: Li+, Na^+, K^+, Ca^{2+}, Mg^{2+}, Cr^{3+}, Fe^{2+}, Co^{3+}, Ni^{2+}, Cu^{2+}, Zn^{2+}, Hg^{2+}, Cd^{2+}, Pd^{2+} and Pb^{2+}); (b) Change in absorption spectra for **L** (20 μM) in presence of varying [Hg^{2+}] (0- 30 equiv); (c) Benesi-Hildebrand (B-H) plots of spectral titration. Good linear fit confirms the 1:1 binding stoichiometry. All studies were performed in aq. solution of 0.4 mM TX100 and HEPES buffer (10 mM; pH 7.2).

The selective binding of **L** to Hg^{2+} among all other metal ions was also studied using the emission spectral response of the solution of **L** (20 μM) in the absence and presence of an excess (30 equiv) of each of these metal ions in aq. solution of HEPES buffer (10 mM; pH 7.2). Upon excitation at 400 nm, a single emission band centered at 464 nm was observed only in presence of Hg^{2+} and this was attributed to the emission from the phenanthroimidazole moiety (Figure 5A.2(a)). This was further confirmed by comparing the emission spectra with those for the model reagent $\mathbf{R_1}$.

Systematic luminescence titrations were carried out for **L** (20 μM) with varying [Hg^{2+}] (0 to 30 mole equiv.) performed in aq. solution of 0.4 mM TX100 and HEPES buffer (10 mM; pH 7.2) using λ_{Ext} of 400 nm and 525 nm. A gradual increase in emission intensity at 583 nm was accompanied with a partial decrease in emission intensity at 464 nm upon addition of Hg^{2+} solution (Figure 5A.2 (b)). The binding stoichiometry for the adduct formation between the receptor **L** and the Hg^{2+} was evaluated as 1:1 from the Benesi-Hildebrand plot of the data obtained from the systematic fluorescence titration (Figure 5A.2(c)). B-H plots, obtained by using data available from systematic absorption spectral titrations at 25 °C, revealed association constant of (2.3 ± 0.5) x 10^3 M^{-1}.

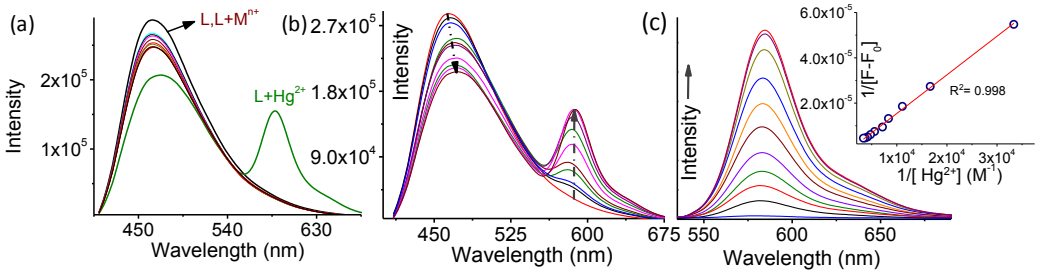

Figure 5A.2. Changes in (a) luminescene of the receptor **L** (20 μM) in presence and absence of different metal ions (M^{n+}: Li+, Na^+, K^+, Ca^{2+}, Mg^{2+}, Cr^{3+}, Fe^{2+}, Co^{3+}, Ni^{2+}, Cu^{2+}, Zn^{2+}, Hg^{2+}, Cd^{2+}, Pd^{2+} and Pb^{2+}); Change in luminescence spectra for **L** (2.0 x 10^{-5} M) in presence of varying [Hg^{2+}] (0 - 60 x 10^{-5} M mole equiv.) (b) using λ_{Ext} = 400 nm; (c) using λ_{Ext} = 525 nm. Inset Benesi-Hildebrand (B-H) plots of spectral titration. Good linear fit confirms the 1:1 binding stoichiometry. All studies were performed in aq. solution of 0.4 mM TX100 and HEPES buffer (10 mM; pH 7.2) and maintaining a slit width of 1/1.

Emission spectra recorded for such a solution showed emission bands at 464 and 587 nm (λ_{Ext} of 400 nm) (Figure 5A.2). Relative emission quantum yield for Hg^{2+}·**L** (Φ = 0.52) at 464 nm was less compared to that observed for free **L** (Φ = 0.78). Emission spectra for **L** (20 μM) were recorded (λ_{Ext} of 400 nm) at different pH values and results of these studies revealed that the spirocyclic form of **L** was stable in the pH range 5 - 10. Upon further lowering the solution pH (below 4.0), a significant lowering of the imidazole-based emission band at 464 nm was observed along with a barely detectable emission intensity enhancement at around 587 nm. However,

excitation of a similar solution at 530 nm showed an intense emission band at 587 nm (Figure 5A.3). These results revealed two important aspects: firstly, the acyclic xanthene form was produced in solution having pH < 4.0;[5] however, the absence of any absorption below 420 nm for the acyclic xanthene form failed to give any sensible emission band beyond 530 nm for λ_{Ext} of 400 nm.[5] Secondly, the absence of any emission band beyond 500 nm for the model reagent **R_1** also excluded the possibility of any FRET process using benzimidazole as a donor and the rhodamine moiety as an acceptor.

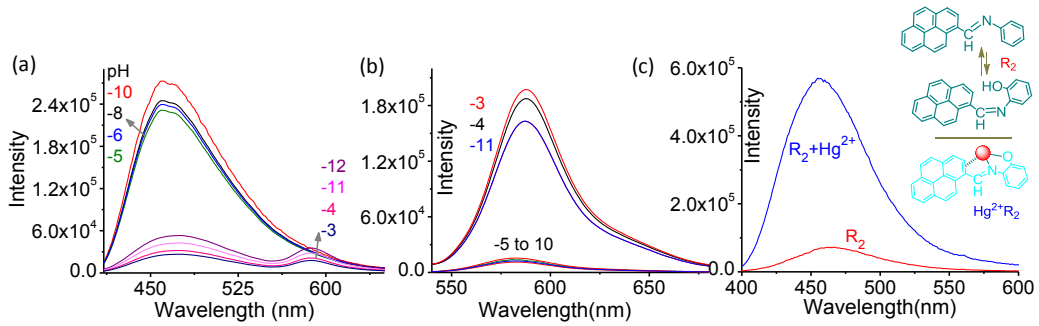

Figure 5A.3**.** Studies were performed in aq. solution of 0.4 mM TX100 and HEPES buffer (10 mM; pH 7.2) by using (a) λ_{Ext} = 400 nm; (b) λ_{Ext} = 530 nm and slit width of 1/1 nm; (c) Emission spectra of **R_2** (20 μM) and **R_2** in the presence of Hg^{2+} (40 mole equiv.) by using λ_{Ext} = 380 nm and (inset) shows the restriction in *cis–trans* isomerisation of R_2 upon binding to Hg^{2+}.

To understand the fluorescence responses of **L** upon binding to Hg^{2+}, luminescence properties of the model compound **R_2** were examined. Reagent **R_2** showed a low emission quantum yield (Φ_{R2} = 0.009) when excited at 380 nm (Figure 5A.3(c) and Scheme 2), the λ_{Abs}^{Max} for the pyrene-based transition. This low Φ_{R2} value was attributed to a fast non radiative deactivation of the pyrene-based excited state due to a rapid cis–trans isomerization process.[11] However, upon binding to Hg^{2+}, a significant enhancement in its emission quantum yield was observed due to the restricted cis-trans isomerisation. There are literature reports, which support this proposition.[11] Binding of Hg^{2+} to **L** would also impose such restriction on the *cis-trans* isomerization of the benzimidazole derivative of the phenanthrene fragment and was

expected to enhance the quantum yield for the emission spectral band having a maximum at 464 nm. Interestingly, such an enhancement was not observed when solution of **L** was excited at 400 nm, and in contrast a decrease in the emission intensity at 464 nm was observed with the appearance of a new emission band with a maximum at 587 nm upon binding to Hg^{2+}.Further, Φ (λ_{Ext} = 400 nm, λ_{Ems}^{Max} of 587 nm) for Hg^{2+}.B (Scheme 2) was estimated to be 0.025, while that for Hg^{2+}.**L** under identical experimental conditions was 0.54.

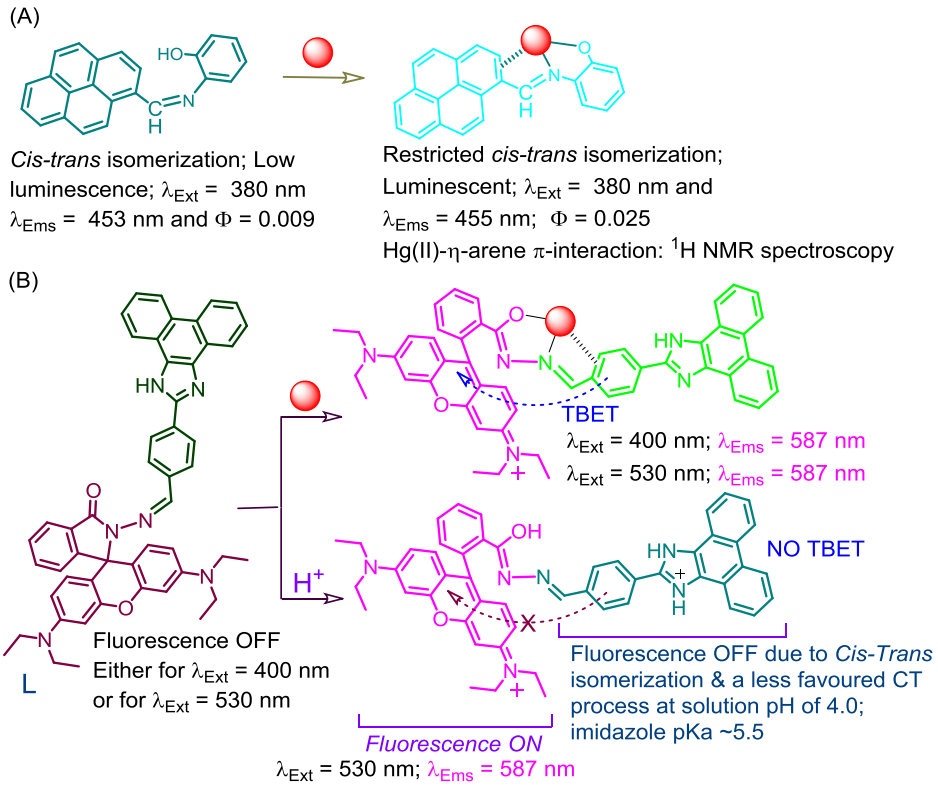

Scheme 2. Proposed mode of binding in (A) Hg^{2+}.$\mathbf{R_2}$ and (B) Hg^{2+}.**L**.

These data clearly indicated that an efficient energy transfer process was operational from the donor Hg^{2+}-bound phenanthroimidazolemoiety to the acceptor Hg^{2+}-bound rhodamine fragment in Hg^{2+}.L. In the absence of any possibility of the FRET process, all these results collectively suggested the possibility of an efficient through bond energy transfer (TBET) from the benzimidazole derivative of the phenanthrene

fragment (donor)[12] to the acyclic xanthene form of the rhodamine moiety (acceptor). Efficiency of the TBET process was estimated to be 87%.[2e,6,13a]

For the efficient TBET process to be operational on binding to Hg^{2+}, one would anticipate a significant and ratiometric decrease in the emission intensity at λ_{Max} of 464 nm, which was not observed in the present study. This apparent anomaly could be explained if we consider the fact that the restricted *cis–trans* isomerization (involving the benzimidazole moiety in Hg^{2+}.**L**) was actually operational and accounted for fluorescence enhancement at ~ 464 nm. This presumption was amply supported by the observed fluorescence enhancement (vide supra) of the model compound $\mathbf{R_2}$ (Figure 5A.3(c)) Thus, these two opposing influences on emission intensity at 464 nm resulted only in a partial decrease in emission intensity at ~ 474 nm and did not allow us to achieve the ratiometric fluorescence response which otherwise was anticipated for a TBET-based luminescence response. Various TBET cassettes that are reported in the literature, including the one reported by one of the research groups authoring this article,[6] have a certain amount of spectral overlap between donor emission and acceptor absorption, which does not completely exclude the possibility of a certain amount of the FRET process along with the TBET process.

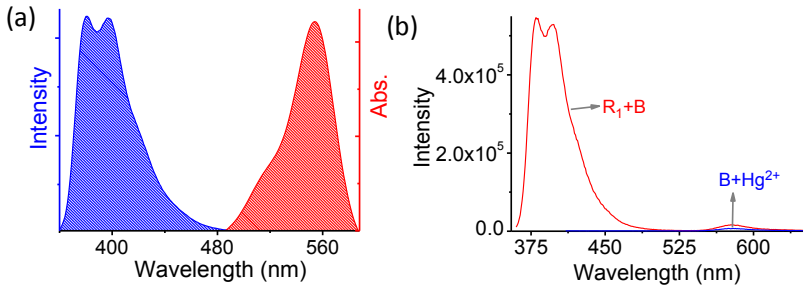

Figure 5A.4. (a) Overlap spectra for emission and an absorption spectrum of the donor ($\mathbf{R_1}$) and acceptor (acyclic xanthene form of B), respectively; (b) Fluorescence spectra of equimolar mixture of $\mathbf{R_1}$ and rhodamine B in presenceof Hg^{2+} (30 equiv.) The concentration is 20 μM for both **R** and rhodamine B using λ_{Ext} = 375 nm; slit width 1/1 nm. This shows there is no inter molecular energy transfer process between acceptor and donor moiety. All studies were performed in aq. HEPES buffer (10 mM; pH 7.2) solution having 0.4 mM TX100.

To the best of our knowledge this is the first report that describes that the donor emission has no spectral overlap with the acceptor absorption (Figure 5A. 4(a)). A closer look at the steady state emission data also reveals that excitation of the benzimidazole derivative of the phenanthrene moiety in **L** (λ_{Ext} of 400 nm) showed an intense emission band with a maximum at ~ 587 nm upon binding to Hg^{2+} in aq. buffer medium having pH 7.2, but no such emission band was observed when analogous spectra were recorded at pH < 4.0 (Scheme 2B). Thus, this offered us the opportunity to use a rhodamine-based reagent to distinguish Hg^{2+} from H^{+} based on the vastly different luminescence responses, which are not common for rhodamine-based receptors.[4]

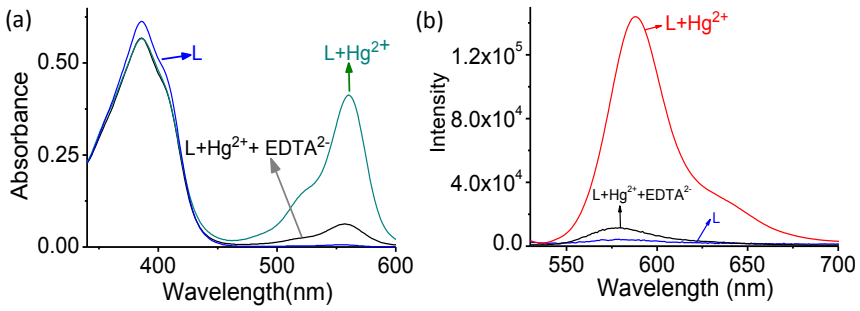

Figure 5A.5. (a) Uv and (b)Fluorescence studies for establishing the reversible binding of Hg^{2+} (30 mole equiv.) to **L** (20 μM) in presence of $EDTA^{2-}$ (2.0 x 10^{-3} M) using λ_{Ext} = 530 nm; and slit width 1/1 nm, in aq. Solution of 0.4 mM TX100 and HEPES buffer (10 mM; pH 7.2).

Further, the difference of 200 nm between the donor absorption (387 nm) and the acceptor emission (587 nm) for Hg^{2+}.**L** was comparable to the highest value of the Stokes shift (202 nm) reported earlier for another TBET-based cassette.[3b] Furthermore, steady state emission spectra recorded for a physical mixture of an equimolar amount of two model reagents, $\mathbf{R_1}$ and Hg^{2+}.B, revealed no detectable quenching or enhancement of luminescence of $\mathbf{R_1}$ and Hg^{2+}.B, respectively, when λ_{Ext} of 375 nm (λ_{Abs}^{Max} for $\mathbf{R_1}$) was used (Figure 5A.4b). These excluded the possibility of any intermolecular energy transfer process,[4] which further corroborated an efficient TBET process. The lowest detection limit (3σ/slope)[13b] was evaluated and

it was found to be as low as 0.48 ppb for Hg^{2+}. The reversibility of the binding process between **L** and Hg^{2+} was also established. On addition of aq. solution of $EDTA^{2-}$ to an aq. HEPES buffer solution (20 μM) of Hg^{2+}.**L** (pH = 7.2), the original spectrum of the spirolactam form of **L** was restored. Higher binding affinity of Hg^{2+} towards $EDTA^{2-}$ led to the formation of Hg^{2+}.$EDTA^{2-}$ and regeneration of **L** (Figure 5A.5).

To have a better insight into the possible binding mode for Hg^{2+} and **L**, detailed NMR studies were performed in DMSO-d_6. Distinct downfield shifts were observed for all protons and these shifts were more significant for -HC=N. Such shifts are anticipated for H_{imine}, where N_{imine} is involved in coordination to a metal ion.[11a,b]

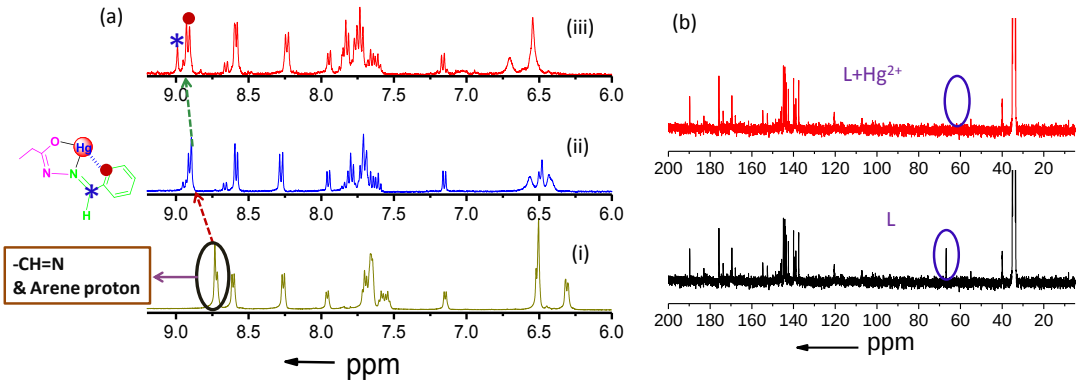

Figure 5A.6. (a) ^1H NMR spectra of **L** (3mM) in absence and in presence of Hg^{2+} (i) 0 equiv.(ii) 50 equiv. (iii) 500 equiv. were recorded in DMSO-d_6; (b) ^{13}C NMR of **L** in absence and in presence of Hg^{2+} in DMSO-d_6.

A relatively high downfield shift ($\Delta\delta$ = 0.23 ppm) for the proton indicated by "•H" (Figure 5A.6 (a)), compared to other aryl protons, suggested a Hg(II)–η^2-arene π-interaction. Such a Hg(II)–η^2-arene π-interaction is not very uncommon in the contemporary literature.[5a,6] Also, ^{13}C NMR spectra revealed that the signal for the tertiary C-atom for the spirocyclic rhodamine moiety for **L** at 66.83 ppm disappeared when **L** was reacted with Hg^{2+} (Figure 5A.6 (b)).

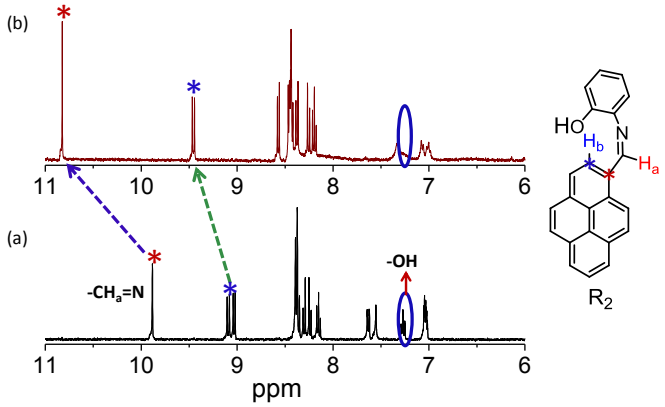

Figure 5A.7. ^{1}H NMR spectra of **R$_2$** (3 mM) in (a) absence and in (b) presence of 50 mole equiv. of Hg^{2+} in CD_3CN.

This signified the formation of the acyclic xanthene form. Based on these NMR and other spectral (electronic, luminescence and ESI-MS) observations, the proposed binding mode of the acyclic xanthene form of **L** to Hg^{2+} involving a Hg(II)–η^2-arene π-interaction is shown in Scheme 2. Further support to such a proposition was achieved from the results of the ^{1}H NMR spectral studies with the analogous model compound **R$_2$** in the absence and presence of Hg(II) in CD_3CN, where a distinct downfield shift ($\Delta\delta$ = 0.32 ppm) was observed for the aryl proton (H*) in **R$_2$** upon binding to Hg^{2+} (Figure 5A.7). This Hg(II)–η^2-arene π-interaction would restrict the *cis–trans* isomerization across the -HC=N functionality in **L** or **R$_2$**.

MTT assay was performed to evaluate the toxicity of this reagent towards Hct116 cells.[13b] After ascertaining the fact that reagent **L** showed only moderate toxicity towards live cancer Hct116 cells, the possibility of using this reagent for the detection of Hg^{2+} uptake in live cancer Hct116 cells was explored using a laser excitation source of 400 nm. Initially, live Hct116 cells were incubated with only **L** (10 μM) for 30 min at 37°C. After necessary and thorough washing, these cells showed intense fluorescence in the green channel due the luminescence from the benzimidazole derivative of the phenanthrene moiety (Figure 5A.8.c). Further, confocal laser microscopic images showed that the Hct116 cells that were pre-treated with 10 μM

reagent **L** (and thoroughly washed for removal of the surface adhered reagent) and subjected to follow-up treatment with Hg^{2+} (4 ppb) led to a distinct decrease in observed fluorescence intensity in the green channel with an onset of strong fluorescence in the red channel (Figure 5A.8.h and i).

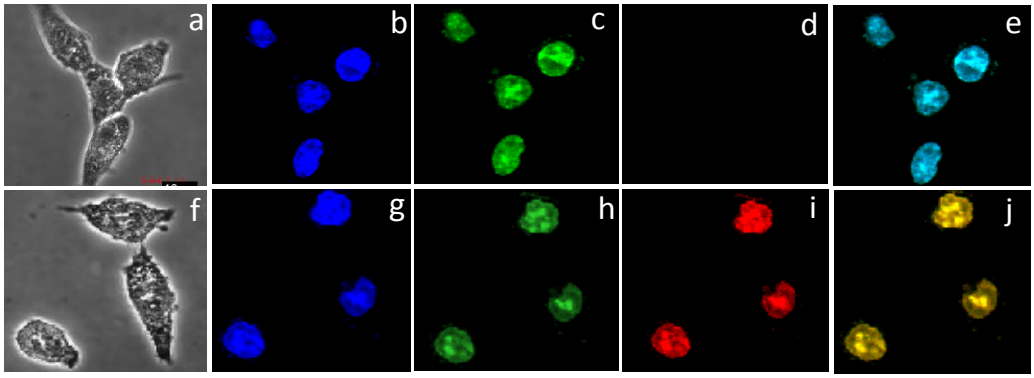

Figure 5A.8. Confocal images of Hct116 cells treated with **L** (10 μM): (a and f) bright field images of Hct116 cells used as a control; (b) and (g) co-staining of **L** with nuclear staining dye DAPI (DAPI: 4',6-diamidino-2-phenylindole) in the blue channel, (c-e) cells incubated with only **L** (10 μM): (c) in the green channel, (d) in the red channel and (e) overlay images of (b) and (c); (h-j) cells incubated with **L** (10 μM) for 30 min and then with then exposed to Hg^{2+} (4 ppb) for 30 min at 37°C; (h) in the green channel, (i) in the red channel, (h) overlay image of (h) and (i); for all studies, a laser source of λ_{Ext} of 400 nm was used.

These results demonstrated two important aspects: reagent **L** was cell membrane permeable and could be used as an imaging reagent for the detection of Hg^{2+} uptake in living cells. Additional studies confirmed that the uptake of Hg^{2+} as low as 0.2 ppb, which is a safe limit for the Hg^{2+} ion concentration (set by the U.S. EPA) based on the environmental primary standard,[8] in live Hct116 cells could be detected from confocal images (Figure 5A.9).

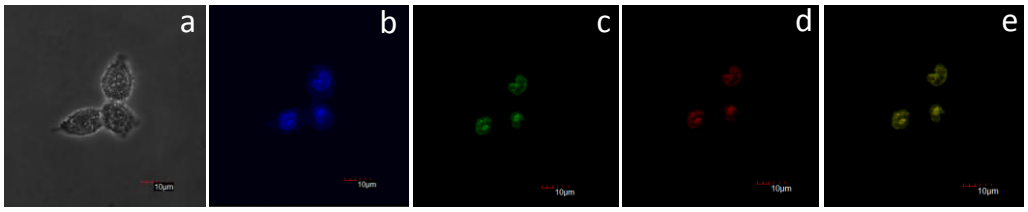

Figure 5A.9. Confocal images of Hct116 cells treated with 0.2ppb of Hg^{2+}: Cells were incubated with **L** (10 μM) for 30 min; (a) Bright filed images of Hct116 cells as control; (b) co-staining of **L** with nuclear staining dye DAPI from blue channel, (c - e) These pre-treated cells were exposed to $Hg(ClO_4)_2$ for 4 hr: (c) at green channel, (d) at red channel and (e) overlay images of (c) and (d); λ_{Ext} = 400 nm.

Further, in order to confirm the ability of reagent **L** to distinguish the cellular pH ≤ 4.0 and cellular Hg^{2+} ion uptake, live Hct116 cells were pre-incubated with buffer solution having pH ~ 4.0 as well as Hg^{2+} solution (pH 7.2) and respective solutions were subsequently exposed to a solution of **L**. Confocal images of these two sets of cells were recorded after excitation at 400 nm (excitation of the imidazolium derivative), and observed confocal images were distinctly different (Figure 5A.10). As anticipated, for cells exposed to a solution having pH ~ 4.0, the TBET process was not operational and only insignificant intracellular emission was observed in red channels; while due to an efficient TBET process, a strong intracellular emission was observed in red channels for cells that were pre-treated with Hg^{2+}.

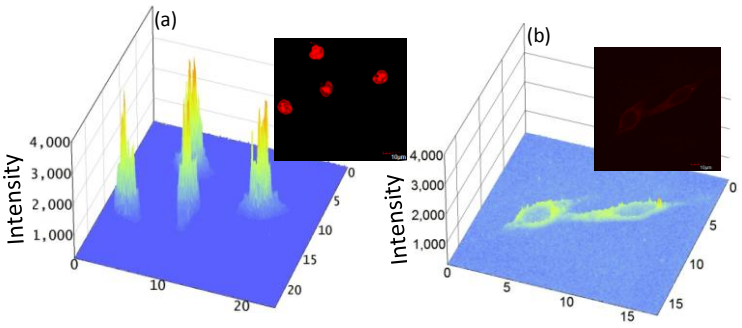

Figure 5A.10. 3D Confocal images of Hct116 cells (pre-treated with **L** (10 μM)) on exposure to a solution having (a) Hg^{2+} (4 ppb) in aq. HEPES buffer (pH 7.2) and (b) pH 4.0 (aq. HEPES buffer) for 30 min at 37°C (λ_{Ext} = 400 nm) at red channel.

Thus, observed results allowed us to distinguish the responses of the reagent towards H^+ and Hg^{2+}. Interestingly, reagent **L** could detect Hg^{2+} ion uptake in the nucleus of theHct116 cells; while that in a solution having pH 4 could only stain the cytosol. Presumably, protonation of **L** at low pH was expected to lead to an increase in its lipophilicity, which adversely affected the uptake of reagent **L** in the nucleus. Such a proposition was put forward recently by Friberg *et al*.[14]

This chapter describes, a new molecular probe **L** showed an efficient TBET-based fluorescence response upon specific binding to Hg^{2+} in an ensemble of several other cations. An appropriate design of the receptor molecule **L** and the Hg(II)–η^2-arene π-

interaction allowed us to exploit the role of the secondary bond in achieving the TBET process with a pseudo-Stokes shift of 200 nm. Interestingly, unlike most other rhodamine-based receptors, this reagent showed distinctly different fluorescence-based output signals upon binding to H^+ in solution having pH $\leq$ 4. This reagent was found to be cell membrane permeable and could be used as a fluorescent probe for imaging Hg^{2+} ion uptake in live Hct116 colon cancer cell lines.

5A.5. References

1. (a) T. Pullerits and V. Sundstro¨m, *Acc. Chem. Res*., 1996, **29**, 381; (b) D. L. Dexter, J. Chem. Phys., 1953, 21, 836.

2. (a) G.-S. Jiao, L. H. Thoresen and K. Burgess, *J. Am. Chem. Soc*., 2003, **125**, 14668; (b) D. Holten, D. Bocian and J. S. Lindsey, *Acc. Chem. Res*., 2002, **35**, 57; (c) O. A. Bozdemir, Y. Cakmak, F. Sozmen, T. Ozdemir, A. Siemiarczuk and E. U. Akkaya, *Chem. – Eur. J*., 2010, **16**, 6346; (d) S. Diring, F. Puntoriero, F. Nastasi, S. Campagna and R. Ziessel, *J. Am. Chem. Soc*., 2009, **131**, 6108; (e) C.Thivierge, J. Han, R.M. Jenkins and K. Burgess, *J. Org. Chem*., 2011, **76**, 5219; (f) J. Fan, M. Hu, P. Zhan and X. Peng, *Chem. Soc. Rev*., 2013, **42**, 29.

3. (a) S. Speiser, *Chem. Rev*., 1996, **96**, 1953; (b) R. Bandichhor, A. D. Petrescu, A. Vespa, A. B. Kier, F. Schroeder, K. Burgess, J. *Am. Chem. Soc*., 2006, **128**, 10688; (c) M. Kumar, N. Kumar, V. Bhalla, H. Singh, P. R. Sharma and T. Kaur, *Org. Lett*., 2011, **13**, 1422; (d) V. Bhalla, Roopa, M. Kumar, P. R. Sharma, and T. Kaur, *Inorg. Chem*., 2012, **51**, 2150; (e) X. Y. Qu, Q. Liu, X. N. Ji, H. C. Chen, Z. K. Zhou and Z. Shen, *Chem. Commun*., 2012, **48**, 4600; (f) L. Zhou, X. Zhang, Q. Wang, Y. Lv, G. Mao, A. Luo, Y. Wu, Y. Wu, J. Zhang and W. Tan, *J. Am. Chem. Soc*., 2014, **136**, 9838; (g) Y.-J. Gong, X.-B. Zhang, C.-C. Zhang, A.-L. Luo, T. Fu, W. Tan, G.-L. Shen and R.-Q. Yu, *Anal. Chem*., 2012, **84**, 10777; (h) J. Han, J. Jose, E. Mei and K. Burgess, *Angew. Chem*., 2007, **119**, 1714; (i) J. Otsuki, Y. Kanazawa, A. Kaito, D.-M. Shafiqul Islam, Y. Araki and O. Ito, *Chem. Eur. J*., 2008, **14**, 3776.

4. W. Lin, L. Yuan, Z. Cao, Y. Feng and J. Song, *Angew. Chem., Int. Ed*., 2010, **49**, 375.

5. (a) P. Mahato, S. Saha, P. Das H. Agarwalla and A. Das, *RSC Adv*., 2014, **4**, 36140; (b) P. Mahato, S. Saha, E. Suresh, R. D. Liddo. P. P. Parnigotto, M. T. Conconi, M. K. Kesharwani, B. Ganguly and A. Das, *Inorg. Chem*., 2012, **51**, 1769; (c) S. Saha, P. Mahato, U. Reddy G, E. Suresh, A. Chakrabarty, M. Baidya, S. K. Ghosh and A. Das, *Inorg. Chem*., 2012, **51**, 336; (e) H. N. Kim, M. H. Lee, H. J. Kim, J. S. Kim and J. Yoon, *Chem. Soc. Rev*., 2008, 1465; (f) E. Karakus, M. U¨çu¨ncu¨ and M. Emrullahog˘lu, *Chem. Commun*., 2014, **50**, 1119; (g) K.-B. Li, Y. Zang, H. Wang, J. Li, G.-R. Chen, T. D. James, X.-P. He and H. Tian, *Chem. Commun*., 2014, DOI: 10.1039/c4cc04568h; (h) N. Kumar, V. Bhalla and M. Kumar, *Analyst*., 2014, **139**, 543; (i) M. Beija, C. A. M. Afonso and J.´ M. G. Martinho, *Chem. Soc. Rev*., 2009, **38**, 2410-2433.

6. (a) S. Saha, P. Mahato, M. Baidya, S. K Ghosh and A. Das*, Chem. Commun*., 2012, **48**, 9293; (b) M. Hörner, A. J. Bortoluzzi, J. Beck, M. Serafin, *Z. Anorg.Allg., Chem.* 2002, **628**, 1104; (c) M. Hörner, G. M. de Oliveira, M. B. Behm, H. Fenner, *Z. Anorg. Allg. Chem.,* 2006, **632**, 615.

7. (a) M. Harada, *Crit. Rev. Toxicol*., 1995, **25**, 1; (b) P. Grandjean, P Weihe, R. F White and F. Debes, *Environ. Res*., 1998, **77**, 165.

8. (a) National Primary Drinking Water Regulations, EPA–HQ–OW–2008–0747; FRL–9156–6; (b) Mercury: Human Exposure; United States Environmental Protection Agency (EPA)-2010-10-01. Retrieved 2011-04-09.

9. (a) J. Du, M. Hu, J. Fan, X. Peng, *Chem. Soc. Rev*., 2012, **41**, 4511; (b) S. Park, W. Kim, K. M. K. Swamy, H. Y. Lee, J. Y. Jung, G. Kim, Y. Kim, S.-J. Kim, J. Yoon, *Dyes and Pigments*., 2013, **99**, 323; (c) E. M. Nolan, S. J. Lippard, *Chem. Rev*., 2008, **108**, 3443; (d) Y. Wu, H. Jing, Z. Dong, Q. Zhao, H. Wu, F. Li, *Inorg. Chem*., 2011, **50**, 7412; (e) S.

Saha, H. Agarwalla, H. Gupta, M. Baidya, E. Suresh, S. K. Ghosh and A. Das, *Dalton Trans*., 2013, **42**, 15097.

10. (a) H. Lee, H.-S. Lee, J. H. Reibenspies and R. D. Hancock, *Inorg. Chem*., 2012, **51**, 10904; (b) McClure, *D. S. J. Chem. Phys*., 1949, **17**, 905.

11. (a) M. Suresh, A. K. Mandal, S. Saha, E. Suresh, A. Mandoli, R. D. Liddo, P. P. Parnigotto and A. Das, *Org. Lett*., 2010, **12**, 5406; (b) A. K. Mandal, M. Suresh, P. Das, E. Suresh, M. Baidya, S. K. Ghosh and A. Das, *Org. Lett*., 2012, **12**, 2980; (c) L. Zang, D. Wei, S. Wang and S. Jiang, *Tetrahedron*., 2012, **68**, 636.

12. (a) W. Lin, L. Long, L. Yuan, Z. Cao, B. Chen and W. Tan, *Org. Lett*., 2008, **10**, 5577; (b) M.-S. Tsai, Y.-C. Hsu, J. T. Lin, H.-C. Chen and C.-P. Hsu, *J. Phys. Chem. C*., 2007, **111**, 18785.

13. (a) U. Reddy G, R. Lo, S. Roy, T. Banerjee, B. Ganguly and A. Das, *Chem. Commun*., 2013, **49**, 9818; (b) U. Reddy G, H. Agarwalla, N. Taye, S. Ghorai, S. Chattopadhyay and A. Das, *Chem. Commun*., 2014, **50**, 9899.

14. (a) H. J. Kim, C. H. Heo and H. M. Kim*, J. Am. Chem. Soc.,* 2013, **135**, 7969; (b) E. G. Friberg, B. Cunderlíková, E. O. Pettersen and J. Moan, *Cancer Letters.*, 2003, **195**, 73.

5B. A new turn on Pd^{2+}-specific fluorescence probe and its use as an imaging reagent for cellular uptake in Hct116 cells

5B.1. Introduction

Palladium in its various oxidation states, is being widely used in organic synthesis, drug design, pharmaceuticals and commercial materials, such as fuel cells, dental crowns, medical instruments, jewellery, etc., owing to its inertness, biocompatibility and versatility as a catalyst.[1] The diverse role of Pd-complexes in different coupling reactions is explored extensively by synthetic chemists as well as for the production of a range of crucial fine chemicals and drug molecules.[2] Despite exhaustive purification processes, a certain amount of palladium could remain as an impurity in the final product,[2b,3] which is consumed along with the drug. Previous reports reveal that palladium has the propensity to coordinate to DNA, certain proteins/thiol-containing amino acids, and vitamin B6 and disrupt some cellular processes, which account for some health problems.[4] Apart from consumption of certain drugs/pharma products that are contaminated with trace amounts of palladium ions, human population also gets exposed to palladium through dental alloys, jewellery, food and emissions from automobile catalytic converters. Average dietary intake of palladium for an adult is estimated to be ~1.5 - 15 mg per day as per WHO report and its permitted threshold level in drugs is 5 - 10 ppm.[3] It has been argued that excretion of palladium happens mostly through urine and its concentration in urine typically lies in the range of 0.006 to $<$ 0.3 $\mu g.L^{-1}$ in adults.[5] All these have necessitated the development of an efficient fluorescent probe that could bind specifically and reversibly to Pd(II) species, as 2+ is the most abundant oxidation state of the palladium metal that could exist under physiological conditions or in live cells. Such a molecular probe could be ideal for detection of cellular uptake of Pd(II) or for diagnostic applications. Apart from these, the reagent that also allows instantaneous infield analysis of environmental samples has a distinct edge over other analytical

methods and procedures. Conventional methods for palladium detection rely mostly on analytical methodologies like atomic absorption spectrophotometry, solid-phase micro-extraction high-performance liquid chromate-graphy and ion-coupled plasma emission-mass spectrometry. Such procedures are generally expensive, time-consuming and need involvement of skilled individuals.[6] Such methodologies also involve complicated sample preparation procedures. These limitations have further exemplified the scope of an efficient and sensitive molecular probe that allows turn-on fluorescence response upon specific binding to Pd(II) ions in aqueous buffer medium having physiological pH as well as an imaging reagent.[7]

Pd(II) is generally known to be an efficient quencher for luminescence, as it favours an effective spin–orbit coupling and non-radiative deactivation of the excited states.[8] Thus, examples of the fluorescence off-based receptors for palladium are abundant in the contemporary literature.[8] Among limited fluorescence on-based receptors reported in the literature,[9] very few have been utilized either as imaging reagents or for detection of palladium in biological fluids.[10] More importantly, none of such receptors are found to be specific towards Pd(II).[8f,9i,j,10g–i] This motivated us to develop a rhodamine based molecular probe (**L**; Scheme 1) that was specific towards Pd(II) among all other metal ions under physiological conditions and could be utilized also as an imaging reagent or for detection of Pd(II) present in biological fluids like human urine samples. Conversion of the cyclic lactam form (fluorescence off mode) to the acyclic xanthene form (fluorescence-on mode) of a suitably substituted rhodamine derivative (**L**) upon specific binding to Pd(II) has been described in the present chapter. Possibility of using this as an imaging reagent for detection of cellular uptake of Pd(II) and its estimation in human urine samples is also discussed. Edge of such a reagent over conventionally used chemodosimetric reagents is discussed.[11]

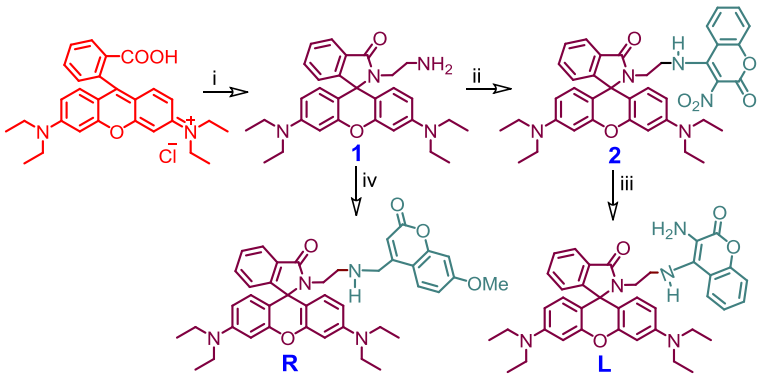

i. Ethylene diamine, EtOH, D 24 hr; **ii.** 4-Chloro-3-nitrocoumarin, CH_2Cl_2, K_2CO_3, 2hr; **iii.** Fe-HCl, MeOH-H_2O, D 1hr; **iv.** 4-Bromomethyl-7-methoxy coumarin Et_3N, Dry THF/N_2, D 10 hr.

Scheme 1. Methodologies that were adopted for synthesis of **1, 2, R** and **L**.

5B.2. Experimental Section

5B.2.1. Materials

Rhodamine B, Ethylenediamine, 4-Chloro-3-nitrocoumarin and Fe powder all metal perchlorate salts such as $NaClO_4$, $KClO_4$, $Mg(ClO_4)_2$, $Ca(ClO_4)_2$, $Cu(ClO_4)_2$, $Zn(ClO_4)_2$, $Co(ClO_4)_2$, $Ni(ClO_4)_2$, $Cr(ClO_4)_3$, $Fe(ClO_4)_2$, $Cd(ClO_4)_2$, $Hg(ClO4)_2$, $Pb(ClO_4)_2$ salts and $PdCl_2$ were obtained from Sigma-Aldrich and were used as received. Solvents used for synthesis of intermediates and final compounds were of AR grade; while HPLC grade solvents were used for spectroscopic studies. Such solvents were procured from S.D. Fine Chemicals in India.

5B.2.2. Analytical Methods

^1H NMR spectra were recorded AV 400 MHz or AV-500 MHz Bruker NMR spectrometers using $CDCl_3$-d_3 as the solvent and tetra methyl silane (TMS) as an internal standard. ESI-Ms measurements were carried out on a Waters QTof-Micro instrument. Electronic spectra were recorded with a Shimadzu UV-3101 PC spectrophotometer; while fluorescence spectra were recorded using Quanta Master 400, PTI spectrofluorometer.

5B.2.3. General experimental procedure for UV-Vis and Fluorescence studies

$5x10^{-2}$ M solution of the perchlorate salts of the respective ion (Na^+, K^+, Fe^{3+}, Na^+, Mg^{2+}, Ni^{2+}, Co^{2+}, Cu^{2+}, Cd^{2+}, Pb^{2+}, Zn^{2+}, Cr^{3+} and Hg^{2+}) were prepared in pure aqueous medium, while $PdCl_2$ in brine solution for all studies. A stock solution of the receptor **L** (1.0×10^{-4} M) was prepared in 10 mM HEPES buffer:CH_3CN (1:1, v/v; pH 7.2). Solution of the compound **L** was further diluted for spectroscopic titrations, and the effective final concentration of the solution of compound **L** used for the fluorescence studies was 10 μM, while the final analyte (Pd(II)) concentration during emission spectral scanning was 1.0×10^{-4} M. For all luminescence measurements, λ_{Ext} = 530 nm with an emission slit width of 2/2 nm. The relative fluorescence quantum yields (Φ_f) were estimated using Rhodamine B (Φ_f = 0.3 in aqueous medium at RT) as a reference.

5B.2.4. Methodology adopted for evaluation of $[Pd^{2+}]$ in human urine sample

Urine was diluted (fresh urine sample was diluted 100 times with water:acetonitrile (1: 1, v/v) medium before measurement and some solutions were spiked with known concentration of Pd^{2+} as an internal standard without further treatment. These solutions along with solutions spiked with known $[Pd^{2+}]$ (1 μM, 2 μM and 3 μM) as an internal standard were used for emission measurements without further treatment. Fluorescence intensity of such urine samples spiked with 1 μM, 2 μM and 3μM of Pd^{2+} were mentioned as $I_{urine+1}$, $I_{urine+2}$ and $I_{urine+3}$, respectively. Fluorescence intensities for aqueous HEPES buffer solution having pH of 7.2 was evaluated for $[Pd^{2+}]$ of 1, 2 and 3 μM and these values were I_1, I_2 and I_3, respectively. Average of three differences ($I_{urine+1}$-I_1), ($I_{urine+2}$-I_2) and ($I_{urine+3}$-I_3) and use of the the calibration plot for Pd^{2+} led us to evaluate the actual $[Pd^{2+}]$ of (0.2 μg/litre) in the urine sample.

5B.3. Synthesis and Characterization

5B.3.1. Synthesis of 2

A mixture of **1** (300 mg, 0.62 mmol), 4-Chloro-3-nitrocoumarin (140 mg, 0.62 mmol) were dissolved in dichloromethane (10 mL) stirred it room temperature for 2 hr under inert atmosphere. Progress of the reaction was monitored by TLC and stopped after 2 hr. The crude product was subjected to silica gel chromatography using DCM: Methanol (99: 1, v/v) as eluent. Major fraction was collected and dried under vacuum, which afforded a red solid (Yield: 400 mg, 95.92%). ESI-Ms (m/z) calculated for $C_{39}H_{39}N_5O_6$: 673, observed: 696 [M +Na]. ^{1}H NMR [500 MHz, $CDCl_3$-d_3: δ (ppm)]: 8.49 (1H, s, -NH); 8.22 (1H, d, 8Hz, ArH); 7.96 (1H, d, *J* = 6.5 Hz, ArH); 7.64 (1H, t, *J*= 8 Hz, ArH); 7.53 - 7.49 (3H, m, ArH); 7.33 (1H, d, *J* = 8 Hz, ArH); 7.15 (1H, d, *J* = 6.5Hz, ArH); 6.42 (2H, s, ArH); 6.37 (2H, d, *J* = 9Hz, ArH); 6.28 (2H, d, *J* = 8.5 Hz, ArH); 3.55 (2H, t, *J* = 4 Hz, CH_2); 3.38 (8H, t, *J* = 7 Hz, CH_2); 2.90 (2H, t, *J* = 4 Hz, CH_2); 1.21 (12H, t, *J* = 7 Hz, CH_3). ^{13}C NMR (125 MHz, $CDCl_3$-d_3, δ (ppm)): 133.34, 129.92, 12844, 127.92, 124.94, 124.11, 123.47, 122.95, 117.79, 114.29, 108.39, 103.57, 97.82, 66.12, 45.99, 44.44, 39.83 and 12.57.

5B.3.2. Synthesis of L

Methodology for the synthesis of this reagent was adopted from an earlier report with necessary modification.[12] Mixture of **2** (220 mg, 0.326 mmol) and Fe powder (116 mg, 2.071 mmol) were dissolved in methanol (15 mL) to this water 6 mL was added. Start the reflux by the time 6M HCl (4mL) was added. By monitoring TLC, after 1.5 hr reaction was stopped. The crude product was subjected to silica gel chromatography using DCM:Methanol (99: 3, v/v) as eluent. Major fraction was collected and dried under vacuum, which afforded a sticky red solid. Yield: 190 mg, 90.47 %. ESI-Ms (m/z) calculated for $C_{39}H_{41}N_5O_4$: 643, observed: 666.37 [L+ Na]. ^{1}H NMR [400 MHz, $CDCl_3$-d_3: δ (ppm)]: 7.98 (1H, s, -ArH); 7.62 (1H, d, *J* = 6.4 Hz, ArH); 7.50 (1H, d, *J* = 6.8 Hz, ArH); 7.33 (1H, t, *J* = 6 Hz, ArH); 7.28-7.22(3H, m, ArH); 7.13(1H, t, *J* = 6.4

Hz, ArH); 6.42 (1H, s, ArH); 6.39 (3H, t, *J* = 5.2 Hz, ArH); 6.18 (2H, d, *J* = 5.6 Hz, ArH); 5.27 (1H, s, -NH); 3.55 (2H, t, *J* = 4.4 Hz, CH_2); 3.32 (8H, q, *J* = 5.6 Hz, CH_2); 3.23 (2H, t, *J* = 4.4 Hz, CH_2); 1.16 (12H, t, *J* = 5.6 Hz, CH_3). ^{13}C NMR (400 MHz, $CDCl_3$-d_3, δ (ppm)): 170.06, 161.23, 153.33, 148.92, 136.75, 132.92, 130.61, 128.61, 128.35, 128.00, 123.93, 128.83, 122.90, 121.61, 117.48, 116.71, 111.96, 108.04, 104.81, 97.65, 65.43, 60.41 46.59, 44.34, 40.32 and 12.55.

5B.3.3. Synthesis of R

Synthetic procedure used for synthesis of **R** was adopted from one of our previous literature reports.[13]

5B.4. Results and Discussions

All UV-Vis and luminescence spectra of **L** (10 μM) were recorded in aq. HEPES buffer (10 mM)-CH_3CN (1:1, v/v; pH 7.2) medium. Electronic spectra revealed two absorption bands: a weak band at 352 nm (8000 M^{-1} cm^{-1}) and a prominent sharp band at 321 nm (20000 $M^{-1}cm^{-1}$). No detectable absorbance beyond 400 nm was observed, which further corroborated that **L** was present almost exclusively in the spirolactam form under the experimental condition (pH 7.2). A characteristic signal at ~ 65.43 ppm for the tertiary C-atom in the ^{13}C NMR spectrum for **L** also confirmed its spirolactam structure.[14] Absorbance spectra of **L** (10 μM) were recorded in the absence and the presence of 100 μM of various metal ions (Na^+, K^+, Ag^+, Hg^{2+}, Pb^{2+}, Cd^{2+}, Cu^{2+}, Cr^{3+}, Ni^{2+}, Fe^{3+}, Co^{3+}, Zn^{2+}, Ca^{2+}, Al^{3+}, Pt^{2+} and Mg^{2+}) including Pd^0 and Pd^{4+} in aq. buffer-CH_3CN medium (1:1, v/v; pH 7.2) (Figure 5B.1a). Among all these cationic analytes, a distinct new spectrum having a band maximum at 567 nm appeared only in the presence of Pd^{2+} and this accounted for the visually detectable change in solution colour from colourless to purple. It may be mentioned that the spectral changes were instantaneous and showed a linear dependency for [Pd^{2+}] of 0

to 20 x 10^{-5} M. B-H. plots, obtained by using data available from systematic absorption titrations at 25°C, revealed association constant of (4.8 ± 0.5) x 10^{3} M^{-1}.

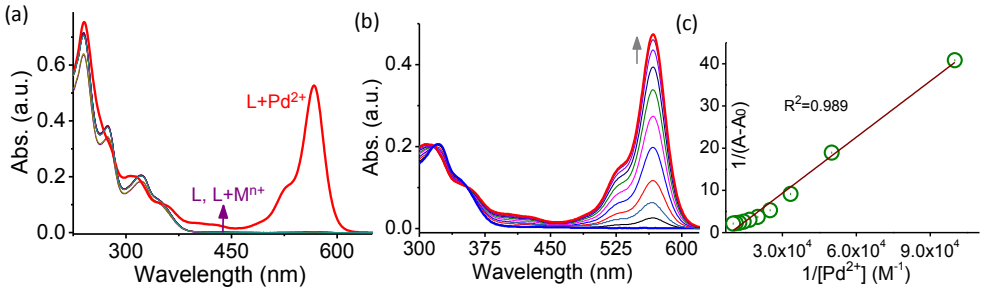

Figure 5B.1. Changes in (a) absorption spectra of the receptor **L** (10 μM) in presence and absence of different metal ions (M^{n+}: Li+, Na^{+}, K^{+}, Ca^{2+}, Mg^{2+}, Cr^{3+}, Fe^{2+}, Co^{3+}, Ni^{2+}, Cu^{2+}, Zn^{2+}, Hg^{2+}, Cd^{2+}, Pb^{2+}, Pt^{2+}, Pd^{2+}, Pd^{0} and Pd^{4+} (b) Change in absorption spectra for **L** (10 μM) in presence of varying [Pd^{2+}] (0 - 20 μM); (c) Benesi-Hildebrand (B-H) plots of spectral titration. Good linear fit confirms the 1: 1 binding stoichiometry. All studies were performed in aq. HEPES buffer-acetonitrile (1: 1, v/v; pH 7.2) medium.

Binding stoichiometry of 1:1 was ascertained from the good 'linear fit of the B.H plot and ESI-Ms spectrum of the Pd^{2+}-complex shows peaks at m/z 783.63 was attributed to [L+ Pd^{2+}- H^{+}]. Further, this ratio between the metal and **L** was also confirmed by the Job plot. The selective binding of **L** to Pd^{2+} among all other metal ions was also studied using the emission spectral response of the solution of **L** (10 μM) in the absence and presence of an excess of each of these metal ions in aq. solution of HEPES buffer-CH_3CN (1:1, v/v; pH 7.2) medium

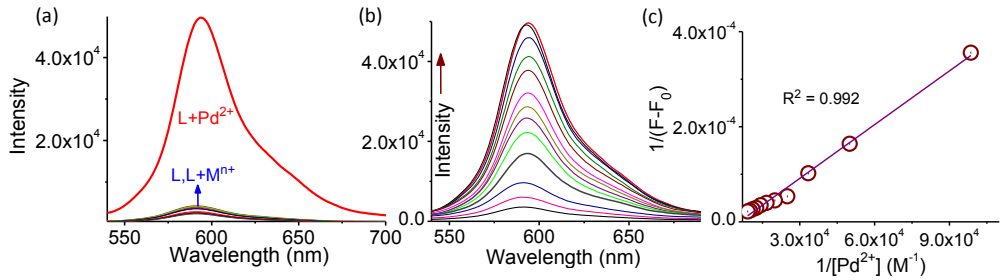

Figure 5B.2. Changes in (a) luminescence spectra of the receptor **L** (10 μM) in presence and absence of different metal ions (M^{n+}: Li+, Na^{+}, K^{+}, Ca^{2+}, Mg^{2+}, Cr^{3+}, Fe^{2+}, Co^{3+}, Ni^{2+}, Cu^{2+}, Zn^{2+}, Hg^{2+}, Cd^{2+}, Pb^{2+}, Pt^{2+}, Pd^{2+}, Pd^{0} and Pd^{4+} (b) Change in luminescence spectra for **L** (10 μM) in presence of varying [Pd^{2+}] (0 - 20 μM); (c) B-H plots of spectral titration. Good linear fit confirms the 1:1 binding stoichiometry. All studies were performed in aq. HEPES buffer-acetonitrile (1:1, v/v; pH 7.2) medium by using λ_{Ext} = 530 nm; and slit width 2/2 nm.

Upon addition of Pd^{2+}, solution of **L** showed strong emission bond at 594 nm under excitation at 530 nm (Figure 5B.2). No such change or insignificant changes was/were observed for all other cations that we studied, including Pd^{4+} or Pd^{0}.

These results revealed that apart from Pd^{2+}, all other metal ions (including Pd^{0} and Pd^{4+}) either failed to bind to **L** or binding of **L** to any of these metal ions was too weak to convert the non luminescent spirolactam derivative to the acyclic and luminescent xanthene forms.[14] The results of the ^{1}H and ^{13}C NMR studies further confirmed this. The emission quantum yield for **L** was evaluated as Φ_L = 0.011 for λ_{Ems} of 594 nm (λ_{Ext} = 530 nm), while this value was found to be 0.245 in the presence of Pd^{2+}. Peng and his co-workers have contributed significantly to the development of efficient and specific receptors for Pd(II) species. However, most of their receptors for Pd(II) also showed sluggish but similar responses towards Pd(0).[9b] In few instances, receptors for Pd(II) showed distinct interference for Pd(IV).[8f,9i,j,10g–i] To the best of our knowledge, this present molecular probe is the first example of a receptor that showed specificity towards Pd(II) under physiological conditions.

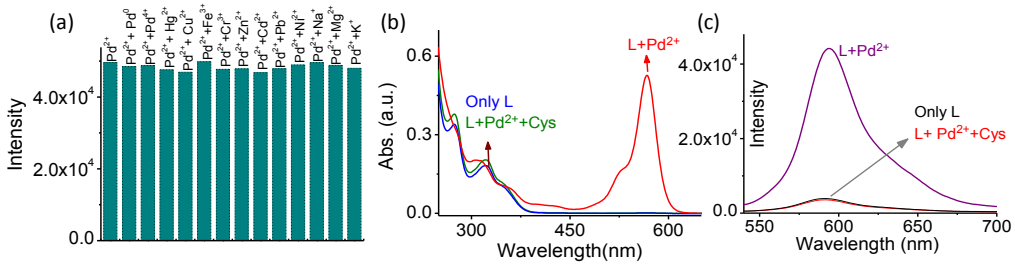

Figure 5B.3. (a) Spectrophotometric interference study of **L** (10 μM) for Pd^{2+}(10 μM) in presence of various metal ions (20 μM); (b) UV and (c) Fluorescence studies for establishing the reversible binding of Pd^{2+} (2 mole eq) to **L** (10 μM) in presence of Cysteine (4 eq) and using λ_{Ext} = 530 nm; and slit width 2/2 nm, in aq. solution of HEPES buffer-CH_3CN (1:1, v/v; pH 7.2).

Systematic luminescence titrations were carried out for **L** (10 μM) with varying [Pd^{2+}] (0 to 20 μM) in aq.HEPES buffer: CH_3CN (1:1, v/v, pH 7.2) medium. Increase in [Pd^{2+}] caused a concomitant increase in emission intensity at ~ 597 nm (Figure 5B.2). B-H. plots, obtained by using data available from systematic absorption

titrations at 25°C, revealed association constant of (5.8 ± 0.5) x 10^3 M^{-1}. Binding stoichiometry of 1:1 was ascertained from the good linear fit of the B.H plot.

The lowest detection limit (3σ/slope) for Pd^{2+} detection (using data available from fluorescence titration) was found to be 0.106 ppm.[15] Furthermore, interference studies in the presence of 10 mole excess of all other metal ions, including Pd^0 and Pd^{4+}, ensured that the reagent **L** was specific towards Pd^{2+} even in the presence of competing cationic analytes (Figure 5B.3).

Reversibility of the binding process between **L** and Pd^{2+} was established by allowing Pd^{2+} to form an even more stable complex $Pd(Cys)_2$ (Cys is Cysteine and $K_{Association}$ for Pd(N-acetyl cys)$_2$ is reported to be ~10^8).[16] The purple solution of Pd^{2+}.**L** turned colourless upon addition of 2 mole equiv. of Cys and both electronic as well as luminescence spectra of **L** were restored (Figure 5B.3).

The luminescence switch *ON* response of the reagent (**L**) occurred at pH 7.2 only upon specific binding to Pd(II), which led to the transformation from a non-luminescent cyclic lactam form to an acyclic luminescent xanthene form. At a similar media pH (7.2), reagent **L** alone remained in the non luminescent lactam form

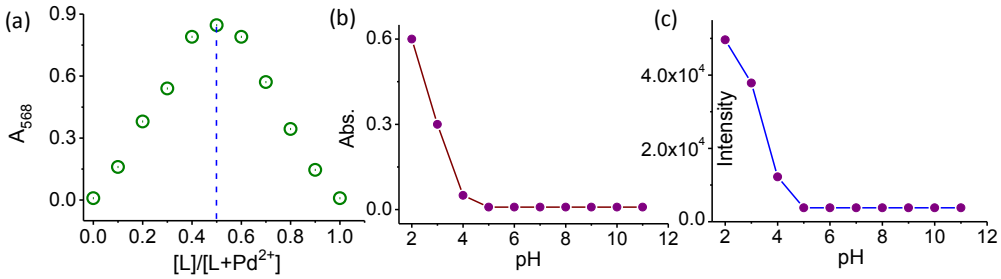

Figure 5B.4. (a) Job's plot between **L** and Pd^{2+} confirmed 1:1 adducts; (b) UV; (c) Fluorescence response of **L** (10 μM) as a function of pH in acetonitrile-universal buffer (1:1, v/v), pH is adjusted by using aqueous solutions of 1 M HCl or 1 M NaOH.

. UV-vis and luminescence spectra were recorded for **L** (10 μM) at varying solution pH and the results of such studies revealed that the conversion from spirocyclic to acyclic xanthene form of the reagent (**L**) could occur only at pH < 4.5 (Figure 5B.4). This confirmed that luminescence in response to ~ 594 nm was only due to the

specific binding of the reagent (**L**) to Pd(II). Most importantly, none of the metals including Pd^0 and Pd^{4+} could influence the optical response of **L**. Emission spectra were recorded for **L** (with λ_{Ext} = 360 nm) and these showed significant luminescence quenching of the coumarin moiety (λ_{max}^{Ems} at 450 nm) in the presence of Pd(II) and an insignificant spectral overlap (Figure 5B.5(b)) with the absorption spectral band with maxima at ~ 567 nm for Pd^{2+}.**L** nullified the possibility for any FRET process being operational.

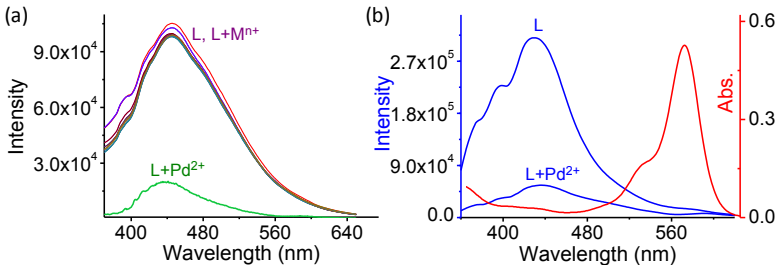

Figure 5B.5. (a) Changes in emission spectra (λ_{Ext} of 360 nm; slit = 2/2 nm) of the receptor **L** (10 μM) in absence and presence of different metal ions (M^{n+} = Li^+, Na+, K^+, Mg^{2+}, Al^{3+}, Ca^{2+}, Ba^{2+}, Sr^2+, Cu^{2+}, Ni^{2+}, Zn^{2+}, Cd^{2+}, Co^{2+}, Fe^{2+}, Fe^{3+}, Cr^{3+}, Pb^{2+}, Pd^{2+} , Pt^{2+}, Pd^0, Pd^{4+}); All studies were performed in aq. solution of aq.HEPES buffer (10 mM):CH_3CN (1:1, v/v; pH 7.2). (b) Overlap spectra of **L** (λ_{Ext} = 360 nm was used for recording emission spectra).

In two of our previous reports we have shown that Hg(II)-η^2-arene π-interaction in a rhodamine–coumarin hybrid could induce a through bond energy transfer (TBET) process.[13,17] Pd(II) is also known to form a stable M^{n+}-η^2-arene π bond.

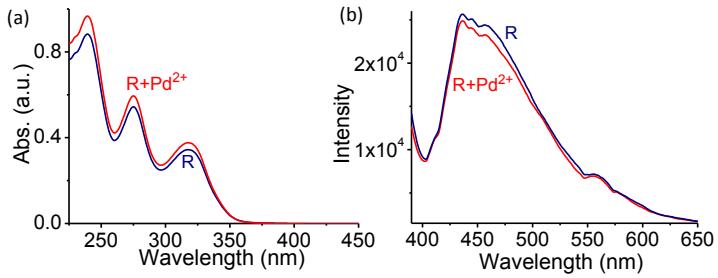

Figure 5B.6. Changes in (a) absorption and (b) emission spectra (λ_{Ext} of 530 nm; slit = 2/2 nm) of the receptor **R** (10 μM) in absence and presence of Pd^{2+}; Studies were performed in aq. HEPES buffer-acetonitrile (1: 1, v/v; pH 7.2) medium.

Presumably, coordination of the 3-amino functionality of the coumarin moiety did not favour such an interaction. In absence of such an interaction the possibility of any

TBET process was nullified. Model reagent **R** (Scheme 1) was synthesized following the literature report to unveil the crucial role that this 3-amino functionality played a crucial role in binding to Pd^{2+}. No detectable change in UV-vis and fluorescence spectra for **R** was evident when spectra were recorded in absence and presence of Pd^{2+} under the identical experimental conditions (Figure 5B.6). This corroborates that the amine group of **L** played a pivotal role in achieveing the desired specificity towards Pd^{2+} ion.

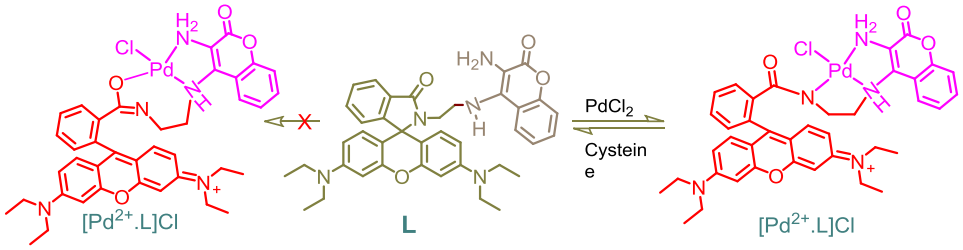

Scheme 2. Proposed mode of coordination for $[Pd^{2+}.L]Cl$.

The interactions between Pd^{2+} and **L** were investigated by IR, ^{1}HNMR and ^{13}CNMR spectroscopic studies. Stretching frequencies for the C=O group in FTIR spectra of the coumarin moiety in **R** and **2** appeared at ~1714 and ~1719 cm^{-1}, respectively.

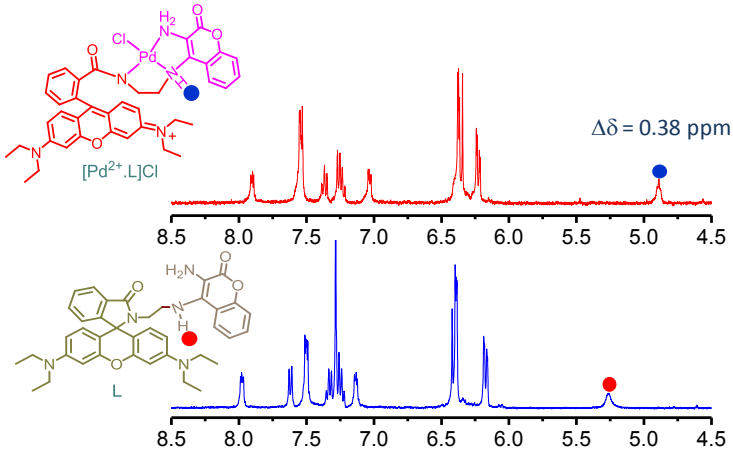

Figure 5B.7. Partial ^{1}H NMR spectra of **L** (3 mM) in absence and presence of Pd^{2+} in CD_3CN-d_3.

The absence of such a band for **L** could be ascribed to a strong hydrogen bonding interaction between O_C=O of the coumarin moiety and the H_3-amino functionality,

which induced a shift to higher energy and eventually got masked within the strong band at ~1685 cm^{-1}, the stretching band for the $C=O_{Amide}$ of the rhodamine moiety. This band appeared almost in a similar frequency region for all three rhodamine derivatives (e.g. **R**, **2** and **L**) and it remained almost invariant upon binding of **L** to Pd^{2+}. This tend to leave us with an impression that $O_C=O_{[Amide]}$ of the rhodamine moiety was not involved in coordination with the Pd^{2+}-centre in Pd^{2+}.**L**.

^{13}C NMR spectra recorded for **L** confirmed that that the band for $C_C=O$ of the coumarin moiety was up field shifted by 5 ppm (-Δδ B 5 ppm; 161 ppm to 156 ppm) upon binding of **L** to Pd^{2+}, while an insignificant shift (Δδ ~ 1 ppm; 161 ppm to 162 ppm) for $C_C=O_{[Amide]}$ of the rhodamine moiety was observed (Figure 5B.8). This further corroborated our presumption that $O_C=O_{[Amide]}$ of the rhodamine moiety was not involved in coordination to Pd^{2+} either in keto form or in enolate form.[10h] FTIR spectra also revealed that the N-H stretching frequency of the $–NH_2$ functionality became broad and shifted to lower energy (by ~120 cm^{-1}) upon binding of **L** to Pd(II).

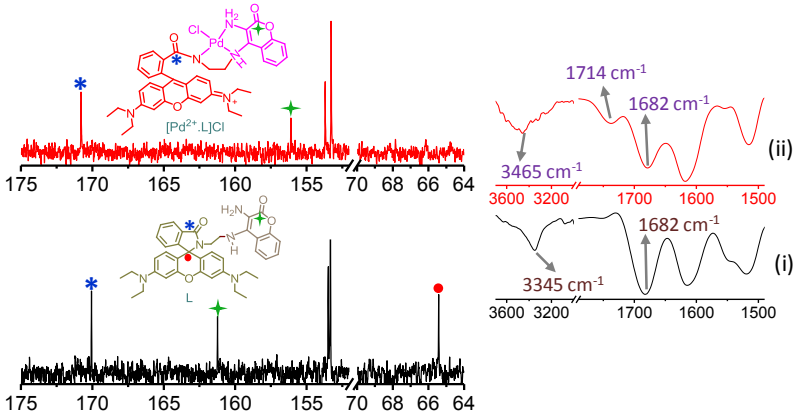

Figure 5B.8. Partial ^{13}C NMR spectra of **L** and [Pd^{2+}.**L**]Cl in CD_3CN; inset; partial IR spectra of **L** in (i) absence and (ii) presence of Pd^{2+}.

All these corroborate that amine group of **L** played a crucial role in the specific binding of **L** to Pd^{2+} ion. Strong coordination and binding of amino functionality to Pd^{2+} could contribute to this high affinity and further, favoured the coordination-induced ring-opening of **L**. The binding stoichiometry between Pd^{2+} and **L** was

ascertained by ESI-Ms studies also. ESI-Ms signal at m/z of 784.32 was attributed to [**L**+ Pd^{2+}+H^{+}].

Urine sample analysis:

The Pd^{2+} levels in urine typically lies in the range of 0.006 - < 0.3 μg/L in adults.[5] To explore the possibility of evaluating unknown [Pd^{2+}] in urine, a standard curve was generated from the plot of the ΔI (I_0- I) vs. known [Pd^{2+}] (0 to 7 μM) (Figure 5B.9). A detailed methodology and the generation of the calibration curve with the linear fluorescence response range for estimation of unknown Pd^{2+} in mixed aq. buffer (pH 7.4) solution as well as in the adult urine sample (Figure 5B.9) are discussed in detail in experimental section (*vide supra*).

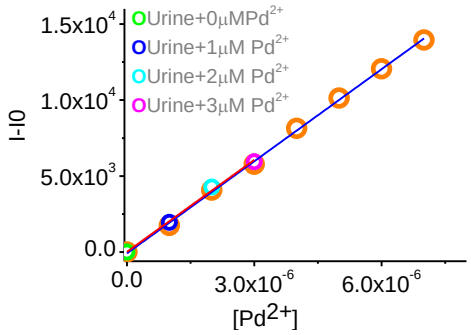

Figure 5B.9. Plot of ΔI (I_0 - I) vs. [Pd^{2+}], where I_0 and I are emission intensities of receptor **L** at 594 nm (λ_{Ext} = 530 nm) in the absence and the presence of known [Pd^{2+}] and urine samples spiked with known [Pd^{2+}], respectively.

The final concentration of the probe molecule **L** in each solution used for estimation of Pd^{2+} in urine sample was maintained at 10 μM. Then, urine was diluted before use and Pd^{2+} was spiked into the urine as an internal standard without further treatment (the urine was totally diluted 100 times with water:acetonitrile (1:1, v/v) before measurement). This solution along with solutions spiked with known [Pd^{2+}] (1 μM, 2 μM and 3 μM) as an internal standard were used for emission measurements without further treatment. The Pd^{2+} concentration in urine was determined to be 0.2 μg/L, which is within the allowed limit for Pd^{2+} content in adult urine sample of a healthy human being.

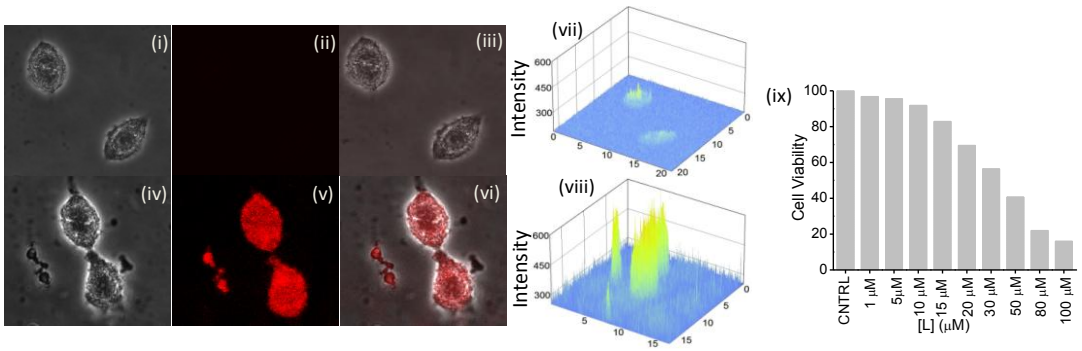

Figure 5B.10. (i)–(iii) Confocal laser scanning microscopy (CLSM) images of Hct116 colon cancer cells incubated with L (10 μM) as control: (i) a bright field image, (ii) an image observed in the red channel and (iii) an overlay image of (i) and (ii); (iv)–(vi) CLSM images of Hct116 cells incubated with **L** (10 μM) for 30 min and then further exposed to Pd^{2+} (0.1 ppm) for 30 min at 37 °C: (iv) a bright field image, (v) an image observed in the red channel and (vi) overlay images of (iv) and (v); graphical 3D CLSM images of Hct116 cells (vii) pre-exposed to **L** (10 μM) only and (viii) pre-treated with **L** (10 μM) for 30 min and then further exposed to a Pd^{2+} (0.1 ppm) (λ_{Ext} = 530 nm); (ix) MTT assay to determine the cell viability percentage in Hct116 colon cancer cells. The concentration of the **L** ranges from 1- 100 μM and treated for 24 hours.

MTT assay was performed to evaluate the toxicity of this reagent towards Hct116 cells (Figure 5B.10(ix)). After ascertaining the fact that reagent **L** showed only moderate toxicity towards live cancer Hct116 cells, the possibility of using this reagent for the detection of Pd^{+2} uptake in live cancer Hct116 cells was explored using a laser excitation source of 530 nm. Initially, live Hct116 cells were incubated with only **L** (10 μM) for 30 min at 37 °C. After necessary and thorough washing, these cells showed no fluorescence was observed. Further, CLSM images revealed that Hct116 cells that were pre-treated with 10 μM reagent **L** (and thoroughly washed for removal of the surface adhered reagent) and subjected to follow-up treatment with Pd^{2+} (0.1 ppm) showed a strong fluorescence in the red channel (Figure 5B.10). These results demonstrated two important aspects: reagent **L** was cell membrane permeable and could be used as an imaging reagent for the detection of Pd^{2+} uptake in live cells. Additional studies confirmed that the uptake of Pd^{2+} as low as 0.1 ppm could be detected in live Hct116 cells, which was significantly lower than the specified threshold value in drugs (5-10 ppm).

In brief, studies with a new coumarin-rhodamine conjugate are described for specific detection of Pd^{2+} from an ensemble of several other competing cations, including Pd^{0} and Pd^{4+}. This reagent showed a turn *ON* fluorescence response on binding to Pd^{2+} ion. Further, scope of such a reagent for use as an imaging reagent for the detection of the cellular uptake of Pd^{2+} ions in live Hct116 colon cancer cell lines and human urine sample analysis is discussed.

5B.5.References

1. (a) R. F. Heck, Palladium Reagents in Organic Syntheses, Academic Press, New York, 1985; (b) R. Chinchilla and C. Nájera, *Chem. Rev.*, 2007, **107**, 874; (c) T. W. Lyons and M. S. Sanford, *Chem. Rev.*, 2010, **110**, 1147; (c) J. Kielhorn, C. Melber, D. Keller, I. Mangelsdorf, *Int. J. Hyg. Environ. Health*, 2002, **205**, 417.

2. (a) J. S. Carey, D. Laffan, C. Thomson, M. T. Williams, *Org. Biomol.Chem*., 2006, **4**, 2337; (b) A. O. King, N. Yasuda, *Top. Organomet. Chem*., 2004, 205; (c) S. L. Buchwald, C. Mauger, G. Mignani and U. Scholz, *AdV. Synth. Catal*., 2006, **348**, 23.

3. C. E. Garrett and K. Prasad, *AdV. Synth. Catal*., 2004, **346**, 889.

4. (a) J. C. Wataha and C. T. Hanks, *J. Oral Rehabil*., 1996, **23**, 309; (b) C. L. S. Wiseman and F. Zereini, *Sci. Total Environ*., 2009, **407**, 2493; (c) T. Gebel, H. Lantzsch, K. Plebow and H. Dunkelberg, Mutat. Res., Genet. *Toxicol. Environ. Mutagen*, 1997, **389**,183; (d) J. Kielhorn, C. Melber, D. Keller and I. Mangelsdorf, *Int. J. Hyg. Environ. Health*, 2002, **205**, 417.

5. World Health Organization. Fenitrothion, Environmental Health Criteria Document No. 226. WHO: Geneva, 2002. D. Keller and I. Mangelsdorf.

6. (a) K. Van Meel, A. Smekens, M. Behets, P. Kazandjian and R. V. Grieken, *Anal. Chem*., 2007, 79, 6383; (b) C. Locatelli, D. Melucci and G. Torsi, *Anal. Bioanal. Chem*., 2005, **382**, 1567; (c) B. Dimitrova, K. Benkhedda, E. Ivanova and F. Adams, *J. Anal. At. Spectrom*., 2004, **19**, 1394.

7. (a) H. Li, J. Fan and X. Peng, *Chem. Soc. Rev*., 2013, **42**, 7943; (b) Y. Yang, Q. Zhao, W. Feng and F. Li, *Chem. Rev*., 2013, **113**, 192; (c) U. Reddy G, P. Das, S. Saha, M. Baidya, S. K. Ghosh and A. Das, *Chem. Commun*., 2013, **49**, 255; (d) H. N. Kim, M. H. Lee, H. J. Kim, J. S. Kim and J. Yoon, *Chem. Soc. Rev*., 2008, 1465; (e) H. N. Kim, W. X. Ren, J. S. Kim and J. Yoon, *Chem. Soc. Rev*., 2012, **41**, 3210-3244.

8. (a) A. Harriman, *J. Chem Soc, Faraday Trans*., 1981, **77**, 1281-1291; (b) D. Eastwood, M. Gouterman, *J. Mol. Spectrosc*., 1970, **35**, 359; (c) J.-P. Li, H.-X. Wang, H.-X. Wang, M.-S. Xie, G. R. Qu, H,-Y. Niu and H.-M. Guo, *Eur. J. Org. Chem*., 2014, 2225; (d) L. P. Duan, Y. F. Xu and X. H. Qian, *Chem. Commun*., 2008, 6339; (e) B. Liu, Y. Bao, F. Du, H. Wang, J. Tian and R. Bai, *Chem. Commun*., 2011, **47**, 1731; (f) A. Kumar, M. Chhatwal, A. K. Singh, V. Singh and M. Trivedi, *Chem. Commun*., 2014, **50**, 8488.

9. (a) F. L. Song and K. Koide, *J. Am. Chem. Soc*., 2009, **131**, 5163; (b) H. Li, J. Fan, M. Hu, G. Cheng, D. Zhou, T. Wu, F. Song, S. Sun, C. Duan and X. Peng, *Chem. Eur. J*., 2012, **18**, 12242; (c) F. Song, A. L. Garner and K. Koide, *J. Am. Chem. Soc*., 2007, **129**, 12354; (d) S. Goswami, D. Sen, N. K. Das, H.-Kun Fun and C. K. Quah, *Chem. Commun*., 2011, **47**, 9101; (e) J. Jiang, H. Jiang, W. Liu, X. Tang, X. Zhou, W. Liu and R. Liu, *Org. Lett*., 2011, **13**, 4922; (f) M. E. Jun and K. H. Ahn, *Org. Lett*., 2010, **12**, 2790; (g) T. Schwarze, C. Dosche, R. Flehr, T. Klamroth, H.-G. Löhmannsröben, P. Saalfrank, E. Cleve, H.-J. Buschmann and H.-J. Holdt, *Chem. Commun*., 2010, **46**, 2034; (h) S. Cai, Y. Lu, S. He, F. Wei, L. Zhaoab and X. Zeng, *Chem. Commun*., 2013, **49**, 822; (i) D. Keum, S. Kim and Y. Kim, *Chem. Commun*., 2014, **50**, 1268; (j) M. Arca, C. Caltagirone, G. D. Filippo, M. Formica, V. Fusi, L.

Giorgi, V. Lippolis, L. Prodi, E. Rampazzo, M. A. Scorciapino, M. Sgarzi and N. Zaccheronic, *Chem. Commun*., 2014, **50**, 15259.

10. (a) M. Santra, S.-K. Ko, I. Shin and K. H. Ahn, *Chem. Commun*., 2010, **46**, 3964; (b) M. Kumar, N. Kumar and V. Bhalla, *RSC Adv*., 2013, **3**, 1097; (c) H. Chen, W. Lin and L. Yuan, *Org. Biomol. Chem*., 2013, **11**, 1938; (d) W. Liu, J. Jiang, C. Chen, X. Tang, J. Shi, P. Zhang, K. Zhang, Z. Li, W. Dou, L. Yang and W. Liu, *Inorg. Chem*., 2014, **53**, 12590; (e) B. Zhu, C. Gao, Y. Zhao, C. Liu, Y. Li, Q. Wei, Z. Ma, B. Du and X. Zhang, *Chem. Commun*., 2011, **47**, 8656; (f) J. Wang, F. Song, J. Wang and X. Peng, *Analyst*., 2013, **138**, 3667; (h) X. Wang, Z. Guo, S. Zhu, H. Tian and W. Zhu, *Chem. Commun*., 2014, **50**, 13525; (i) S. Sun, B. Qiao, N. Jiang, J. Wang, S. Zhang and X. Peng, *Org. Lett*., 2014, **16**, 1132; (j) H. Li, J. Fan, J. Du, K. Guo, S. Sun, X. Liu and X. Peng, *Chem. Commun*., 2010, **46**, 1079-1081.

11. (a) J. Jiang, H. Jiang, W. Liu, X. Tang, X. Zhou, W. Liu, and R. Liu, *Org. Lett*., 2011, **13**, 4922; (b) X. Chen, H. Li, L. Jin, B. Yin *Tetrahedron Lett*., 2014, **55**, 2537.

12. H. Lu, L. Xiong, H. Liu, M. Yu, Z. Shen, F. Li and X. You, *Org. Biomol. Chem*., 2009, **7**, 2554.

13. S. Saha, P. Mahato, M. Baidya, S. K Ghosh and A. Das, *Chem. Commun*., 2012, **48**, 9293

14. (a) P. Mahato, S. Saha, P. Das, H. Agarwalla and A. Das, *RSC Adv*., 2014, **4**, 36140; (b) S. Saha, P. Mahato, U. Reddy G, E. Suresh, A. Chakrabarty, M. Baidya, S. K. Ghosh and A. Das, *Inorg. Chem*., 2012, **51**, 336.

15. U. Reddy G, H. Agarwalla, N. Taye, S. Ghorai, S. Chattopadhyay and A. Das, *Chem. Commun*., 2014, **50**, 9899.

16. J. Giljanović, M. Brkljača and A. Prkić, *Molecules*., 2011, **16**, 7224.

17. U. Reddy G, V. Ramu, S. Roy, N. Taye, S. Chattopadhyay and A. Das, *Chem. Commun*., 2014, **50**, 14421.

5C. A FRET-based probe for monitoring subtle pH changes in endoplasmic reticulum

5C.1. Introduction

Intracellular pH (pH_i) is an important physiological parameter in various biological processes for studying cellular metabolisms and gaining insights into physiological and pathological processes.[1,2] It is being argued that the abnormal level of intracellular pH could be used as an important early stage symptom for crucial diseases like cancer,[3a] Alzheimer's disease,[3b] etc. Different organelles of Eukaryotic cells have different pH values. For example, pH in mitochondria is around 8.0, where as other organelles such as lysosomes and endosomes have intracompartmental pHs of 4.0 to 6.0.[4] Among various organelles, endoplasmic reticulum (ER) is one of the largest compartment of the eukaryotic cells having pH 7.2 ± 0.2. Very little is understood about the ionic composition of the endoplasmic reticulum (ER), one of the major compartments of the secretory pathway.[5] This has been primarily due to the inaccessibility of ER to exogenous probes. Secretion of proteins that follow secretory pathway has its origin in the endoplasmic reticulum. It has been argued that the pH within individual organelles of the secretory pathway is an important factor for their biosynthetic activity. The importance of pH in the secretory pathway is also revealed by the adverse influence induced by inhibitors of the major organelles proton pump, the vacuolar H^+-ATPase, or V-ATPase.[6] The V-ATPase is an ATP-driven enzyme that transforms the energy of ATP hydrolysis to pump protons across diverse biological membranes via the primary active transport of H^+.[7] Considering the fact that wide range of cells used and approaches adopted for measuring the pH of the different compartments of the secretory pathway, little disparity in the reported pH of an individual compartment is noticed.[8] Despite such variations, a general agreement has been reached regarding the absolute pH of the individual organelles. The endoplasmic reticulum pH is generally thought to be near neutral. However, the

compartments of the secretory pathway become progressively more acidic thereafter, as the products of secretion approach their final destination.[9] Any deviation from such precisely maintained lumenal pH for ER and other compartments involved in secretory pathway would have disrupted the activation of enzymes, sorting and processing of secretory proteins, lipid biosynthesis and calcium storage.[10] These reports have clearly revealed that the pH within the individual organelles of the secretory pathway is crucial for maintaining their biosynthetic activity and the precise measurement of the pH in the secretory organelles is essential for developing a better insight in understanding the processes associated with secretion of proteins. Much research effort has been devoted to the development of new pH probes for monitoring minor changes in pH in lysosome[11] and mitochondria.[12] To the best of our knowledge, example of molecular probe for non-invasive dynamic measurement of pH in the lumen of the endoplasmic reticulum, a lipid dense region, is scanty in the contemporary literature.[13] First report for estimation of the pH of the ER revealed that the measurement was made by quantifying the partition of a permeant weak base by immune electron microscopy,[14] and since then there are attempts for developing an efficient ER specific fluorescent probe. However, such attempts are mostly restricted in utilizing probes for monitoring ER redox poise using derivatives of green fluorescent proteins with a small stokes shift value.[15] A recent report reveals the use of a naphthalenediimide derivative as imaging reagent for estimation of pH_{ER} in aq. buffer-DMSO (9:1, v/v) medium with Stokes shifts of ~ 75 nm.[13a] Parker and his co-workers have reported an unique UV-excitable Eu(III)-based luminescent reagent for efficient probing of subtle changes in intracellular (NIH 3T3 cells) pH with delayed longer wavelength emission.[13b] Till date there is no report on a Förster Resonance Energy Transfer (FRET) based efficient ER specific fluorescent probe for monitoring minor changes in intracellular pH; though such an imaging probe has an obvious edge over the others: primarily for achieving a large Stokes shift value and also to

minimize the problem like photobleaching.[16] It has been argued by many researchers that any evaluation of the change in pH of the ER (pH_{ER}) region provides information on overall cytosolic pH. Considering these, design of an ER specific and FRET based imaging reagent for monitoring changes in Intracellular pH has significance. In this chapter, we have described a new molecular probe (**L**, Scheme 1) for monitoring the subtle changes in pH_{ER} based on FRET mechanism.

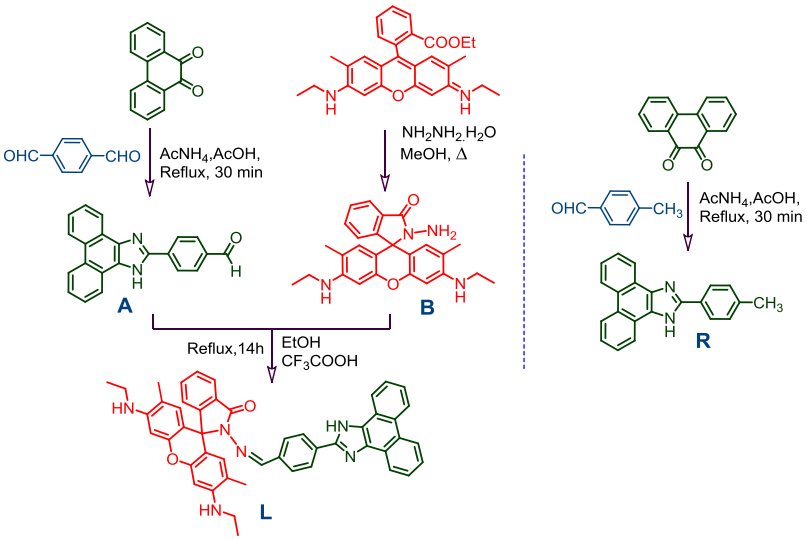

Scheme 1: Methodologies that were adopted for synthesis of **A**, **B**, **L** and **R**.

5C.2. Experimental Section

5C.2.1. Materials

Rhodamine 6G, Hydrazene monohydrate, 9,10-Phenanthrenequinone, Terephthal aldehyde, 4-Methylbenzaldehyde, Trifluoroacetic acid, all metal perchlorate salts such as $NaClO_4$, $KClO_4$, $Mg(ClO_4)_2$, $Ca(ClO_4)_2$, $Cu(ClO_4)_2$, $Zn(ClO_4)_2$, $Co(ClO_4)_2$, $Ni(ClO_4)_2$, $Cr(ClO_4)_3$, $Fe(ClO_4)_2$, $Cd(ClO_4)_2$, $Hg(ClO4)_2$, $Pb(ClO_4)_2$ salts and $PdCl_2$ were obtained from Sigma-Aldrich and were used as received. Solvents used for synthesis of intermediates and final compounds were HPLC grade solvents for spectroscopic studies from S.D. Fine Chemicals in India.

5C.2.2. Analytical Methods

^{1}H NMR spectra were recorded AV-500 MHz Bruker NMR spectrometers using DMSO-d_6 as the solvent and tetra methyl silane (TMS) as an internal standard. ESI-Ms measurements were carried out on a Waters QTof-Micro instrument. Electronic spectra were recorded with a Shimadzu UV-3101 PC spectrophotometer; while fluorescence spectra were recorded using Quanta Master 400, PTI spectrofluorometer.

5C.2.3. General experimental procedure for UV-Vis and Fluorescence studies

5.0 x 10^{-2} M solution of the perchlorate salts of the respective ion (Na^+, K^+, Fe^{3+}, Na^+, Mg^{2+}, Ni^{2+}, Co^{2+}, Cu^{2+}, Cd^{2+}, Pb^{2+}, Zn^{2+}, Cr^{3+} and Hg^{2+}) was prepared in pure aqueous medium. A stock solution of the receptor **L** (5.0 x 10^{-4} M) was prepared in DMSO. Solution of the compound **L** was further diluted for spectroscopic titrations, and the effective final concentration of the solution of compound **L** used for the fluorescence study was 10 μM, while the final analyte concentration during emission spectral scanning was 2.0 x 10^{-4} M. For all luminescence measurements, λ_{Ext} = 400 nm with an emission slit width of 2/2 nm. The relative fluorescence quantum yields (Φ_f) were estimated using Rhodamine B (Φ_f = 0.3 in aqueous medium at RT) as a reference.

5C.2.4. Cell culture and fluorescence imaging: Intracellular pH calibration

Hct116 cells were seeded on coverslips placed in 6 well plates. After 24 hours cells were treated with **L** (10 μM) for 20 minutes. Cells were then washed thrice with phosphate buffer saline (1 x PBS) and fixed with 4% PFA for 10 minutes and washed again with phosphate buffer saline (1 x PBS). The **L**-stained colon cancer cells Hct116 incubated with different pH solutions for 20 min. Solutions were decanted and cover slips mounted using mounting medium. Nail paints was used to seal the cover slips mounted on the glass slides. Images were acquired in Olympus Fluoview

Microscope. Then, the intensity of fluorescence images was measured, and the pH calibration curve was constructed.

Dexamethanose (DMT) treatment:

Hct116 cells were pre-treated with media containing **L** (10 μM). The media were replaced with PBS containing Dexamethanose (2.0 μM) and incubated for either 20 min at 37°C. The cells were washed three times with PBS. Fluorescent confocal images were then recorded using an excitation wavelength of 400 nm and band-path emission filter 586 ± 30 nm.

5C.3. Synthesis and Characterization

5C.3.1. Synthesis of B

Synthetic procedure that was adopted for synthesis of B from our previously reported procedure (Discussed in details in the synthesis section of Chapter 5A).

5C.3.2. Synthesis of A and R

Synthetic procedure that was adopted for synthesis of **A** and **R** from our previously reported procedure (Discussed in details in the synthesis section of Chapter 5A).

5C.3.3. Synthesis of L

Rhodamine 6G hydrazine (200 mg, 0.467 mmol) and compound **A** (150 mg, 0.467mmol) were dissolved in 40 mL of ethanol. To this, approximately 0.5 ml of acetic acid was added and the resulting solution was refluxed for 18 h. A yellow precipitate appeared. The solution was filtered hot and yellow precipitate was collected. The residue was washed thoroughly with methanol and acetone to isolate pure form of **L**. Yield: 315 mg, 92 %. ESI-Ms (m/z) calculated for $C_{50}H_{46}N_6O_2$: 732, observed: 733 [M + H^+]. ^{1}H NMR [500 MHz, DMSO-d_6: δ (ppm)]: 8.86 (2H, d, *J* = 8.4 Hz, ArH); 8.61 (1H, s, -CH=N); 8.58 (2H, d, *J* = 7.6 Hz, ArH); 8.29 (2H, d, *J* = 8.0 Hz, ArH); 7.95 (1H, d, *J* = 7.2 Hz, ArH); 7.75 (2H, t, *J* = 7.2 Hz, ArH); 7.68-7.59 (6H, m, ArH); 7.06 (1H, d, *J* = 7.2 Hz, ArH); 6.40 (2H, s, ArH); 6.28 (2H, s, ArH); 3.16 (4H, q,

J = 6.8 Hz, -CH_2); 1.87 (6H, s, CH_3); 1.22 (6H, t, *J* = 6.8 Hz, CH_3). ^{13}C NMR (500 MHz, DMSO-d_6, δ (ppm)): 164.38, 160.19, 152.12, 151.36, 148.33, 145.38, 135.75, 134.52, 127.74, 127.71, 127.28, 126.11, 124.43, 123.59, 122.56, 118.89, 105.29, 9634, 65.89, 56.49.

5C.4. Results and Discussions

All UV-Vis and luminescence spectra of **L** (10 μM) were recorded in aq. phosphate buffer solution (PBS-DMSO; 98:2, v/v) solution. An intense absorption band for π-π*-based transition of the imidazole derivative of the phenanthrene moiety was observed at 388 nm (Figure 5C.1a). Electronic spectral band with maximum at ~ 380 nm for the model reagent **R** confirmed this assignment. This further corroborated the fact that **L** was present exclusively in its spirolactam form under the experimental conditions and accounted for its colourless solution (pH > 6.5). A characteristic signal at ~ 65.89 ppm for the tertiary C-atom in the ^{13}C NMR spectrum for **L** also confirmed its Spiro lactam structure.[17] Absorption spectra for **L** were recorded in presence of different cations (Figure 5C.1a) that are important for human physiology.[16a,b] Significant changes in absorption spectra were observed when solution pH was adjusted at pH 3.5. To explore the sensitivity of this reagent towards solution pH, systematic pH titrations were carried out.

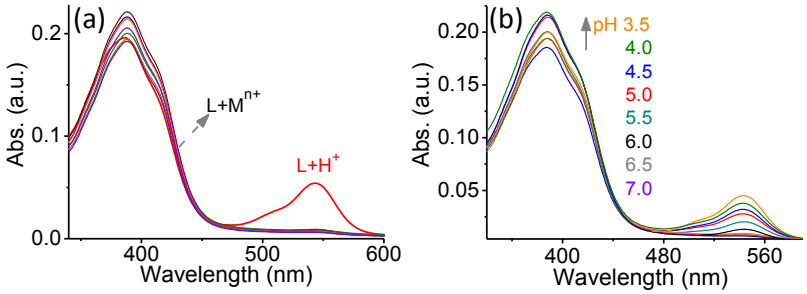

Figure 5C.1. (a) Absorption intensity for **L** (10 μM) in the absence and the presence of 30 mole equiv. of different metal ions (M^{n+}= Na^+, K^+, Mg^{2+}, Hg^{2+}, Cu^{2+}, Zn^{2+}, Cr^{3+}, Fe^{3+}, Co^{2+}, Cr^{3+}, Pd^{2+}, Pb^{2+}, Ni^{2+}, Cd^{2+}), glutathione (GSH), cysteine (Cys), and homocysteine (Hcy) as well as at different solution pH); (b) systematic changes in absorption spectral patterns for **L** (10 μM) at different pH (3.5 – 8).

A new absorption band appeared at 542 nm (Figure 5C.1b) with gradual decrease in solution pH from 8.0 to 3.5 due to the conversion to the xanthenes derivative (H^+.**L)** with a visually detectable change in solution colour to pink. For such changes in solution pH, no significant change was observed for the absorption band at 388 nm.

Fluorescence studies performed with λ_{Ext} = 400 nm or 505 nm also revealed the specificity of the reagent **L** towards H^+ (~ pH 4.0) in aq. PBS buffer-DMSO (98: 2, v/v) medium (Figures 5C.2a & b). Interference studies performed in presence of higher concentration of the above referred metal ions, GSH, Cys and Hcy failed to alter with the luminescence response of the reagent **L** towards media pH (aq. PBS buffer-DMSO; 98: 2, v/v).

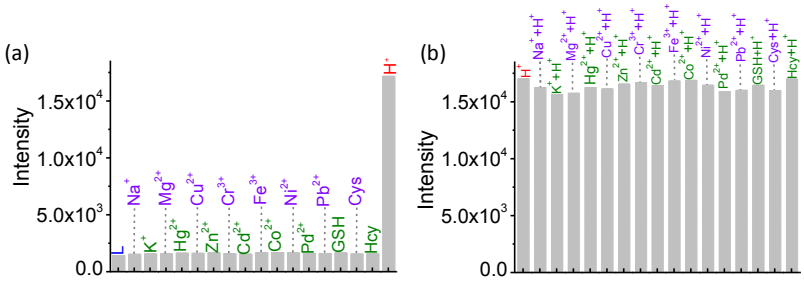

Figure 5C.2. Changes in luminescence intensity of **L** (10 μM) in the absence and the presence of 30 mole equiv. of different metal ions (M^{n+} = Na^+, K^+, Mg^{2+}, Hg^{2+}, Cu^{2+}, Zn^{2+}, Cr^{3+}, Fe^{3+}, Co^{2+}, Cr^{3+}, Pd^{2+}, Pb^{2+}, Ni^{2+}, Cd^{2+} GSH, Cys, Hcy and H^+); (b) Interference study for **L** (10 μM) in presence of various metal ions (40 equiv.) in HEPES buffer to reveal the specific of the reagent L towards H^+ (pH 3.5) by using λ_{Ext} = 505 and λ_{Mov} = 552nm.

These results further confirmed the specificity in response of **L** towards the change in solution pH. Luminescence band at 492 nm (λ_{Ext}: 400 nm) was observed for **L** and the model reagent **R** for solution with pH 7.0. Accordingly, the luminescence band at ~ 490 nm for **L** was assigned for the imidazole derivative of the phenantherene moiety. Even the reagent **L** did not show any detectable emission band following excitation at ~ 505 nm. This confirmed the spirolactam structure for **L** at neutral pH. However, on lowering the solution pH from 8.0 to 3.5, gradual bleach in emission intensity at 492 nm (λ_{Ext}: 400 nm) was observed (Figure 5C.3). Interestingly, a new emission band appeared at 552 nm on excitation either at 400 nm or at 505 nm;

though the relative emission quantum yields (Φ) were found to be different (Φ[λ_{Ext} of 400 nm] = 0.02 & Φ[λ_{Ext} of 505 nm] = 0.78; rhodamine 6G was used as standard).

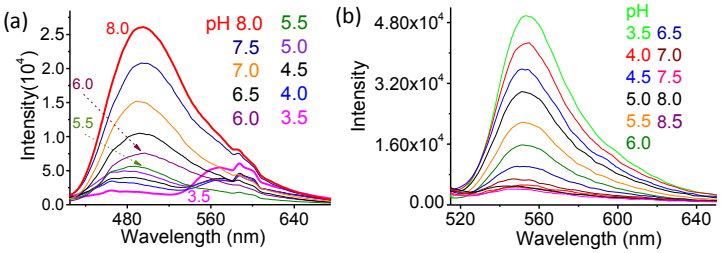

Figure 5C.3. (a) Emission spectra of **L** (10 μM) (λ_{Ext} = 400 nm; slit width 1/1 nm) at various pH (3.5 – 8.0); (b) Emission spectra of **L** (10 μM) (λ_{Ext} = 505 nm; slit width 1/1nm) at various pH (3.5 – 8.0). All studies were performed in aq.Phosphate buffer solution having 2% DMSO.

Appearance of the new emission band at ~ 552 nm on increase in media acidity further supported formation of H^+.**L** and the conversion to the acyclic xanthenes form.[17] Conversion from lactam form (**L**) to the corresponding xanthenes (H^+.**L**) form the was attributed for the first set of changes for pH changes from 3.5 to 5.5 with an iso-emission point at 540 nm; while deprotonation of **L** at the $HN_{Imidazole}$ moiety accounted for the observed increase in emission intensity at ~ 490 nm (Figure 5C 3a). Interestingly, further studies revealed that there was a definite spectral overlap between the emission spectra of the model reagent **R** and the analogous rhodamine derivative (H^+.B) (Figure 5C.4a); a condition that was favourable for FRET process.

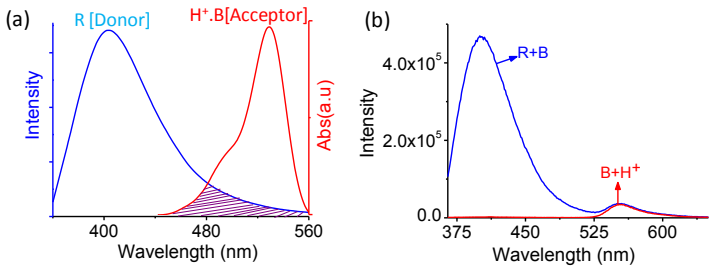

Figure 5C.4. (a) Overlap spectra: for emission spectrum of the donor (R) and the absorption spectrum of the acceptor acyclic xanthene form (H^+.B); (b) fluorescence spectra of equimolar mixture of R and B in presence of H^+ (pH ≤5). The concentration is 20 μM for both R and B using λ_{Ext} = 350 nm; slit width 1/1 nm. This shows there is no inter molecular energy transfer process between acceptor and donor moiety.

Emission spectra recorded for rhodamine 6G or H^+.B did not show any significant emission band at 552 nm for λ_{Ext} of 400 nm. Thus, the observed emission band with

maximum at 552 nm for aq. buffer solution of **L** (λ_{Ext} of 400 nm) at pH ≤ 6.5 could only be explained based on the FRET based response. Efficiency of the FRET process between donor imidazole and the acceptor rhodamine moieties in **L** was evaluated using the steady state emission quantum yield data (Φ_f) mentioned above and was found to be 42% under the experimental conditions.[18]Furthermore; we have recorded the steady state emission spectra for a physical mixture of an equimolar amount of two model reagents, **R** and H^+.**B** (Figure 5C.4b)**.** These studies revealed that the resultant spectrum was basically a summation of the spectra of two independent luminophores, which nullified any possibility for the intermolecular energy transfer process.

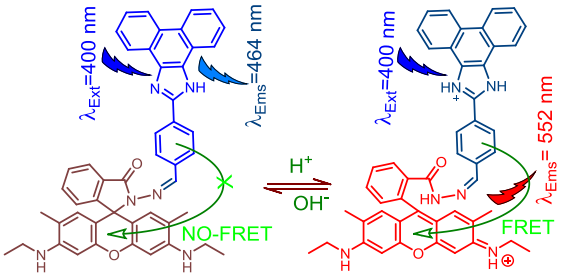

Scheme 2. (a) Schematic presentation of the observed emission response at pH ≤ 6.0.

It may be noted that the observed difference of 165 nm between the donor absorption (388 nm) and the acceptor emission (553 nm) for H^+.**L** is the highest Stokes shift value reported till date for any visible light excitable pH probe.

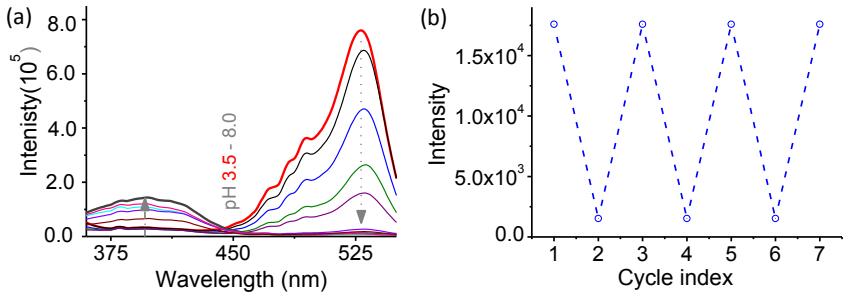

Figure 5C.5. (a) Excitation spectra of **L** (10 μM) for λ_{Ems} = 552 nm and this confirms its dual excitation ratiometric pH sensing ability; (b) reversible fluorescence changes of probe **L** (10 μM) between pH 3.5 and pH 8.0 for λ_{Ext} of 505 nm in aq. PBS buffer-DMSO (98:2, v/v) solution at 25°C.

Reversibility of the luminescence responses on excitation at 505 nm (Figures 5C & 5b) was also established by altering the solution pH between 3.5 and 8.0. Linearity of the luminescence responses either at 490 nm or at 552 nm (for λ_{Ext} = 505 nm) was also confirmed for pH 3.5 & 8.0.

MTT assay studies revealed that this reagent showed insignificant toxicity towards live Hct116 cells. After ensuring the FRET based luminescence response of the biologically benign reagent **L** towards media pH, possibility of using this reagent for tracking intracellular pH of Hct116 cells was explored using CLSM studies. Analysis of CLSM images of Hct116 cells, labelled with the reagent **L**, revealed distinctly different intracellular emission responses from cells incubated at different media pH.

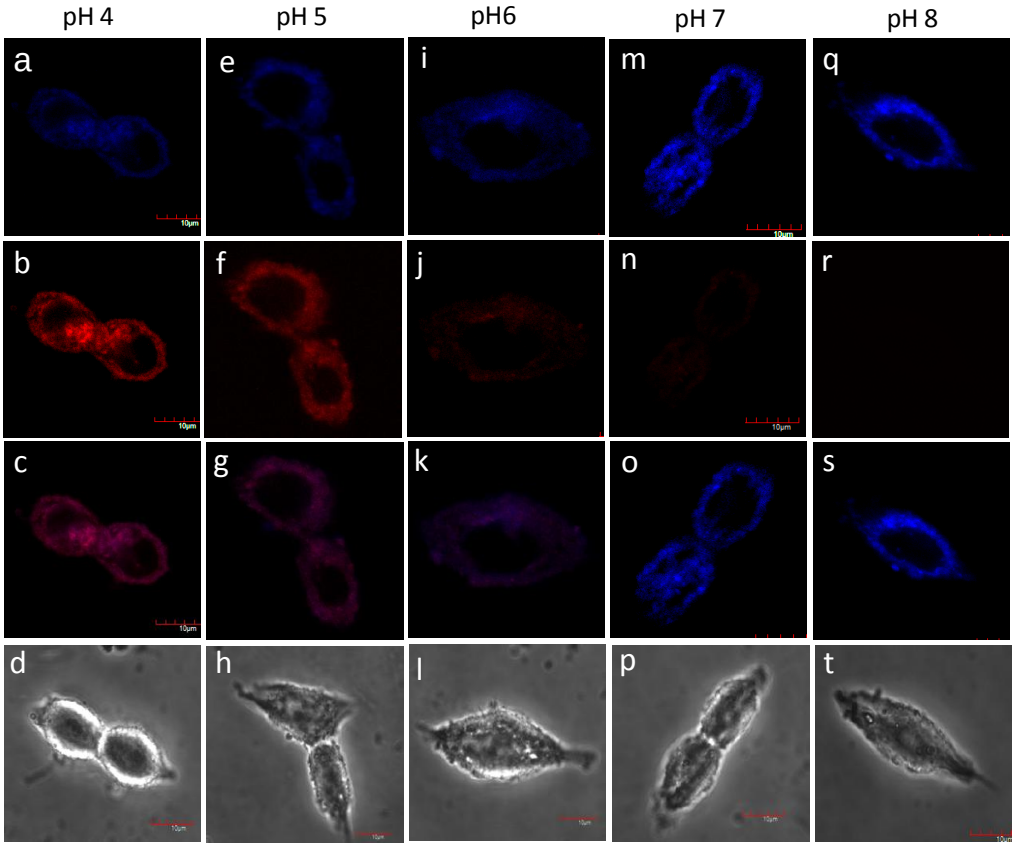

Figure 5C.6. CLSM images of recorded for Hct116 cells clamped at pH 4 (a–d), 5 (e–h), 6 (i–l), 7 (m–p), and 8 (q–t) using probe **L** (10 μM). The excitation wavelength was 400 nm and the images were collected at 460 ± 30 nm (first row) and 586 ± 30 nm (second row). Ratio images obtained from the blue and red channels (third row) and the corresponding contrast images (fourth row).

Only red intracellular emission, primarily from the xanthene form of the reagent **L**, was observed when images were viewed using red channel (586 ± 30 nm) and a weak intracellular emission was observed when viewed through blue channel (460 ± 30 nm) for cells incubated in media having pH 4.0 (Figure 5C.6). Analogous studies for media pH of 8.0 showed distinct blue intracellular emission (primarily from imidazole derivative of the phenanthrene moiety) when viewed through blue channel and no intracellular emission was observed when red channel was used. These observations agreed well with the emission responses of the reagent **L** towards solution pH (Figure 5C.4). Figure 5C.6 further revealed that on regular increase in media pH from 4.0 to 8.0, in which Hct116 cells were incubated, a gradual increase in blue intracellular emission was observed (viewed through blue channel) with concomitant decrease in red intracellular emission (viewed through red channel). Interestingly, intracellular emissions at both channels were observed for Hct116 cells incubated at pH 6.0 (Figure 5C.6i & 6j). Thus, above described results clearly revealed that the present reagent **L** could be used as FRET-based dual imaging probe for tracking the subtle changes in intracellular pH (4.0-8.0).

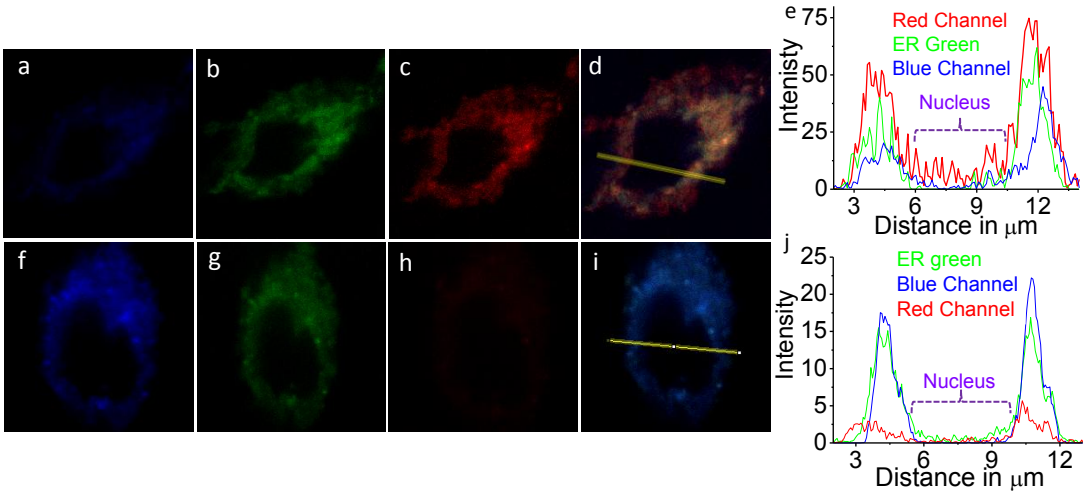

Figure 5C.7. Co-localization experiments using reagent **L** and ER-Tracker green (ERTG) in for Hct116 cells. Cells were incubated with **L** (10 μM) for 20 min at 37°C, and the medium was replaced with fresh medium containing ERTG (1μM) and incubated for 30 min. CLSM images with reagent **L** were collected for blue channel (460 ± 30 nm) and red channel (586 ± 30 nm) following excitation with laser source of 400 nm. CLSM image with ERTG (b and g)

were recorded using laser excitation source of 495 nm and emission filter of 519 ± 30 nm; d and I are the merged image of c & b and g & h, respectively. Note: first row images were collected at pH 5 and second row images were collected at pH 7.2 medium.

Further, co-localization experiments were performed using **L** and organelle-specific fluorescent dye (ER-8 Tracker™ Green (ERTG)) to identify the location or localization of the reagent **L** in Hct116 cells, which accounted for the intracellular blue and red fluorescence. Close comparison of the CLSM images as well as the images of the co-staining experiments with ERTG ((Figures 5C.7a-d) clearly revealed that intracellular emissions for **L** were found to be exactly superimposed with those for ERTG and distributed mainly in the lipid dense region of ER. Interestingly, for intracellular pH ≥ 7.0 no FRET-based red emission from the xanthene moiety of **L** was observed. Hct116 cells incubated with solution having pH ≤ 6.0 revealed a strong FRET-based red emission, while emission intensity was enhanced with lowering of the media pH.

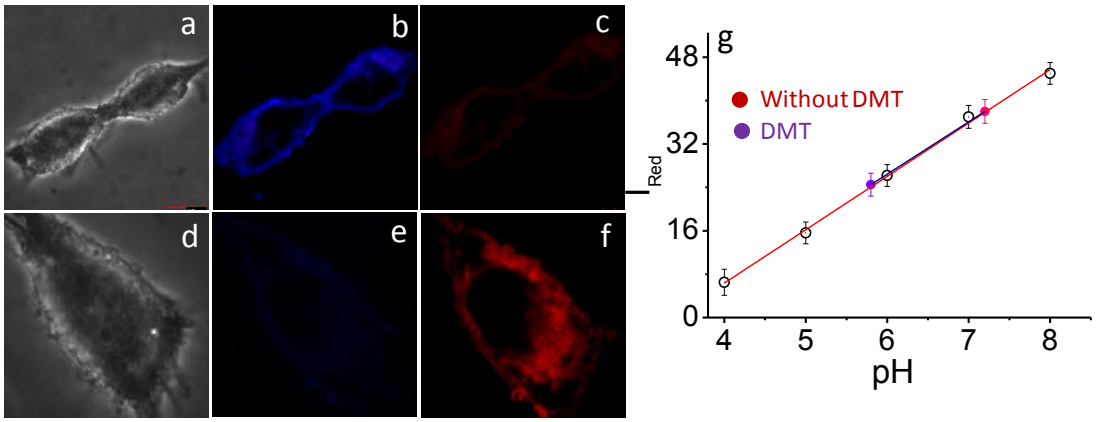

Figure 5C.8. CLSM images of Hct116 colon cancer cells incubated with **L** (10 μM) as a control: (a) a bright field image, (b & c) an images observed in the blue and red channel; (d) and (e) CLSM images of Hct116 cells incubated with **L** (10 μM) for 20 min and then further exposed to DMT (2 μM) for 20 min at 37 °C: (d) a bright field image, (e & f) an images observed in the blue & red channel; (g) Intracellular pH calibration curve of probe **L** in Hct116 cells, generated from red fluorescence intensity (I_{Red}) of cells exposed to different media pH and each data is an average of three independent measurements.

Further, Pearson's correction coefficient (Pcc) was evaluated from the overlay of fluorescence images of Hct116 cells stained with **L** and ERTG. These evaluated Pcc were 0.94 (586 ± 30 nm filter) & 0.76 (460 ± 30 nm filter) at pH 5.0 and 0.96 (586 ±

30 nm) & 0.12 (460 ± 30 nm filter) at pH 7.2. This confirmed that the reagent **L** was solely localized in the ER region of the Hct116 cells. To the best of our knowledge, this is the first report in the literature for an imaging reagent that is capable of monitoring subtle changes in pH in endoplasmic reticulum, the lipid dense region Hct116 cells based on FRET mechanism.[13] Intracellular pH is known to be closely associated to cell growth and apoptosis.[19] Dexamethanose (DMT) is known to lower the pH of the cytosol by inhibiting the H^+-ATPase activity and any knowledge gained on the pH change in the ER region is expected to provide insight in overall change in cytosolic pH.[13b,20] H^+-ATPase is a proton pump that accounts for maintaining the cellular pH at physiological pH range. It has been argued that DMT interferes with the H^+-ATPase activity and effectively reduces the intracellular pH, which eventually causes cell apoptosis. To examine the possibility monitoring the changes in cellular pH induced by DMT, Hct116 cells were pre-exposed to a buffer solution (pH 7.2) of 10 μM of **L** for 20 min, in absence and presence of DMT. Pre-treated cells were exposed to DMT (2 μM) in aq. HEPES buffer medium (pH 7.2) and were visualized under a laser scanning confocal microscope. The more intense red intracellular luminescence was observed for cells loaded with DMT. A plot of I_{586nm} (red channel) (measured from confocal images of cells in respective pH) vs pH helped in generating a calibration plot (Figure 5C.8g). This calibration curve was used for measuring possible intracellular pH, which was evaluated as 7.2 ± 0.2 and 5.8 ± 0.2, respectively, before and after treatment with 2 μM DMT for 20 min. This study clearly revealed that DMT was responsible for lowering of the cellular pH and the reagent **L** could be used for monitoring this change in intracellular pH.

In this chapter we have described a new FRET based ER specific imaging probe with Stokes shift of 165 nm for monitoring pH changes in aq. buffer medium under physiological condition as well as in monitoring subtle changes in intracellular pH in the ER region of the Hct116 cells induced by DMT.

5C.5.References

1. J. R. Casey, S. Grinstein and Orlowski, *J. Nat. Rev. Mol. Cell Biol*., 2010,**11**, 50.

2. (a) A. Roos and W. F. Boron, *Physiol. Rev*., 1981, **61**, 296; (b) J. Srivastava, D. L. Barber and M. P. Jacobson, *Physiology,* 2007, **22**, 30.

3. (a) H. Izumi, T. Torigoe, H. Ishiguchi, H. Uramoto, Y. Yoshida, M. Tanabe, T. Ise, T. Murakami, T. Yoshida, M. Nomoto and K. Kohno, *Cancer Treat. Rev*., 2003, **29**, 541; (b) T. A. Davies, R. E. Fine, R. J. Johnson, C. A. Levesque, W. H. Rathbun, K. F. Seetoo, S. J. Smith, G. Strohmeier, L. Volicer, L. Delva and E. R. Simons, *Biochem. Biophys. Res. Commun*., 1993, 194, 537.

4. J. Han and K. Burgess, *Chem. Rev*., 2010, **110**, 2709-2728.

5. J. H. Kim, L. Johannes, B. Goud, C. Antony, C. A. Lingwood, R. Daneman, S. Grinstein, *Proc. Natl. Acad. Sci*.; 1998, **95**, 2997-3002.

6. (a) M. Yilla, A. Tan, K. Ito, K. Miwa, and H. L. Ploegh, *J. Biol. Chem*., 1993, **268**, 19092-19100; (b) A. Serrano, J.R. Pérez-Castiñeira, M. Baltscheffsky, H. Baltscheffsky; IUBMB Life, 2007, **59**, 76-83.

7. K.W. Beyenbach and H. Wieczorek, *J. Exp Biol*., 2006, **209**, 577-589.

8. P. Paroutis, N. Touret and S. Grinstein, *Physiology*., 2004, **19**, 207.

9. M. M. Wu, M. Grabe, S. Adams, R. Y. Tsien, H. P. Moore and T. E. Mache, *J. Biol. Chem*., 2001, **276**, 33027-33035.

10. (a) I. Mellman, R. Fuchs, A. Helenius, *Annu. Rev. Biochem*., 1986, **55**, 663-700; (b) P. A. Halban and J. C. Irminger, *Biochem. J*., 1994, **299**, 1-18; (c) W.K. Schmidt, H.P. Moore, *Mol. Biol. Cell*., 1995, **6**, 1271-1285; (d) M. K. Brown and N. Naidoo, *Frontiers in Integrative Physiology*., 2012, **3**, 1.

11. (a) M. H. Lee, J. H. Han, J. H. Lee, N. Park, R. Kumar, C. Kang and J. S. Kim, *Angew. Chem. Int. Ed*., 2013, **52**, 6206; (b) Q. Wan, S. Chen, W. Shi, L. Li and H. Ma, *Angew. Chem. Int. Ed*., 2014, **53**, 10916; (c) S. Wu, Z. Li, J. Han and S. Han, *Chem. Commun*., 2011, **47**, 11276; (d) H. Zhu, J. Fan, Q Xu, H. Li, J Wang, P Gao and X. Peng, *Chem. Commun*., 2012, **48**, 11766; (e) J. Fan, H Dong, M. Hu, J.Wang, H. Zhang, H. Zhu, W. Sun and X. Peng, *Chem. Commun*., 2014, ***50***, 882; (f) Y. M. Ho, N. P. Au, K. L. Wong, C. T. Chan, W. M. Kwok, G. L. Law, K. K. Tang, W. Y. Wong, C. H. Ma and M. H. Lam, *Chem. Commun*., 2014, **50**, 4161; (g) L. Wang, Y. Xiao, W. Tian and L. Deng, *J. Am. Chem. Soc*., 2013, **135**, 2903;

12. (a) M. H. Lee, N. Park, C.Yi, J. H. Han, J. H. Hong, K. P. Kim, D. H. Kang, J. L. Sessler, C. Kang and J. S. Kim, *J. Am. Chem. Soc*., 2014, **136**, 14136; (b) S.Chattoraj, R. Chowdhury, S. K. Dey, S. S. Jana and K. Bhattacharyya, *J. Phys. Chem. B*, DOI: 10.1021/jp503808z; (c) Q. Zhang, R. Cao, H. Feia and M. Zhou, *Dalton Trans*., 2014, **43**, 16872; (d) Y. Chen, C. Zhu, J. Cen, Y. Bai, W. He and Z. Guo, *Chem. Sci*., 2015, **6**, 3187.

13. (a) N. V. Ghule, R. S. Bhosale, K. Kharat, A. L. Puyad, S. V. Bhosale and S. V. Bhosale, *ChemPlusChem*, 2015, **80**, 485-489; (b) B. K. McMahon, R. Pal and D. Parker, *Chem. Commun*., 2013, **49**, 5363.

14. L. Orci, M. Ravazzola, M. Amherdt O. Madsen, A. Perrelet, J.-D.Vassalli and R. G. Anderson, *J Cell Biol*., 1986, **103**, 2273-2281.

15. J. Birk, T. Ramming, A. Odermatt, C. A. -Herzog, *Frontiers in Genetics*, 2013, **4**, 1-10.

16. (a) J. Fan, M. Hu, P. Zhan and X. Peng, *Chem. Soc. Rev*., 2013, **42**, 29; (b) L.Yuan, W.Lin, K. Zheng and S. Zhu, *Acc. Chem. Res*., 2013, **46**, 1462-1473; (c) Y.-X. Wu, X. -B. Zhang, J.-B. Li, C. -C. Zhang, H. Liang, G. -J. Mao, L. -Y. Zhou, W. Tan and R. -Q. Yu, *Anal. Chem*., 2014, **86**, 10389; (d) R. J. Meier, J. M. B. Simburgera, T. Soukka and M. Schaferling, *Chem. Commun*., 2015, **51**, 6145.

17. (a) P. Mahato, S. Saha, P. Das, H. Agarwalla and A. Das, *RSC Adv*., 2014, **4**, 36140; (b) S. Saha, P. Mahato, U. Reddy G, E. Suresh, A. Chakrabarty, M. Baidya, S. K. Ghosh and A. Das, *Inorg. Chem*., 2012, **51**, 336; (c) U. Reddy G, V. Ramu, S. Roy, N. Taye, S. Chattopadhyay and A. Das, *Chem. Commun*., 2014, **50**, 14421.

18. U. Reddy G, R. Lo, S. Roy, T. Banerjee, B. Ganguly and A. Das, *Chem. Commun*., 2013, **49**, 9818.

19. X. Zhou, F. Su, H. Lu, P. S.-Willis, Y. Tian, R. H. Johnson and D. R. Meldrum, *Biomaterials*., 2012, **33**, 171-180.

20. (a) C. Nauclér, R. Sundler and H. Tapper, J. of Leukoc. Biol., 2000, **67**, 876; (b) M. R. Gill, D. Cecchin, M. G. Walker, R. S. Mulla, G. Battaglia, C. Smythe and J. A. Thomas, *Chem. Sci*., 2013, **4**, 4512.

Conclusion of the Thesis:

The thesis entitled “Recognition and sensing of Biologically and Environmentally Significant Analytes” describes the synthesis of several organic receptor molecules along with their recognition studies for analytes that have implications in various biological processes. The thesis contains overall six chapters. The first chapter is basically the introductory chapter, which describes “various photoinduced processes that are being used for designing receptors for recognition of the desired analyte with preferred optical responses”. Emphasis of this chapter is different photoinduced process that led to a luminescence *ON* response on binding to a target analyte, as this provides the option of using such reagent for imaging application. Also, processes like FRET and TBET are discussed in details, as such processes help in achieving largest Stokes shift value - a preferred criterion for imaging and biological application.

Chapter 2 provides a discussion on the design strategy that is adopted for synthesis of an Ir(III)-based cyclometallated complex having a pendant Cu(II)-moiety (**1.Cu**) for the recognition of biologically relevant anion like CN^-. Strong affinity of the cyanide species towards Cu(II) helps in achieving the demetallation reaction in **1.Cu** and this eventually results in a luminescence *ON* response. This is utilized for the detection of CN^- in virtual aq. HEPES buffer medium (10 mM aq. HEPES buffer-CH_3CN, 99.6:0.4, v/v; pH 7.6) with associated *turn-on* phosphorescence response. Additionally, this reagent could also be used as an imaging reagent for detection of the cellular uptake of CN^- ions in HeLa cells from aqueous-buffer media (pH 7.6) with [CN^-] as low as 0.2 ppm as well as for developing an assay for probing the in situ release of cyanide from a cyanohydrin by the HNL enzyme under physiological conditions, is also described.

Chapter 3 provides, the design and syntheses of a new thiourea based receptor **A** by multistep procedure with reasonable yield for specific recognition of fumaric acid and

maleic acid in aqueous solution. Once again our design strategy helps in achieving a FRET based response on specific recognition of these two acids. Fumaric and maleic acid plays key role in many crucial biological functions. More importantly, presence of these acids in concentration higher than the threshold value is known to have adverse influence towards human physiology. To confirm the photoinduced process that is associated with the recognition of these two acids, studies with model reagents (**B** and **R**) are discussed. An energy efficiency of 75% is observed for the FRET process involving the donor naphthyl and acceptor dansyl moieties under the experimental conditions (10 mM aq. HEPES buffer- CH_3CN (1:1, v/v; pH 6.0) medium; λ_{Ext} = 290 nm, λ_{Mon} = 542 nm). Results of the computational studies are also discussed for a developing better insight in understanding the preferential binding to fumaric and maleic acids. More importantly, results of our studies also establish that this reagent could also be used for quantitative estimation of the fumarate ion in commercial fruit juice sample.

In chapter 4 we have discussed a new chemodosimetric receptor, bis-Cu(II)-complex, this is suitable for specific recognition of Cys and His. Interestingly, this reagent is also found useful for estimating total and individual concentrations of Cys and His in biofluids like human blood plasma. This reagent is also found to be permeate through cell membrane and could be used as an imaging reagent for the detection of intracellular Cys in live cells. Results of various spectroscopic studies help in distinguishing the two different mechanistic pathways for interaction of Cys and His with this reagent **R**.

Chapter 5 describes different newly synthesized rhodamine derivatives as molecular probes for recognition of analytes like Hg^{2+}, Pd^{2+} and H^{+} in physiologically relevant medium. Design strategy for achieving the desired specificity of the respective receptors towards an analyte is also discussed.

Chapter 5A describes the design and synthesis of phenanthroimidazole–rhodamine conjugate for specific binding to Hg^{2+} in an ensemble of several other cations based on TBET-based fluorescence response with high Stokes shift value. Additionally, this reagent showed distinctly different fluorescence-based output signals upon binding to H^+ in solution having pH $\leq$ 4 and this reagent was found to be cell membrane permeable and could be used as a fluorescent probe for imaging Hg^{2+} ion uptake in live Hct116 colon cancer cell lines.

Chapter 5B describes a new coumarin–rhodamine conjugate probe **L** for specific Pd(II) ion over other potential interfere metal ions including Pd(0) and Pd(Iv) ions. Moreover, this reagent could also be used for quantitative estimation of the Pd(II) in human urine as well as an imaging reagent for the detection of Pd(II) in live Hct116 colon cancer cells.

In chapter 5C, we have described a new FRET based ER specific imaging probe **L** with Stokes shift of 165 nm for monitoring pH changes in aq. buffer medium under physiological condition as well as in monitoring subtle changes in intracellular pH in the ER region of the Hct116 cells induced by commonly prescribed drug DMT.

Future Scope of my research:

Reagents described in the present thesis shows specificity towards certain important analytes having biological significance. However, most of the reagents, described in this thesis, are visible light excitable dyes which show emission in or around 580 nm. Ideally one would like to have a dye that shows response in the NIR region of the spectrum as well as capable of showing delayed emission response, i.e., phosphorescence. These two criteria are more preferred for completely overcoming the autofluorescence response from living organisms.

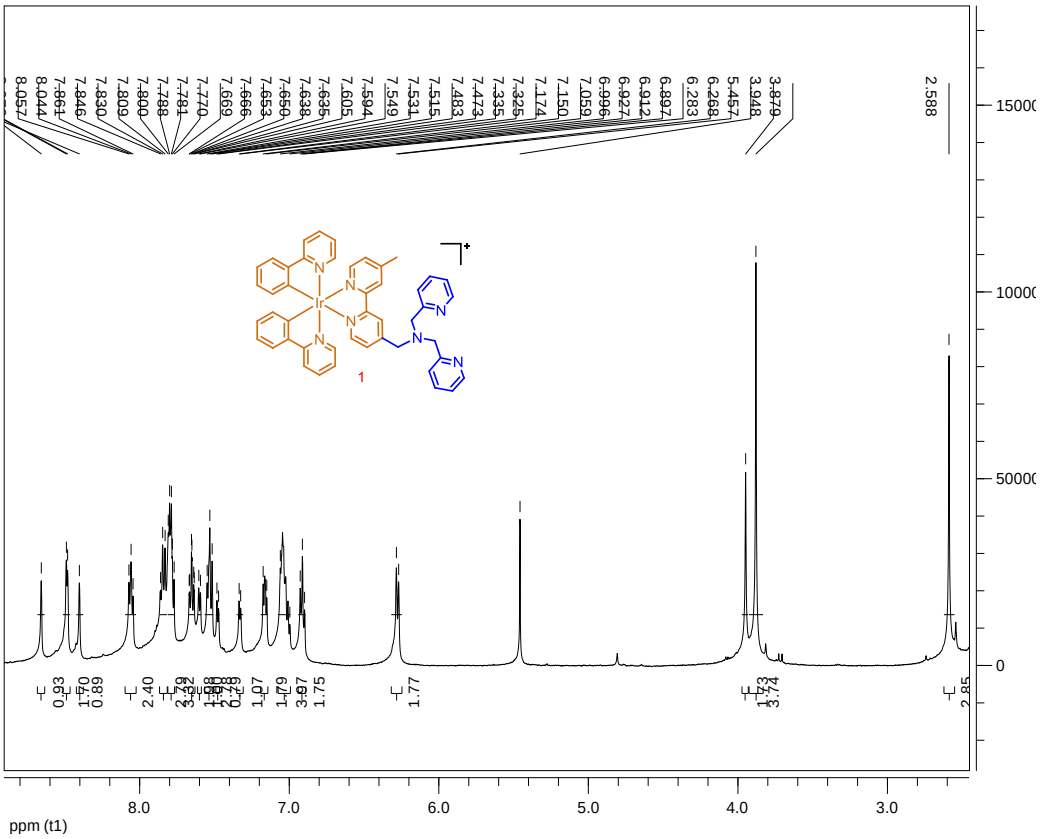

Figure 1. ^{1}H NMR spectra recorded in CD_3CN.

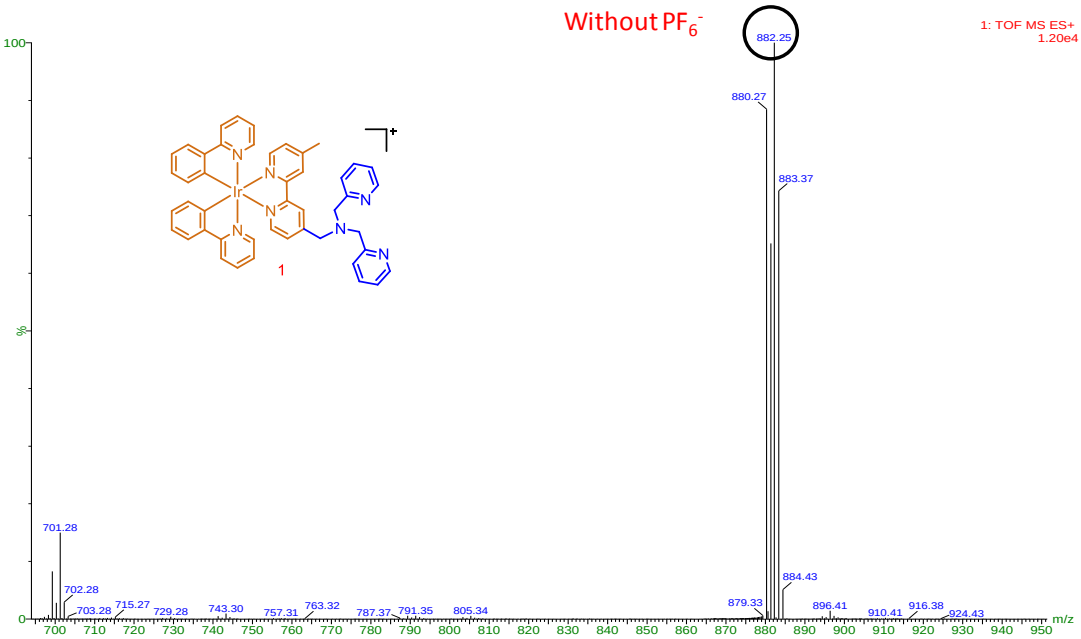

Figure 2. ESI Mass spectra recorded in MeOH.

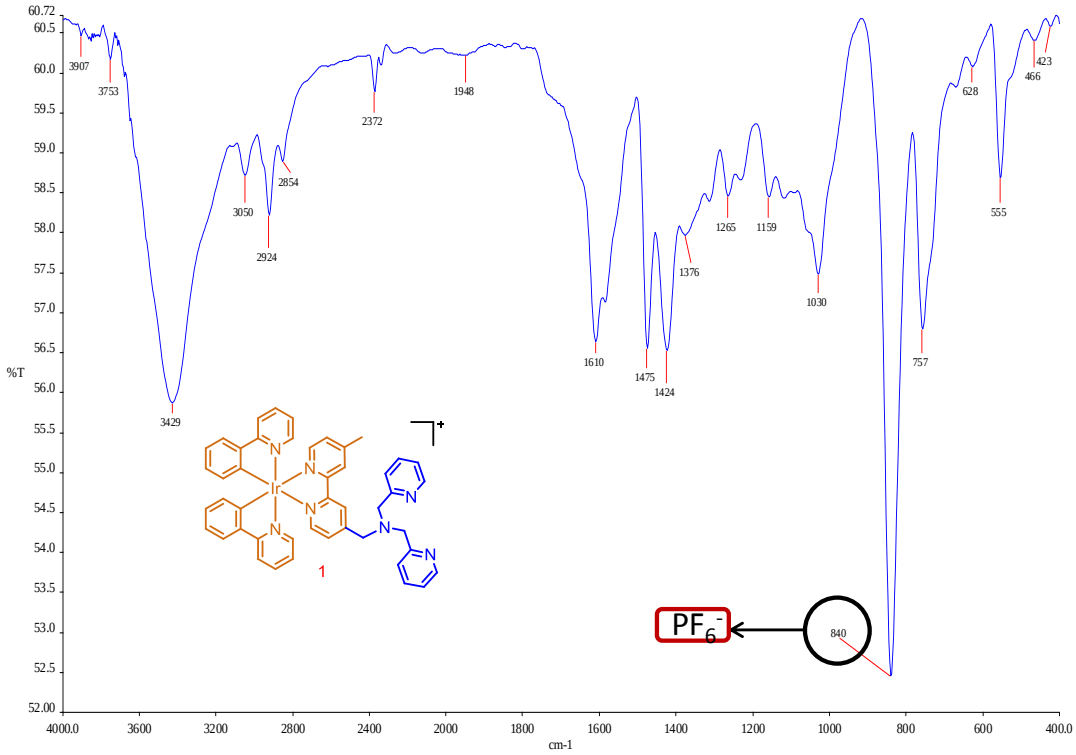

Figure 3. FTIR spectra of **L** as a KBR pellet.

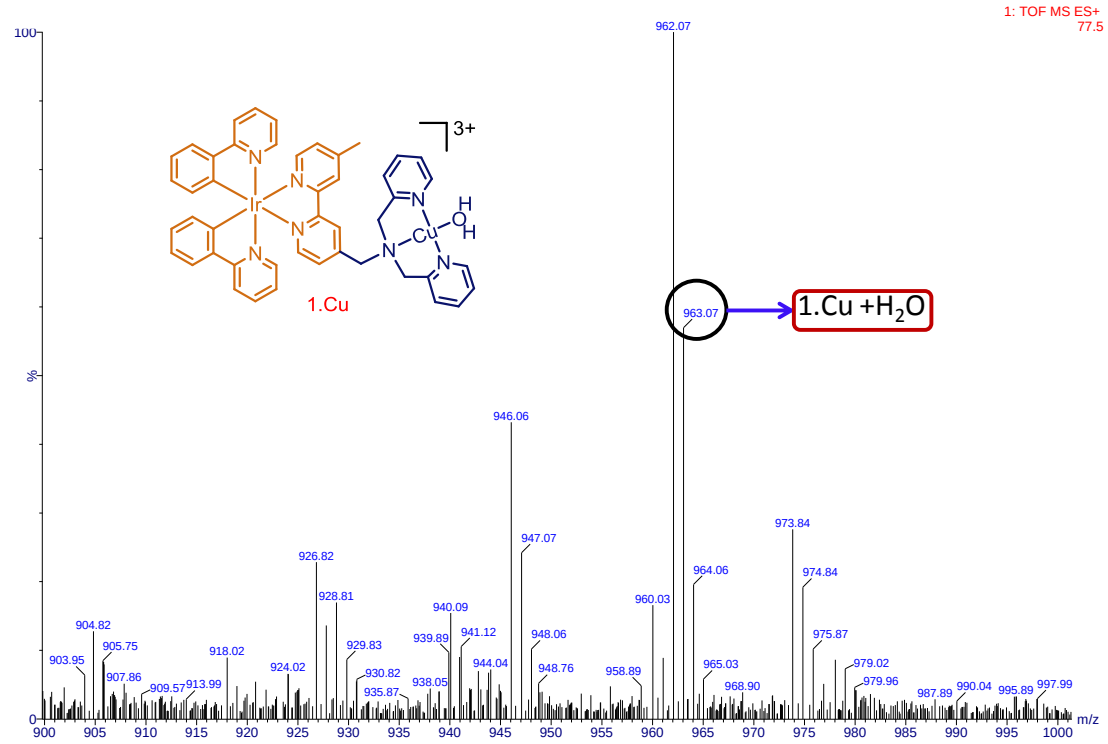

Figure 4. ESI Mass spectra recorded in MeOH.

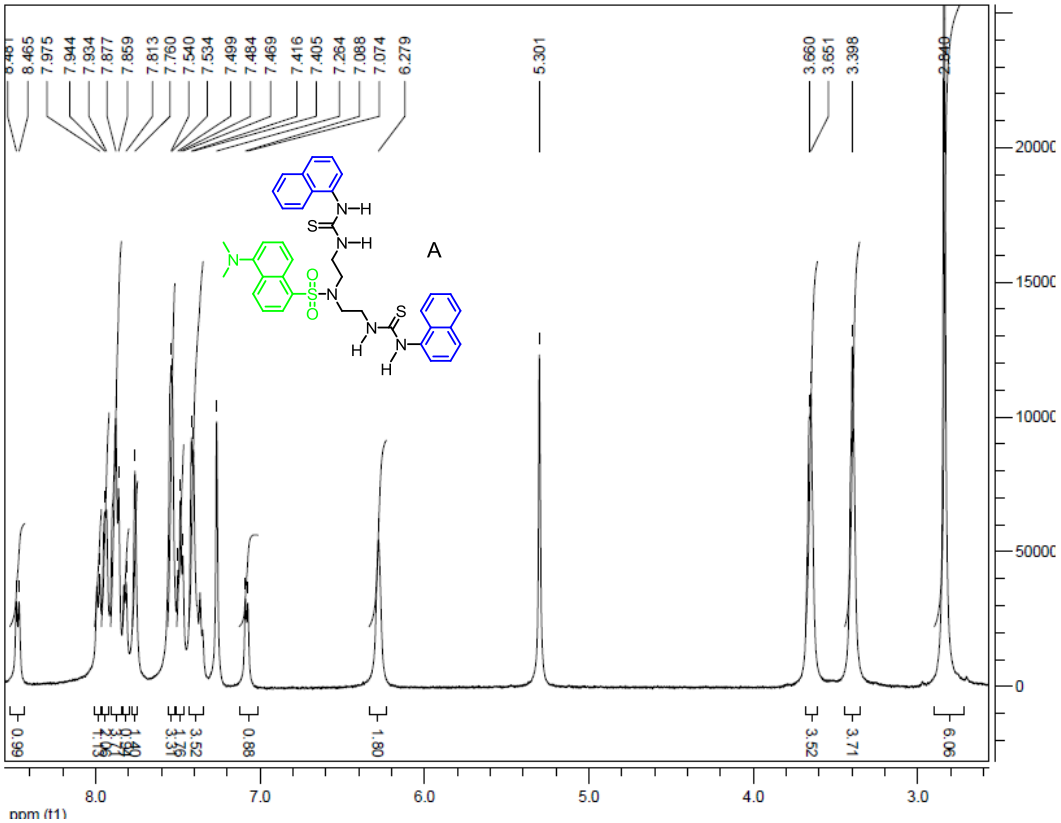

Figure 5. ^{1}H NMR spectra recorded in $CDCl_3$ medium.

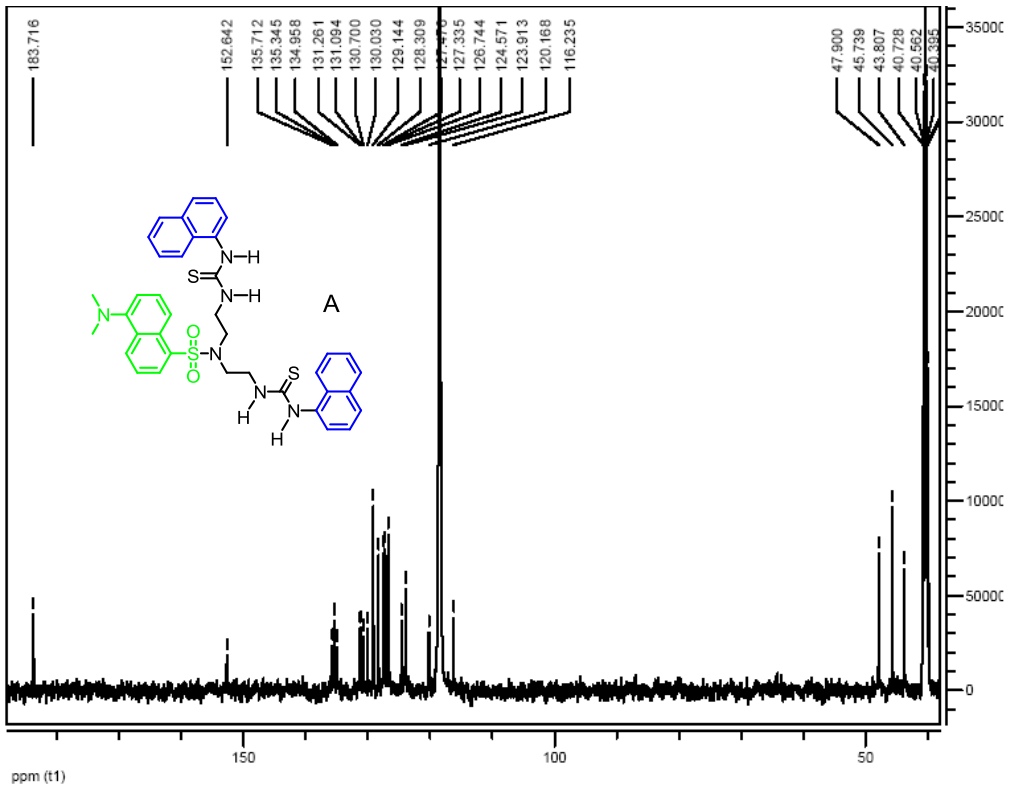

Figure 6. ^{13}C NMR spectra recorded in $CDCl_3$ medium.

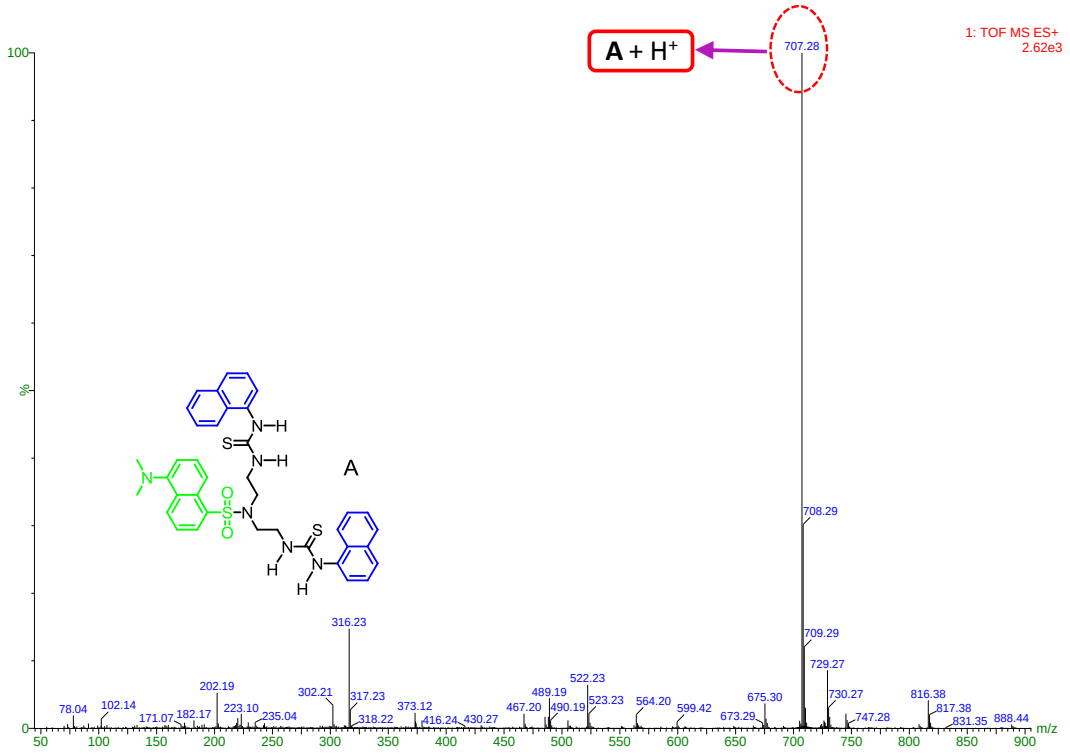

Figure 7. ESI Mass spectra recorded in MeOH.

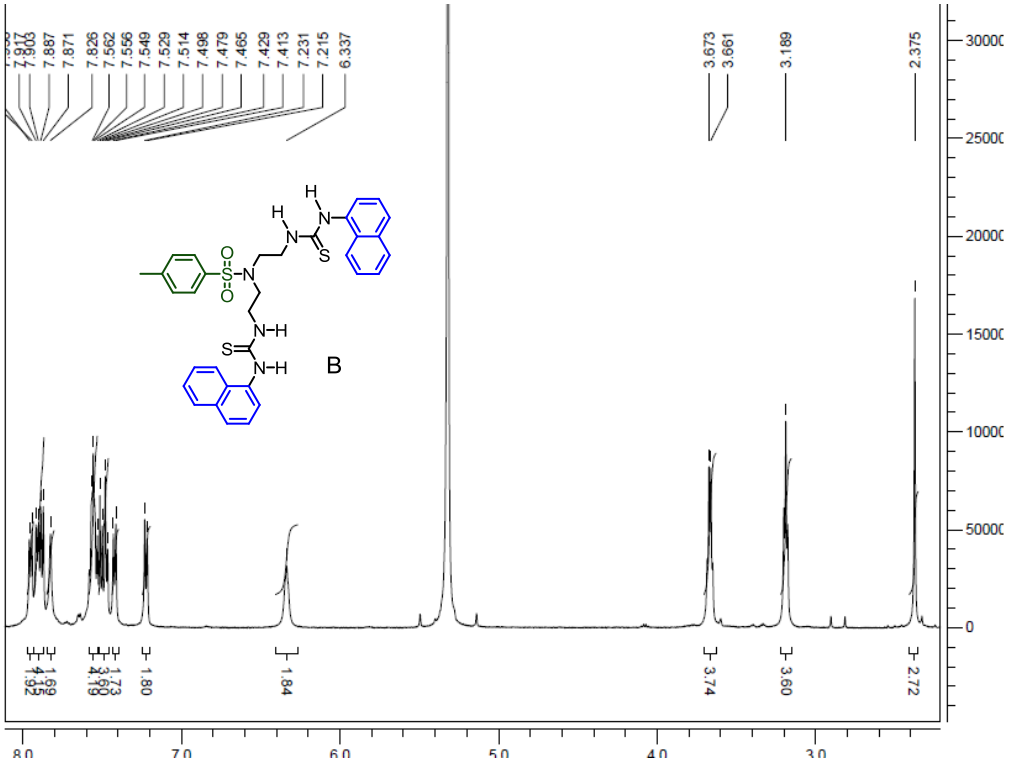

Figure 8. ^{1}H NMR spectra recorded in CD_2Cl_2 medium.

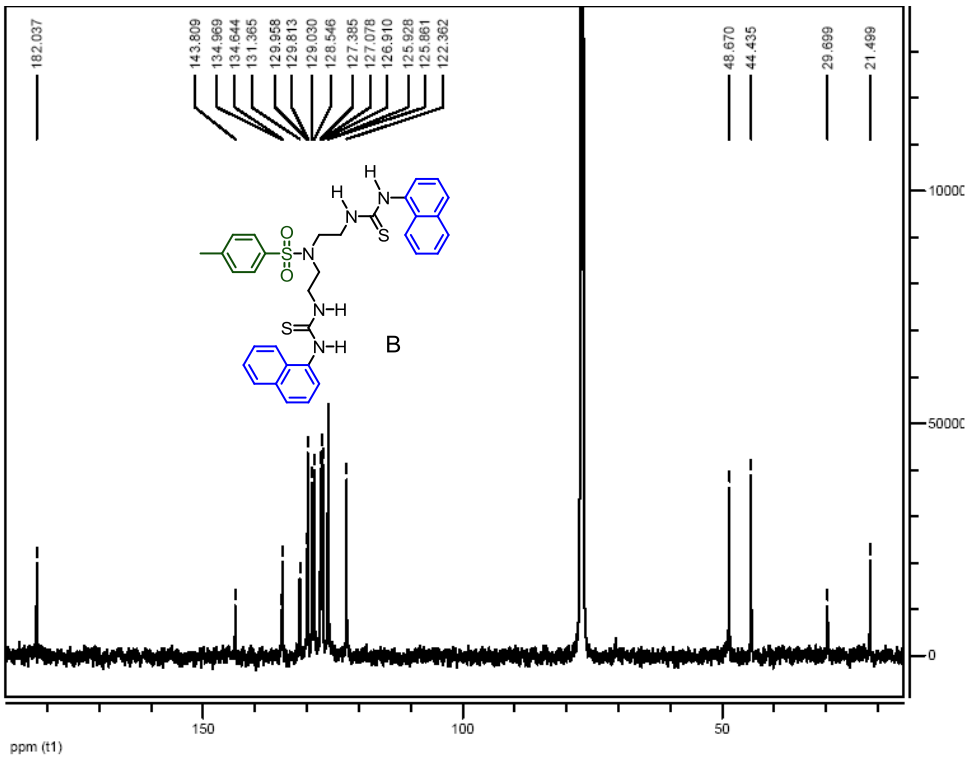

Figure 9. ^{13}C NMR spectra recorded in CD_2Cl_2 medium.

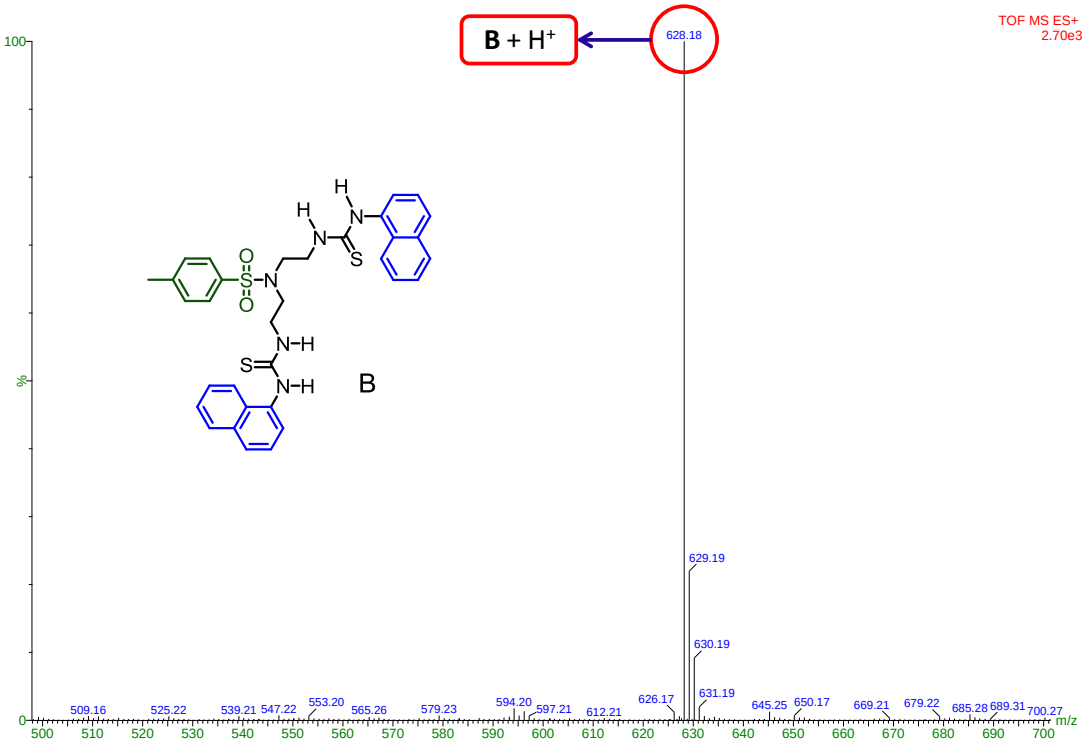

Figure10. ESI Mass spectrum recorded in MeOH.

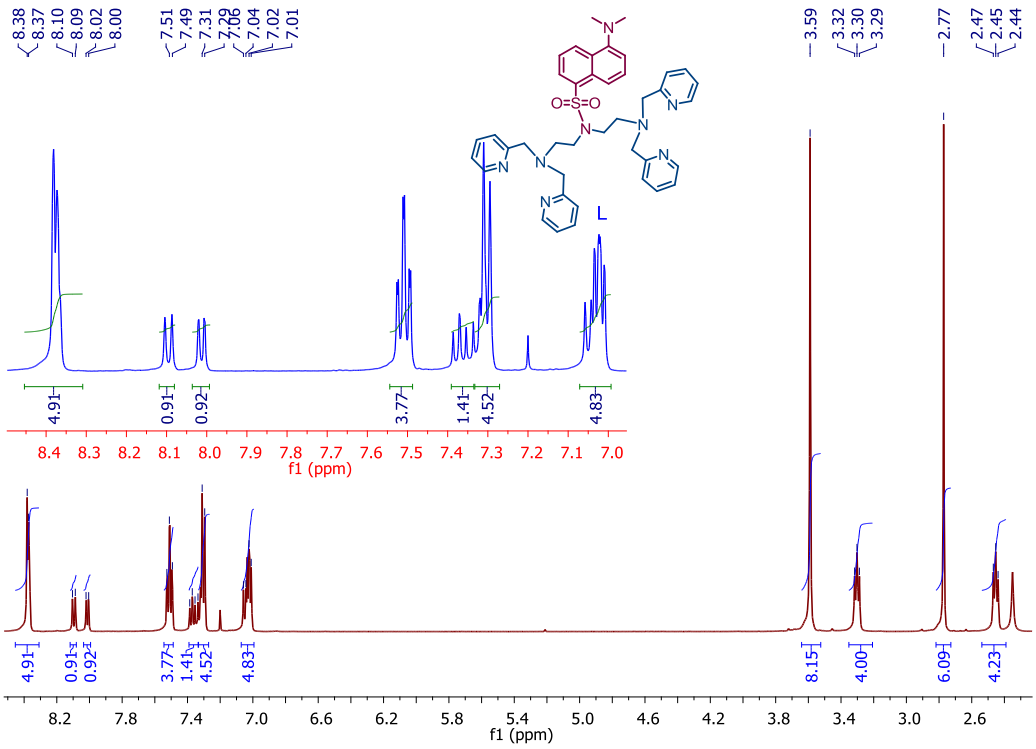

Figure 11. ^{1}H NMR spectra recorded in $CDCl_3$ medium.

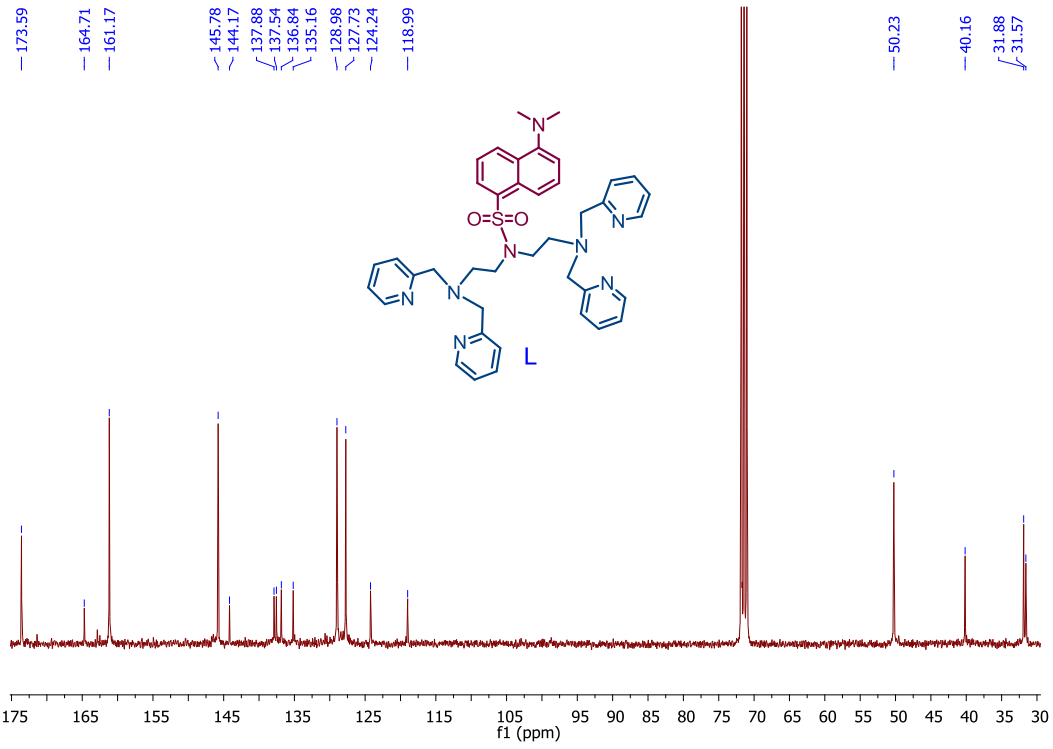

Figure 12. ^{13}CNMR spectrum recorded in $CDCl_3$ medium.

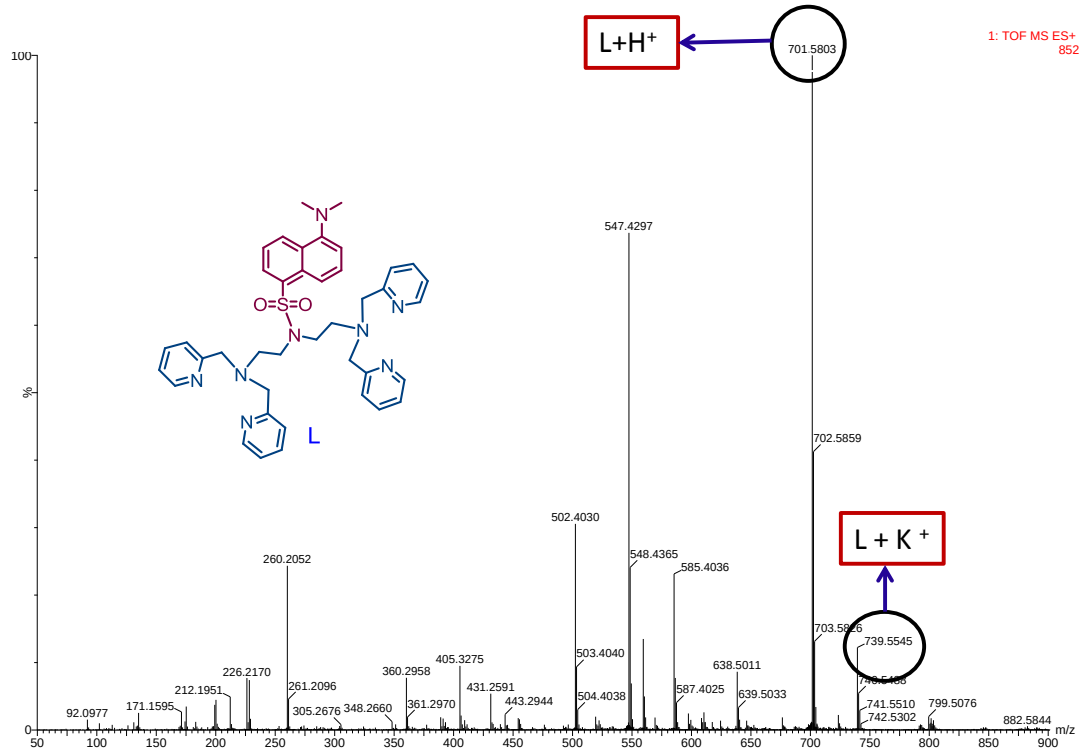

Figure 13. ESI Mass spectrum recorded in MeOH.

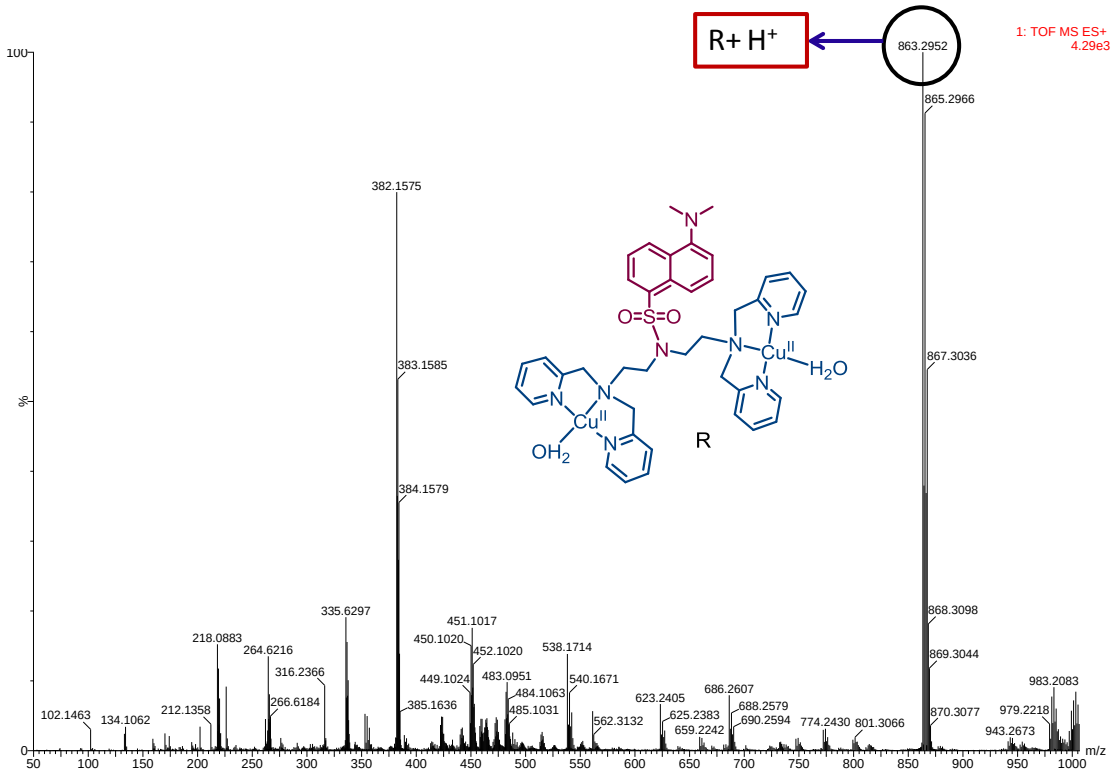

Figure 14. ESI Mass spectrum recorded in MeOH.

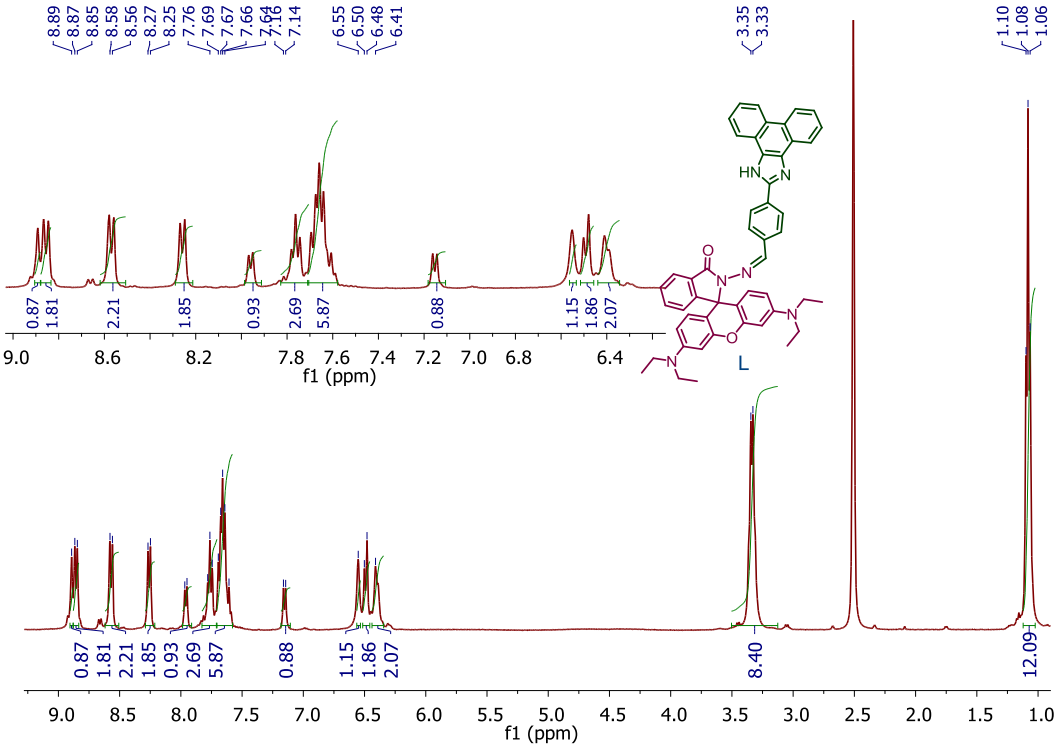

Figure 15.^{1}H NMR spectra recorded in DMSO-$d_6$medium.

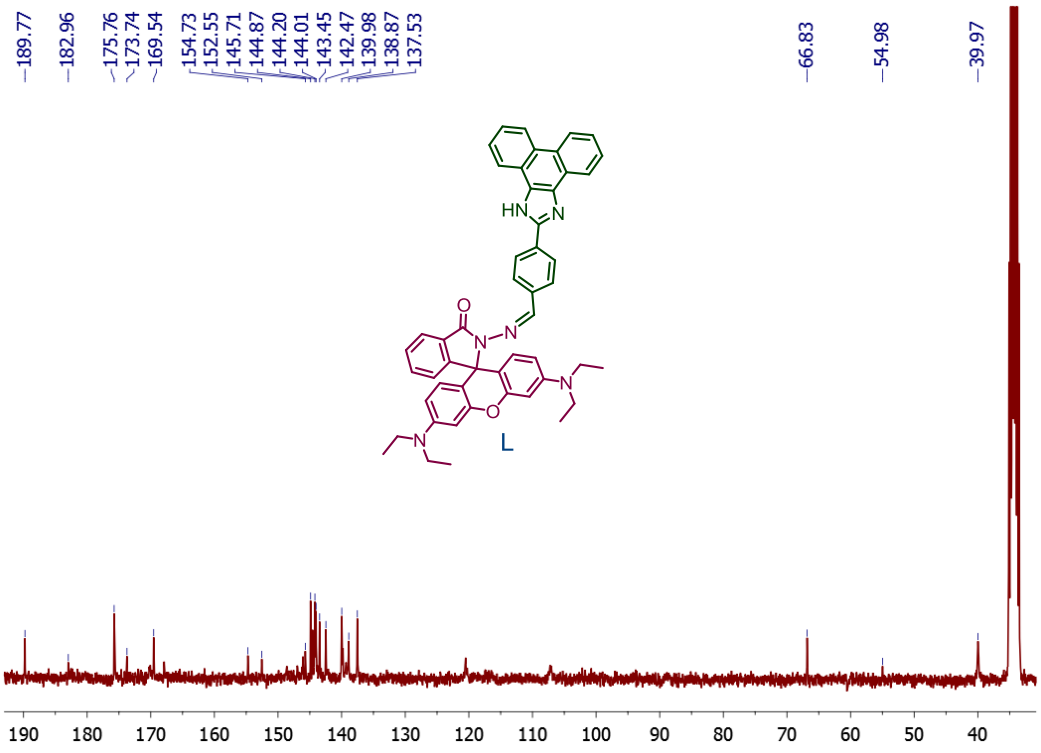

Figure 16. ^{13}C NMR spectra recorded in DMSO-$d_6$medium.

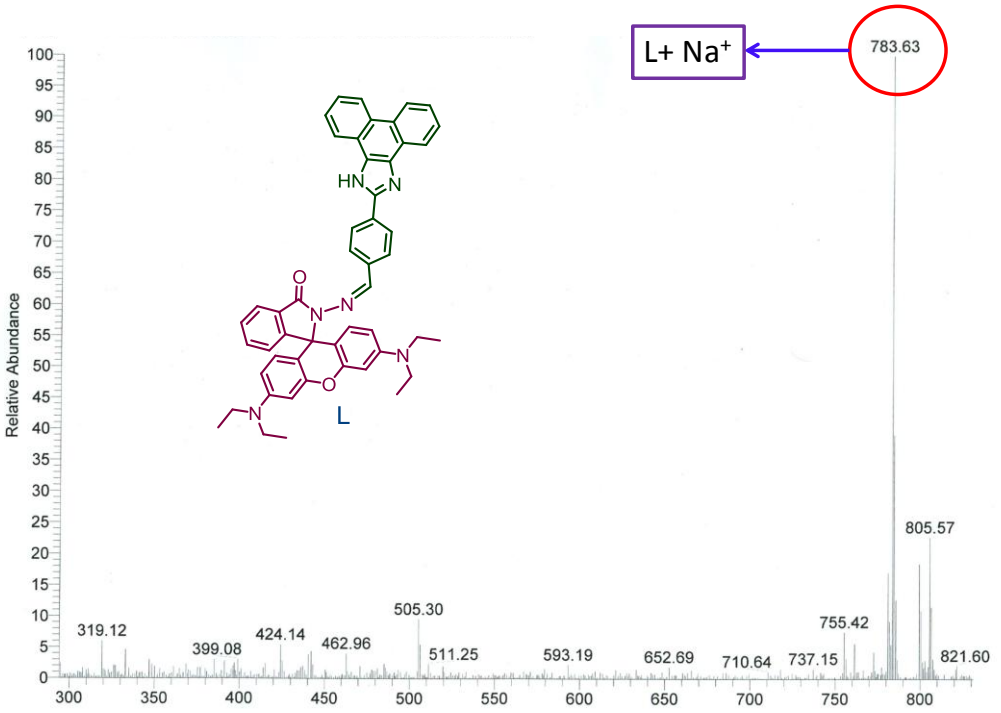

Figure 17. ESI Mass spectra recorded in MeOH.

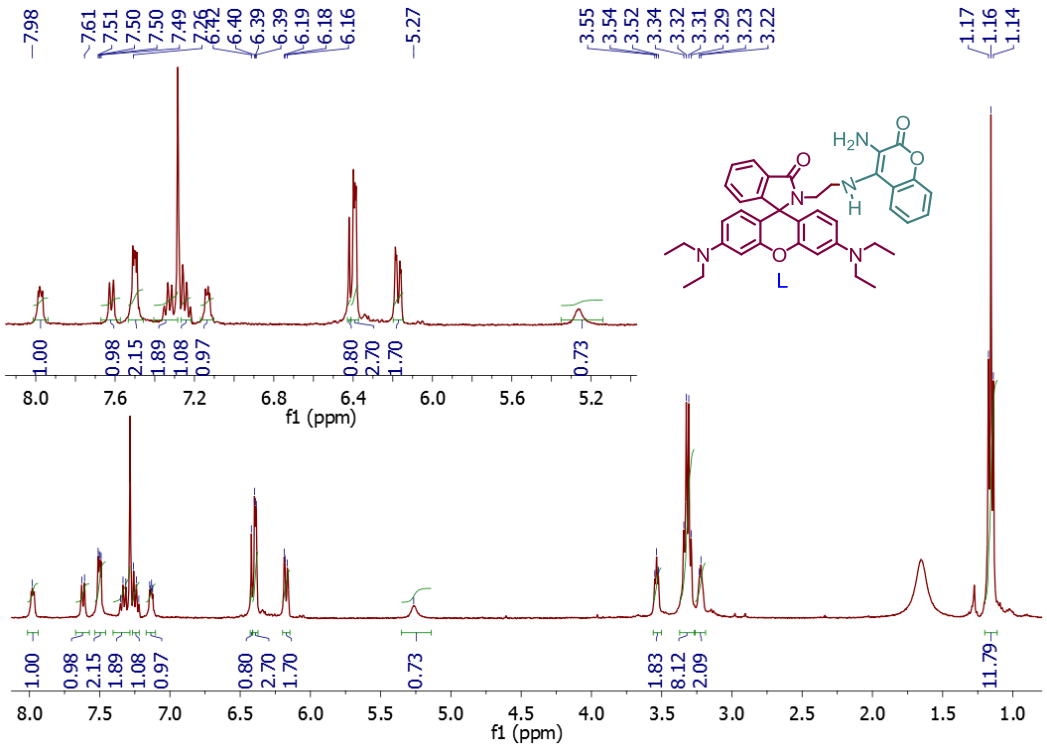

Figure 18.^{1}H NMR spectra recorded in $CDCl_3$-$d_3$medium.

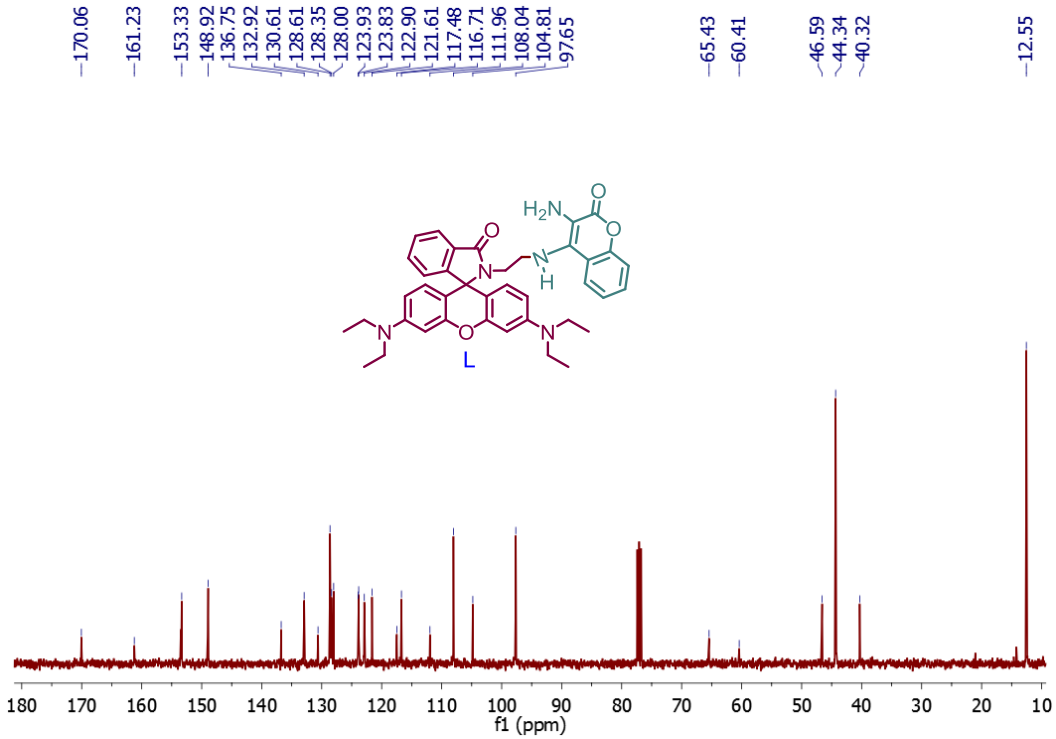

Figure 19. ^{13}C NMR spectra recorded in $CDCl_3$-$d_3$medium.

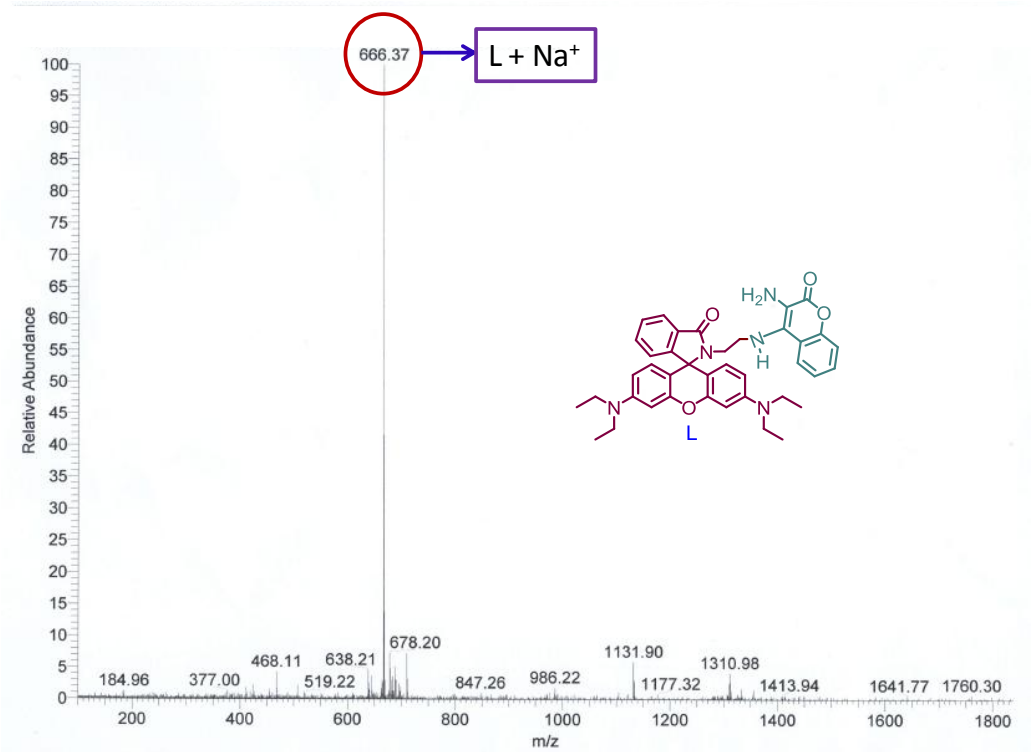

Figure 20. ESI Mass spectra recorded in MeOH.

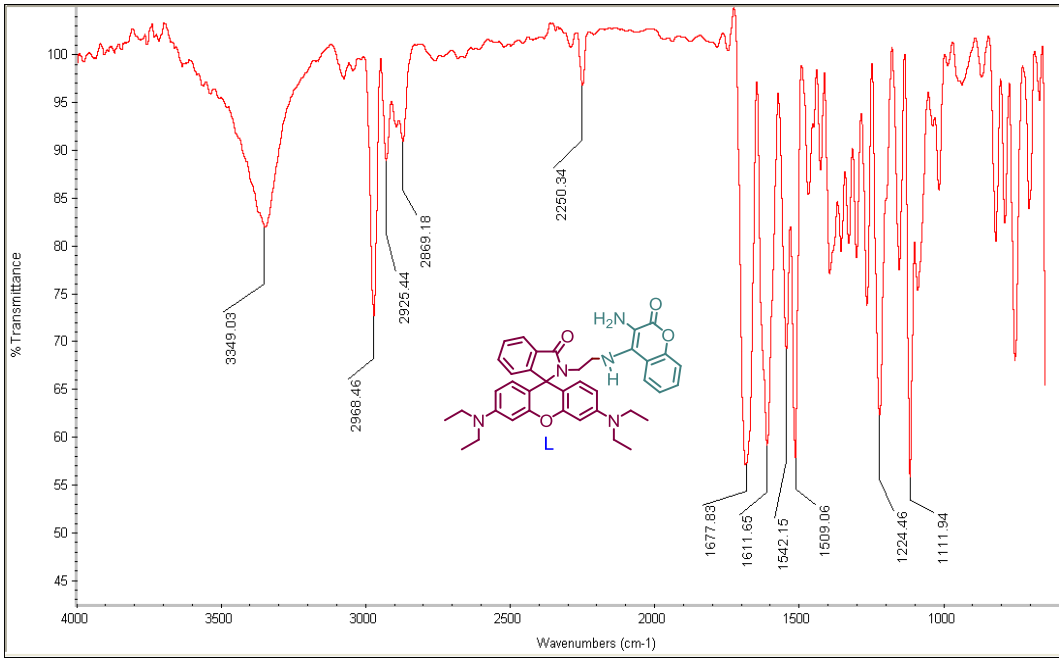

Figure 21. FTIR spectra recorded in MeOH.

1. **Upendar Reddy G**., Priyadip Das, Sukdeb Saha, Mithu Baidya, Sudip K. Ghosh and Amitava Das, ***Chem. Commun****.,* 2013, *49*, 255-257.
2. **Upendar Reddy G**., Rabindranath Lo, Sovan Roy, Tanmay Banerjee, Bishwajit Ganguly and Amitava Das, ***Chem. Commun****.,* 2013, *49*, 9818-9820.
3. **Upendar Reddy G**., Hridesh Agarwalla, Nandaraj Taye, Suvankar Ghorai, Samit Chattopadhyay and Amitava Das, ***Chem. Commun****.,* 2014, 50, 9899-9902.
4. **Upendar Reddy G**., Vadde Ramu, Sovan Roy, Nandaraj Taye, Samit Chattopadhyay and Amitava Das, ***Chem. Commun****.,* 2014, 50, 14421-14424.
5. **Upendar Reddy G**., Firoj Ali, Nandaraj Taye, Samit Chattopadhyay and Amitava Das, ***Chem. Commun.,*** 2015, 51, 3649-3652.
6. Sukdeb Saha, Prasenjit Mahato, **Upendar Reddy G**., E. Suresh, Arindam Chakrabarty, Mithu Baidya, Sudip. K. Ghosh and Amitava Das, ***Inorg. Chem.***, 2012, *51*, 336.
7. Priyadip Das, Amal Kumar Mandal, **Upendar Reddy G**, Mithu Baidya, Sudip K. Ghosh and Amitava Das, ***Org. Biomol. Chem***., 2013, 11, 6604.
8. Tanmay Banerjee, Abul Kalam Biswas, **Upendar Reddy G.**, Tuhin Subhra Sahu, Bishwajit Ganguly, Hirendra Nath Ghosh and Amitava Das, ***J. Phys. Chem. C***, 2014,118, 3864.
9. **Upendar Reddy G**., Anila H. A, Nandaraj Taye, Samit Chattopadhyay and Amitava Das, **Manuscript communicated.**
10. Anila H. A., **Upendar Reddy G.**, Firoj Ali, Nandaraj Taye, Samit Chattopadhyay and Amitava Das, **Manuscript communicated.**
11. Firoj Ali**,** **Upendar Reddy G.**, Anila H. A, Nandaraj Taye, Samit Chattopadhyay and Amitava Das, **Manuscript to be communicated.**

List of Patents

1. Amitava Das, Samit Chattopadhyay **Upendar Reddy G** and Hridesh Agarwalla. Patent filed application no. 2864/DEL/2014; New reagent for selective detection of cysteine and histidine in pure aqueous environment and in human blood plasma.
2. Amitava Das, Anila H.A. **Upendar Reddy G.**, Firoj Ali. Patent filed application no. 1061/DEL/2015. New reagent for selective detection of cysteine in aqueous solution as well as on silica coated TLC test strips
3. Amitava Das, Samit Chattopadhyay, Firoj Ali, **Upendar Reddy G**, Anila H.A. Nandaraj Taye. **Patent filed** (109NF2015). New reagent for specific detection of free cysteine.

1. Oral presentation in "3rd National Symposium on Functional Applications of Colorants (NSFAC -2013)" during October 29-30, 2013, conducted by Department of Chemistry, ICT- Bombay, India.
2. Oral presentation in "Modern Trends in Inorganic Chemistry [MTIC-XV]" during December 13-16, 2013, conducted by Department of Chemistry, IIT Roorkee, India.
3. Poster presentation in "4th International Conference on Molecular Sensors and Molecular Logic Gates (MSMLG)" during November 9-12, 2014, conducted by East China University of Science and Technology (ECUST), Shanghai, China.
4. Poster presentation in "Indo-German Conference on Bio-inspired Chemistry (IGCBIC-2014)" during September 10-12, 2014, conducted by IISc Bangalore, India.
5. Poster presentation in "JSPS-DST Asian Academic Seminar and School" during March 6-10, 2015, jointly conducted by IACS& IISER, Kolkata, India.
6. Poster presentation in "National Conference on Recent Trends in Drug Development (RTDD-2015)" during March 12-14, 2015, conducted by Savitribai Phule Pune University, Pune, India.
7. Poster presentation in "National Science day for 2014" in CSIR-NCL, Pune, India. February 25-28, 2015.
8. Participated in "International Conference on Structural and Inorganic Chemistry" during December 4-5, 2014, jointly conducted by CSIR-NCL& IISER- Pune, India.
9. Participated in "Chemical Research Society of India (CRSI) National Conference "during February 7-9, 2015, jointly conducted by CSIR-NCL, IISER- Pune & SP Pule University India

ChemComm

RSC Publishing

COMMUNICATION

View Article Online
View Journal | View Issue

Cite this: *Chem. Commun.*, 2013, **49**, 255

Received 4th October 2012,
Accepted 30th October 2012

DOI: 10.1039/c2cc37243f

www.rsc.org/chemcomm

A CN^- specific *turn-on* phosphorescent probe with probable application for enzymatic assay and as an imaging reagent†

Upendar Reddy G.,[a] Priyadip Das,[a] Sukdeb Saha,[a] Mithu Baidya,[b] Sudip K. Ghosh*[b] and Amitava Das*[a]

A new "*turn-on*" luminescence probe for imaging the uptake of 0.2 ppm inorganic CN^- in live HeLa cells as well as for probing the CN^- generation through an enzymatic process in a virtual aqueous medium at appropriate pH.

Acute toxicity of the cyanide ion towards mammalians results from its ability to interfere with the electron transport process and thus, inhibits the cellular respiration. Despite such a detrimental effect on human health, cyanide as a reagent has been used widely in various industries.[1] Accumulation of a higher level of cyanide could also happen through consumption of certain foods and plants.[2] Its acute toxicity accounts for a very low tolerance limit and according to the regulatory bodies (U.S. EPA) the maximum acceptable level of cyanide in drinking water and environmental primary standards is 0.2 and 0.5 ppm, respectively.[3] Prevalent industrial use as well as the increasing threat of its use with malicious intention has actually led to a recent surge of interest for the development of suitable reagents for selective detection of CN^- in water or in an aqueous environment. Further, the possibility of using such a reagent to develop an enzymatic assay for probing the *in situ* CN^- generation initiated by an important enzyme like hydroxynitrile lyase (HNL) is an added motivation and challenge.[4] Several methodologies have been adopted for designing an efficient CN^- sensor, which include recognition through hydrogen bonded adduct formation,[5] chemodosimetric detection,[6] utilizing the metal–cyanide ion coordination in a metal ion based receptor,[7] or by adopting the displacement reaction pathway.[8] However, many such systems suffer from the problem of achieving the specificity either due to the interference of other anions like fluoride, acetate, phosphate *etc.*, and/or the desired sensitivity owing to the high solvation energy of CN^- in water (-339 kJ mol^{-1}).[9] The affinity of CN^- towards Cu^{2+}-ions and the consequential displacement methodology is utilized for its recognition in an aqueous environment.[10] Hydrated CN^-, which is present predominantly in aq. medium, also attributes to its poor reactivity as a neucleophile toward a chemodosimetric reagent. Thus, the issue of specific, efficient and instantaneous recognition of CN^- in aqueous medium is a challenging one and any new reagent that works under physiological conditions as well as address these issues has significance in the area of cyanide detection.[5–8,11]

The fluorescence-based process for probing the binding induced phenomena is generally preferred over others owing to the possibility of attaining higher sensitivity as well as developing an imaging reagent for detection of the cellular uptake of the analyte with spatial resolution. In this regard cyclometallated Ir(III)-complexes have received recent attention due to their better stability towards photo-bleaching and favourable photophysical properties.[12] For such Ir(III)-complexes, an efficient spin–orbit coupling process favours the ISC process and thus helps in populating the first excited triplet state having a longer lifetime.[12] This has been utilized successfully in designing Ir(III)-polypyridyl and Ir(III)-cyclometallated complexes as the phosphorescence-based signalling unit as well as an imaging reagent for intracellular studies.[13] Generally, a higher degree of localization of these Ir(III)-complexes in the perinuclear region occurs due to interactions of these complexes with hydrophobic organelles.[13c] In the present study, we have used a Ir(III)-based cyclometallated complex having a pendant Cu(II)-moiety (**1·Cu**) for recognition of CN^- in virtual aq. HEPES buffer medium (10 mM aq. HEPES buffer–CH_3CN, 99.6 : 0.4, v/v; pH 7.6) with associated turn-on phosphorescence response. This reagent could also be used as an imaging reagent for detection of the cellular uptake of CN^- ions in HeLa cells from aqueous-buffer media (pH 7.6) with [CN^-] as low as 0.2 ppm as well as for developing an assay for probing the *in situ* release of cyanide from a cyanohydrin by the HNL enzyme under physiological conditions.

The absorption and photoluminescence spectra of **1** (Scheme 1 and ESI†) were recorded in virtual aq. HEPES buffer (pH 7.6) medium at room temperature (Fig. 1A). The intense absorption band maximum at 260 nm ($\varepsilon = 5.2 \times 10^4$ mol^{-1} L cm^{-1}) was

[a] *CSIR-Central Salt & Marine Chemicals Research Institute, Bhavnagar 364002, Gujarat, India. E-mail: amitava@csmcri.org*
[b] *Department of Biotechnology, Indian Institute of Technology, Kharagpur, West Bengal 721302, India. E-mail: sudip@hijli.iitkgp.ernet.in*

† Electronic supplementary information (ESI) available: Synthesis, characterization details of $\mathbf{L_1}$, $\mathbf{L_2}$, **1** and **1·Cu**, experimental methodologies and sample preparation. See DOI: 10.1039/c2cc37243f

ChemComm

RSC Publishing

COMMUNICATION

View Article Online
View Journal | View Issue

Cite this: *Chem. Commun.*, 2013, **49**, 9818

Received 5th July 2013,
Accepted 27th August 2013

DOI: 10.1039/c3cc45051a

www.rsc.org/chemcomm

A new receptor with a FRET based fluorescence response for selective recognition of fumaric and maleic acids in aqueous medium†

Upendar Reddy G.,[a] Rabindranath Lo,[b] Sovan Roy,[a] Tanmay Banerjee,[a] Bishwajit Ganguly*[b] and Amitava Das*[a]

Preferential binding of a new reagent to fumaric acid could be utilized for its estimation in aqueous medium and in commercial fruit juice.

Molecular recognition studies of dicarboxylic acids have gained importance because of their presence as key structural moieties in many bioactive molecules, their role in various metabolic processes and involvement in the biosynthesis of some important intermediates.[1] Fumaric (Fum) and maleic (Mal) acids find a broad range of uses in medicine, food and polymer industries.[1] More recently, fumaric acid derivatives have been tested for treatment of multiple sclerosis and patients with psoriasis.[2] Maleic acid is known for its role as an inhibitor of the Krebs cycle and in different kidney diseases.[2] Due to the widespread use of these two acids as ingredients in food as well as beverages and their possible adverse influences on human health upon prolonged exposure, it is important to develop an efficient reagent for their recognition and quantitative estimation in aqueous medium. In the recent past, considerable progress has been made in the recognition of various dicarboxylic acids through hydrogen bonded adduct formation using hydrogen bond donor units like urea/thiourea/amide, guanidium groups, and allosteric phosphate-based receptors.[3–6] Among these, the only report that reveals the recognition of certain dicarboxylate ions in pure aqueous tris buffer medium of pH 7.5 shows the lack of the desired specificity towards maleate or fumarate.[4a] Alternative approaches to investigate the coordinative interactions of these dicarboxylate ions with certain metal ions or Lewis acid based receptors for recognition studies are truly limited and in these examples the key issue of specificity remains unaddressed.[4,7] A chemodosimetric reagent was reported to be able to discriminate between maleate and fumarate ions.[8] However, this reagent was also found to bind to *ortho*- and *meta*-dibenzoic acids in mixed aq. buffer medium at nearly neutral pH. A synthetic molecular probe was reported for estimation of citrate or tartrate–malate in mixed aq. buffer medium.[4b] Thus, the issue of developing a reversible sensor specific to maleate and fumarate ions in an ensemble of common mono- and di-carboxylate ions in aqueous medium has eluded researchers to date.[3–8]

A new thiourea based receptor **A** was synthesized following a multistep procedure with reasonable yield and purity of this reagent was ensured.† Model reagents (**B** and **R**) were synthesized for unambiguous assignment of the spectral responses of **A** upon binding to fumarate or maleate ions (Scheme 1).

The electronic and emission spectra of compounds **A** and **B** were recorded in aq. HEPES buffer–CH_3CN (1 : 1, v/v; pH 7.4) medium at room temperature. The electronic spectrum of compound **A** showed three shoulders at ~353 nm, ~290 nm and ~244 nm, whereas in the case of compound **B** one distinct absorption band at 290 nm was observed.† The common shoulder observed at 290 nm could be ascribed to a charge transfer (CT) transition that is typical for the naphthalene moiety. A shoulder at ~353 nm for **A** was ascribed to a dansyl-based CT transition. UV-vis spectra of **A** and **B** remained unchanged in the presence of excess of all mono and di-carboxylate ions under identical experimental conditions.†

A solution of **A** in aq. HEPES buffer–CH_3CN (1 : 1, v/v; pH 6.0) medium showed a strong emission band at 542 nm (λ_{Ext} = 290 nm).† Emission spectra recorded for compound **B**, having only a comparable naphthalene moiety as the fluorescence active unit (λ_{Ext} of 290 nm), showed three emission bands at 313, 390 (broad) and 464 nm.† Bands at 313 and 390 nm were

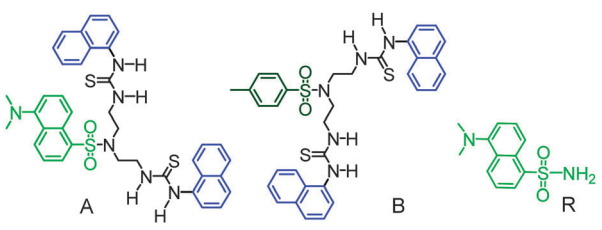

Scheme 1 Molecular structures of **A**, **B** and **R**.

[a] *Organic Chemistry Division, CSIR-National Chemical Laboratory, Pune-411008, India. E-mail: a.das@ncl.res.in; Fax: +91 2025902629; Tel: +91 2025902385*

[b] *CSIR-Central Salt & Marine Chemicals Research Institute, Bhavnagar – 364002, India. E-mail: ganguly@csmcri.org; Fax: +91 278 2567562*

† Electronic supplementary information (ESI) available: Synthesis and characterization details of **A**, **B** and **R**. Energy optimized structures and analysis of fumaric acid in fruit juice by HPLC.See DOI: 10.1039/c3cc45051a

ChemComm

COMMUNICATION

View Article Online
View Journal | View Issue

Cite this: *Chem. Commun.*, 2014, **50**, 9899

Received 2nd June 2014,
Accepted 2nd July 2014

DOI: 10.1039/c4cc04214j

www.rsc.org/chemcomm

A novel fluorescence probe for estimation of cysteine/histidine in human blood plasma and recognition of endogenous cysteine in live Hct116 cells†

Upendar Reddy G.,[a] Hridesh Agarwalla,[a] Nandaraj Taye,[b] Suvankar Ghorai,[b] Samit Chattopadhyay*[b] and Amitava Das*[a]

A new Cu(II)-complex is used as a "*Turn-On*" luminescence probe for specific detection of endogenous Cys in live Hct116 cells and Cys present in human blood plasma without any interference from other amino acids, especially GSH and Hcy. Difference in the mechanistic pathway for Cys and His recognition is discussed.

High sensitivity and spatiotemporal resolution are two key issues that have made molecular probes with *fluorescence on* response an efficient tool for detection and visualization of minute amounts of the desired analytes(s) in live cells and tissues. Accordingly, a number of such molecular probes are reported for vital biothiols, like cysteine (Cys) and histidine (His), as these play vital roles in many critical bioactivities.[1] Among these, Cys acts as an intracellular redox buffer that influences detoxification and critical metabolic functions.[1] Deficiency in Cys causes oxidative damage, haematopoiesis, psoriasis, leukocyte loss and metabolic disorders. A higher level of Cys in the human blood plasma (HBP) is known to cause cardiovascular and Alzheimer's diseases.[2] His can act as a neurotransmitter in the central nervous system of mammals. Its deficiency could affect the human growth factor and may cause the impaired nutritional state of patients with chronic kidney disease.[3] A higher level of His could cause metabolic disorders like histidinemia.[4] Estimation of these amino thiols in HBP is essential for understanding the role of these in the pathogenesis of vascular diseases and these have provoked researchers to develop molecular probes that could quantitatively delineate these biothiols from other amino acids.[2,3b] However, examples of molecular probes capable of detecting Cys and His in biological fluids in the presence of Hcy and GSH are rather limited.[5e,n] Molecular probes that are generally being used for detection of biothiols either under physiological conditions or in biological fluids are mostly based on chemodosimetric reaction and such a process often suffers from the relatively large incubation time ranging from 20 minutes to 1 h or more.[5a–c,h,i,k–m] An alternate approach utilizes the higher affinity of Cu(II) towards S-donor nucleophiles for designing molecular probes with *fluorescence on* response.[5e,g] Such reactions mostly occur within a millisecond time scale and thus, this methodology has an edge over the other for application in diagnostics. Examples of molecular probes that could specifically detect Cys, even in the presence of Hcy and GSH, under pure physiological conditions are scanty,[5a–c] while limited such probes are known for His.[5fj] However, a majority of such reagents relied on chemodosimetric detection and estimation of the total thiol content in HBP.[6] Use of certain fractions of organic solvents was described in most such reports for solubilising the reagent. In our attempt to develop a molecular probe for instantaneous and selective detection of endogenous Cys or Cys/His in HBP, we have synthesized a novel bis-Cu(II)-complex (**R**, Scheme 1) using a new bis-dipicolyl amine derivative (**L**). A lower pK_a value of the thiol group in the side chain in Cys (8.00), as compared to that in Hcy (8.87) and GSH (9.20), is utilized for its specific detection without any interference from these two commonly interfering biothiols at pH 7.4. At this pH, Cys exists predominantly in its thiolate form and thus acts as a better coordinating ligand for Cu(II) than other biothiols.[5d] Also, the well known affinity of His to form a stable complex with Cu(II) is utilized in the present study for its recognition.[7] Thus, this reagent (**R**) could be utilized for specific and quantitative estimation of Cys and His in HBP as well as for specific imaging of endogenous Cys

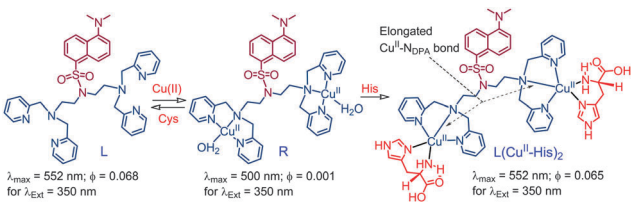

Scheme 1 Molecular structure of receptor **R** and its reactions with Cys and His with associated steady state fluorescence properties.

[a] *Organic Chemistry Division, CSIR-National Chemical Laboratory, Pune-411008, India. E-mail: a.das@ncl.res.in; Fax: +91 2025902629; Tel: +91 2025902385*

[b] *Chromatin and Disease Biology Lab, National Centre for Cell Science, Pune 411007, India. E-mail: samit@nccs.res.in*

† Electronic supplementary information (ESI) available: Synthesis, characterization details for **1**, **L** and **R**, other methodologies and sample preparation. See DOI: 10.1039/c4cc04214j

ChemComm

COMMUNICATION

View Article Online
View Journal | View Issue

Cite this: *Chem. Commun.*, 2014, 50, 14421

Received 27th August 2014,
Accepted 15th September 2014

DOI: 10.1039/c4cc06740a

www.rsc.org/chemcomm

A specific probe for Hg^{2+} to delineate even H^+ in pure aqueous buffer/Hct116 colon cancer cells: Hg(II)–η^2-arene π-interaction and a TBET-based fluorescence response†

Upendar Reddy G.,[a] Vadde Ramu,[a] Sovan Roy,[a] Nandaraj Taye,[b] Samit Chattopadhyay*[b] and Amitava Das*[a]

A new molecular probe that demonstrates a distinct TBET process, induced by the Hg(II)–η^2-arene π-interaction, in pure aqueous medium with a large pseudo-Stokes shift of 200 nm.

Intramolecular triplet–triplet energy transfer is being pursued more recently for developing efficient fluorescence-based receptors, as the average lifetime of the triplet state is much longer than the singlet state.[1] However, such a triplet–triplet energy transfer is spin-forbidden by the dipole–dipole mechanism (Förster-type mechanism) and is only allowed by the electron exchange mechanism (Dexter-type mechanism).[1] Such a triplet–triplet energy transfer requires either an effective orbital overlap or coupling mediated by an appropriate conduit. More importantly, such a through bond energy transfer (TBET) process is not limited by the fact that donor and acceptor fragments ought to have a spectral overlap. This offers the opportunity to achieve a large pseudo-Stokes shift to avoid self-quenching of the donor fluorophore and fluorescence detection errors because of excitation back-scattering effects.[2] Additionally such an energy transfer dyad also helps in avoiding the problem of photo-bleaching of the probe fluorophore.[2,3] For fluorophore dyad systems that have an insignificant spectral overlap between the donor emission and acceptor absorption, the FRET process could be operational along with the TBET process. The challenge of demonstrating the TBET process in a small molecule based fluorophore dyad without the complete absence of the spectral overlap has not been met to date, barring one recent example.[4]

Among various fluorophores, acyclic xanthene forms of different rhodamine derivatives have been widely used as imaging reagents because of their high emission quantum yield, cell membrane permeability, non-toxic nature towards live cells and finally the *switch on* fluorescence response upon conversion of a cyclic lactam form to the acyclic one.[5] However, such reagents generally have a Stokes shift of about 50 nm and respond to H^+ as well as certain metal ion(s) with a fluorescence on response.[5] More recently, a much larger Stokes shift was reported for a receptor with TBET-based response on specific binding to Hg^{2+}.[6] However, there existed a small spectral overlap between the donor and the acceptor fragments and this did not completely exclude the possibility of the FRET-based response along with the predominant TBET process. Thus, examples of TBET-based cassettes for intracellular imaging applications are actually rare.[3,6]

Among various metal ions, Hg^{2+} is one of the most potent neurotoxins known and its deleterious influences on human as well as plant physiology are well documented in a range of literature reports and the lowest Hg(II) concentration that is allowed in safe drinking water is 0.2 ppb.[7–9] Keeping this in mind, it is imperative to develop a reagent that could specifically recognize, detect and quantitatively estimate mercury ion concentration as low as the above referred limit in pure aqueous/buffer medium having physiological pH. Hg^{2+} is known to be an efficient quencher of molecular fluorescence due to a facile spin–orbit coupling process.[10] The solvation enthalpy for Hg^{2+} is also significant (1824 kJ mol^{-1}). Thus, designing an ultrasensitive fluorescence-based specific probe for Hg(II) with a high Strokes shift is a challenging issue.

In the present communication, we have described a new probe molecule that allowed us to achieve specificity in detecting Hg^{2+} in aqueous buffer medium through formation of a Hg(II)–η^2-arene complex. This not only allowed us to delineate Hg^{2+} from H^+ based on a distinctly different fluorescence response, but also helped us to achieve a significant pseudo-Stokes shift of ~200 nm through a TBET-based response. Such an example is rare in the contemporary literature.

Detailed synthesis of **L**, $\mathbf{R_1}$ and $\mathbf{R_2}$ (Scheme 1), their spectral (^{1}H NMR and ^{13}C NMR) and analytical characterization data are provided in the ESI.† Reagent **L** showed an intense absorption band at 386 nm for the benzimidazole derivative of the phenanthrene moiety and apart from this, no other absorption band was observed when spectra were recorded for 20 μM solution of **L** in aq. buffer medium (aq. HEPES buffer; 10 mM; pH 7.2) containing 0.4 mM Triton X100 (TX100) (Fig. 1a (inset)). This assignment was based on the observed electronic spectral band for the model compound $\mathbf{R_1}$ at 375 nm. A biologically benign neutral surfactant (TX100) allowed

[a] *Organic Chemistry Division, CSIR-National Chemical Laboratory, Pune-411008, India. E-mail: a.das@ncl.res.in; Fax: +91 2025902629; Tel: +91 2025902385*
[b] *Chromatin and Disease Biology Lab, National Centre for Cell Science, Pune-411007, India. E-mail: samit@nccs.res.in*

† Electronic supplementary information (ESI) available. See DOI: 10.1039/c4cc06740a

ChemComm

COMMUNICATION

View Article Online
View Journal | View Issue

Cite this: *Chem. Commun.*, 2015, 51, 3649

Received 19th December 2014,
Accepted 20th January 2015

DOI: 10.1039/c4cc10171e

www.rsc.org/chemcomm

A new turn on Pd^{2+}-specific fluorescence probe and its use as an imaging reagent for cellular uptake in Hct116 cells†

Upendar Reddy G.,[a] Firoj Ali,[a] Nandaraj Taye,[b] Samit Chattopadhyay*[b] and Amitava Das*[a]

A new coumarin–rhodamine conjugate is used as a specific probe for Pd^{2+} ions and this could even delineate Pd(II) from Pd(0) or Pd(IV) in aqueous buffer medium (pH ~ 7). Laser confocal microscopic studies reveal that efficient cellular internalization of this reagent helps in imaging the cellular uptake of Pd^{2+} as low as 0.1 ppm in Hct 116 cells. This reagent could even be used for estimation of Pd^{2+} in human urine samples.

Palladium has found a wide range of applications in organic synthesis, drug design, pharmaceuticals and commercial materials, such as fuel cells, dental crowns, medical instruments, jewellery, *etc.*, owing to its inertness, biocompatibility and versatility as a catalyst.[1] The role of diverse Pd-complexes in different coupling reactions is explored extensively by synthetic chemists as well as for the production of a range of crucial fine chemicals and drug molecules.[2] Despite exhaustive purification processes, a certain amount of palladium could remain as an impurity in the final product,[2b,3] which is consumed along with the drug. Previous reports reveal that palladium has the propensity to coordinate to DNA, certain proteins/thiol-containing amino acids, and vitamin B6, and disrupt some cellular processes, thereby leading to health problems.[4] Apart from consumption of certain drugs/pharma products that are contaminated with trace amounts of palladium ions, human population in general gets exposed to palladium through dental alloys, jewellery, food and emissions from automobile catalytic converters. Average dietary intake of palladium for an adult is estimated to be ~1.5–15 μg per day as per WHO report and its permitted threshold level in drugs is 5–10 ppm.[3] It has been argued that excretion of palladium happens mostly through urine and its concentration in urine typically lies in the range of 0.006 to $<0.3\ \mu g\ l^{-1}$ in adults.[5] All these have necessitated the development of an efficient fluorescent probe that could bind specifically and reversibly to Pd(II) species, as 2+ is the most abundant oxidation state of the palladium metal that could exist under physiological conditions or in live cells. Such a molecular probe could be ideal for detection of cellular uptake of Pd(II) or for diagnostic applications. Apart from these, the reagent that also allows instantaneous infield analysis of environmental samples has a distinct edge over other analytical methods and procedures. Conventional methods for palladium detection rely mostly on analytical methodologies like atomic absorption spectrophotometry, solid-phase micro-extraction-high-performance liquid chromatography and ion-coupled plasma emission-mass spectrometry. Such procedures are generally expensive, time-consuming and need highly skilled individuals.[6] Such methodologies also involve complicated sample preparation procedures. These limitations have further exemplified the scope of an efficient and sensitive molecular probe that allows turn-on fluorescence response upon specific binding to Pd(II) ions in aqueous buffer medium having physiological pH as well as an imaging reagent.[7]

Pd(II) is generally known to be an efficient quencher for luminescence, as it favours an effective spin–orbit coupling and non-radiative deactivation of the excited states.[8] Thus, examples of the fluorescence off-based receptors for palladium are abundant in the contemporary literature.[8] Among limited fluorescence on-based receptors reported in the literature,[9] very few have been utilized either as imaging reagents or for detection of palladium in biological fluids.[10] More importantly, none of such receptors are found to be specific towards Pd(II).[8f,9i,j,10g–i] This motivated us to develop a rhodamine based molecular probe (**L**; Scheme 1) that was specific towards Pd(II) among all other metal ions under physiological conditions and could be utilized also as an imaging reagent or for detection of Pd(II) present in biological fluids like human urine samples. Conversion of the cyclic lactam form (fluorescence-off mode) to the acyclic xanthene form (fluorescence-on mode) of a suitably substituted rhodamine derivative (**L**) upon specific binding to Pd(II) has been described in the present communication. We could demonstrate that this new molecular probe could bind to Pd(II) in the presence of all other common metal ions, including Pd(0) or Pd(IV), under physiological conditions with associated

[a] *Organic Chemistry Division, CSIR-National Chemical Laboratory, Pune-411008, India. E-mail: a.das@ncl.res.in; Fax: +91 2025902629; Tel: +91 2025902385*
[b] *Chromatin and Disease Biology Lab, National Centre for Cell Science, Pune 411007, India. E-mail: samit@nccs.res.in*

† Electronic supplementary information (ESI) available: Synthesis, characterization, methodologies for cellular imaging studies and different evaluation procedures. See DOI: 10.1039/c4cc10171e